HYDROPHOBINS FROM *PLEUROTUS OSTREATUS* IN BIOTECHNOLOGICAL INDUSTRY

Alfredo Maria Gravagnuolo

Dottorato in Scienze Biotecnologiche – XXVII ciclo
Indirizzo Biotecnologie Industriali e Molecolari
Università di Napoli Federico II

Dottorato in Scienze Biotecnologiche – XXVII ciclo
Indirizzo Biotecnologie Industriali e Molecolari
Università di Napoli Federico II

HYDROPHOBINS FROM *PLEUROTUS OSTREATUS* IN BIOTECHNOLOGICAL INDUSTRY

Alfredo Maria Gravagnuolo

Dottorando: Alfredo Maria Gravagnuolo

Relatore: Prof.ssa Paola Giardina

Coordinatore: Prof. Giovanni Sannia

A chi mi sorprende
giorno per giorno

INDICE / INDEX

RIASSUNTO

A. INTRODUZIONE

Idrofobina Vmh2 da *Pleurotus ostreatus*

Le idrofobine sono piccole proteine (circa 100 residui amminoacidici) ad alta attività superficiale, note da circa 10 anni per le loro peculiari proprietà. Prodotte da funghi filamentosi, sono bio-surfattanti e auto-assemblano in membrane anfifiliche alle interfacce solido-liquido o aria-liquido. Per le loro proprietà, le idrofobine hanno diversi ruoli biologici, ad esempio sono coinvolte nella formazione ed il rivestimento di ife aeree, spore, corpi fruttiferi e nell'adesione delle ife a superfici idrofobiche durante le interazioni simbiotiche o patogene (Wösten et al. 2001).
Le proteine di questa famiglia hanno bassa identità di sequenza, ma sono caratterizzate da un motivo ben conservato di otto cisteine legate tra loro da ponti disolfurici (Sunde et al. 2008).

La famiglia delle idrofobine fungine è stata divisa in due classi in base a caratteristiche strutturali e funzionali: le idrofobine di classe I formano un film estremamente robusto costituito da strutture di tipo amiloide chiamate "*rodlet*" che possono essere depolimerizzate solo in acidi forti (i.e. TFA 100%), mentre i polimeri formati dalle idrofobine di classe II sono non fibrillari e meno stabili, possono essere sciolti in etanolo o soluzioni acquose di sodio dodecil solfato (SDS) (Zampieri et al. 2010). Le principali caratteristiche dei film d'idrofobine rispetto agli altri film proteici sono la loro maggiore resistenza chimica e l'abilità di modificare sensibilmente la bagnabilità della superficie di materiali (Hou et. al 2009), Infatti, per la loro natura anfifilica, il rivestimento di idrofobine converte superfici idrofobiche in idrofiliche e vice versa.

A causa delle loro proprietà peculiar,i queste proteine sono di grande interesse per vari settori dell'industria (Hektor et al. 2005, Linder et al. 2009). Sono stabilizzanti di emulsioni e sono in grado di produrre schiume; da questo le loro applicazioni nell'industria cosmetica ed alimentare. Inoltre, alcune di loro sono prodotte da organismi GRAS (*generally recognized as safe*) o addirittura edibili. Sono molto interessanti anche dal punto di vista della scienza delle superfici e possono essere usate in applicazioni di alto livello tecnologico (Bayry et al., 2012) come ad esempio adesione di cellule (Li X et al. 2009; Zhang M et al., 2011), sistemi di *drug delivery* (Sarpanta et al., 2012; Valo et al., 2010) e biosensori (Corvis et al. 2005; Zhao et al., 2007; Zhao et al., 2009).

Le ultrastrutture formate da idrofobine di classe I, chiamate "*rodlets*" (letteralmente dall'inglese, a forma di bastoncelli), rivestono la superficie di molti funghi sporigeni ed è stato dimostrato che questo strato è in grado di prevenire il riconoscimento di spore fungine disperse nell'aria da parte del sistema immunitario [Aimanianda et al. 2009]. La loro abilità di formare membrane immunolgicamente inerti ed altamente stabili le rende attraenti candidati per impianti ortopedici (Scholtmeijer et al. 2002; Boeuf et al., 2012). E' stato anche dimostrato che uno strato monomolecolare formato da alcune idrofobine su substrati solidi è in grado di mediare l'adesione di un secondo strato proteico (De Stefano et al. 2009; Wang Z. et

al. 2010). Questo sistema è utilizzabile per la modifica di superfici di elettrodi e nella biosensoristica (Corvis et al. 2006; Zhao et al. 2007).

Tuttavia, i livelli di produzione della maggior parte delle idrofobine note sono bassi ed i costi di produzione troppo elevati per applicazioni di uso comune. Fanno eccezione l'idrofobina di classe II, HFBI per la quale è stato costruito un ceppo di *Trichoderma reesei* iperproduttore, ottenendo una resa di proteina di 600mg per litro di coltura (Askolin et al. 2001), e l'idrofobina di classe I H*Protein A prodotta come proteina ricombinante di fusione dalla multinazionale BASF su impianto pilota per la produzione su scala di chilogrammi (Wohlleben et al. 2010).

Nonostante la difficile estrazione e manipolazione, le idrofobine di Classe I sono proteine molto interessanti per la scienza delle superfici perché formano strati altamente stabili che possono resistere in SDS 2% (peso/volume, w/v). SC3 da *Schizophyllum commune* è una delle idrofobine di Classe I più studiate. Questa è in grado di formare fibrille di tipo amiloide che hanno una caratteristica morfologia a *rodlet*. I *rodlet* sono ultrastrutture proteiche di circa 100 nm di lunghezza che condividono molte delle caratteristiche strutturali delle fibrille di tipo amiloide; la loro formazione è accompagnata da cambi conformazionali verso strutture ordinate di tipo β, in grado di legare la Tioflavina T (ThT) così come avviene per le strutture amiloidi (Biancalana and Koide 2010). In particolare, SC3 auto-assembla spontaneamente all'interfaccia acqua-aria, formando prima un intermedio ad alto contenuto di α-elica, poi una configurazione finale stabile ad alto contenuto di foglietti β. D'altra parte, SC3 è bloccata nell'intermedio in configurazione α-elica in seguito al contatto con solidi idrofobici (ad esempio Teflon). La transizione verso lo stato stabile finale a foglietti β è promossa da alta concentrazione proteica, oppure dalla presenza di polisaccardi della parete cellulare (schizofillano) oppure in presenza di detergenti ed ad elevate temperature (Scholtmeijer et al 2009).

Sono anche riportate condizioni in grado di indurre auto-assemblamento di altre idrofobine di classe I ricombinanti, H*Proteina A e B (pH > 6, temperatura $\gg$ 5 °C, concentrazione > 0.2 mg/mL) (Wohlleben et al. 2010). Morris e colleghi (2011) hanno studiato l'effetto di alcuni additivi (alcoli, detergenti, liquidi ionici) sulla formazione di rodlet da parte di due idrofobine espresse per via ricombinante, EAS e DewA. E' stato osservato che la velocità di formazione di *rodlet* è rallentata con la diminuzione di tensione superficiale del solvente, prescindendo dalla natura degli additivi. La tensione superficiale della soluzione, il pH, la temperatura, la concentrazione di idrofobina, le caratteristiche dell'interfaccia, la presenza di zuccheri o di altri additivi, sono tutti parametri da considerare per attivare o inibire il processo di auto-assemblamento delle idrofobine *in vitro*. Studiare le condizioni che portano alla formazione di fibrille di tipo amiloide è essenziale per poterle usare nelle applicazioni industriali (Morris et al 2013).

Questo progetto di ricerca è incentrato sull'idrofobina di Classe I, Vmh2 (codice UniProt Q8WZI2) prodotta dal fungo basidiomicete *Pleurotus ostreatus* [Armenante et al. 2010]. Questa proteina è stata localizzata sia associata alla parete cellulare del micelio sia secreta nel brodo di coltura. La proteina è solubile in soluzioni acquose di etanolo, mentre complessi formati tra la proteina e glucani o glucosio, sono solubili in acqua. Inoltre, quando il pH aumenta sopra il valore di 6, avvengono cambi conformazionali irreversibili con formazione di strutture di tipo β che auto-assemblano nella soluzione in presenza di etanolo mentre quando la polarità del solvente aumenta si osserva una maggiore tendenza a raggiungere interfacce idrofobico/idrofiliche, in assenza di cambi conformazionali [Longobardi et al., 2012].

Vmh2 sembra essere l'idrofobina più idrofobica caratterizzata fino ad ora, la sua sequenza è composta di 111 amminoacidi che includono un singolo amminoacido basico (Lys 19), un singolo amminoacido aromatico (Phe 96) e 8 residui di cisteina che formano il caratteristico motivo di 4 ponti disolfurici conservato in tutte le idrofobine di Classe I. La struttura di Vmh2 mostra alta identità di sequenza con SC3. Tuttavia, SC3 contiene all'N terminale della proteina matura un peptide addizionale ricco in T e glicosilato (T *stretch*), che rende la proteina più solubile in acqua rispetto a Vmh2. Infatti, SC3 può essere solubilizzata in acqua fino a 1mg mL^{-1} (Wang X et al., 2004), anche se le idrofobine di classe II sono riportate essere ancora più solubili, fino a 10 mg mL^{-1} (Kisko et al., 2008).

```
Vmh2  MFSR---VIFCTFLILPLLAAAT--AIPRTDTP----------------- 28
SC3   MFARLPVVFLYAFVAFGALVAALPGGHPGTTTPPVTTTVTVTTPPSTTTI 50
      **:*   *:: :*: :  *.**   . * * **

Vmh2  ----SCSTGSLQCCSSVQKATDPLASLLIGLLGIVLGPLDLLVGVTCSPI 74
SC3   AAGGTCTTGSLSCCNQVQSASSSPVTALLGLLGIVLSDLNVLVGISCSPL 100
          :*:****.**..**.*:.. .: *:*******. *::***::***:

Vmh2  TVIGVGGTSCTQQTVCCTGNSFNGLIAIGCSPINISL 111
SC3   TVIGVGGSGCSAQTVCCENTQFNGLINIGCTPINIL- 136
      *******:.*: ***** ...***** ***:****
```

Fig.1. Allineamento della struttra primaria di Vmh2 con SC3.

Vmh2 è stata utilizzata per funzionalizzare superfici di silicio. Il film di Vmh2 di spessore nanometrico, depositato su silicio cristallino, si è rivelato un'efficiente protezione per l'*etching* con KOH in fase liquida lasciandone inalterate le proprietà ottiche [De Stefano et al., 2007; De Stefano et al., 2008]. Sono stati inoltre verificati, con misure di angolo di contatto di una goccia d'acqua con la superficie (*water contact angle,* WCA), cambi nella bagnabilità di superficie dovuti alla presenza dello strato proteico auto-assemblato sia su silicio cristallino che poroso. Lo strato nanometrico è molto stabile dal punto di vista chimico, essendo presente dopo lavaggi in NaOH o SDS 100°C. Lo strato proteico monomolecolare è utilizzabile per l'immobilizzazione non covalente di altre proteine, quali la BSA e la laccasi. E' stato anche dimostrato che l'immobilizzazione di enzimi sul film d'idrofobine ne migliora la stabilità [De Stefano et al., 2009].

Tuttavia, applicazioni a livello industriale di Vmh2, così come di altre idrofobine di classe I, possono essere difficilmente attuabili a causa del costo di produzione e/o della richiesta di grandi quantità di proteina. L'espressione ricombinante può essere una valida alternativa, dato che può consentire di ottenere alti livelli di proteina pura; inoltre, l'ingegneria proteica fornisce uno strumento per migliorare le caratteristiche e le funzioni delle idrofobine, adattandole alle specifiche applicazioni (Linder et al. 2002; Scholtmeijer et al. 2002; Valo et al., 2010; Boeuf et al., 2012; Reuter et al., 2013). Un sistema di espressione ricombinante per Vmh2 in *E. coli* è stato già messo a punto e la proteina mostra proprietà comparabili alla proteina nativa [Longobardi et al., 2012].

B. Studio delle proprietà di solubilità e caratterizzazione delle forme aggregate di Vmh2.

B1. *Scale-up* della produzione di Vmh2

E' stato ottimizzato il protocollo per l'estrazione di Vmh2 dal micelio di *P. ostreatus*, ottenendo circa 230mg di proteina pura per litro di coltura ed aumentando la produttività di estrazione fino a 50 volte. Brevemente, il micelio è trattato con SDS bollente per rimuovere la maggior parte delle proteine solubili, metaboliti e contaminanti dal fungo. In seguito il micelio è lavato varie volte con acqua e una con 60% etanolo per rimuovere completamente il detergente. Il residuo è quindi liofilizzato, trattato con acido trifluoroacetico (TFA) al 100% in bagno a ultrasuoni. Dopo centrifugazione il sovranatante è seccato sotto flusso di azoto, ed estratto usando una miscela di metanolo-cloroformio-acqua in grado di eliminare principalmente i componenti lipidici. Dopo questo trattamento la proteina aggregata è trattata di nuovo in 100% TFA e dopo centrifugazione il sovranatante è seccato sotto flusso di azoto e solubilizzato in 60% etanolo. Nel passaggio finale, la soluzione è stata chiarificata per centrifugazione.
La massa molecolare della proteina (8564 Da) è stata confermata per spettrometria di massa MALDI-TOF, mentre non si è verificata la presenza di altre proteine. Analisi di dicroismo circolare hanno confermato la struttura di Vmh2, e l'alta concentrazione proteica ottenuta.

B2. L'idrofobina di classe I, Vmh2, adotta meccanismi atipici per auto-assemblare in fibrille di tipo amiloide. (Gravagnuolo et al., articolo sottomesso)

L'idrofobina Vmh2 prodotta dal fungo basidiomicete *P. ostreatus*, può essere solubilizzata in tamponi acquosi, ma solo a pH ≥ 7. I risultati ottenuti ci hanno permesso di concludere che: i) in soluzioni acquose Vmh2 forma due tipi di strutture assemblate di dimensioni differenti, la cui quantità e rapporto relativo, dipendono dalla concentrazione proteica, ii) Vmh2 auto-assembla spontaneamente in strutture di tipo amiloide ed il processo è controllato da temperatura, pH e presenza di ioni Ca^{2+}, iii) l'esposizione di soluzioni di Vmh2 a interfacce di carattere idrofilico-idrofobico non induce aggregazione. Abbiamo quindi dimostrato che la conversione di Vmh2 in forme assemblate ricche di strutture di tipo β, avviene in condizioni differenti da quelle delle altre idrofobine di Classe I studiate, che sono note auto-assemblare in film anfifilici alle interfacce idrofiliche-idrofobiche. E' stato anche proposto un modello per il cambio conformazionale e l'auto-assemblamento di Vmh2 in strutture di tipo amiloide.

B3. Caratterizzazione spettroscopica mediante ATR-FTIR di film auto-assemblante di Vmh2 per la biofunzionalizzazione del TEFLON (Portaccio M. et al., articolo sottomesso)

Avvalendosi della spettroscopia ATR-FT-IR, è stato studiato il processo di formazione di film di Vmh2 estratta da *P. ostreatus* su membrana di TEFLON. In particolare, lo strato proteico è stato caratterizzato sia quantificando la banda dell'ammide I caratteristica delle proteine, che il rapporto lipidi/ammide e carboidrati/ammide. In più è stata determinata la struttura secondaria della proteina nel film attraverso la procedura di deconvoluzione della banda dell'amide I, analisi che ha indicato un prevalente contributo di strutture secondarie di tipo β in tutti i campioni analizzati. E' interessante notare che la percentuale di struttura β varia in

dipendenza delle condizioni di formazione dello strato proteico. I risultati ottenuti sono stati anche confermati attraverso immagini SEM.

C. Miglioramento di proprietà di superficie di materiali attraverso rivestimento con Vmh2 auto-assemblata per applicazioni biotecnologiche.

C1 Uso di piastre porta campioni MALDI rivestite dall'idrofobina Vmh2 per il miglioramento dell'analisi di miscele complesse di peptidi e proteine (Longobardi S. et al., *Analytical Biochemistry*, 2014, 449: 9-16, articolo di copertina)

Le proprietà auto-assemblanti dell'idrofobina Vmh2 sono state sfruttate per sviluppare un nuovo metodo di rivestimento di piastre d'acciaio in uso come porta campioni nella spettrometria di massa MALDI. Il rivestimento con Vmh2 permette l'analisi di miscele di proteine standard e digeriti triptici in concentrazioni nano-femto molare, in presenza di sali e denaturanti, in quanto è possibile desalificare facilmente il campione *in situ*. Come campione reale complesso è stato utilizzato siero umano non trattato e sono stati acquisiti spettri MALDI-TOF in un largo intervallo di m/z (rapporto massa carica). E' stata eseguita una comparazione di questo nuovo metodo di rivestimento e desalificazione sia con tecniche di desalificazione standard che con tecniche di desalificazione su piastra più recentemente riportate in letteratura. I risultati dimostrano che il rivestimento tramite Vmh2 di piastre porta campioni per MALDI, permette una desalificazione molto semplice ed efficiente, utilizzabile per sviluppare piattaforme integrate per applicazioni in proteomica.

C2 Uso di piastre porta campioni per spettrometria di massa MALDI rivestite dall'idrofobina Vmh2 per digestioni seriali multi-enzimatiche di proteine *in situ* (Longobardi S. et al. *Analytical and Bioanalytical Chemistry*, 2015, 407: 487-96)

Lo sviluppo di metodi efficienti e rapidi per l'identificazione di proteine con alta copertura di sequenza è uno degli obiettivi principali nella moderna proteomica. La digestione di proteine su supporti solidi bio-funzionalizzati può essere un approccio vantaggioso, che permette di accoppiare la digestione *in situ* di proteine attraverso l'uso di enzimi immobilizzati ad analisi di spettrometria di massa MALDI-TOF o MALDI-TOF/TOF. Il passaggio decisivo nello sviluppo di una tecnica d'immobilizzazione enzimatica è la funzionalizzazione dei materiali di supporto. Piastre d'acciaio funzionalizzate con Vmh2 sono in grado di adsorbire peptidi e proteine, e sono compatibili con analisi MALDI-TOF-MS (sezione C4.A). Abbiamo quindi sviluppato un "laboratorio su piastra" immobilizzando diversi enzimi in maniera non covalente. Gli enzimi scelti sono d'interesse comune per l'identificazione e la caratterizzazione di proteine, come ad esempio la tripsina, la proteasi V8, la PNGaseF, e la fosfatasi alcalina. Sono state eseguite digestioni multi-enzimatiche seriali di proteine modello ottenendo alte coperture di sequenza in bassi tempi di reazione. Infine abbiamo dimostrato la possibilità di sfruttare questo metodo per l'analisi di campioni su piastra anche utilizzando la tecnica di spettrometria di massa tandem, MALDI-TOF/TOF, sia su proteine modello sia su un intero proteoma di latte, quale esempio di sistema complesso.

C3 Produzione e bio-funzionalizzazione *in situ* di nanomateriali a base di grafene privo di difetti strutturali (Gravagnuolo A.M. et al., articolo accettato in *Advanced Functional Materials* DOI: 10.1002/adfm.201500016)

L'interfacciamento del grafene, uno dei nanomateriali più promettenti, con molecole biologiche è un aspetto fondamentale per il miglioramento della biocompatibilità e dispersibilità di questo materiale e per la sua implementazione con funzioni necessarie per applicazioni biomediche. La bio-funzionalizzazione del grafene, senza apportare difetti nella struttura planare ad atomi di carbonio ibridizzati sp^2, è una sfida ancora più difficile. In questo studio abbiamo definito un processo per la sintesi di grafene privo di difetti strutturali attraverso esfoliazione per ultrasonicazione in fase liquida di materiale grafitico grezzo, assistita dall'idrofobina fungina auto-assemblante Vmh2. Le proprietà uniche di Vmh2, soprattutto la sua idrofobicità e stabilità, ci hanno permesso di ottenere nanomateriale esfoliato stabile (potenizale-ζ, +40 ÷ +70) ed altamente concentrato (~440-510 μg mL^{-1}). Inoltre, attraverso centrifugazione controllata, sono stati selezionati foglietti micrometrici di carbonio bio-funzionalizzato dotato di pochi strati molecolari, privi di difetti strutturali, come dimostrato attraverso spettroscopia Raman, AFM, SEM ed analisi di mobilità elettroforetica. Questo prodotto ibrido rappresenta un materiale ad alto valore aggiunto per le emergenti applicazioni del grafene in settori d'interesse biotecnologico come la nanomedicina, il *sensing* e la bioelettronica.

C4 Rapida e semplice immobilizzazione di nanomateriali e proteine su substrato auto-assemblante di Vmh2 (Gravagnuolo A.M. et al, articolo in preparazione)

Il film anfifilico di Vmh2 è stato utilizzato come metodo semplice per il rivestimento di superfici di vetro e come efficiente substrato per l'immobilizzazione di proteine e nanomateriali, quail l'ossido di grafene e i *quantum dots* sintetizzati nei laboratori dell'ICN2. I supporti di vetro così funzionalizzati sono stati caratterizzati usando la tecnologia dei microarray. Inoltre, tramite un saggio biologico è stata dimostrata la funzionalità di anticorpi immobilizzati su film di Vmh2 seguendo la metodologia proposta. Il tempo richiesto per la fabbricazione di questi supporti per microarray è minore rispetto alle funzionalizzazioni chimiche più comuni per l'immobilizzazione delle proteine su vetro.

SUMMARY

Biological interfacing of novel materials is a key step to improve their biocompatibility, biofunctionality and selectivity toward bio-technological applications such as nanomedicine, bioelectronics, and in bioanalytical chemistry.

Self-assembling of proteins, “nanomachines” with a wide variety of functions, has been intensively studied in the past few decades as fundamental and green strategy to build hierarchical structures in both living systems and hybrid functional assemblies for bionanotechnological purposes.

The Class I hydrophobin, called Vmh2, is a peculiar, surface active, and versatile fungal protein that is known to self-assemble into very chemically stable amphiphilic film, able to change wettability of surfaces and to strongly adsorb other proteins in their active form. Moreover the Vmh2 nanometer-scale layer is perfectly compatible with optical applications.

However, the production and handling of this protein, which has been characterized in our laboratories, is very arduous due to its low solubility and natural propensity to self-assemble into amyloid-like stable nano-structures.

As a first goal, productivity of protein extraction and purification has been sensibly increased to obtain adequate amount of protein for laboratory scale applications. Moreover the conditions for Vmh2 solubilization in aqueous media and for Vmh2 self-assembling have been explored characterizing the aggregated forms in solution and the stable film on Teflon support. A molecular model for Vmh2 self-assembly has also been proposed.

The protein film has been exploited to easily coat the sample-loading steel plate used in MALDI-TOF mass spectrometry. The hybrid surface is able to stably and homogenously adsorb peptides and proteins whereas salts or denaturants can be washed out allowing fast and high-throughput on-plate desalting prior to MS analysis. The functions of the Vmh2 coating have been expanded immobilizing enzymes of interest in proteomics. Rapid and efficient multiple enzyme digestions have been performed to achieve high sequence coverage of model proteins and to analyze a whole proteome. Since Vmh2 can be de-polymerized in specific conditions, the functionalized supports can be reused for indefinite cycles.

Moreover Vhm2 has been exploited to disperse quite high amount of highly hydrophobic graphene based materials, produced by ultrasonic wave exfoliation of low cost graphite. Notably, the non-covalent nature of the amphiphilic protein-carbon interactions preserves the band structure of sp^2-carbon lattice. The bio-hybrid material is endowed with the self-assembling properties of Vmh2, controlled by environmental factors, and is a valuable material for biomedical applications.

Finally, Vmh2 layer has been used as a facile method of glass surface coating and efficient substrate for the immobilization of proteins and nanomaterials, such as graphene oxide and home-made quantum dots. The functionalized slides have been tested in microarray technology. Notably, immobilized antibodies have proved functional and used in a bioassay. The time needed for fabrication of these new microarray slides is lower than that of the most efficient methods for chemical functionalization.

In conclusion the unique properties of Vmh2 have provided new biotechnological solutions that could boost the applications of bio-hybrid materials in biomedical and bioanalytical fields.

ABBREVIATIONS

ATR-FT-IR: Attenuated Total Reflection-Fourier Transform-Infrared (spectroscopy)
DLS: Dynamic Light Scattering
FT-IR: Fourier Transform-Infrared (spectroscopy)
GBMs: Graphene Based Materials
GRMs: Graphene Related Materials
GRAS: Generally Recognized As Safe
MALDI-TOF-MS: Matrix-Assisted Laser Desorption/Ionization-Time Of Flight-Mass Spectroscopy
SDS: Sodium Dodecyl Sulfate
SDS-PAGE: Sodium Dodecyl Sulfate-Polyacrylamide Gel Electrophoresis
TFA: Trifluoroacetic acid
ThT: Thioflavine T
WCA: Water Contact Angle

1. INTRODUCTION

The PhD project entitled "HYDROPHOBINS FROM *PLEUROTUS OSTREATUS* IN BIOTECHNOLOGICAL INDUSTRY", has been carried out in the Biotecnologie Industriali Molecolari e Ambientali (BIMA) research group, Department of Chemical Sciences, University of Naples Federico II under the supervision of Prof. Paola Giardina.

The multiple attractive potential applications of hydrophobins and the interest for the industrial use of this class of proteins, both as emulsion stabilizer and for surface modification, are demonstrated by the conspicuous number of research articles and patents which have been published and registered in the last 10-15 years.

This project deals with the exploitation of the properties of the Class I hydrophobin Vmh2 [Peñas et al. 1998, Armenante et al. 2010, Longobardi et al., 2012], extracted from the mycelium of the edible fungus *Pleurotus ostreatus*, for the development of new bio-technological applications. Vmh2 (UniProt accession number Q8WZI2), seems to be the most hydrophobic hydrophobin characterized so far. The sequence is composed by 111 amino acids including a signal peptide (chain 1-24), a single basic residue (Lys 19), a single aromatic one (Phe 96) and 8 cysteine residues forming the characteristic pattern of 4 disulfide bonds conserved in all Class I hydrophobins.

As a general introduction about hydrophobins, including a focus on Vmh2, the review published in 2013 on "Rendiconti dell'Accademia Nazionale delle Scienze" is reported below (**section 1**).

This thesis is then split in two macro sections: **section 2**, production of Vmh2, analysis of its soluble and aggregated forms; **section 3**, use of Vmh2 self-assembled coating to enhance the surface properties of materials for biotechnological purposes.

RENDICONTI
DELLA
ACCADEMIA NAZIONALE
DELLE SCIENZE
DETTA DEI XL

MEMORIE DI SCIENZE
FISICHE E NATURALI

COMITATO SCIENTIFICO

A.BALLIO – E.GATTI – A.GRANITI – E.MANELLI
G.MARINO – A.MOTTANA – E.PICASSO
E.PORCEDDU – G.SETTI

SERIE V, VOL. XXXVII, PARTE II, TOMO I, 2013
131° ANNO DALLA FONDAZIONE (1782)
ROMA

1. INTRODUCTION

Rendiconti Accademia Nazionale delle Scienze detta dei XL
Memorie di Scienze Fisiche e Naturali
ISBN 987-88-548-7171-7
DOI 10.4399/97888548717173
pag. 65–76

Self–assembling fungal proteins and their biotechnological applications

SARA LONGOBARDI, ALFREDO MARIA GRAVAGNUOLO, LUCA DE STEFANO, ILARIA REA, PAOLA GIARDINA

1. Summary

Hydrophobins are small secreted proteins playing diverse roles in the life cycle of filamentous fungi. They are capable of self–assembling at hydrophilic–hydrophobic interfaces, resulting in the formation of amphipathic films. This film can make hydrophobic surfaces of a liquid or a solid material wettable, while a hydrophilic surface can be turned into a hydrophobic one. These properties, among others, make hydrophobins of interest for medical, bio–technological and technical applications.

The class I hydrophobin Vmh2 from the basidiomycete fungus *Pleurotus ostreatus* seems to be the most hydrophobic hydrophobin characterized so far. Structural and functional properties of the protein as a function of environmental conditions have been determined. The self–assembled film has been characterized and tested as masking material in the KOH wet etch of crystalline silicon. Because of the high persistence of the protein film, the hydrophobin–coated silicon surface is fully protected during the standard KOH micromachining process. The Vmh2 film has also been exploited as coating material of a commercial steel sample–plate of a MALDI–TOF mass spectrometer. The presence of self–assembled Vmh2 on MALDI wells allowed us to perform on plate desalting of protein and peptide samples, and to immobilize trypsin to perform on–plate digestion of protein mixtures.

Key words: fungal proteins, self–assembling, hybrid surfaces, amyloid fibrils

2. Introduction

Hydrophobins are proteins produced by filamentous fungi. Their functions are mainly based on their capability to self–assemble into a highly surface active film at a hydrophilic–hydrophobic interface [1,2]. The presence of hydrophobins is not associated with a specific microbial lifestyle — they are produced by saprophytic fungi, pathogenic fungi and fungi that establish a mutually beneficial symbiosis. They play a key role in growth and morphogenesis in the majority of these fungi, as a coating/protective agent, in adhesion, surface modification, or other types of function that require surfactant–like properties [3]. Hydrophobins can be secreted out in the surroundings or retained in the fungal structures, such as fruiting bodies or mycelium. Their biological functions seem to be diverse, but always in some manner related to interactions with interfaces or surfaces. They allow fungi to escape an aqueous environment, confer hydrophobicity to air–exposed fungal surfaces, mediate the attachment of fungi to hydrophobic solid substrates such as the surface of a host, facilitate dispersion of spores and contribute to invasion of abiotic and biotic substrates [4].

Aerial growth is mediated by hydrophobins that are secreted by the hyphae into the moist substrate. Through a process of self–assembly, these structures reduce the water surface tension of the substrate–air interface, which eliminates this physical barrier and thereby allows the hyphae to grow into the air. The aerial hyphae continue to secrete hydrophobins, which assemble at the hyphal surface. The hydrophilic side of the amphipathic film is positioned next to the cell wall, whereas the hydrophobic side is exposed. As a result, aerial hyphae are water repellent. Similarly, water–soluble hydrophobins assemble at the surfaces of spores that have developed from differentiated aerial hyphae. The coating of spores by hydrophobins facilitates their dispersal by wind [5].

The intriguing properties of these proteins make them of significant interest to biotechnologists, as they have potential for numerous applications, ranging from medical and technical coatings to the production of proteinaceous glue and cosmetics [6].

Although hydrophobins show differences in their primary sequence, they share eight conserved cysteine residues that form four disulphide

bridges [7]. The Cys residue pattern has a striking symmetry and can be easily recognized in the primary structure. The second and third Cys and the sixth and seventh Cys residues follow each other immediately in sequence, forming two pairs, the rest of the Cys residues does not have other Cys residues as near neighbours. Based on the spacing of the cysteine residues and their biophysical properties, hydrophobins can be divided in two classes. The members of the group named class I share a functional similarity since the aggregates that they formed are highly insoluble in aqueous solution, whereas the members of class II form aggregates that are much easier to dissolve. So far, class II hydrophobins have been observed only in Ascomycetes, whereas class I hydrophobins are produced both in Ascomycetes and Basidiomycetes.

3. Class I hydrophobins

In this paper we will focus our attention on class I hydrophobins. These proteins self–assemble at hydrophilic–hydrophobic interfaces into an amphipathic membrane that consists of a mosaic of amyloid–like fibrils known as rodlets [8].

Amyloid fibrils have historically been associated with pathology in a class of degenerative diseases including Alzheimer's disease and Creutzfeldt–Jakob disease. Amyloid fibrils share a structural motif — the cross–β structure — which indicates that these fibrils have common properties [9]. This structure consists of β–sheets that are stacked in the direction perpendicular to the fibril axis, with hydrogen bonds parallel or perpendicular to it. The similarity in structure implies a common mechanism of fibril formation and that the fibrils themselves have common properties. Indeed, all amyloids increase the fluorescence of the dye thioflavin T, exhibit green–gold birefringence on binding the dye Congo red, and cause a red–shift in the absorbance spectrum of Congo red.

Recent data have shown that amyloid fibril formation can also provide biologically functional molecules [9,10]. Functional amyloids have been identified on the surfaces of both fungi and some bacteria (i.e. curli). The deployment of amyloid hydrophobins contributes to the presence of several hundred, and sometimes thousand, fungal

spores per cubic metre of air. These spores can attach onto the surface of a plant or an animal, or can enter the body by inhalation, a lesion in the skin or an implant to which spores have adhered. There is experimental evidence that the amyloid layer forms a protective "coat" to allow microorganisms to evade the immune system of the host [11].

Class I hydrophobin, SC3 from *Schizophyllum commune* has been extensively studied from the point of view of structure/function relationships. It spontaneously self–assembles via an α–helical intermediate state into a stable β–sheet end configuration at a water–air interface. In contrast, upon contact with hydrophobic solids (e.g., Teflon) in water, SC3 is arrested in the intermediate α–helical configuration. The transition to the stable β–sheet end form is promoted by high protein concentration, the presence of cell wall polysaccharides, and the combination of heat and detergents [12].

The most detailed structural work on a class I hydrophobin has been obtained for the EAS hydrophobin from *Neurospora crassa* [13]. The monomer consists of a four–stranded β–barrel core, an additional two–stranded β–sheet and two sizeable disordered regions (Fig. 1). EAS is cross–linked by the four disulphide bridges connecting C1–C6, C2–C5, C3–C4 and C7–C8. Notably, the charged residues are localized at one side of the surface of the protein. This strongly suggests that the water–soluble form of EAS is amphipathic. The largest disordered region of EAS (M22–S42) is contained between the third and the fourth cysteine residue. This part is the least conserved portion of class I hydrophobins in terms of both size and makeup. Importantly, the disordered regions of EAS do not seem to be important in the self–assembly process. Mutated EAS, in which half of the largest disordered region was deleted, was still able to self–assemble. More recent mutagenesis studies identified the F72–N76 segment of EAS as the critical amyloidogenic segment [14]. These results demonstrate that the F72–I75 region directly forms the core of the cross–β structure in EAS hydrophobin functional amyloid rodlets. Moreover a peptide encompassing the sequence of this region can form amyloid fibrils on its own. Therefore Macindoe *et al.* [14] postulate that a conformational change in the protein monomer leads to expose a previously buried segment that is prone to cross–β stacking, leaving the bulk of the native fold of the protein largely unchanged.

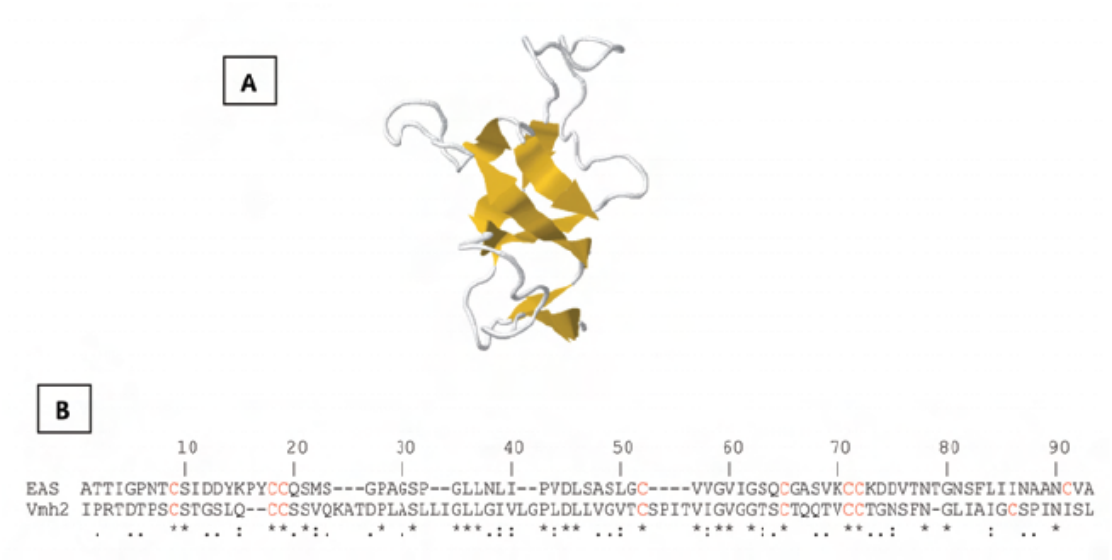

Figure 1. a) 3D structure of the Class I hydrophobin EAS; b) alignment of EAS and Vmh2 class I hydrophobin sequences. In red the eight Cys residues, highlighted in gray the F72–N76 segment.

This conformational change model is analogous to those designed to describe the behavior of proteins that "switch" to an amyloidogenic state due to a localized conformational change under appropriate conditions.

4. The class I hydrophobin Vmh2 from the basidiomycete fungus *Pleurotus ostreatus*

A class I hydrophobin secreted by the basidiomycete fungus *Pleurotus ostreatus* has been purified and identified as Vmh2. According to Peñas *et al.* [15], this protein is specific to vegetative mycelium, is produced throughout the culture time, and is found both as cell wall–associated protein and in the bulk medium. The pure protein is not soluble in pure water, but in ethanol solution, whereas complexes formed between the protein and glucans, produced in culture broth containing amylose, are soluble in water. Vmh2 seems to be the most hydrophobic hydrophobin characterized so far because both SC3 and EAS can be dissolved in water up to 1 mg/mL [16]. It has been verified that glucose is also able to solubilize the hydrophobin in water. Interaction between Vmh2 and glucose has been verified

by the finding that both molecules elute in a unique peak by gel filtration. The aqueous solution of the protein, in the presence of glucans, showed propensity to self–assembly, while the pure protein dissolved in less polar solvent (60% ethanol) is not prone to self–assembly [17].

Structural and functional properties of the protein as a function of the environmental conditions have been determined. By increasing the pH of the solution (pH $\geq$ 6), Vmh2 undergoes a conformational change, forming a self–assembled β–sheet rich state (a significantly increased association at alkaline pH has also been demonstrated for SC3). Analogous behavior was observed in the presence of Ca^{2+}, while a monovalent cation, Na^{+}, has quite an opposite effect, inhibiting the conformational change and self–assembly occurring at pH 6. Another class I hydrophobin has showed propensity to self–assembly in the same conditions [18]. It has been suggested that the formation of large agglomerates can be triggered by bivalent cations bridging and prevented by charge screening with monovalent cations. However, it is worth noting that in the case of Vmh2 we do not observe conversion into the β–sheet rich, assembled form, triggered by migration to hydrophobic/hydrophilic interfaces, as demonstrated for the other known hydrophobins.

In summary, the following events occur starting from the Vmh2 helical structure observed in low polarity solvents:

a) Irreversible conformational change toward a β–structure followed by self–assembling when the pH increases above 6, or in the presence of Ca^{2+} ions.
b) Increased tendency to reach hydrophobic/hydrophilic interfaces when the solvent polarity increases, with no detectable conformational change.
c) Reversible conformational change toward a disordered structure and reversible aggregation at high temperature.

A schematic representation of the behavior of Vmh2 by changing the environmental conditions is shown in Fig. 2.

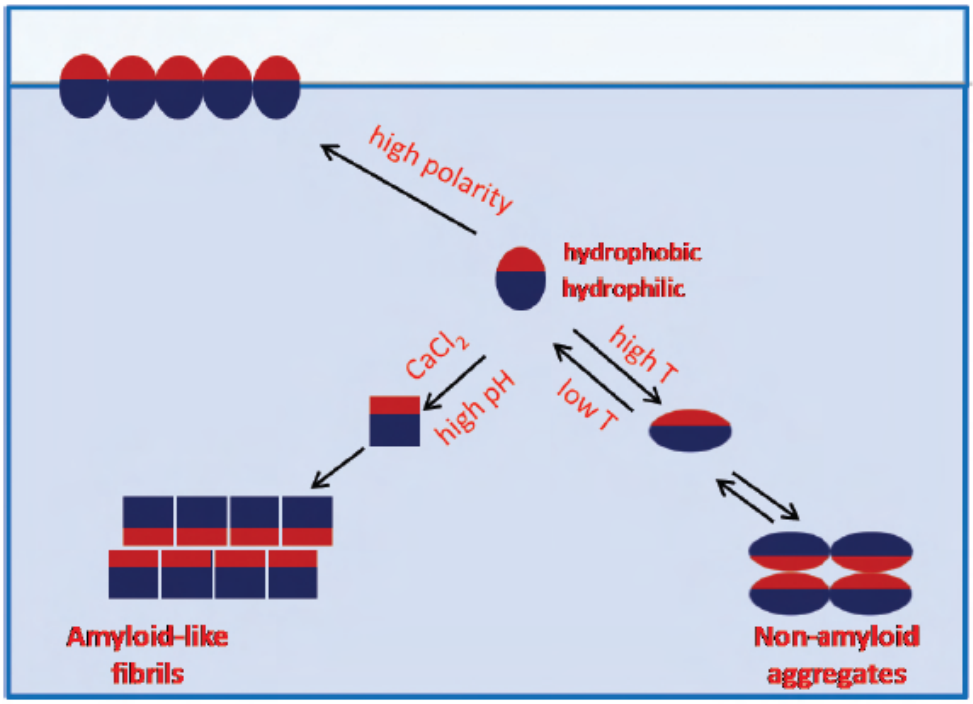

Figure 2. Schematic representation of the Vmh2 behavior in different conditions.

5. Functional surfaces based on Vmh2 biofilms

Silicon is the most used solid support in all micro– and nanotechnologies developed for the integrated circuits industry. For this reason, silicon is also used in many commercial technological platforms for biomedical and biosensing applications. The anisotropic wet micromachining of silicon, based on a water solution of potassium hydroxide (KOH), is a standard fabrication process that is extensively exploited in the realization of very complex microsystems such as cantilevers or membranes.

Vmh2, deposited on crystalline silicon forms a chemically and mechanically stable layer of self–assembled proteins. The Water Contact Angle (WCA) of the silicon surface after the Vmh2 deposition falls down from 90° to 44°; so that the dramatic increase in the surface wettability is well evident [19]. Atomic Force Microscopy (AFM) highlighted the presence of nanometric rodlet–like aggregates on the biofilm surface (Fig. 3).

This biomolecular membrane has been tested as masking material in the KOH wet etch of the crystalline silicon. Because of the high

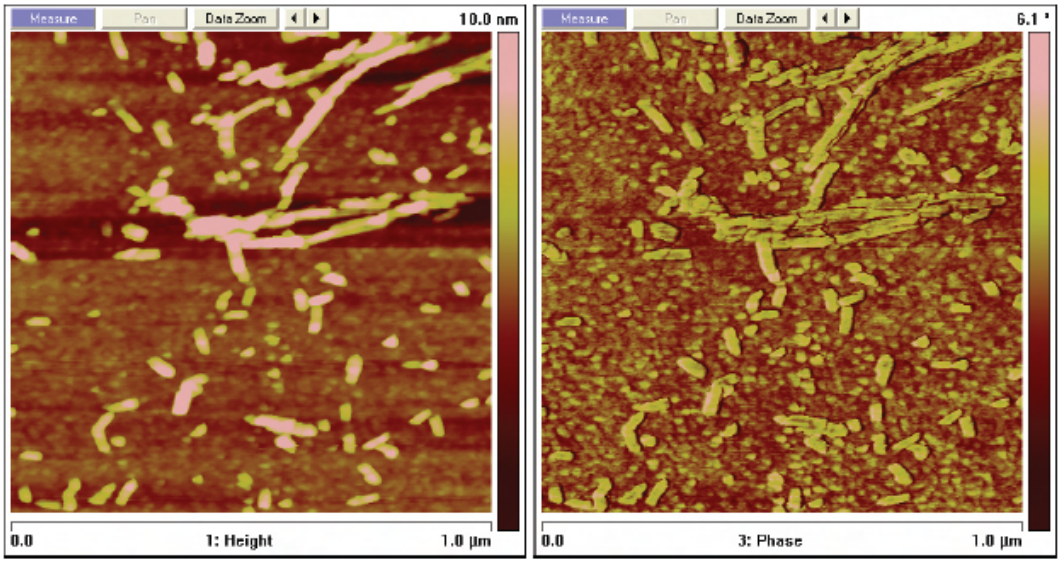

Figure 3. AFM images of Vmh2 film on silicon. On the left topography image and phase image on the right.

persistence of the protein biofilm, the hydrophobin–coated silicon surface is perfectly protected during the standard KOH micromachining process [19].

We have found that Vmh2–glucose complexes forms a chemically stable biofilm on silicon, containing 35% of glucose. The wettability of a silicon surface, covered by the organic layer of Vmh2–glucose, strongly changed: WCA decreased from 90° down to 17°, a decrease of about 27° higher than the pure protein–coated surface [20].

The protein modified silicon surface is suitable for immobilization of other proteins. Two different proteins were successfully immobilized on the HFBs–coated chips: bovine serum albumin and an enzyme, a laccase, which retains its catalytic activity after binding to the chip. Moreover enzyme immobilization on the hydrophobin layer improves the enzyme stability [21].

The Vmh2 self–assembled layer has also been exploited as a coating of a Matrix–Assisted Laser Desorption Ionization (MALDI) steel sample–loading plate, aimed at developing lab–on–plate platforms focused on proteomic applications [22].

The Vmh2 film coating on steel was homogeneous and compact, as shown by Scanning Electron Microscopy (SEM) (Fig. 4), even if it appears less smooth than that formed on crystalline silicon. Its thickness, fitted by Variable–Angle Spectroscopic Ellipsometry (VASE)

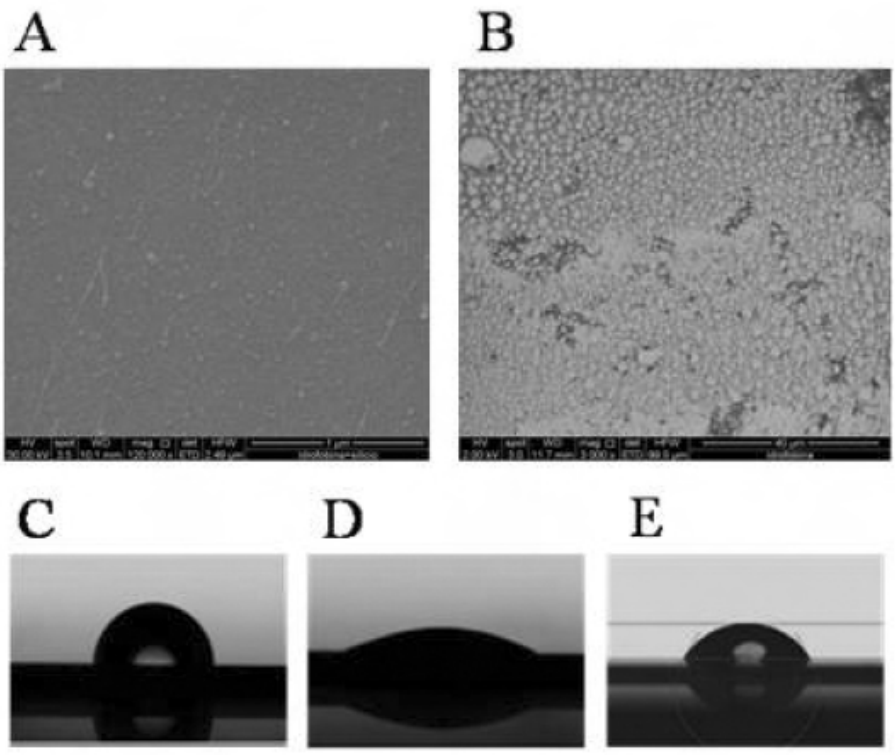

Figure 4. SEM images of Vmh2 coating on silica (A) and on steel (B); WCA of a water drop on steel surface (C), on Vmh2–coated silicon (D) and on Vmh2–coated steel (E).

measurements, was about 10 nm, higher than that found on silicon (about 3 nm). Analysis of the WCA of Vmh2 coated steel compared to the bare surface, showed a change of surface wettability (from 96° to 75°). remarkably less than that in the case of Vmh2 coating on silicon. Therefore the nature of surface affects the characteristics of the Vmh2 film: since hydropathy of bare surfaces (silicon and steel) is almost comparable, the observed differences could be ascribed to other characteristics, such as their different roughness. As a matter of fact, crystalline silicon wafers have a mean roughness of 1–2 nm, whereas steel surface shows roughness values that could be several orders of magnitude greater. However, the self–assembled film showed a strong adhesion to both surfaces.

Vmh2 coating of MALDI plates allows for a very simple and effective desalting method, suitable for development of lab–on–plate platforms focused on proteomic applications [22]. Mixtures of standard proteins, as well as tryptic peptides, in the nanomolar–femtomolar

range, can be analysed in the presence of salts and denaturants. As evidence on a real complex sample, crude human serum has also been analysed and high–quality spectra over a wide mass range have been acquired.

Trypsin has also been immobilized on Vmh2–coated MALDI wells in order to perform on–plate digestion of protein mixtures. The immobilized trypsin is active and able to perform the complete hydrolysis of substrate more quickly than the free enzyme.

The ability of Vmh2 to coat a wide range of different surfaces makes it applicable to several biotechnological fields, from lab–on–plate to biosensing. The Vmh2 self–assembly can serve as intermediate layer for secondary protein immobilization, thus creating hybrid devices applicable in proteomics as well as environmental monitoring, food quality control, etc.

References

[1] LINDER M., 2009. *Hydrophobins: Proteins that self assemble at interfaces*. Curr. Opin. Colloid Interface Sci., 14, 356–363.

[2] LINDER M.B., SZILVAY G.R., NAKARI–SETÄLÄ T., PENTTILÄ M.E., 2005. *Hydrophobins: the protein–amphiphiles of filamentous fungi*. FEMS Microbiol Rev., 29, 877–96.

[3] ZAMPIERI F., WÖSTEN H.A.B., SCHOLTMEIJER K., 2010. *Creating surface properties using a palette of hydrophobins*. Materials, 3, 4607–4625.

[4] WÖSTEN H.A.B., VAN WETTER M.A., LUGONES L.G., VAN DER MEI H.C., BUSSCHER H.J., WESSELS J.G.H., 1999. *How a fungus escapes the water to grow into the air*. Curr. Biol., 9, 85–88.

[5] KERSHAW M.J., TALBOT N.J., 1998. *Hydrophobins and repellents: proteins with fundamental roles in fungal morphogenesis*. Fungal Genet. Biol., 23, 18–33.

[6] HEKTOR H.J., SCHOLTMEIJER K., 2005. *Hydrophobins: proteins with potential*. Curr. Opin. Biotechnol., 16, 434–439.

[7] SUNDE M., KWAN A.H., TEMPLETON M.D., BEEVER R.E., MACKAY J.P., 2008. *Structural analysis of hydrophobins*. Micron. 39, 773–84.

[8] MORRIS V.K., SUNDE M., 2013. *Formation of amphipathic amyloid monolayers from fungal hydrophobin proteins*, Methods Mol. Biol., 996, 119–29.

[9] GEBBINK M.F., CLAESSEN D., BOUMA B., DIJKHUIZEN L., WÖSTEN H.A., 2005. *Amyloids—a functional coat for microorganisms*. Nat. Rev .Microbiol., 3,333–41.

[10] CHERNY I., GAZIT E., 2008. *Amyloids: not only pathological agents but also ordered nanomaterials*. Angew. Chem. Int. Ed. Engl., 47, 4062–9.

[11] AIMANIANDA V., LATGÉ J.P., 2010. *Fungal hydrophobins form a sheath preventing immune recognition of airborne conidia*. Virulence., 1, 185–7.

[12] SCHOLTMEIJER K., DE VOCHT M.L., RINK R., ROBILLARD G.T., WÖSTEN H.A.B., 2009. *Assembly of the fungal SC3 hydrophobin into functional amyloid fibrils depends on its concentration and is promoted by cell wall polysaccharides*. J. Biol. Chem., 284, 26309–26314.

[13] KWAN A.H., WINEFIELD R.D., SUNDE M., MATTHEWS J.M., HAVERKAMP R.G, TEMPLETON M.D., MACKAY JP., 2006. *Structural basis for rodlet assembly in fungal hydrophobins*. Proc. Natl. Acad. Sci. U S A., 103, 3621–6.

[14] MACINDOE I., KWAN A.H., REN Q., MORRIS V.K., YANG W., MACKAY J.P., SUNDE M., 2012. *Self–assembly of functional, amphipathic amyloid monolayers by the fungal hydrophobin EAS*. Proc. Natl. Acad. Sci. U S A. 109, E804–11.

[15] PEÑAS M.M., ASGEIRSDÓTTIR S.A., LASA I., CULIAÑEZ–MACIÀ F.A., PISABARRO A.G., WESSELS J.G., RAMÍREZ L., 1998. *Identification, characterization, and In situ detection of a fruit–body–specific hydrophobin of Pleurotus ostreatus*. Appl. Environ. Microbiol.,64, 4028–34.

[16] LONGOBARDI S., PICONE D., ERCOLE C., SPADACCINI R., DE STEFANO L., REA I., GIARDINA P., 2012. *Environmental conditions modulate the switch among different states of the hydrophobin Vmh2 from Pleurotus ostreatus*. Biomacromolecules, 13, 743–50.

[17] ARMENANTE A., LONGOBARDI S., REA I., DE STEFANO L., GIOCONDO M., SILIPO A., MOLINARO A., GIARDINA P., 2010. The *Pleurotus ostreatus hydrophobin Vmh2 and its interaction with glucans*. Glycobiology, 20, 594–602.

[18] WOHLLEBEN W., SUBKOWSKI T., BOLLSCHWEILER C., VON VACANO B., LIU Y., SCHREPP W., BAUS U., 2010, *Recombinantly produced hydrophobins from fungal analogues as highly surface–active performance proteins*. Eur. Biophys. J. 39, 457–468.

[19] DE STEFANO L., REA I., ARMENANTE A., GIARDINA P., GIOCONDO M. RENDINA I., 2007. *Self–assembled Biofilm of Hydrophobins Protect the Silicon Surface in the KOH Wet Etch Process*. Langmuir 23, 7920–2.

[20] REA I., GIARDINA P., LONGOBARDI S., PORRO F., CASUSCELLI V., RENDINA I., DE STEFANO L., 2012. *Hydrophobin Vmh2–glucose complexes self–assemble in nanometric biofilms*. J. R. Soc. Interface. 9, 2450–6.

[21] DE STEFANO L., REA I., DE TOMMASI E., RENDINA I., ROTIROTI L., GIOCONDO M., LONGOBARDI S., ARMENANTE A., GIARDINA P., 2009. *Bioactive Modification of Silicon Surface using Self–assembled Hydrophobins from Pleurotus ostreatus*. Eur. Phys. J. E–(Soft Matter & Biological Physics), 30, 181–185.

[22] LONGOBARDI S., GRAVAGNUOLO A.M., REA I., DE STEFANO L., MARINO G., GIARDINA P., 2013. *Hydrophobin–coated plates as matrix–assisted laser desorption/ionization sample support for peptide/protein analysis*. Anal. Biochem., 449, 9–16.

Sara Longobardi, Alfredo Maria Gravagnuolo, Paola Giardina
Dipartimento di Scienze Chimiche, Università "Federico II", Napoli
giardina@unina.it
Luca De Stefano, Ilaria Rea
Istituto per la Microelettronica e Microsistemi, CNR, Napoli

2. ANALYSIS OF VMH2 SOLUBILITY AND STRUCTURAL STUDIES OF AGGREGATED FORMS

Structural and functional properties of the hydrophobin Vmh2 as a function of environmental conditions have been studied (Longobardi et al. 2012). At least three distinct phenomena can occur in 60% ethanol solution, being modulated by the environmental conditions: (1) when the pH increases or in the presence of Ca^{2+} ions, an assembled state, β-sheet rich, is formed; (2) when the solvent polarity increases, the protein shows an increased tendency to reach hydrophobic/hydrophilic interfaces, with no detectable conformational change; and (3) a reversible conformational change and reversible aggregation occurs at high temperature. Modulation of the Vmh2 conformational/aggregation features by changing the environmental conditions can be very useful in view of the potential protein applications. Langmuir−Blodgett films of Vmh2 deposited on silicon substrates have been investigated by atomic force microscopy (AFM). Compact and uniform monomolecular layers coexisting with protein aggregates, under the typical rodlet form, have been observed (Houmadi et al. 2008). Moreover, experimental results have shown that the presence of carbohydrates, i.e. cyclodextrins, maltohexaose, and glucose, strongly increases the Vhm2 solubility in water (Armenante et al. 2010). Vmh2-glucose chemically stable films, obtained by drop deposition on silicon, have been characterized in our research group by different techniques.

Further knowledge of the structural properties of Vmh2, by means of methods to trigger self-assembly into the fibrillar rodlet state and techniques to characterize the physicochemical properties of the polymeric forms can be helpful to optimize its production as well as for its use in industrial applications.

In **section 2.1.** an optimized protocol for extraction and purification of Vmh2 from the mycelium of *P. ostreatus* is described.

In **section 2.2.** a study on Vmh2 soluble and aggregated forms is reported. We took advantage of Thioflavin T fluorescence assay to specifically detect amyloid-like structures, and of Circular Dichroism to analyze conformational changes related to their formation. In addition, dynamic light Scattering (DLS) analysis was performed in collaboration with Prof. Luigi Paduano, Dipartimento di Scienze Chimiche, “Università di Napoli”, Naples, Italy. DLS analysis allowed the measurement of hydrodynamic radii of nano- or micro-sized aggregates suspended in liquid solutions.

Moreover, Vmh2 layer prepared on the hydrophobic Teflon membrane in different conditions were structurally characterized by the FT-IR analysis (**Section 2.3.**). Spectra analysis in the range 1700-1500 cm^{-1} made possible to obtain information on the secondary structure of the protein. These analyses were carried out in collaboration with the group of Prof. Marianna Portaccio and Prof. Maria Lepore, Dipartimento di Medicina Sperimentale, Seconda Università di Napoli, Naples, Italy.

2.1. OPTIMIZATION AND SCALE UP OF THE VMH2 PRODUCTION

A protocol was set up to extract high amount of pure Vmh2 from *Pleurotus ostreatus* mycelia in an easy way. Each step was optimized and the yield and productivity maximized. Amount of solvents, lipid depletion and sample dissolving strategies were tested and working time needed for the entire process was reduced. The protein samples were analyzed by circular dichroism, MALDI-TOF mass spectrometry, Pierce 660 protein assay, dry weight measurement, FT-IR and SDS-PAGE to guarantee the quality standard required for our applications.
Extraction from *P. ostreatus* mycelium grown in shaken cultures was performed. Mycelia were treated twice with 2% SDS in a boiling water bath for 15 min to remove most of the soluble proteins, metabolites and contaminants. The mycelium was washed several times with water and once with 60% ethanol to completely remove the detergent. The residue was freeze-dried, and about 1.2 g of dry extract were obtained at this step for Liter of culture medium.
The dry extract was treated with 100% trifluoroacetic acid (TFA) in a water bath sonicator to disassemble the Vmh2 aggregates from the mycelium walls and the solution was then clarified by centrifugation (crude extract). The supernatant was dried in a stream of nitrogen and lipids were extracted in a mixture of water-methanol-chloroform 2:2:1 v/v (5 min in bath sonicator). The aggregated protein pellet was dissolved again in 100% TFA and, after centrifugation, the supernatant was dried in a stream of nitrogen, dissolved in 80% ethanol, and clarified by centrifugation. The supernatant was dried, treated with TFA as above-described and dissolved in the appropriate solution.
The molecular mass, 8564 Da, was confirmed by MALDI-TOF mass spectrometry while no other protein was detected. By circular dichroism analysis the known structure [Longobardi et al. 2012] and high concentration of Vmh2 were confirmed.
In conclusion, exploiting the optimized protocol, the yield of protein increased up to ≈230 mg of Vmh2 per Liter of culture broth, doubling the amount obtained using the old protocol. Moreover the productivity of the process was increased ≈50-fold obtaining up to 20÷50 mg of protein per working day.

CLASS I HYDROPHOBIN VMH2 ADOPTS ATYPICAL MECHANISMS TO SELF-ASSEMBLE INTO FUNCTIONAL AMYLOID FIBRILS

Alfredo Maria Gravagnuolo[1]‡, *Sara Longobardi*[1]‡, *Alessandra Luchini*[1], *Luca De Stefano*[2], *Eugenio Notomista*[3], *Luigi Paduano*[1], *Paola Giardina*[1]*

[1]Department of Chemical Sciences, University of Naples 'Federico II', Via Cintia 4, 80126 Naples, Italy

[2]Unit of Naples, Institute for Microelectronics and Microsystems, National Council of Research, Via Pietro Castellino 111, 80131 Naples, Italy

[3]Department of Biology, University of Naples 'Federico II', Via Cintia 4, 80126 Naples, Italy

KEYWORDS

Fungi, rodlets, interfaces, Dynamic Light Scattering, *Pleurotus ostreatus,* protein self-assembly

2. Analysis of Vmh2 Solubility and Structural Studies of Aggregated Forms

ABSTRACT

Hydrophobins are fungal proteins whose functions are mainly based on their capability to self-assemble into amphiphilic films at hydrophilic-hydrophobic interfaces. It is widely accepted that Class I hydrophobins assemble into amyloid-like structures, named rodlets, when exposed to these interfaces. The hydrophobin Vmh2 produced by the basidiomycete fungus *Pleurotus ostreatus* can be solubilized in low polar solvents and in aqueous buffers at pH ≥ 7. Results allow us to conclude that: i) Vmh2 forms two types of assemblies in aqueous solutions whose amount and ratio, not the size, are dependent on the protein concentration, ii) Vmh2 spontaneously self-assembles into amyloid-like structures and the process is controlled by temperature, pH, and Ca^{2+} ions, iii) exposition of Vmh2 solutions to hydrophilic-hydrophobic interfaces does not induce aggregation. Hence, Vmh2 conversion into the β-sheet rich, assembled form occurs in conditions different from those of the other studied Class I hydrophobins. A model of self-assembly into amyloid-like structures has also been proposed.

Table of Contents Graphic

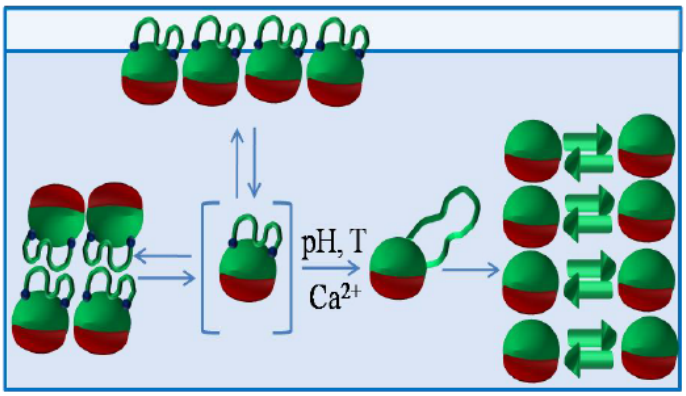

2.2. Class I Hydrophobin Adopts Atypical Mechanisms to Self-assemble into Functional Amyloid Fibrils

INTRODUCTION

Protein self-assembly is a complex phenomenon intensively studied in the past few decades, due to its wide implications in living systems.[1] However this spontaneous process is also becoming more and more attractive from the point of view of potential applications of protein layers in nano-biotechnological field, in particular in the design and production of novel advanced materials.[2,3] Understanding the self-assembling mechanism is crucial to control the process and to exploit the potential of these systems, moreover it might shed light on amyloid diseases and their treatments.

Hydrophobins are fungal proteins whose functions are mainly based on their capability to self-assemble into amphiphilic films at a hydrophobic-hydrophilic interface (HHI).[4,5] They play a key role in growth and morphogenesis in the majority of filamentous fungi.[6] Hydrophobins and their encoding genes have been identified in both the ascomycete and the basidiomycete phyla that represent most species in the fungal kingdom, and more recently in bacteria.[7] The presence of hydrophobins is not associated with a specific microbial lifestyle, since they are produced by saprophytic, pathogenic, and symbiotic fungi. Due to their ability to coat both hydrophobic and hydrophilic solid surfaces and reverse their hydropathy, their main biological functions are to allow fungi to escape an aqueous environment and to facilitate dispersal of the spores by their hydrophobization.[6]

Although hydrophobins show extensive differences in their primary sequence, all of the known 3D structures exhibit a similar β-barrel structure interrupted by some disordered regions and share eight conserved cysteine residues that form four disulphide bridges.[8] Based on the spacing of the cysteine residues and the properties of the layer they form, hydrophobins have been divided in two classes. Class I hydrophobins assemble into a protein layer that can only be

dissociated using pure trifluoroacetic acid or formic acid. In contrast, assemblages of class II hydrophobins can be dissociated in 60% ethanol, or 2% SDS.[5]

Fibrillar structures formed by Class I hydrophobins, called rodlets, share many structural analogies with amyloid fibrils: they bind amyloid specific dyes, Congo red and ThT[9] and exhibit the typical X-ray fibre diffraction pattern.[10] Amyloid fibrils show a common structural motif, the cross-β structure, and have historically been associated with pathologies, such as Alzheimer's and Parkinson diseases. However amyloid-like fibrils formed by class I hydrophobins provide biologically functional molecules, defined functional amyloids. To these group belong other proteins some from bacteria, insect and fish, from spider, from humans.[11]

The mechanism of rodlet formation and the role of HHI in the assembly process have not yet been well understood. The extensively studied class I hydrophobin, SC3 from *Schizophyllum commune* spontaneously self-assembles via an α-helical intermediate state into a stable β-sheet end configuration at a water-air interface.[12,13] It has been also demonstrated that SC3 adopts the amyloid state at the water-Teflon interface by heating the sample in the presence of detergent or at high protein concentration and prolonged incubation. Moreover the presence of some polysaccharides, such as schizophyllan, promotes SC3 amyloid formation.[14]

Morris et coworkers studied the behavior of the class I hydrophobins EAS and DewA.[15] The authors suggest a key role of HHI in rodlet formation related not only to a local protein concentration increase, but also to specific conformational changes that expose amyloidogenic regions and result in cross-β rodlet structure formation. The rodlet assembly rate of these hydrophobins, induced by solution agitation, is reduced when the percentage of apolar solvents increases.

2.2. Class I Hydrophobin Adopts Atypical Mechanisms to Self-assemble into Functional Amyloid Fibrils

In our research group, one of the hydrophobins produced by the basidiomycete fungus *Pleurotus ostreatus*, named Vmh2, has been studied.[16,17] Vmh2 belongs to Class I hydrophobin and forms rodlets, as shown by atomic force microscopy.[18,19] Fluorescence analyses in the presence of ThT, confirm the cross-β structure of these aggregates that can be only disassembled in strong acids.

In a previous paper we have reported that Vmh2 is quite insoluble in water, while its solubility increases in lesser polar solvents (i.e., ethanol, at least 40% v/v).[17] The presence of alcohol in an aqueous environment can be required to mask the large exposed hydrophobic areas of hydrophobin molecules, thus, reducing protein-protein interactions. In these solvents the protein adopts mainly a stable α-helix conformation. A decreased Vmh2 solubility was observed by increasing the solvent polarity, even if no conformational transition was induced. On the other hand, a Vmh2 conformational change occurs by increasing the pH of the alcoholic solution (pH $\geq$ 6), and a self-assembled β-sheet rich state is formed. Vmh2 self-assembling is also induced in the presence of Ca^{2+}. Analogously the recombinant class I hydrophobin H* protein A shows propensity to self-assemble in the same condition.[20]

In this study, we evaluate the self-assembly characteristics of the Class I hydrophobin Vmh2 under an array of experimental conditions in an attempt to define the key factors controlling the process. Since we now assess that Vmh2 can be solubilized in water at pH $\geq$ 7, its behavior can be compared to that of the other Class I hydrophobins in the same conditions. Findings indicate that Vmh2 conversion into the β-sheet rich, assembled form occurs in conditions different from those of the other studied Class I hydrophobins. A model is suggested which can explain the mechanism of protein self-assembling

MATERIALS and METHODS

Vmh2 extraction from *P. ostreatus* mycelia.

White-rot fungus, *P. ostreatus* (Jacq.: Fr.) Kummer (type: Florida; ATCC No. MYA-2306) was maintained at 4 °C through periodic transfer on potato dextrose agar (Difco) plates in the presence of 0.5% yeast extract. Mycelia were inoculated in 1 L flasks containing 500 mL of potato-dextrose broth (24 g/L) supplemented with 0.5% yeast extract, grown at 28 °C in shaken mode (150 rpm). After 10 days of fungal growth, mycelia were separated by filtration through gauze, treated twice with 2% SDS in a boiling water bath for 10 min, washed several times with water and once with 60% ethanol to completely remove the detergent. The residue was dried under nitrogen, grinded and treated with 100% TFA in a water bath sonicator (Elmasonic S30, Elma) for 30 min, and centrifuged (10 min at 3200 *g*). The supernatant was dried, dissolved in 60% ethanol and centrifuged (20 min at 3200 *g*) obtaining a raw extract solution. The ethanol was removed from the raw extract under vacuum at 40 °C using rotavapor and the material was freeze-dried, then lipids were extracted in a mixture of water-methanol-chloroform 2:2:1 v/v (5 min in bath sonicator). After centrifugation, proteins appeared as a solid aggregate at the interface between the water-methanol and the chloroform phases. They were recovered by removal of liquid phases. The aggregated protein was dried, treated with TFA for 30 min in bath sonicator, re-dried and dissolved in 80% ethanol. The sample was centrifuged (90 min at 12000 g) and the supernatant dried, treated with TFA as above-described and re-dissolved in the appropriate solution. All the analyses were performed using samples just after TFA treatment and solubilization, unless specifically indicated.

Protein Concentration Determination.

Protein concentration was evaluated using the PIERCE 660 nm or BCA Protein Assay kit using ovalbumin as standard.

Spectroscopy Techniques.

Far-UV CD spectra were recorded on a Jasco J715 spectropolarimeter equipped with a Peltier thermostatic cell holder in a quartz cell (0.1 cm light path) from 190 to 250 nm. The temperature was kept at 20 °C and the sample compartment was continuously flushed with nitrogen gas. The final spectra were obtained by averaging three scans, using a bandwidth of 1 nm, a step width of 0.5 nm, and a 4 s averaging per point.

Fluorescence spectra were recorded at 25 °C with a HORIBA Scientific Fluoromax-4 spectrofluorometers. Slits were set to 3 and 6 nm spectral bandpass in excitation and emission monochromators, respectively. ThT (Sigma, 30 μM final concentration) was added to the samples. Samples were excited at 435 nm and emission was monitored from 460 to 600 nm.

Dynamic Light Scattering (DLS)

DLS measurements were performed with a home-made instrument composed by a Photocor compact goniometer, a SMD 6000 Laser Quantum 50 mW light source operating at 5325 Å, a photomultiplier (PMT-120-OP/B) and a correlator (Flex02-01D) from *Correlator.com*.[21] The measurements were performed at (25.00 ± 0.05) °C with temperature controlled through the use of a thermostat bath. All experiments were performed at the scattering angle of 90° (θ), the value of the scattering vector $q = 4 \pi n/\lambda \sin(\theta/2)$ where calculated assuming the refractive index of the solution n = 1.33. The scattered intensity correlation function was analyzed using a

regularization algorithm (Precision Deconvolve 32).[22] The measured diffusion coefficients was taken as the z-average diffusion coefficient of the obtained distributions.[23]

For spheres diffusing in a continuum medium at infinite dilution, the diffusion coefficient, $\langle D \rangle \equiv \langle D \rangle_\infty$ and it is dependent on the sphere radius R_H, called hydrodynamic radius, through the Stokes–Einstein equation:

$$R_H = \frac{k\,T}{6\,\pi\,\eta\,\langle D \rangle_\infty}$$

where k is the Boltzmann constant, T is the absolute temperature and η is the medium viscosity. For not spherical particles, R_H represents the radius of equivalent spherical aggregates. In this hypothesis, Stokes–Einstein equation can be reasonably used to estimate the averaged R_H of the aggregates.[24]

In the present case the R_H was estimated from at least three measurements of the diffusion coefficients of the aggregates for each analyzed samples.

Homology modelling of Vmh2

The homology model of Vmh2 was prepared using the "DeepView Project Mode" option of the Swiss-Model homology-modeling server.[25,26] The sequences of the hydrophobins Vmh2, DewA and EAS were aligned using the ClustalW2 server (http://www.ebi.ac.uk/Tools/msa/clustalw2/).[27] The structures of hydrophobins DewA (pdb code: 2LSH) and EAS (pdb code: 2FMC) were superimposed using the DeepView/Swiss-PdbViewer software,[26] hence the sequence of Vmh2 was manually aligned to the structural alignment of the two known structures using the ClustalW2 alignment as reference. Finally, the thus obtained "DeepView project" was uploaded to the Swiss-Model server. Structures and Vmh2 model were analyzed using PyMol ("The PyMOL Molecular Graphics System, Version 1.5.0.4 Schrödinger, LLC" http://www.pymol.org/).

2.2. Class I Hydrophobin Adopts Atypical Mechanisms to Self-assemble into Functional Amyloid Fibrils

RESULTS

Spontaneous and induced Vmh2 self-assembly was studied by means of spectroscopic and scattering techniques in aqueous solution as function of different variables: pH, protein concentration, presence of $CaCl_2$, temperature and HHI increase.

Effect of pH

As above mentioned, in a previous paper we reported that Vmh2 is quite insoluble in pure water, differently from other Class I hydrophobins.[17] To assess Vmh2 solubility in aqueous buffers at different pH, a fixed protein amount (200 μg), upon TFA treatment (see Materials and Methods, and Supporting Information), was dissolved in 1 mL of different buffers at pH values ranging from 4 to 9. Efficient solubilization occurred between pH 7 and 9 (i.e. estimated concentration by protein assay corresponding to the nominal value), while no detectable solubilization occurred at pH 4 and 5. An incomplete solubilization was observed at pH 6 (≈70%). CD spectra of Vmh2 dissolved in aqueous buffers at different pH were also acquired. As shown in Fig. 1A, spectra recorded at pH 7, 8 and 9 were very similar, while spectra corresponding to the baseline were obtained at pH 4 and 5. An atypical spectrum was monitored at pH 6 (Fig. 1A).

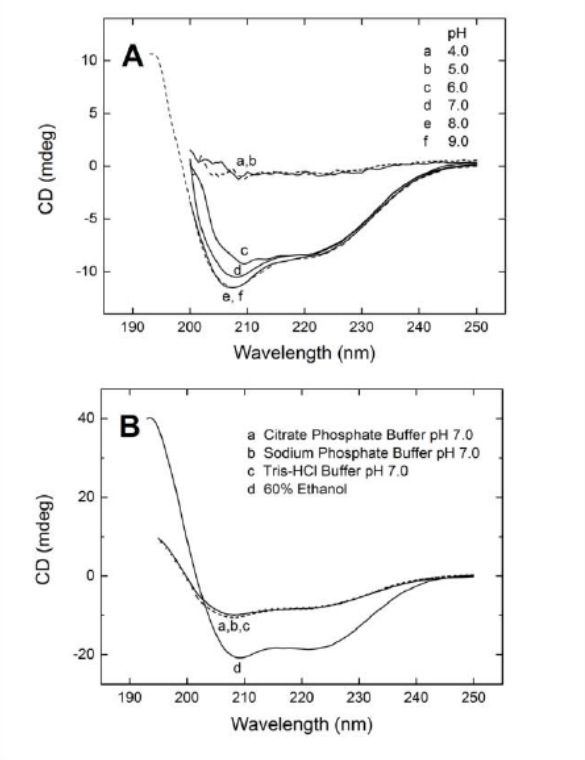

Figure 1. Effect of pH on Vmh2 solubilization. A, CD spectra of Vmh2 (200 µg) dissolved in 1 mL of (a-d) citrate phosphate buffer pH 4÷7 (1:2 diluted), (e-f) 50 mM Tris-HCl pH 8, 9. B, CD spectra of Vmh2 (200 µg) dissolved at pH 7 in 1 mL of (a) citrate phosphate (1:2 diluted), (b) 50 mM sodium phosphate, (c) 50 mM Tris-HCl, in comparison with (d) the same amount of Vmh2 dissolved in 60% ethanol.

When three different buffers were used at the same pH (7), no difference either in protein solubility or conformation was observed, leading to the conclusion that no matter the composition of the buffer, the structure and solubility of Vmh2 in aqueous solution is strictly affected by the pH (Fig. 1B). As expected[28] the protein solubilized in 60% ethanol was more structured then in aqueous buffers as demonstrated by the intense CD spectrum (Fig. 1B, d).

In order to further verify the effect of the pH on Vmh2 in solution, samples of the protein were prepared at pH 7, and then the pH was progressively reduced down to 3.4 by HCl addition. By lowering the pH from 7 to 6.2, no significant conformational change was observed (Figure 2A). On the contrary, CD spectra showed remarkable conformational changes from pH 6.2 to 5.2 and from 5.2 to 3.4.

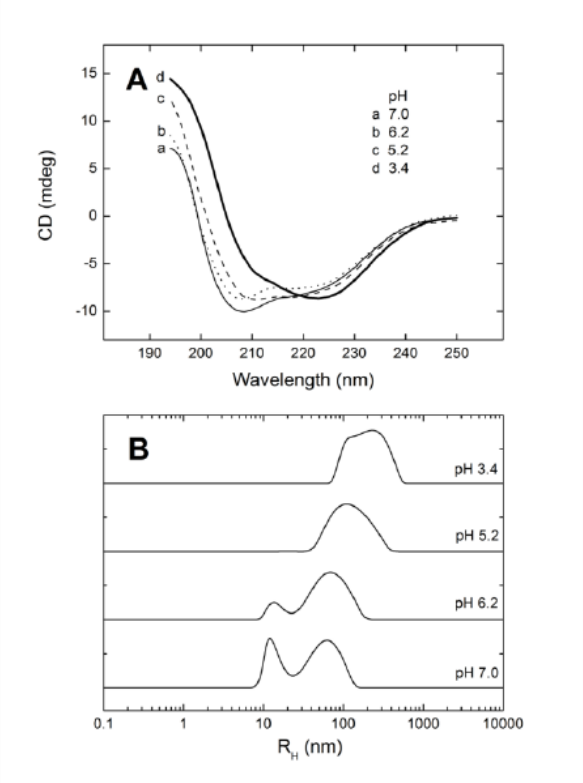

Figure 2. Effect of pH on Vmh2 aggregation. A, CD spectra and, B, R_H distribution of Vmh2 (200µg mL^{-1}) after lowering the pH from 7 to 3.4.

DLS measurements were performed in order to reveal the presence of protein aggregates and to monitor the system evolution as a function of the pH. The hydrodynamic radius (R_H) distribution of Vmh2 was initially obtained at pH 7 and protein concentration corresponding to 200 µg mL^{-1}. Analyses of several samples in the same conditions allowed us to assess that this solution was characterized by the presence of two populations of R_H in the range 10÷20 nm and 50÷80 nm. In Fig. 2B and Table 1 an example of the obtained scattering intensity distribution over R_H and the mean R_H value with the corresponding standard error are respectively reported. When the samples at lower pH were analyzed, an increase of the relative amount of the 50÷80 nm population at pH 6.2 was observed.

Table 1. Mean R_H values observed at different pH values of Vmh2 solution (200 μg mL^{-1}).

pH	R_{H1} *(nm)*	R_{H2} *(nm)*
7.0	12 ± 2	67 ± 5
6.2	15 ± 3	67 ± 4
5.2	----	77 ± 6
3.4	----	125 ± 9

Further decreasing of the pH led to the disappearance of the smaller size population. Moreover the R_H of the larger size population slightly increased at pH 5.2, and further grew up at pH 3.4. As a result, both CD and DLS analyses indicated the occurrence of noticeable changes of the protein state between pH 6 and 5. At lower pH more drastic changes led to massive aggregation and precipitation. ThT assay, which could be useful to verify the formation of amyloid-like-fibrils, is unreliable at the acidic conditions and was not performed.[29]

Effects of protein concentration

CD spectra of Vmh2 solutions were recorded at pH 7 at different concentrations, up to 500 μg mL^{-1} (Fig. SI-1) and no significant conformational transition was detected. In order to rule out the presence of amyloid-like fibrils in these aqueous samples, ThT fluorescence tests were performed. Unexpectedly, ThT fluorescence tests showed the presence of stacked β-sheet structures even at 50 μg mL^{-1} (Fig. SI-2, c), although all the samples were analyzed just after the

TFA treatment and solubilization of the protein. Because this effect could be related to inefficient depolymerization prior to protein dissolution, we firstly optimized the TFA treatment (see Supporting Information). Then the effect of concentration was monitored using the optimized TFA/protein ratio. As shown in Fig. 2A and B, the relationship between ThT fluorescence intensity and protein concentration was clearly not linear, so definitely demonstrating that the formation of amyloid-like structures in aqueous buffer is dependent on protein concentration.

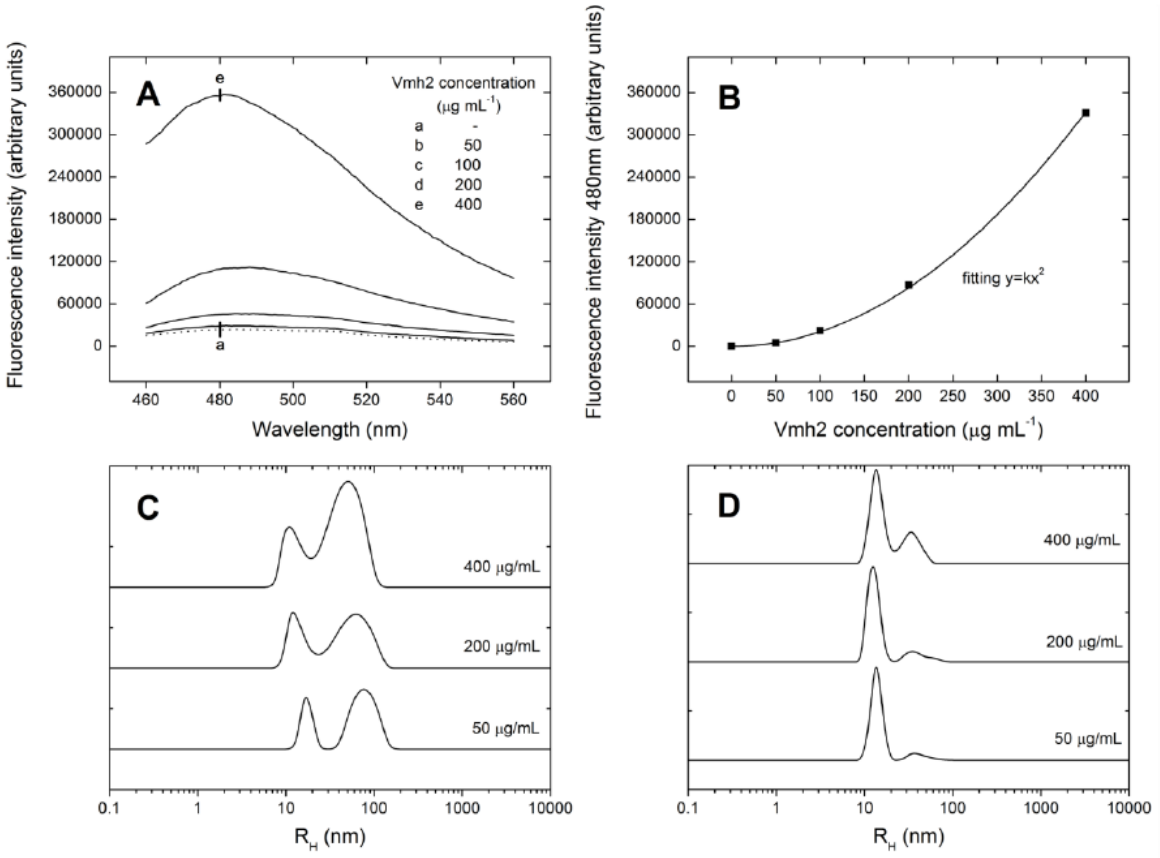

Figure 3. Effect of Vmh2 concentration. A, Fluorescence spectra of 30 μM ThT in the presence of Vmh2 dissolved in 50 mM Na phosphate buffer, pH 7 (b-e). Dotted line (a) is the reference

spectrum of ThT. B, ThT fluorescence intensity at 480 nm of the same samples as in the panel A, upon reference subtraction, as a function of protein concentration. C, distribution of scattering intensity over R_H of Vmh2 (spectra were normalized with respect to the scattering intensity of the small size population). D, aggregate number distribution of Vmh2 estimated from R_H distribution in C (see text for details).

To investigate the aggregation state of Vmh2 in aqueous buffer at pH 7, DLS measurements were performed at protein concentration ranging from 50 to 400 μg mL^{-1}. As it is shown in the Fig. 2C, all the analyzed solutions were characterized by the presence of the two populations of R_H in the range 10÷20 and 50÷80 nm (Table 2) that were slight affected by protein concentration increase.

Table 2. Mean R_H values of the two aggregates populations (R_{H1} and R_{H2}) calculated by three measurements of each sample of Vmh2 in phosphate buffer at pH 7.

Vmh2 concentration (*μg mL^{-1}*)	R_{H1} (nm)	R_{H2} (nm)
50	16 ± 4	68 ± 4
200	13 ± 3	55 ± 5
400	13 ± 5	52 ± 8

In order to have a rough evaluation of the particles concentration, their masses (M) were assumed to follow a scaling law $M = k R_H^3$ (where k is a constant, and the aggregates are approximated to spherical objects) and the scattering intensity distribution were converted in aggregate number distribution. The results reported in Fig. 2D indicated that the systems were dominated by the presence of the population of R_H 10÷20 nm and that the increase of protein concentration determined an increase of the large particles amount. These evidences suggested that the size of the Vmh2 assemblies was independent on the protein concentration while their amount and relative ratio were affected. Taking into consideration that the fluorescence data indicated an increase of the amount of amyloid-like structures depending on concentration, we could infer that the large size population was mainly responsive to the ThT assay. However, the abundance of the small size population over the large one, could explain why CD analyses was not able to show any structural change of the whole system.

Effect of temperature on temporal evolution

The stability of the Vmh2 solution (200 μg mL^{-1} in 50mM Na phosphate buffer, pH 7) and its propensity to self-assemble at different temperatures was also investigated. At 30 °C a reduction of protein concentration (about one third) was observed after 3 days, associated with a conformational change, as evinced by CD analysis (Fig. 4A).

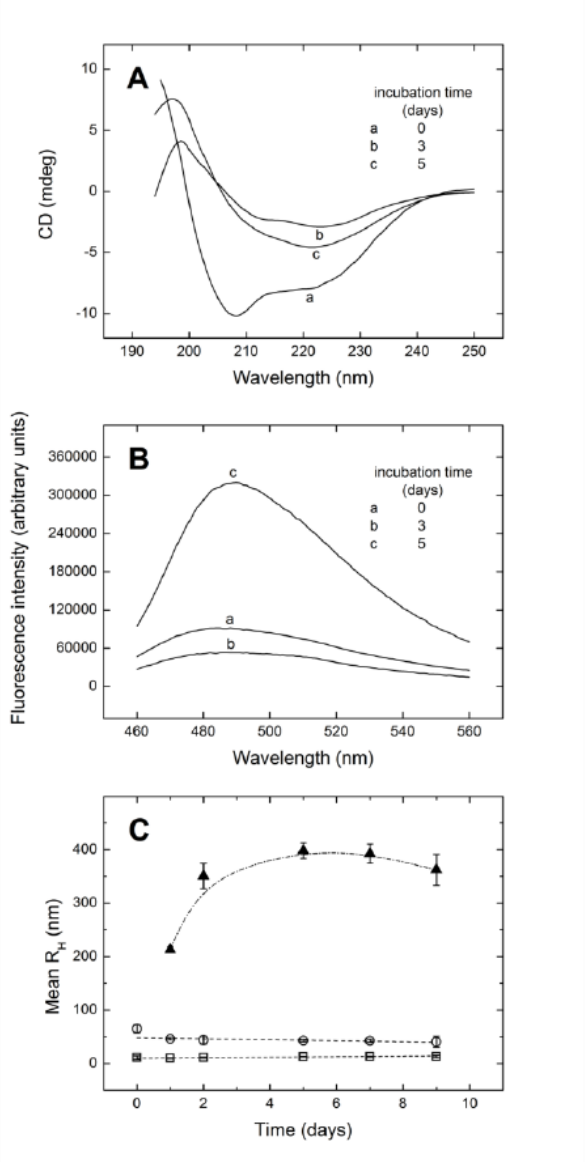

Figure 4. Temporal evolution of Vmh2 (200µg mL^{-1}) in 50mM Na phosphate buffer, pH 7, at 30 °C analyzed by: A, CD spectroscopy; B, ThT fluorescence test; C, DLS (lines depicted as guides for eyes), showing a third distribution of larger particles detectable after one day. Error bars representing the double of the standard deviation calculated on three measurements of the same sample.

A further conformational change and a significant increase of fluorescence intensity of ThT were detected after 5 days (Fig. 4B), moreover complete protein precipitation occurred upon centrifugation (20 min at 3200 g). It is also interesting to analyze the evolution of the process. The presence of a conformational intermediate characterized by a flatter CD spectrum and a lower ThT fluorescence intensity with respect to the initial structure was observed after three days. Indeed the occurrence of less structured intermediates is a common finding in amyloid fibrils formation.[30] Time evolution of the R_H of the different populations in the system was also investigated (Fig. 4C). Inspection of the data revealed that, as time progressed, a third population of aggregates appeared, growing in size. As this latter population reached a size of ≈400 nm, turbidity increased followed by precipitation, observable by naked eyes. However taking into consideration that the scattering intensity of the aggregates is related to the 6th power of R_H, the appearance of the third population by DLS can be detected even when very low amount were formed in the early stages. On the other hand, the increase in ThT fluorescence intensity and the complete CD transition can be detected after accumulation of amyloid-like aggregates.

When Vmh2 was incubated at 60 °C, conformational changes, ThT fluorescence intensity increase, and protein precipitation occurred just after 30 minutes (Fig. SI-3). Conversely, samples stored at 4 °C did not show any variation in 7 days.

Effects of $CaCl_2$ addition

In a previous paper a rapid self-assembly process of Vmh2 dissolved in 60% ethanol as a consequence of $CaCl_2$ addition has been demonstrated.[17] Formation of aggregates some minutes after addition of $CaCl_2$ were observable by naked eyes also when Vmh2 was dissolved in aqueous buffer (pH 7), alongside the occurrence of conformational changes and ThT

fluorescence intensity increase (Fig. SI-4). DLS measurements could not be performed in this case because of the rapid decrease of the scattering intensity due to the precipitation of large particles in the measurement cell.

Effect of HHI

Class I hydrophobins are known to self-assemble forming amyloid-like fibrils by increasing HHI,[5] i.e. by agitation of the solution. Vmh2 samples were analyzed after vortexing, changing several conditions (vortexing time, sample concentration, pH). In any case no significant change was detected by protein assay (after centrifugation), CD and DLS. However, formation of foam stable for at least three days after vortexing, was observed (Fig. SI-5). This foam stabilizing property was lost after Vmh2 aggregation, either at high temperature, or in the presence of calcium ions or at low pH, suggesting that the assembled form of Vmh2 has not tendency to reach HHI.

All reported results allow us to conclude that:

i) Hydrophobin Vmh2 is soluble in aqueous buffers at pH $\geq$ 7; ii) two types of assemblies of different size are present in freshly dissolved Vmh2 at pH 7 and their relative amount, not their size, is dependent on the protein concentration; ii) Vmh2 spontaneously self-assembles into amyloid-like structures and the process is promoted by temperature increase, pH < 6, or in the presence of Ca^{2+} ions - the same final conformation is reached in each case (Fig. 5); iii) only the soluble form of Vmh2 acts as a surfactant (foam stabilizer) and the exposition of Vmh2 solutions to HHI (i.e. by vortexing) does not induce self-assembling.

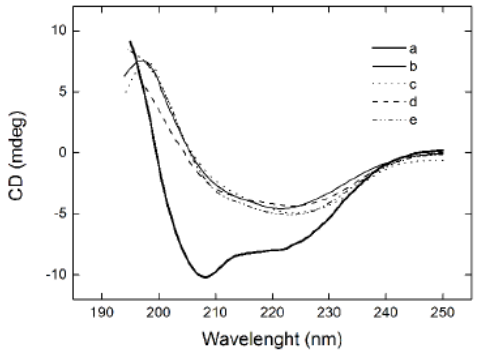

Figure 5. CD spectra of (a) Vmh2 (200µg mL^{-1}) in Na phosphate buffer pH 7, (b) after 5 days at 30 °C, (c) after 30 min at 60 °C, (d) in the presence of 10 mM $CaCl_2$, (e) at pH 3.2 (intensity of spectrum e normalized with respect to spectra b, c and d).

Inference from Vmh2 3D structure model

In order to shed light on the mechanism of self-assembling of Vmh2 the structure of the protein was modeled using the structure of hydrophobin DewA as template (pdb code: 2LSH). The structural alignment (Fig. 6A) of Vmh2 with DewA and EAS, the only two class I hydrophobins of known structure, highlights the significant differences in the sequence and structure of these three proteins.

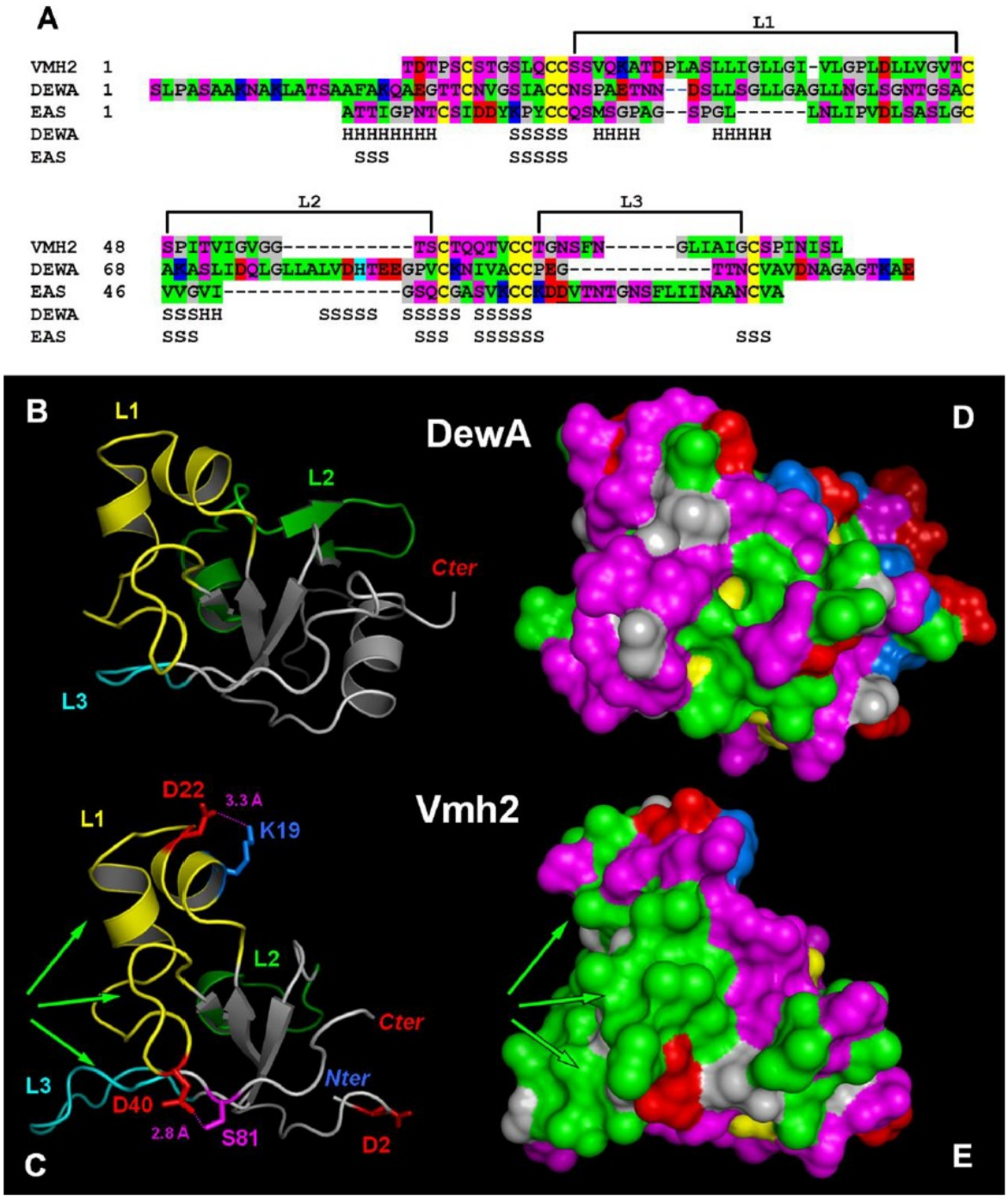

Figure 6. A, Structural alignment of DewA (pdb code: 2LSH), EAS (pdb code: 2FMC) and Vmh2 (UniProt Accession Number Q8WZI2; chain 25-111). The letters H and S at the bottom of

the alignment indicate the position of α-helices and β-strands, respectively, in the two known structures. Residues are colored according to their properties (red, acidic; blue, basic; magenta, hydrophilic; green, hydrophobic, gray, glycine and proline; yellow, cysteine). The region of EAS involved in the formation of rodlets is underlined. The position of loops L1-3 is indicated at the top of the alignment. B-E, Comparison between DewA structure (pdb code: 2LSH; panels B and D) and the homology model of Vmh2 (panels C and E). In B and C the structures are shown as ribbons to highlight position and length of loops L1 (yellow), L2 (green) and L3 (cyan). In panel B the first seven residues are not shown for clarity. In panel C side chains of Asp-2, Asp-22, Asp-40, Ser-81 and Lys-19 are shown as sticks. Hydrogen bonds are shown as magenta dotted lines. Panels D and E show the solvent accessible surface colored according residues properties (colors as panel A). Green arrows in panels C and E indicate the large hydrophobic patch created by the packing of L1 and L3.

Beyond the different length of the loops connecting the conserved cysteines, the three proteins show significant differences in the number and distribution of hydrophobic and charged residues (Fig. 6). For example L1 loop, connecting cysteines 3 and 4 in Vmh2 and DewA is considerably longer than in EAS. The first part of L1 loop of both Vmh2 and DewA is very hydrophilic, whereas the second part is rich in hydrophobic residues in both proteins. It is worth noting that Vmh2 shows an aspartate (Asp40) in this region not present in DewA. L2 loop, connecting cysteines 4 and 5, is much longer in DewA than in EAS and Vmh2. On the contrary L3 loop, connecting cysteines 7 and 8, is much longer in EAS than in DewA, and in Vmh2 it has an intermediate length.

2. Analysis of Vmh2 Solubility and Structural Studies of Aggregated Forms

Vmh2 contains much less charged residues than the other two hydrophobins: only three aspartates and one lysine are present in Vmh2, whereas DewA contains ten aspartates/glutamates, six lysines and a histidine and EAS contains five aspartates and three lysines (Fig. 6A). Except Asp2 that, in our model, is solvent exposed and not involved in stabilizing contacts, the other charged residues are located in crucial positions at both ends of L1 loop: Lys19 and Asp22 form a ionic pair stabilizing the first short helix of L1, whereas Asp40 forms a hydrogen bond with the OH group of Ser81 thus anchoring the turn located at the C-end of L1 to body of the protein (Fig. 6C).

It is worth noting that previous analysis of Vmh2 monolayer, obtained by Langmuir technique and performed using AFM, allowed measurements of local hydropathicity and visco-elasticity, suggesting the localization of a large hydrophobic flexible loop free at the air interface,[19] thus supporting the proposed 3D model.

DISCUSSION

Proteins can use different mechanisms to control their own assembly into fibrils, such as the controlled release of an amyloidogenic region from the folded protein, the inclusion of chaperoning domain, or the adjustment of fibrillation propensity according to pH.[31] It is widely accepted that Class I hydrophobins assemble into amyloid-like structures, the so-called rodlets, when exposed to HHI. A plausible mechanism has been recently described for the *Neurospora crassa* hydrophobin EAS, whose NMR structure is known.[1,10] According to this model, contact with an air/water interface should induce the formation of an amphiphilic secondary structure from a disordered loop. A region of EAS has been identified that drives intermolecular association and formation of the cross-β rodlet structure.

2.2. Class I Hydrophobin Adopts Atypical Mechanisms to Self-assemble into Functional Amyloid Fibrils

The main issue of this work is to explore the self-assembling of Class I hydrophobins showing that it is not regulated by a unique, common mechanism, but different mechanisms can trigger and control functional amyloid formation within this class of proteins. Exposition to HHI does not induce formation of amyloid-like structures in the case of the Class I hydrophobin Vmh2 from *Pleurotus ostreatus* in any of the conditions tested, whereas the phenomenon is controlled by other parameters (i.e. pH, temperature, presence of Ca^{2+}). Among the known Class I hydrophobins, SC3 from *Schizophyllum commune* shows the highest sequence similarity to Vmh2,[16] however SC3 is much more hydrophilic being a glycosylated protein.[32] It is generally reported that SC3, upon assembly at water-air interface, proceeds via an α-helical intermediate state to a stable amyloid-like β-sheet state. On the other hand at water and hydrophobic solid interface, SC3 does not spontaneously form amyloid-like fibrils, but is arrested in the α-helical intermediate state, unless transition to the β-sheet state is induced by particular conditions (heating in the presence of detergent, high protein concentration, presence of cell-wall polysaccharides).[14] Hence, differently from EAS,[33] SC3 requires specific conditions to self assemble at HHI. Moreover, recently Zykwinska *et al.* reported that SC3 nano-rodlets are formed in aqueous solution, tuned by pH and ionic strength.[34] The Class I hydrophobin ABH1 from *Agaricus bisporus* also shows unusual self-assembly properties. As reported by Paslay *et al.*, ABH1 undergoes a direct transition to the β-sheet state at elevated temperature.[35] These examples demonstrated that, although the amphiphilic characteristics of hydrophobins determine their tendency to migrate towards HHI, this migration is not the necessary and sufficient condition to form amyloid-like structures in the case of Class I proteins.

We have previously demonstrated that Vmh2 is soluble in the presence of ethanol (at least 40%) at acid pH. In this condition the protein assumes a α-helical conformation, but does not

show a tendency to reach the air-liquid interface. It has been reported that interface properties are of critical importance for the rodlet formation of both EAS and DewA. The process is strongly affected by the surface tension of the solution,[33] being so slow to be no detectable, i.e. in the case of DewA in 20% ethanol. Therefore to compare the behavior of Vmh2 in the presence of HHI to that of other Class I hydrophobins, analysis of ethanol solutions of Vmh2 were not appropriate. Since we have now assessed that Vmh2 can be solubilized in water at pH $\geq$ 7, we can compare its behavior to that of the other Class I hydrophobins in these conditions. Our results clearly indicate that Vmh2 rodlets formation is not induced by exposition to HHI. Indeed, we previously reported the formation of a Vmh2 monolayer at water-air interface.[18,19] The monolayer formed at HHI was shown by AFM analysis of LB films, whereas rodlets embedded in the monolayer were only observed after repeated compression-expansion cycles.

As a matter of fact, Vmh2 fibrillation phenomenon is controlled by other parameters, being Vmh2 water soluble only at neutral or alkaline pH and forming aggregates when the pH decreases at acidic values. Vmh2 shows a very high hydrophobic index (GRAVY, +0.829)[36] and just one Lys and three Asp are present in the sequence of the mature protein (pI about 4). It is conceivable that at low pH the protein has low net charge and is only soluble in low polar solvent (40÷60% ethanol), whilst it is soluble in aqueous buffers at neutral and basic pH (7-9) where it is negatively charged.

When aqueous solutions of Vmh2 at neutral pH were analyzed by DLS, two populations were detected whose smallest R_H (10÷20nm) is larger than that one expected from a single molecule (≈1.5nm), as in the case of ABH1, therefore comparable to an oligomer. On the other hand, on the basis of the DLS analysis and ThT test, the large size population (R_H 50÷80nm) is rich in amyloid-like structures and its relative amount increases as a function of protein concentration.

These results were obtained using proteins freshly dissolved after TFA depolymerization treatment. However, extensive conformational changes were detected by CD few days after protein dissolution, with a concomitant increase of aggregate size and amount, as revealed by DLS and by ThT assay. As expected, the kinetic of the self-assembly process depends on temperature, the higher the temperature, the faster the aggregate formation. Hence Vmh2 spontaneously self-assemble evolving into large amyloid-like aggregates in aqueous solutions, whereas it is stable many months in low polar solvents (e.g. 60% ethanol) at room temperature.

Moreover, it has been previously reported that the presence of Ca^{2+}, triggers Vmh2 self-assembling in 60% ethanol. Herein we show that the protein rapidly undergoes conformational changes in the presence of Ca^{2+} also in aqueous buffer forming large amyloid-like aggregates.

Even if the 3D structure of Vmh2 is not known, we have speculated on possible mechanisms of formation of amyloid-like structures on the basis of a homology model. Sunde and co-workers demonstrated by a mutational and deletion analysis that L3 loop of EAS is able to trigger aggregation when transferred to a non-amyloidogenic hydrophobin.[1] Moreover, they proposed a molecular model for the formation of amyloid-like fibrils. According to this model, regions D64-T68 and S71-I75 of L3 loop would form the stems of a β-hairpin responsible for the aggregation process. More recently the same research group analyzed the structure of DewA[15] and observed that the L3 loop in this protein is too short and does not contain amyloidogenic sequences so they proposed that the long L2 loop could drive the self-assembly process of DewA. However, at the moment, this hypothesis has not been verified.

Even if the L3 loop of Vmh2 shows a region very similar in sequence (residues 71-78) to the second stem of the β-hairpin responsible for the self-assembly process in EAS (Fig. 6A), this loop seems too short to be the sole or the main responsible for the aggregation, as in the case of

DewA. Moreover the L3 loop does not contain charged residues that could explain the pH and calcium dependence of the process.

It could be speculated that protonation of the two aspartates in Vmh2 would induce a destabilization of the L1 loop thus triggering a conformational change that in turn would determine the aggregation of the protein. Both L1 and L3 loops could participate to the process, in fact, the two loops are closely packed in the model (Fig. 6C) but a conformational change of the L1 loop could expose the L3 loop to the solvent thus making this loop available to intermolecular contacts. Notably, both loops contain very hydrophobic stretches that could contribute to the interaction with hydrophobic surfaces (green arrows in Fig 6C, E). Obviously calcium ions, whose affinity for aspartate is well known, could trigger a similar conformational switch thus explaining the efficacy of calcium in the induction of aggregation.

It is interesting to note that AFM analysis of Vmh2 rodlets, obtained by Langmuir technique after repeated compression expansion cycles at the air-water interface, have led to similar conclusions.[19] Indeed, local hydropathicity and visco-elasticity measures suggested that rodlets are hydrophobic structures in which the flexible loops, occurring in the monolayer, are no longer freely located at the air interface, possibly because of structural modifications, involving intermolecular interactions.

CONCLUSIONS

Vmh2 conversion into the β-sheet rich, assembled form occurs in conditions different from those of the other Class I hydrophobins. Exposition of Vmh2 to water-air HHI does not induce self-assembly, whereas the aggregation process is promoted by temperature increase, at pH < 6, or in the presence of Ca^{2+} ions. The aqueous solution of Vmh2 at pH 7 contains a population of

soluble oligomers and another one of small amyloid-like aggregates, whose ratio is affected by protein concentration. Their spontaneous evolution into larger aggregates is accelerated in the conditions previously mentioned and leads to the same final protein conformation. On the basis of the 3D structure model of the protein, a self-assembling mechanism can be inferred. Protonation of two aspartates, as well as the interaction with Ca^{2+} ions or increase of temperature would induce a destabilization of a long loop thus triggering a conformational change that in turn would determine rapid and extensive aggregation of the protein and the formation of amyloid-like structures.

ASSOCIATED CONTENT

Supporting Information.

Description of optimization of TFA treatment.

Figures:

- CD spectra of Vmh2 samples prepared at different concentrations and ThT test of Vmh2 (treated with different TFA volumes) at different protein concentrations.
- ThT test of Vmh2 upon different TFA treatments
- CD and ThT test of Vmh2 at 60 °C, 30 min.
- CD and ThT test of Vmh2 in the presence of Ca^{2+}.
- Samples of Vmh2 in buffer at pH 7 and in 60% ethanol upon agitation.

This material is available free of charge via the Internet at http://pubs.acs.org.

AUTHOR INFORMATION

Corresponding Author

*Paola Giardina. Department of Chemical Sciences, University of Naples 'Federico II', Via Cintia 4, 80126 Naples, Italy - Email: giardina@unina.it - Tel: +39 081 674319 - Fax +39 081 674 310

Author Contributions

The manuscript was written through contributions of all authors. All authors have given approval to the final version of the manuscript. ‡These authors contributed equally.

Funding Sources

This work was supported by grant from the Ministero dell'Università e della Ricerca Scientifica -Industrial Research Project "Integrated agro-industrial chains with high energy efficiency for the development of eco-compatible processes of energy and biochemicals production from renewable sources and for the land valorization (EnerbioChem)" PON01_01966, funded in the frame of Operative National Programme Research and Competitiveness 2007–2013 D. D. Prot. n. 01/Ric. 18.1.2010. Research activity was also supported by P.O.R. Campania FSE 2007-2013, Project CREMe.

ABBREVIATIONS

HHI, hydrophilic-hydrophobic interface; SDS, Sodium Dodecyl Sulphate; ThT, Thioflavin T; TFA, trifluoroacetic acid; CD, Circular Dichroism; DLS, Dynamic Light Scattering; AFM, atomic force spectroscopy

REFERENCES

(1) Macindoe, I.; Kwan, A. H.; Ren, Q.; Morris, V. K.; Yang, W.; Mackay, J. P.; Sunde, M. Proc. Natl. Acad. Sci. U. S. A. 2012, 109, E804–E811.

(2) Wetzel, R.; Shivaprasad, S.; Williams, A. D. Biochemistry 2007, 46, 1–10.

(3) Zganec, M.; Zerovnik, E. Biochim. Biophys. Acta 2014, 1840, 2944–2952.

(4) Linder, M. B. Curr. Opin. Colloid Interface Sci. 2009, 14, 356–363.

(5) Wösten, H. a; de Vocht, M. L. Biochim. Biophys. Acta 2000, 1469, 79–86.

(6) Bayry, J.; Aimanianda, V.; Guijarro, J. I.; Sunde, M.; Latgé, J.-P. PLoS Pathog. 2012, 8, e1002700.

(7) Hobley, L.; Ostrowski, A.; Rao, F. V; Bromley, K. M.; Porter, M.; Prescott, A. R.; MacPhee, C. E.; van Aalten, D. M. F.; Stanley-Wall, N. R. Proc. Natl. Acad. Sci. U. S. A. 2013, 110, 13600–13605.

(8) Sunde, M.; Kwan, A. H. Y.; Templeton, M. D.; Beever, R. E.; Mackay, J. P. Micron 2008, 39, 773–784.

(9) Butko, P.; Buford, J. P.; Goodwin, J. S.; Stroud, P. A.; McCormick, C. L.; Cannon, G. C. Biochem. Biophys. Res. Commun. 2001, 280, 212–215.

(10) Kwan, a H. Y.; Winefield, R. D.; Sunde, M.; Matthews, J. M.; Haverkamp, R. G.; Templeton, M. D.; Mackay, J. P. Proc. Natl. Acad. Sci. U. S. A. 2006, 103, 3621–3626.

(11) Fowler, D. M.; Koulov, A. V; Balch, W. E.; Kelly, J. W. Trends Biochem. Sci. 2007, 32, 217–224.

(12) De Vocht, M. L.; Reviakine, I.; Ulrich, W.-P.; Bergsma-Schutter, W.; Wösten, H. a B.; Vogel, H.; Brisson, A.; Wessels, J. G. H.; Robillard, G. T. Protein Sci. 2002, 11, 1199–1205.

(13) Wang, X.; Graveland-bikker, J. F.; Kruif, C. G. De; Robillard, G. T.; Kruif, C. G. D. E. 2004, 810–821.

(14) Scholtmeijer, K.; de Vocht, M. L.; Rink, R.; Robillard, G. T.; Wösten, H. a B. J. Biol. Chem. 2009, 284, 26309–26314.

(15) Morris, V. K.; Kwan, A. H.; Sunde, M. J. Mol. Biol. 2013, 425, 244–256.

(16) Armenante, A.; Longobardi, S.; Rea, I.; De Stefano, L.; Giocondo, M.; Silipo, A.; Molinaro, A.; Giardina, P. Glycobiology 2010, 20, 594–602.

(17) Longobardi, S.; Picone, D.; Ercole, C.; Spadaccini, R.; De Stefano, L.; Rea, I.; Giardina, P. Biomacromolecules 2012, 13, 743–750.

(18) Houmadi, S.; Ciuchi, F.; De Santo, M. P.; De Stefano, L.; Rea, I.; Giardina, P.; Armenante, a; Lacaze, E.; Giocondo, M. Langmuir 2008, 24, 12953–12957.

(19) Houmadi, S.; Rodriguez, R. D.; Longobardi, S.; Giardina, P.; Fauré, M. C.; Giocondo, M.; Lacaze, E. Langmuir 2012, 28, 2551–2557.

(20) Wohlleben, W.; Subkowski, T.; Bollschweiler, C.; von Vacano, B.; Liu, Y.; Schrepp, W.; Baus, U. Eur. Biophys. J. 2010, 39, 457–468.

(21) Mangiapia, G.; D'Errico, G.; Simeone, L.; Irace, C.; Radulescu, A.; Di Pascale, A.; Colonna, A.; Montesarchio, D.; Paduano, L. Biomaterials 2012, 33, 3770–3782.

(22) Lomakin, A.; Teplow, D. B.; Benedek, G. B. Methods Mol. Biol. 2005, 299, 153–174.

(23) Zhang, H.; Annunziata, O. J. Phys. Chem. B 2008, 112, 3633–3643.

(24) Paduano, L.; Sartorio, R.; D'Errico, G.; Vitagliano, V. J. Chem. Soc. Faraday Trans. 1998, 94, 2571–2576.

(25) Arnold, K.; Bordoli, L.; Kopp, J.; Schwede, T. Bioinformatics 2006, 22, 195–201.

(26) Guex, N.; Peitsch, M. C.; Schwede, T. Electrophoresis 2009, 30 Suppl 1, S162–S173.

(27) Larkin, M. A.; Blackshields, G.; Brown, N. P.; Chenna, R.; McGettigan, P. A.; McWilliam, H.; Valentin, F.; Wallace, I. M.; Wilm, A.; Lopez, R.; Thompson, J. D.; Gibson, T. J.; Higgins, D. G. Bioinformatics 2007, 23, 2947–2948.

(28) Buck, M. Q. Rev. Biophys. 1998, 31, 297–355.

(29) Khurana, R.; Coleman, C.; Ionescu-Zanetti, C.; Carter, S. A.; Krishna, V.; Grover, R. K.; Roy, R.; Singh, S. J. Struct. Biol. 2005, 151, 229–238.

(30) Kelly, J. W. Curr. Opin. Struct. Biol. 1998, 8, 101–106.

(31) Landreh, M.; Johansson, J.; Rising, A.; Presto, J.; Jörnvall, H. Biochem. J. 2012, 447, 185–192.

(32) De Vocht, M. L.; Scholtmeijer, K.; van der Vegte, E. W.; de Vries, O. M.; Sonveaux, N.; Wösten, H. a; Ruysschaert, J. M.; Hadziloannou, G.; Wessels, J. G.; Robillard, G. T. Biophys. J. 1998, 74, 2059–2068.

(33) Morris, V. K.; Ren, Q.; Macindoe, I.; Kwan, A. H.; Byrne, N.; Sunde, M. J. Biol. Chem. 2011, 286, 15955–15963.

(34) Zykwinska, A.; Guillemette, T.; Bouchara, J.-P.; Cuenot, S. Biochim. Biophys. Acta 2014, 1844, 1231–1237.

(35) Paslay, L. C.; Falgout, L.; Savin, D. a; Heinhorst, S.; Cannon, G. C.; Morgan, S. E. Biomacromolecules 2013, 14, 2283–2293.

(36) Gasteiger, E.; Hoogland, C.; Gattiker, A.; Duvaud, S.; Wilkins, M. R.; Appel, R. D.; Bairoch, A. In The Proteomics Protocols Handbook; Walker, J. M., Ed.; Humana Press: Totowa, NJ, 2005; pp. 571–607.

2.2. Class I Hydrophobin Adopts Atypical Mechanisms to Self-assemble into Functional Amyloid Fibrils (Supporting Information)

SUPPORTING INFORMATION

Optimization of TFA treatment

The efficiency of Vmh2 de-polymerization by TFA treatment was tested. The same amount of Vmh2 dry-aggregates (50 µg) was treated in a bath sonicator with different amounts of TFA (50 and 500 µL). After TFA removal in a stream of nitrogen, 1mL of Na phosphate at pH 7 was added to each sample and ThT fluorescence measurements were carried out. The results indicated that an efficient de-polymerization was obtained using the highest volume of TFA (Fig. SI-2). The same experiment was carried out using a higher amount of Vmh2 (200 µg) and TFA/protein ratios spanning the same range. In this case a remarkable effect of the TFA/protein ratio was observed, however high fluorescence emission was detected even when 2 mL of TFA were used. When higher TFA/protein ratios were used inconclusive results were obtained (i.e. low final protein concentration). Therefore all the experiments were performed using the optimized TFA/protein ratio, 1ml of TFA/100 µg of protein.

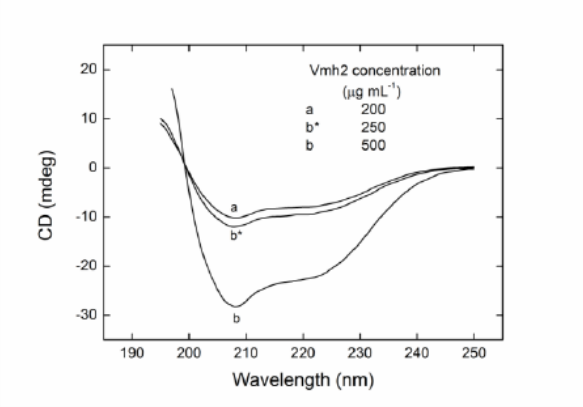

Fig. SI-1. CD spectra of Vmh2 samples prepared at 0.2 mg mL^{-1} (a) and 0.5 mg mL^{-1} (b) in 50 mM Na phosphate buffer, pH 7. The latter has been diluted twofold (b*) for an easy comparison to the sample dissolved at lower concentration.

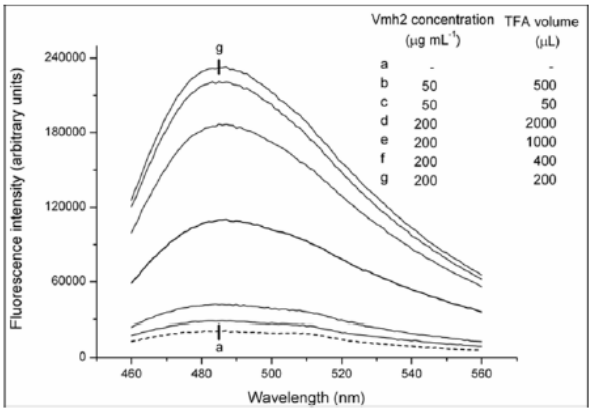

Fig. SI-2. Fluorescence spectra of ThT 30 μM in the presence of Vmh2 dissolved in 50mM Na phosphate buffer, pH 7 at different protein concentration (50 or 200 μg of Vmh2 in 1mL buffer) previously treated with different TFA volumes.

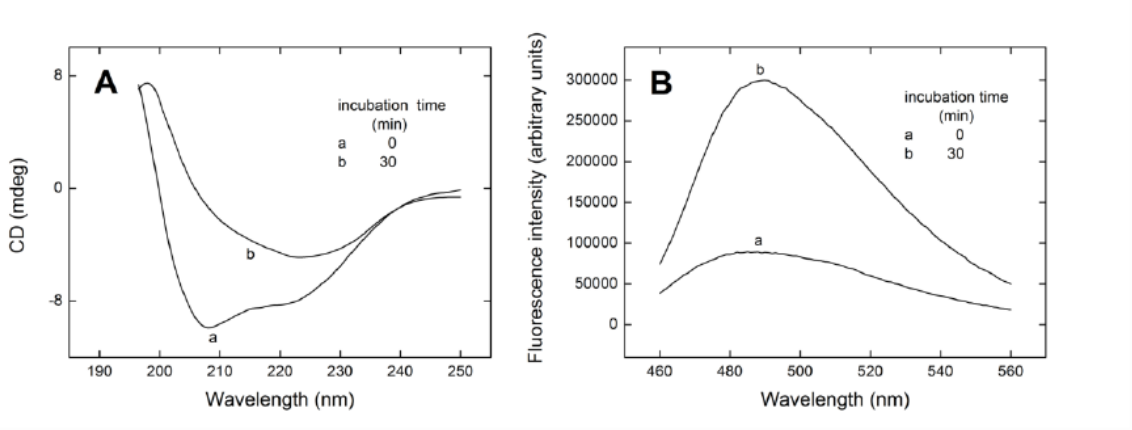

Fig. SI-3. A, CD and B, ThT fluorescence spectra of Vmh2 dissolved in 50mM Na phosphate buffer pH 7, incubated at 60 °C

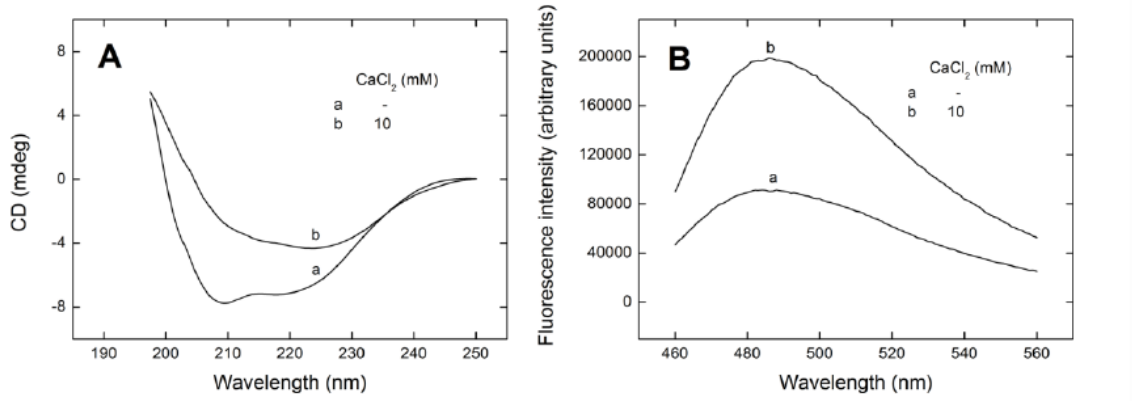

Fig. SI-4. A, CD and B, ThT fluorescence spectra of Vmh2 dissolved in 50 mM Na phosphate buffer, pH 7, in the presence of Ca^{2+}.

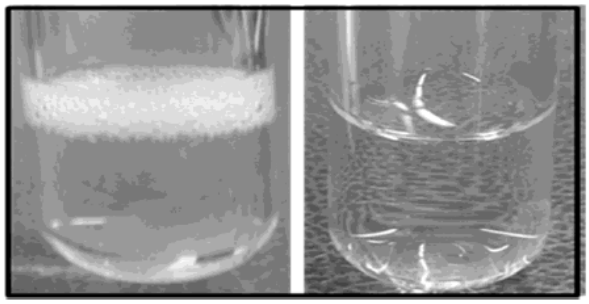

Fig SI-5. Agitated samples, by 15 min vortexing, of Vmh2 in Na Phosphate buffer at pH 7 after 3 days (left) and 60% ethanol after 1 minute (right).

ATR FT-IR SPECTROSCOPY ON HYDROPHOBIN SELF-ASSEMBLED LAYERS FOR TEFLON MEMBRANE BIO-FUNCTIONALIZATION

M. Portaccio[1], A. M. Gravagnuolo[2], S. Longobardi[2], P. Giardina[2], I. Rea[3], L. De Stefano[3], M. Cammarota[1], M. Lepore[1].

[1] Dipartimento di Medicina Sperimentale – Seconda Università di Napoli, Via S.M. di Costantinopoli,16-80134 Napoli, ITALY; E-mails: marianna.portaccio@unina2.it, marcella.cammarota@unina2.it, maria.lepore@unina2.it

[2] Dipartimento di Scienze Chimiche, Università "Federico II", Via Cintia, 21- 80126 Napoli, ITALY; E-mails: sara.longobardi@unina.it; alfredomaria.gravagnuolo@unina.it, paola.giardina@unina.it

[3] Institute for Microelectronics and Microsystems, CNR, Via P. Castellino, 111 -80131 Napoli, ITALY; E-mails: ilaria.rea@na.imm.cnr.it, luca.destefano@na.imm.cnr.it

Corresponding Author: Prof. Maria Lepore (E-mail: maria.lepore@unina2.it, tel +39 0815665839, fax +39 0815667500)

Abstract

Hydrophobins are small, amphiphilic proteins that can form a compact and stable nanometric layer at solution-solid interface, thus offering a promising approach in green modification of surfaces. The layering process of the Vmh2 hydrophobin from *Pleurotus ostreatus* on Teflon membrane in different conditions has been investigated by Attenuated Total Reflection Fourier Transform Infrared (ATR-FT-IR) spectroscopy. In particular, the protein layer has been characterized by quantifying the amide I band together with the lipid/amide ratio and carbohydrate/amide ratio. These values can be very useful in evaluating the removal efficiency of each class of non-proteic contaminants from fungal hydrophobin extracts as well as some key characteristics of the protein layer. In addition the secondary structure has been determined through amide I deconvolution procedure indicating the prevalent contribution from β-sheet state. The results inferred by infrared spectroscopy have been also confirmed by scanning electron microscopy imaging.

Keywords: Hydrophobin; Teflon membrane bio-functionalization; ATR-FT-IR spectroscopy

1. Introduction

Surface modification is often the key to successful use of metals, ceramics, carbon and polymers in applications such as biosensors, microarrays, medical implants and cell culturing [1-3]. Surface modification is a process that changes the material surface composition, structure, morphology and functionality. While the intrinsic mechanical properties are scarcely affected, stability, bio-functionality and/or biocompatibility of the material are significantly tuned by surface coating [4]. The result is driven by changes in the physical micro-architecture of the surface or in biochemical properties, and/or in viscous-elastic properties. Besides many wet or dry chemical procedures available, a promising approach to surface modification can be offered by hydrophobins, small self-assembling proteins, which can provide new green ways with great technological potential [5]. Hydrophobins, consisting approximately of 100 amino acid residues, are the most powerful surface-active proteins known [6]. They are ubiquitously produced by filamentous fungi playing various roles in fungal physiology related to surface phenomena, such as adhesion, formation of surface layers and lowering of surface tension [7]. As a remarkable property, hydrophobins have hydrophobic and hydrophilic patches and can self-assemble into strong, highly ordered, amphiphilic layer of nanometric thickness at almost any interfaces, helping fungi in facing the wide variety of environmental conditions and also in the adhesion to various surfaces. Depending on the type of surface, several molecular interactions, such as van der Waals interactions, hydrogen bonding, electrostatic interactions, or hydrophobic interactions, may be involved in the self-assembling process [7]. Since the first hydrophobin was identified in early 1990s [8], a big family has been isolated from many fungi. The sequence similarity of hydrophobins is generally weak, except for the characteristic and unique pattern of eight Cys residues forming four disulfide bridges [6, 9]. On the basis of differences in hydropathy patterns of the amino acid sequences and biophysical properties, two different types of hydrophobins are distinguished, namely class I and class II [10]. The members of both classes share properties such as high interfacial activity and high tendency to adhere to surfaces, which are essential for the surface modifying applications. However, the class I hydrophobins tends to form amyloid-like aggregates and surface layers that are highly stable and insoluble, i.e. they can only be dissolved in pure strong acids such as trifluoroacetic acid or formic acid, whereas the dissolution of class II hydrophobin assemblages seem to be relatively easier, for example, they dissolve in 2% sodium dodecyl sulfate or 60% ethanol [7]. Among Class I hydrophobins, the self-assembled process of a protein extracted from *Pleurotus ostreatus*, named Vmh2, has been used for bioactive modification of silicon surface [11]. The Vmh2 modified silicon surface shows an improvement in wettability and is suitable for the immobilization of other proteins. Variable-angle spectroscopic ellipsometry, water contact angle, and fluorescence measurements

have demonstrated that the proposed approach in silicon surface bio-activation is a feasible strategy for the fabrication of a new class of hybrid devices [12]. Vmh2 is soluble in solvents less polar than water (i.e., ethanol, at least 40%), not in pure water [13]. By increasing the solvent polarity, the Vmh2 solubility decreases, although any conformational transition is observed. On the other hand, Vmh2 undergoes a conformational change by increasing the pH of the alcoholic solution (pH ≥ 6), forming a self-assembled β-sheet rich state. In this paper, we aim to extend the investigation on Vmh2 layering process on hydrophobic surface by means of Attenuated-Total-Reflected Fourier-Transformed Infrared (ATR-FT-IR) spectroscopy, a powerful technique in chemical and structural characterization of very thin interfaces [14, 15]. In particular, we estimated the amide content, the lipid/amide and carbohydrate/amide ratios of the protein layer for different preparation procedures [16, 17]. Moreover, we had a deeper insight in the secondary structure of protein that has been demonstrated to be of extreme relevance in monitoring hydrophobin self-assembling process [18, 19]. The infrared analysis suggested the best conditions for uniform and homogeneous protein deposition and scanning electron microscopy (SEM) imaging confirmed the results of FT-IR spectroscopy.

2. Materials and methods

2.1 Materials

P. ostreatus mycelia (type: Florida no. MYA-2306) were purchased from American Type Culture Collection (ATCC; Italian distributor: LGC Standards, Sesto San Giovanni, Italy). As support surface we used 150 μm tick Teflon membranes from Gelman Science (Ann Arbor, MI, USA). Teflon has been already used both for hydrophobin structural studies [19] and for different applications [20, 21] due to its hydrophobic characteristics that makes it an ideal support for protein self-assembling. Moreover, Teflon IR spectrum presents only few absorption bands (see Results and Discussion paragraph), so that these plastic membranes are well suited for FT-IR spectra acquisition in macro-ATR geometry.

2.2 Vmh2 purification and self-assembled layer preparation

White-rot fungus, *P. ostreatus* (Jacq.: Fr.) Kummer (type: Florida; ATCC No. MYA-2306) was maintained at 4 °C through periodic transfer on potato dextrose agar (Difco) plates in the presence of 0.5% yeast extract. Mycelia were inoculated in 1 L flasks containing 500 mL of potato-dextrose broth (24 g/L) supplemented with 0.5% yeast extract, grown at 28 °C in shaken mode (150 rpm). After 10 days of fungal growth, mycelia were separated by filtration through gauze, treated twice

with 2% SDS in a boiling water bath for 10 min, washed several times with water and once with 60% ethanol to completely remove the detergent. The residue was freeze-dried and grinded to obtain the "washed-dry" mycelia, then it was treated with 100% trifluoroacetic acid (TFA) in a water bath sonicator (Elmasonic S30, Elma) for 25 min, and centrifuged 10 min at 3200g. The supernatant was dried in a steam of nitrogen, dissolved in 60% ethanol, centrifuged (10 min at 3200g) obtaining the raw extract. The ethanol was removed from the new supernatant under vacuum at 40 °C using rotavapor and after freeze-drying, two different procedures were carried out in order to remove contaminant molecules:

Extraction procedure A - The freeze-dried residue was washed 3 times with methanol/chloroform, 1:2 v/v (5 min in bath sonicator) and dried in a stream of nitrogen. Afterwards the solid material was treated with TFA for 30 min in bath sonicator, dried, dissolved in 60% ethanol and centrifuged at 3200g [22].

Extraction procedure B - The freeze-dried material was washed in a mixture of water/methanol/chloroform 2:2:1 v/v (5 min in bath sonicator). After centrifugation, proteins appeared as a solid aggregate at the interface between the water-methanol and the chloroform phases, and were recovered by liquid phases removal. The aggregated protein was dried, treated with TFA for 10 min in bath sonicator, re-dried, dissolved in 60% ethanol and centrifuged at 3200g [23].

Protein concentration was evaluated using the Pierce 660 nm protein assay kit (Thermo Scientific) using ovalbumin as standard protein.

Teflon membranes coating was achieved by casting 800µl of Vmh2 solutions at 0.2 mg/ml and the efficiency of A and B extraction procedures was evaluated. We explored the effect of protein solvent concentration (20% and 60% ethanol concentration), drying temperature (60 °C fixed temperature or room temperature) and pH (addition or not of NH_3 during drying process) on Vmh2 self-assembling layer on the hydrophobic surface of Teflon.

2.3 Circular Dichroism measurements

Far-UV CD spectra were recorded by a Jasco J715 spectropolarimeter equipped with a Peltier thermostatic cell holder (Jasco model PTC-348) in a quartz cell (0.1-cm light path) from 190 to 250 nm. The temperature was kept at 25° C and the sample compartment was continuously flushed with nitrogen gas. The final spectra were obtained by averaging three scans, using a bandwidth of 1 nm, a step width of 0.5 nm and a 4 sec averaging per point.

2.4 FT-IR spectroscopy

A Perkin Elmer Spectrum One FT-IR spectrometer equipped with a MIR TGS detector was used to record FT-IR spectra. Spectral acquisitions were performed in macro-ATR mode using a HATR ZnSe Flat-Plate 45-Degree (Perkin Elmer Part Number: L1200313) on which samples were placed with the hydrophobin layer in contact with ZnSe plate. Particular care was employed in order to achieve the same degree of contact for all measurements. Once good contact was achieved, the ATR FT-IR spectrum of the selected area on the surface was collected. The background spectrum was collected from the ZnSe plate without samples. All spectra were collected using 16 scans in the range from 4.000 to 600 cm^{-1} with a 4 cm^{-1} spectral resolution. Each sample was analyzed in triplicate. It is worth to note that, thanks to the adopted approach for data collection, no particular sample preparation was required. The spectra were preliminarily analyzed using the application routines provided by the software package ("Spectrum" User Guide, Perkin Elmer Inc. USA) controlling the whole data acquisition system. "Spectrum" (release 5.0.2, 2004) is the main Perkin Elmer software package for collecting, viewing and processing IR spectra.

Different samples prepared with A and B procedure was examined by FT-IR spectroscopy. All the spectra were preliminarily normalized with respect to the Teflon intense peaks located at 1210 and 1152 cm^{-1} and the Teflon spectrum was subsequently subtracted. This normalization procedure allowed us to quantitatively compare the spectra of different samples. As reported by different authors [24-27] the amount of protein detectable in different samples was estimated by evaluating the area of amide I and amide II bands in the 1700-1500 cm^{-1} region. Relative lipid content was determined by calculating the ratio of area in the 2990-2830 cm^{-1} region to the amide I band area. In a similar way, relative carbohydrate content was determined by calculating the ratio of the carbohydrate (1150 – 780 cm^{-1}) band area to the amide I band area [17, 25, 27] .

Protein structure was determined following the procedure described by Goormaghtigh et al. [28, 29] by curve fitting the amide I band into its respective secondary structure components. In particular, we analyzed the band in terms of the sum of six mixed Lorentzian-Gaussian curves, whose characteristics (intensity, position and width) were obtained using GRAMS Software.

2.5 SEM Characterization

The morphology of hydrophobin layer was studied by using a Carl Zeiss model SUPRA 40 SEM. The Teflon membranes coated by Vmh2 layer were directly mounted on a stub and coated with gold-palladium (Denton Vacuum Desk V) before observation.

3. Results and discussion

3.1 Purification and Circular Dichroism analysis of Vmh2

The Vmh2 hydrophobin was extracted from *P. ostreatus* by TFA treatment of "washed-dry" mycelia. The dry weight of the raw extract was about 130 mg per gram of "washed-dry" mycelia. On the other hand, the protein amount of this sample dissolved in 60% ethanol, estimated by Pierce 660 nm protein assay, was about 90 mg per gram, suggesting the presence of non-protein components in the raw extract. Therefore two different protocols (A and B) of solvent extraction were applied to this rough material and their efficiency evaluated characterizing these samples by different techniques.

CD spectra of samples before and after the two extraction procedures were acquired. However, no difference between the two samples could be detected, which means that the secondary structure was not affected by the presence of contaminants. A typical CD spectrum is reported in Fig. 1, showing the characteristic minima at 208 nm and 223 nm and the positive absorption at 198 nm, corresponding to a significant contribution of α-helix structure (30% of α-helix with respect to 20% of β-sheet).

In order to evaluate the efficiency of the two different extraction procedures (A and B) further analysis was performed by FT-IR spectroscopy.

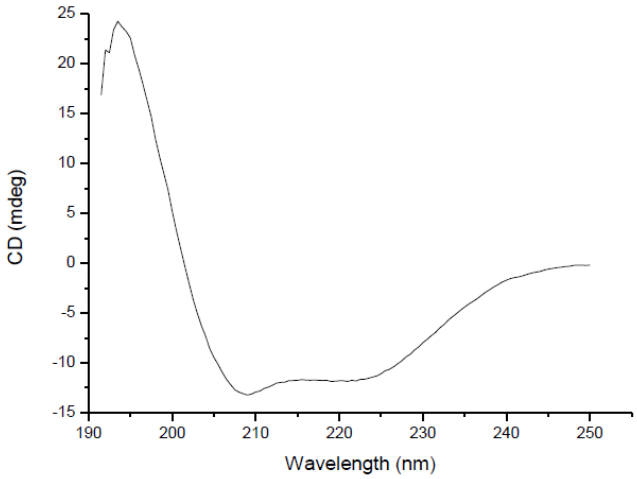

Fig. 1 – A typical CD spectrum of Vmh2 hydrophobin in 60% ethanol

3.2 FT-IR spectra of hydrophobin layer

In Fig. 2 FT-IR spectra of Vhm2 protein layers before and after purification procedures A and B are shown.

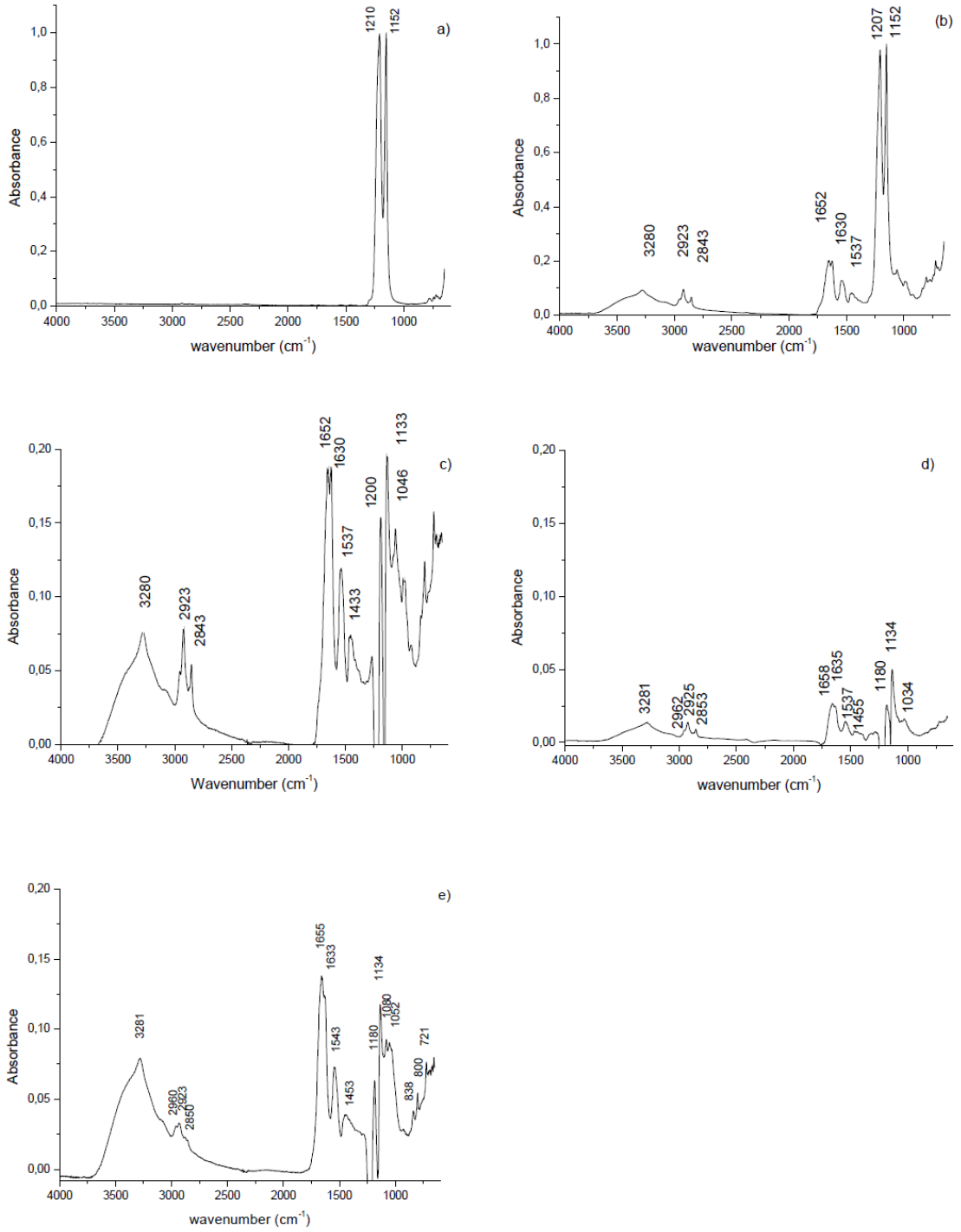

Fig. 2 - Representative FT-IR spectra of hydrophobin layers: bare Teflon membrane (a); Vmh2 layer obtained on Teflon membrane using raw extract before (b) and after (c) Teflon contribution subtraction; hydrophobin layer prepared following A purification procedure after Teflon contribution subtraction (d), hydrophobin layer prepared following B purification procedure after Teflon contribution subtraction (e).
Portaccio et al.

Teflon membrane is a good support material since its spectrum (Fig. 2a) presents only two strong peaks at 1210 cm^{-1} and 1152 cm^{-1} due to CF_2 stretching in a region where our samples don't show any significant infrared absorption. Fig. 2b shows a spectrum of Vmh2 protein layer obtained from a not purified sample, the raw extract (Fig. 2b), in which the contribution from the Teflon membrane, hydrophobin structures and non-proteic contaminants are represented. A better insight into the protein layer can be obtained after Teflon contribution subtraction (Fig. 2c). Analogously the normalized FT-IR spectra of Vhm2 layers prepared with A (Fig. 2d) and B procedure (Fig. 2e) are reported. The spectra of Fig. 2c, Fig. 2d and Fig. 2e are characterized by the presence of similar contributions. In particular in the Fig. 2e the large band centred at 3281 cm^{-1} can be attributed to Amide A. On its right tail, three small peaks at 2960 cm^{-1}, 2923 cm^{-1} and 2850 cm^{-1} are present and can be attributed to CH asymmetric stretching of CH_3, CH asymmetric stretching and symmetric of CH_2, respectively. A strong peak is evident at 1655 cm^{-1} with a small feature at 1633 cm^{-1}: they can be both attributed to the C-O stretching of amide I. Its position and shape is of fundamental importance for the characterization of the protein secondary structure and it will be further discussed in the next paragraph. Another relevant peak is located at 1543 cm^{-1} and it is related to N-H bending of amide II, whereas the structure at 1453 cm^{-1} can be related to O-H bending. The peaks at 1134 cm^{-1} and 1052 cm^{-1} can be assigned to the C-O-C asymmetric and symmetric stretching contributions, respectively. The peaks at 1080 cm^{-1} and 1023 cm^{-1} are due to asymmetric and symmetric C-O stretching, respectively. The weak peak at 838 cm^{-1} can be related to C-H bending, while the one at 800 cm^{-1} to NH_3 rocking. The last faint structure at 721 cm^{-1} can be due to the contribution of Amide IV and/or Amide V. In Table 1, the main peaks and related assignment in agreement with Refs. [30-33] have been reported. It is evident that the normalized spectra of Vmh2 layer upon purification procedure A (Fig. 2d) and B (Fig. 2e) showed peaks located at the same positions (within the spectral resolution) but with a higher intensity in the case of last one.

Table 1 - Main peaks in FT-IR spectrum of a hydrophobin layer in the range 4000 - 700 cm^{-1} and tentative assignment in agreement with Refs.30-33.

Peak (cm^{-1})	Assignments
Teflon support (see Figure 2 a)	
1210	CF_2 stretching
1152	CF_2 stretching
Hydrophobin layer ((see Figures 2d and 2e)	
3281	Amide A
2960	CH asymmetric stretching in CH_3
2923	CH asymmetric stretching in CH_2
2851	CH symmetric stretching in CH_2
1655-1633	C-O stretching dell'ammide I
1543	N-H bending dell'amide II
1453	asymmetric CH_2 and CH_3 bending
1184	C-O and CC stretching
1134	C-O-C asymmetric stretching
1080	C–O stretching
1052	C-O and CC stretching
838	C-H bending
800	NH_3 rocking
721	Amide IV e/o ammide V

3.3 Amide content, lipid/amide ratio and carbohydrate/amide ratio analysis

The amount of protein detectable in different samples was estimated by evaluating the area of amide I and amide II bands in the 1700-1500 cm^{-1} region. Relative lipid content in different samples was determined by calculating the ratio of area of the 2990-2830 region to the amide I band area even though in this case also contribution from methyl side groups in protein has to be taken into account in the above-mentioned region. In a similar way, relative carbohydrate content was determined by calculating the ratio of the carbohydrate (1150– 780 cm^{-1}) band area to the amide I band area [17]. All samples prepared following A purification procedure for protein extraction showed lower value of amide content, higher values of lipid/amide and carbohydrate/amide ratio in comparison with samples prepared following B procedure. In Table 2 the above-mentioned quantities have been averaged for samples prepared with the two different procedures in the deposition conditions reported at the end of the paragraph concerning Vmh2 purification and self-assembled layer preparation.

Table 2– Results of the detected amide content, lipid/amide ratio and carbohydrate/amide ratio analysis for layers prepared using hydrophobin from the two different procedures of protein purification. The results are expressed as the mean ± standard deviation of five samples for each condition of Vmh2 deposition.

	Amide content (a.u.)	**Lipid/ Amide ratio**	**Carbohydrates/ Amide ratio**
Samples from A procedure	4.0 ± 0.3	0.17 ± 0.02	1.84 ± 0.19
Samples from B procedure	17 ± 2	0.09 ± 0.01	0.88 ± 0.09

The lowest values of lipid/amide ratio and carbohydrate/amide ratio were obtained using samples prepared by the procedure B, which has thus been considered the most useful for Vmh2 purification.

In Table 3 the amide content values, the lipid/amide ratio and the carbohydrate/amide ratio of hydrophobin-Teflon samples prepared using the B procedure, but whose protein layers were obtained in different conditions (solvent concentration, drying temperature and pH) have been shown.

Table 3 - Results of the detected amide content, lipid/amide ratio and carbohydrate/amide ratio analysis for samples prepared using procedure B for protein purification and different conditions for film deposition. The results are expressed as the mean ± standard deviation of five samples for each kind of samples.

Sample	Protein solvent	Layer formation conditions	**Amide content (a.u.)**	**Lipid/ Amide ratio**	**Carbohydrates/ Amide ratio**
B1	60% Ethanol	Dry at 60° C	7.7 ± 1.3	0.11 ± 0.01	0.80 ± 0.05
B2	60% Ethanol	NH_3 addition, dry at 60° C	13.7 ± 1.3	0.21 ± 0.03	0.81 ± 0.05

B3	60% Ethanol	Dry at RT	22 ± 4	0.09 ± 0.01	0.99 ± 0.07
B4	60% Ethanol	NH_3 addition, dry at RT	14± 3	0.19 ± 0.04	1.03 ± 0.06
B5	20% Ethanol	Dry at 60° C	12 ± 2	0.10 ± 0.01	0.82 ± 0.03
B6	Ethanol 20%	Dry at RT	27 ± 4	0.08 ± 0.01	0.93 ± 0.08

It can be noted that the drying process at room temperature (B3 vs. B1, B6 vs. B5) shows a higher amide content with respect to the other, even if the protein amounts deposited on the Teflon membranes were always the same. Since the obtained value for amide content are related to the average on the whole membrane surface analysed, this result can be due to a more uniform and homogeneous distribution of the protein samples slowly dried at room temperature with respect to that quickly dried at 60°C. On the other hand, when the pH was increased by adding NH_3 (B2, B4), the obtained values of amide content were very similar, independently from the drying temperature. In this case the layer formation process was mainly triggered by the pH change leading to a quick aggregation, as previously demonstrated [13]. Moreover the B6 samples prepared in 20% ethanol and dried at room temperature are characterized by the highest amide content, the lowest lipid/amide ratio and a carbohydrates/amide ratio with an intermediate value among the ones shown in Table 3.

3.4 Secondary structure analysis

de Vocht et al [18, 19] used secondary structure analysis of amide I region of FT-IR spectra for monitoring the changes that accompany the self-assembly of the hydrophobin SC3 with ATR-FTIR and PM-IRRASS spectroscopy relating them to changes in morphology and structure.

In the present case, we noticed in Fig. 2e that the amide I band is characterized by a peak located at 1655 cm^{-1} that is generally attributed to the α-helical state but it is also present a peak at 1633 cm^{-1} that is characteristic of β-sheet state. Then we examined in more detail the amide I band region and the results of deconvolution procedure are reported in Fig. 3 (for details about the procedure, see Material and Methods section).

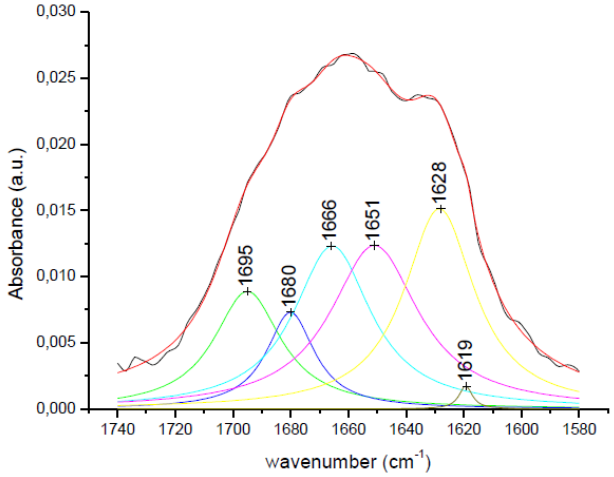

Fig. 3 - FT-IR and deconvoluted spectra of amide I region of the Fig. 2e spectrum.

Numerical deconvolution highlights three several distinct peaks: the bands at 1628, 1680 and 1695 cm^{-1} can presumably be assigned to β-sheet structures with the 1680 cm^{-1} band characteristic of anti-parallel β-sheet structure [31, 34, 35]. Quantifying the deconvolution results, we can assume that the β-sheets contribution constitutes the 54 % of the secondary structures. The band around 1651 cm^{-1} is characteristic of an α-helical structure, and the area of this component accounts for 27 % of the total band area, while the β-turn structure (about 18 %) contributes to the bands at 1672 cm^{-1}. The results are summarized in Table 4.

Table 4 - Results of Amide I band deconvolution for a typical hydrophobin layer. Peak spectral ranges (in agreement with refs. [30, 31]) and secondary structure subcomponent contributions are reported.

	β-sheet	α-helix	Random coil	β-Turn	Other
Spectral Range (cm^{-1})	1623–1641 1674–1695	1648–1657	1642-1657	1662-1686	
Hydrophobin film	1628 1695; 1680	1651		1666	
(%)	54	27		18	1

The predominance of β-sheet contribution is in agreement with other data reported in literature for hydrophobin on Teflon surface [13, 14, 15]. The deconvolution procedure has been performed on all spectra and the results of this analysis are summarised in Fig. 4 as far as concerns β-sheet, β-turn, β-tot (the sum of β-sheets and β-turn) and α-helical contributions. It is evident that the β-sheet structure is always dominant. It has been previously demonstrated that pH increase by NH_3 addition leads to amyloid-like fibrils formation [13].

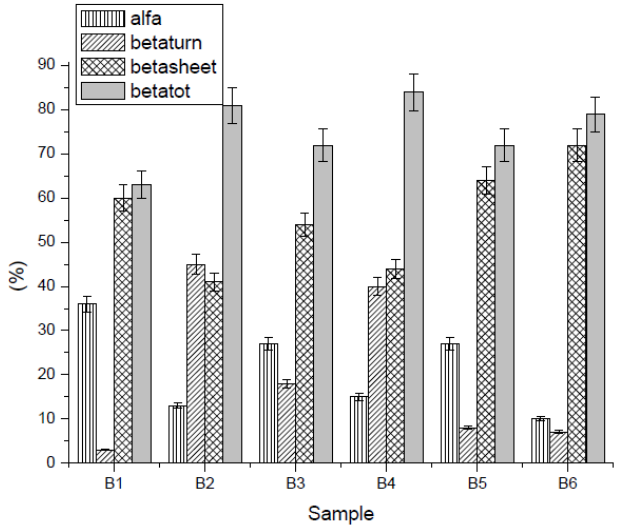

Fig. 4 - Comparison of the mean values of secondary structure α- helix, β-sheet and β-turn components for different samples. The numerical values are expressed as the mean ± standard deviation of five samples for each kind of samples.

FT-IR spectra analysis showed a decrease of α-helical, as expected, and an increase of β-turn contribution, rather than β-sheets, phenomenon usually ascribed to an increase of disorder. On the other hand, B5 and B6 samples were characterized by high amide content and also the highest β-sheet contribution. These samples contained a high percentage of water (80%), therefore the drying process was slower than in the case of samples dissolved in 40% water (60% ethanol), especially when protein layers were obtained by drying at room temperature (B6). Therefore these results indicated that a slow process favours the formation of a more uniform layer with a higher β-sheet contribution. Conversely when the pH values were quickly increased by NH_3 addition, a sudden and probably less ordered self-assembling process was induced.

3.5 SEM characterization results

In Fig. 5 micrographs at different magnifications have been reported for some Vmh2 layers prepared following the purification procedure B. B1 and B3 samples are less homogeneous with some cavities that are visible at a 15000X magnification. Micrographs of B4 samples show inhomogeneities even at 500X magnification. In the case of B6 sample layer, micrographs show a greater uniformity at all magnifications. Therefore, also from a morphological point of view, the conditions employed for preparing samples of B6 type seem to be the most suitable to obtain an ordered and homogeneous layer of Vmh2 on Teflon support.

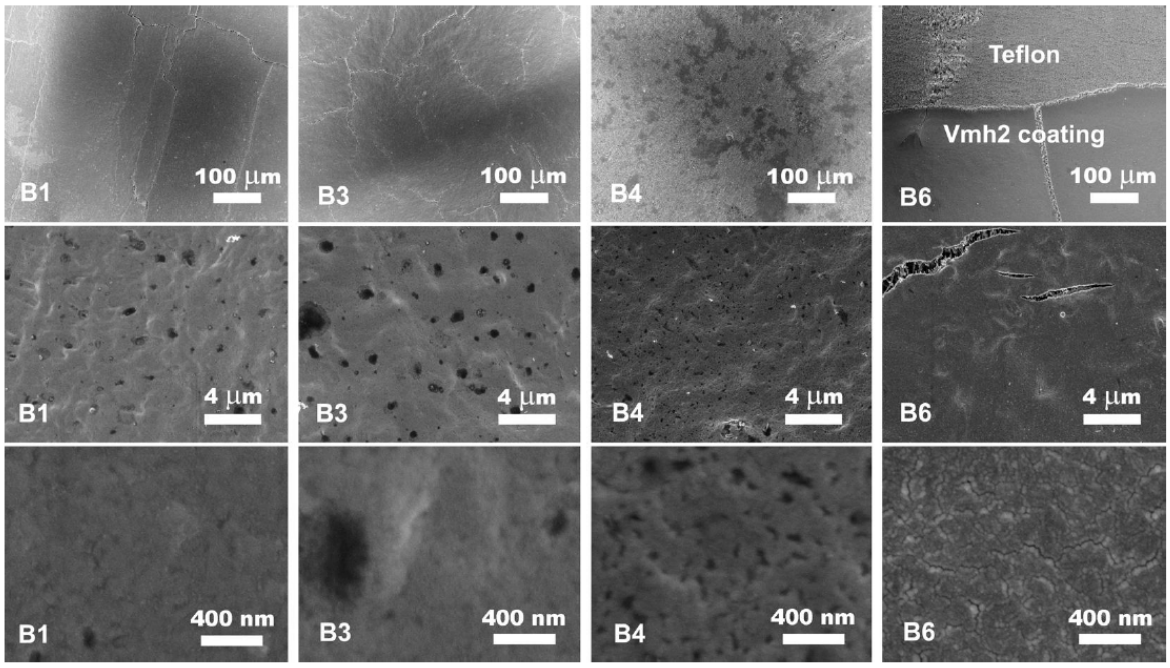

Fig. 5 - SEM micrographs of the different Vmh2 layer surfaces. For sample characteristics please refer to Table 3. Pictures were taken at different magnification.

4. Conclusions

In the present paper the layering process of Vmh2 hydrophobin from *Pleurotus ostreatus* on Teflon membrane has been investigated using ATR-FT-IR spectroscopy. In particular the characteristics of the protein layer have been evaluated from amide I band together with the lipid/amide ratio and carbohydrate/amide ratio. Moreover, the changes induced in the secondary structure has been monitored by means of amide I deconvolution procedure. The results of this investigation suggest which are the best preparation conditions of the Vmh2 hydrophobin layer in terms of surface homogeneity and low non proteic content that are both important in biomaterials surface modification.

References

1) B. Kasemo, Surf. Sci. 500 (2002) 656-677.
2) L. De Chiffre, H. Kunzmann, G.N. Peggs, D.A. Lucca, CIRP Annals—Manufacturing Technol. 52 (2003) 561-577.
3) A. Kurella, N.B. Dahotre, J. Biomater. App. 20 (2005) 5-50.
4) T. Hanawa, J. R. Soc. Interface 6 (2009) S361-S369.
5) J. Bayry, V. Aimanianda, J.I. Guijarro, M. Sunde, J.P. Latgé, PLoS Pathog. 8 (2012) doi:10.1371/journal.ppat.1002700
6) J.Hakanpä, A. Paananen, S. Askolin, T. Nakari-Setälä, T. Parkkinen, M. Penttilä, M.B. Linder, J. Rouvinen. J. Biol. Chem. 279 (2004) 534-539.
7) M.B. Linder, G.R. Szilvay, T. Nakari-Setälä, H. Söderlund, M. Penttilä, Protein Sci. 11 (2002) 2257-2266.
8) J.G. Wessels, O.M. De Vries, S.A. Asgeirsdottir, J. Springer, J. Gen. Microbiol. 137 (1991) 2439-2445.
9) H.J. Hektor, K. Scholtmeijer, Curr. Opin. Biotechnol. 16 (2005) 434-439.
10) J.G. Wessels, Annu. Rev. Phytopathol. 32 (1994) 413-437.
11) L. De Stefano, I. Rea1, E. De Tommasi, I. Rendina, L. Rotiroti, M. Giocondo, S. Longobardi, A. Armenante, P. Giardina, Eur. Phys. J. E 30 (2009) 181-185.
12) L. De Stefano, I. Rea, P. Giardina, A. Armenante, I. Rendina, Adv. Mater. 20 (2008) 1529-1533.
13) S. Longobardi, D. Picone, C. Ercole, R. Spadaccini, L. De Stefano, I. Rea, P. Giardina, Biomacromolecules 13 (2012) 743-750.
14) S.E. Glassford, B. Byrne, S.G. Kazarian, Biochim. & Biophys. Acta 1834 (2013) 2849-2858.
15) I. A. Mudunkotuwa, A. Al Minshid, V. H. Grassian, Analyst 139 (2014) 870-881.
16) Z. Wang, S. Feng, Y. Huang, S. Li, H. Xu, X. Zhang, Y. Bai, M. Qiao, Protein Expression & Purification 72 (2010) 19-25.
17) A.P. Dean, D.C. Sigee, B. Estrada, J.K. Pittman, Bioresource Technology 101 (2010) 4499-4507.
18) M.L. de Vocht, K. Scholtmeijer, E.W. van der Vegte, O.M.H. de Vries, N. Sonveaux, H.A.B. Wösten, J.M. Ruysschaert, G. Hadzïoannou, J.G.H. Wessels, G.T. Robillard, Biophys. J. 74 (1998) 2059-2068.
19) M. de Vocht, I. Reviakine, W.P. Ulrich, W. Bergsma-Schutter, H. A.B.Wosten, H. Vogel A.Brisson, J.G.H. Wessels, G.T. Robillard, Protein Science 11 (2002) 1199-1205.
20) M.I. Janssen, M.B.M. van Leeuwen, T.G. van Kooten, J. de Vries, L. Dijkhuizen, H.A.B. Wosten, Biomaterials 25 (2004) 2731-2739.
21) Y. Corvis, A. Walcarius, R. Rink, N.T. Mrabet, Anal. Chem. 77 (2005) 1622-1630.
22) T. Kurihara, Y. Nishizawa, Y. Takahashi, Biochem. J. 165 (1977) 135-140.
23) D. Wessel, U.I. Flügge, Anal. Biochem. 138 (1984) 141-143.
24) Y. Mei, L. Miller, W. Gao, R.A. Gross, Biomacromolecules 4 (2003) 70-74.
25) D.L. Jurgen-Lohmann, C. Nacke, R.L. Legge, L.C. Simon, J Sol-Gel Sci. Technol. 50 (2009) 77-86.
26) M. Portaccio, B. Della Ventura, D.G. Mita, N. Manolova, O. Stoilova, I. Rashkov, M. Lepore, J Sol-Gel Sci. Technol. 57 (2011) 204-211.
27) I. Delfino, M. Portaccio, B. Della Ventura, D.G. Mita, M. Lepore, Mat. Sci. & Eng. C 33 (2013) 304-310.
28) E. Goormaghtigh, V. Cabiaux, J.M. Ruysschaert, Eur. J. Biochem. 193 (1990) 409-420.
29) E. Goormaghtigh, V. Cabiaux, J.M. Ruysschaert, Subcell. Biochem. 23 (1994) 329-362.
30) J. Coates, Interpretation of infrared spectra. A practical approach, J. Wiley and Sons Ltd, Chichester 2000.
31) A. Barth, Biochim. Biophys. Acta 1767 (2007) 1073-1101.

32) M. Ibrahim, M. Alaam, H. El-Haes, A.F. Jalbout, A. de Leo, Ecl. Quím., 31 (2006) 15-21.
33) R.S. Tipson Infrared Spectroscopy of Carbohydrates National Bureau of Standards Monograph (1968) 110.
34) H. Susi, D.M. Byler, Methods Enzymol. 130 (1986) 290-311.
35) S. Krimm, J. Bandekar, Adv. Protein Chem. 38 (1986) 181-264.

3. VMH2 SELF-ASSEMBLED COATING ENHANCES THE SURFACE PROPERTIES OF MATERIALS FOR BIOTECHNOLOGICAL APPLICATIONS

In this project, Vmh2 is exploited for improving surface features of materials of interests for industrial applications, even in high technology fields. The following macro-section is split in two areas of applicative interest in surface science. **Section 3.1** concerns the use of Vmh2 for analysis of peptides and proteins by mass spectrometry. **Section 3.2** concerns the use of Vmh2 in nanomaterials-based applications.

3.1. A VERSATILE MALDI-MS PLATFORM BASED ON SELF-ASSEMBLED THIN FILM OF HYDROPHOBIN

Matrix-Assisted Laser Desorption/Ionization - Time of Flight - Mass Spectrometry (MALDI-TOF MS) is a widely used tool for the analysis of biomolecules, such as proteins and peptides. In proteomic research very complex biological samples are analyzed, usually requiring buffer for maintaining their structure or activities. The presence of relatively high concentration of salts or other reagents results in a significant decrease of MS signal sensitivity (Xu et al., 2003; Pan et al. 2007) due to ion suppression phenomena. Therefore, time-consuming pre-treatments of samples prior to MS analysis, such as purification and separation of proteins, are often required, also employing high amount of sample.

The ability of Vmh2 to coat a wide range of different materials and to adsorb proteins to its surface makes it applicable to perform on-plate enrichment and desalting of peptides/proteins. Moreover the Vmh2 film is a low cost coating, easy to be prepared and easy to be removed, allowing reuse of the same plate.

In **section 3.1.1**, the use of Vmh2 self-assembled layer to develop a novel coating of steel MALDI sample plate is reported. The propensity of Vmh2 film to adsorb proteins (De Stefano et al. 2009) has been investigated to set up in situ desalting strategies for MALDI-MS or MS/MS of real biological samples (i.e. protein mixes and/or peptide mixes in presence of salts).

In **section 3.1.2** an expanded use of the Vmh2 film adding new functionalities to the MALDI coating is described. The immobilization of proteolytic and demodifying enzymes on the Vmh2 layer has been tested, developing a lab-on-plate platform focused on proteomic applications.

3.1.1 HYDROPHOBIN-COATED PLATES AS MATRIX-ASSISTED LASER DESORPTION/IONIZATION SAMPLE SUPPORT FOR PEPTIDE/PROTEIN ANALYSIS (Front Cover)

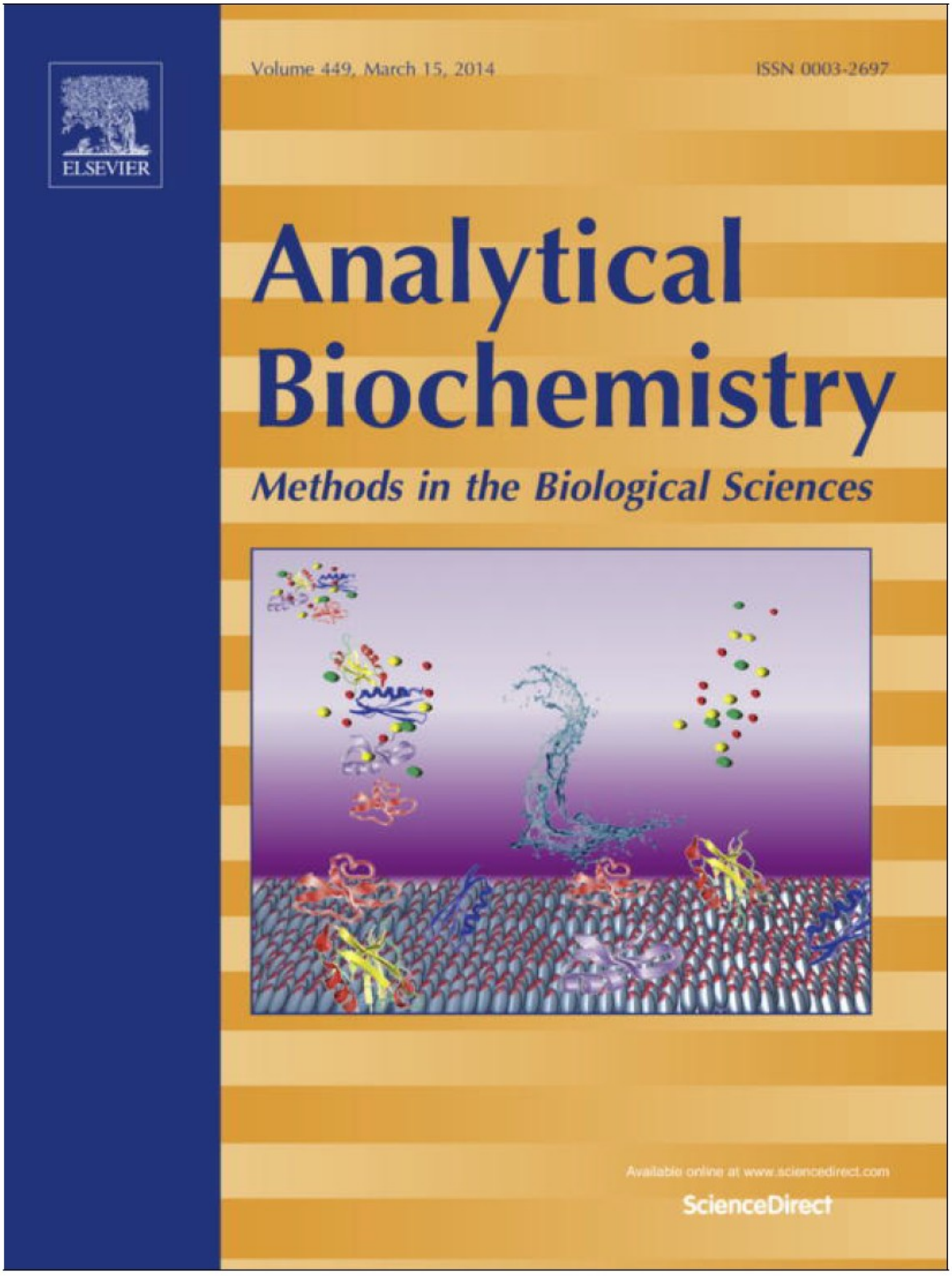

3.1 A VERSATILE MALDI-MS PLATFORM BASED ON SELF-ASSEMBLED THIN FILM OF HYDROPHOBINS

3.1 A VERSATILE MALDI-MS PLATFORM BASED ON SELF-ASSEMBLED THIN FILM OF HYDROPHOBINS

Analytical Biochemistry 449 (2014) 9–16

Contents lists available at ScienceDirect

Analytical Biochemistry

journal homepage: www.elsevier.com/locate/yabio

Hydrophobin-coated plates as matrix-assisted laser desorption/ionization sample support for peptide/protein analysis

Sara Longobardi [a], Alfredo Maria Gravagnuolo [a], Ilaria Rea [b], Luca De Stefano [b], Gennaro Marino [a], Paola Giardina [a,*]

[a] Department of Chemical Sciences, University of Naples "Federico II", 80126 Naples, Italy
[b] Unit of Naples–Institute for Microelectronics and Microsystems, National Council of Research, 80131 Naples, Italy

ARTICLE INFO

Article history:
Received 24 October 2013
Received in revised form 15 November 2013
Accepted 18 November 2013
Available online 25 November 2013

Keywords:
Thin films
Fungal proteins
Self-assembly
Lab-on-a-plate

ABSTRACT

Fungal hydrophobins are amphipathic self-assembling proteins. Vmh2 hydrophobin, prepared from mycelial cultures of the basidiomycete fungus *Pleurotus ostreatus*, spontaneously forms a stable and homogeneous layer on solid surfaces and is able to strongly absorb proteins even in their active forms. In this work, we have exploited the Vmh2 self-assembled layer as a novel coating of a matrix-assisted laser desorption/ionization (MALDI) steel sample-loading plate. Mixtures of standard proteins, as well as tryptic peptides, in the nanomolar–femtomolar range were analyzed in the presence of salts and denaturants. As evidence on a real complex sample, crude human serum was also analyzed and spectra over a wide mass range were acquired. A comparison of this novel coating method with both standard desalting techniques and recently reported on-plate desalting methods was also performed. The results demonstrate that Vmh2 coating of MALDI plates allows for a very simple and effective desalting method suitable for development of lab-on-a-plate platforms focused on proteomic applications.

Hydrophobins are a family of small amphipathic proteins (comprising ~100 amino acid residues) produced by filamentous fungi. They are able to self-assemble on hydrophobic or hydrophilic solid surfaces into thin amphiphilic layers, changing the hydropathy character of the surfaces [1]. Based on the structural features and properties of their aggregates, hydrophobins have been classified into two groups: class I and class II. Layers formed by class II hydrophobins are soluble in ethanol or sodium dodecyl sulfate (SDS)[1] aqueous solutions, whereas class I hydrophobins form highly insoluble membranes that can be solubilized only by strong acids such as trifluoroacetic acid (TFA) [2]. Various biotechnological applications have been reported by exploiting the interesting properties of these fungal proteins [3–5]. In particular, hydrophobin coating has been used as an intermediate layer to attach cells, proteins, or other biomolecules to surfaces for development of several biotools such as biosensors and DNA/protein microarrays [6–9].

A class I hydrophobin secreted by the basidiomycete fungus *Pleurotus ostreatus* has been purified and identified as Vmh2 [10]. Vmh2 behavior has been widely investigated both in solution [11] and in assembled form [12–14]. We have demonstrated that Vmh2 is spontaneously able to form a stable and homogeneous layer on hydrophilic or hydrophobic surfaces, changing their wettability [12]. The stability of the self-assembled coating has also been investigated in order to protect nanocrystalline material, such as porous silicon, used in optical devices for biosensing [13]. Furthermore, we have shown that Vmh2-coated surfaces are able to strongly bind proteins, including enzymes in their active form [14].

Following these results, Vmh2 hydrophobin layers have been tested in coating steel matrix-assisted laser desorption/ionization (MALDI) sample plates with the aim to develop a lab-on-a-plate platform focused on proteomic applications [15].

Ion suppression phenomena, due to salts, denaturants, and/or other reagents, in peptide/protein samples result in a significant decrease of signal sensitivity in MALDI analysis [16,17]. Most of the common desalting methods (e.g., high-performance liquid chromatography [HPLC], ZipTip, PD10) require relatively large sample volumes and/or are associated with sample loss [18]. These drawbacks can limit the advantages of MALDI–MS (mass spectrometry) in terms of sensitivity. To overcome these limits, several authors have suggested the use of *on-plate* sample treatment by

* Corresponding author. Fax: +39 081674313.
E-mail address: giardina@unina.it (P. Giardina).

[1] *Abbreviations used:* SDS, sodium dodecyl sulfate; TFA, trifluoroacetic acid; MALDI, matrix-assisted laser desorption/ionization; MS, mass spectrometry; AMBIC, NH_4HCO_3; TOF, time-of-flight; CHCA, α-cyano-4 hydroxycinnamic acid; S/N, signal-to-noise; DHB, 2,5-dihydroxybenzoic acid; SEM, scanning electron microscopy; S/N, signal/noise.

0003-2697/$ - see front matter © 2013 Elsevier Inc. All rights reserved.
http://dx.doi.org/10.1016/j.ab.2013.11.021

3. VMH2 SELF-ASSEMBLED COATING ENHANCES THE SURFACE PROPERTIES OF MATERIALS FOR BIOTECHNOLOGICAL APPLICATIONS

properly treating the MALDI plate surface [15,19]. It is worth recalling that surface-enhanced laser desorption/ionization (SELDI) mass spectrometry, introduced by Hutchens and Yip in 1993 [20,21], was the first approach to exploit on-plate sample desalting/enrichment. A number of in-house methods to cover MALDI plates with hydrophobic layers aimed at on-plate desalting/enrichment of samples have been further suggested [22–25].

In this article, we describe the surface treatment of MALDI sample plates with hydrophobin Vmh2, resulting in a simple and effective desalting method prior to MALDI analysis. To the best of our knowledge, this is the first report on the use of a biomaterial to improve the efficiency of MALDI–MS analysis of peptides/proteins. A comparative evaluation of the described technique with respect to other off-plate and on-plate desalting techniques—ZipTip microcolumns and paraffin-coated plates—has been made showing specific benefits of Vmh2 as a coating material of MALDI sample plates.

Materials and methods

Materials

Lysozyme from chicken egg white, ovalbumin from chicken egg white, myoglobin from equine heart, ribonuclease from bovine pancreas, α-lactalbumin from bovine milk, trypsin from bovine pancreas, and paraffin wax were purchased from Sigma (St. Louis, MO, USA). *P. ostreatus* mycelia (type: Florida no. MYA-2306) were purchased from American Type Culture Collection (ATCC; Italian distributor: LGC Standards, Sesto San Giovanni, Italy). PD-10 desalting columns were purchased from GE Healthcare (Milan, Italy). $ZipTip_{C18}$ microcolumns were purchased from Millipore (Vimodrone Italy). Calibration mixtures were purchased from AB SCIEX (Framingham, MA, USA).

Tryptic digests

Lysozyme and ovalbumin were dissolved at 5 μM in 0.5 M Tris–HCl (pH 8.0) containing 6 M guanidinium chloride and then reduced in 10 mM dithiothreitol for 2 h at 37 °C and carboxamidomethylated in 50 mM iodoacetamide for 30 min, in the dark, at room temperature.

Samples were desalted on a PD10 column using 10 mM NH_4HCO_3 (AMBIC) as eluting buffer. Fractions containing proteins were pooled, concentrated, and treated with trypsin (substrate/enzyme ratio, 50:1, w/w) for 18 h at 37 °C. Samples were lyophilized and dissolved in four different solutions—namely 0.1% formic acid, 10 mM AMBIC, 1 M NaCl, and 2 M urea—to test the effectiveness of on-plate washing of hydrophobin-coated plates.

$ZipTip_{C18}$ desalting

Desalting of peptide samples was performed by using $ZipTip_{C18}$ microcolumns according to manufacturer's instructions. Briefly, 0.1% TFA was added to samples to get pH < 4.0. The $ZipTip_{C18}$ was wetted with 10 μl of 50% acetonitrile and 0.1% TFA (three times) and equilibrated with 10 μl of 0.1% TFA (three times). Samples were slowly aspirated and dispensed 10 times, and then desalting was achieved by aspirating and dispensing 10 μl of 0.1% TFA (5 times). Finally, peptides were eluted with 10 μl of 50% acetonitrile and 0.1% TFA.

Standard proteins preparation

Standard proteins (lysozyme, myoglobin, ribonuclease, and α-lactalbumin) were dissolved at 0.1 mg ml^{-1} in 0.1 M sodium acetate (pH 3.6), 0.1 M sodium acetate (pH 5.8), 0.05 M sodium bicarbonate (pH 7.5), or 0.05 M sodium bicarbonate (pH 9.6).

Serum proteins preparation

Human serum, obtained from blood of a healthy donor and prepared by following the standard laboratory procedures, was provided by the blood bank center of the "Federico II" university hospital and used without any further treatment and/or purification.

Vmh2 purification

Vmh2 was prepared from *P. ostreatus* mycelia as described previously [10]. Preparation basically involves growing mycelia at 28 °C in static cultures in 2-L flasks containing 500 ml of potato dextrose (24 g/L) broth with 0.5% yeast extract. After 10 days of fungal growth, hydrophobins released into the medium were aggregated by air bubbling using a Waring blender and collected by centrifugation at 4000*g*. The precipitate was freeze-dried, left to dissolve under mechanical agitation with TFA for 2 h, and treated in a bath sonicator (operating at 35 kHz and 240 W) for 30 min. The TFA solution was dried in a stream of air, and Vmh2 was dissolved in 60% ethanol, resulting in a stock solution (100 μg ml^{-1}) that was further used to coat MALDI plates.

MALDI plate coating

Vmh2 solution (1 μl) was spotted on each MALDI plate well. After 1 h, samples were dried for 10 min at 80 °C and washed with 60% ethanol. Deposition was repeated twice, and finally the plate was washed with 2% SDS at 100 °C for 10 min. To obtain mass spectra, 1 μl of sample (tryptic peptides, standard proteins, or human serum) was spotted on MALDI plate wells coated by Vmh2. After 5 min of incubation at room temperature, wells were washed three times with water. Finally, the appropriate matrix was added and left to crystallize. Vmh2 coating can be removed by washing the MALDI plate with 10% TFA (by gently polishing the surface) followed by washing with acetonitrile, water, and acetone.

Other coating methods were tested in comparison with hydrophobin coating. Mineral oil, glycerol [25], and paraffin wax [26] were used according to the procedures described previously.

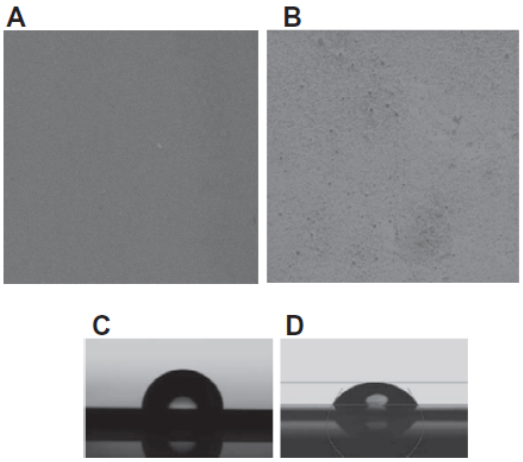

Fig.1. (A, B) SEM images of bare steel (A) and Vmh2-coated steel (B). (C, D) Water contact angle of a water drop on steel (C) and on Vmh2-coated steel (D).

3.1.1 Hydrophobin-coated Plates as Matrix-assisted Laser Desorption/Ionization Sample Support for Peptide/Protein Analysis (Supporting Material)

Briefly, a cotton applicator was dipped in mineral oil, glycerol, or chloroform saturated solution of paraffin wax. The applicator was used to coat the steel MALDI plate with one smooth movement across a single lane.

MALDI–MS analyses

Mass spectra were registered by a Voyager-DE STR MALDI–TOF (time-of-flight) mass spectrometer (Applied Biosystems, Framingham, MA, USA) equipped with a nitrogen laser (337 nm). Peptides were detected in reflector mode using α-cyano-4 hydroxycinnamic acid (CHCA, 10 mg ml^{-1} in acetonitrile/0.1% TFA, 7:3, v/v) as matrix. Spectra were acquired using a mass range of 500 to 5000 amu. Acceleration and voltages were set up as follows: target voltage at 20 kV, grid at 66% of target voltage, and delayed extraction at 150 ns to obtain the best signal-to-noise (S/N) ratios and the best possible isotopic resolution. Spectra were accumulated in multiples of 50 laser shots, with 50 to 2000 shots in total. The molecular weight standards for the calibration of the Voyager-DE STR system were AB SCIEX calibration mixtures 1 and 2.

Proteins were detected in linear mode using sinapinic acid (20 mg ml^{-1} in acetonitrile/0.1% TFA, 7:3, v/v) or 2,5-dihydroxybenzoic acid (DHB, 20 mg ml^{-1} in acetonitrile/0.1% TFA, 7:3, v/v) as matrix. Acceleration and voltages were set up as follows: target voltage at 22 kV, grid at 85% of target voltage, and delayed extraction at 250 ns. Spectra were accumulated in multiples of 250 laser shots, with 500 to 20,000 shots in total. The molecular weight standards for the calibration of the Voyager-DE STR system were AB SCIEX calibration mixture 3.

Characterization of Vmh2 coating

The characterization of the Vmh2 layer covering stainless steel MALDI plates was performed by variable-angle spectroscopic ellipsometry (UVISEL, Horiba–Jobin–Yvon), and by water contact angle analysis, using KSV Instruments' CAM 200 Optical Contact

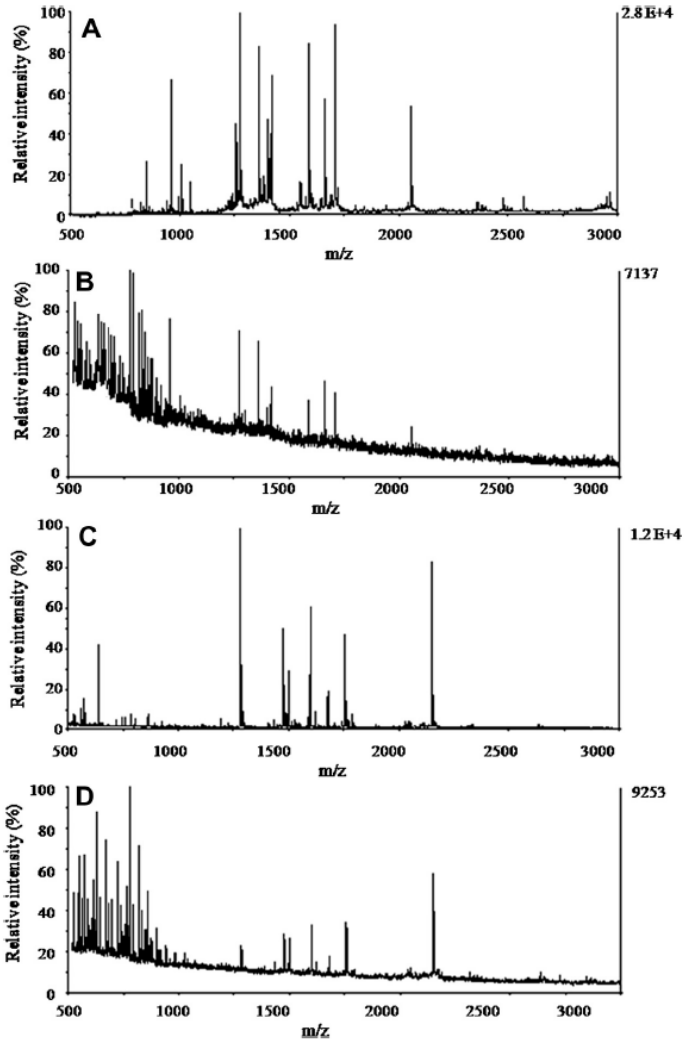

Fig.2. MALDI spectra of tryptic peptides in 2 M urea spotted on Vmh2-coated wells. (A, B) Lysozyme after on-plate washing (A) and undesalted (B). (C, D) Ovalbumin after on-plate washing (C) and undesalted (D).

3. VMH2 SELF-ASSEMBLED COATING ENHANCES THE SURFACE PROPERTIES OF MATERIALS FOR BIOTECHNOLOGICAL APPLICATIONS

Table 1
Numbers of matched peptides dissolved in 2 M urea, obtained by trypsin hydrolysis of different protein amounts.

Protein	Amount (fmol)	Peptide number (% of sequence coverage)					
		No desalting	ZipTip μ-column	Paraffin coating	Mineral oil coating	Glycerol coating	Vmh2 coating
Lysozyme	500	8 (53)	16 (84)	14 (56)	10 (53)	11 (72)	17 (94)
	50	5 (32)	15 (84)	0–6[a]	0–3[a]	0–2[a]	17 (94)
	5	–	–	–	–	–	16 (94)
Ovalbumin	500	10 (33)	16 (63)	13 (58)	8 (27)	7 (26)	16 (63)
	50	3 (10)	14 (60)	0–2[a]	–	–	16 (63)
	5	–	–	–	–	–	14 (60)

Note: Results of different desalting methods are reported. The data were obtained collecting at least 10 replicates.
[a] By using paraffin, mineral oil, and glycerol coatings, erratic data were obtained. The ranges of peptide numbers observed in the replicates are reported.

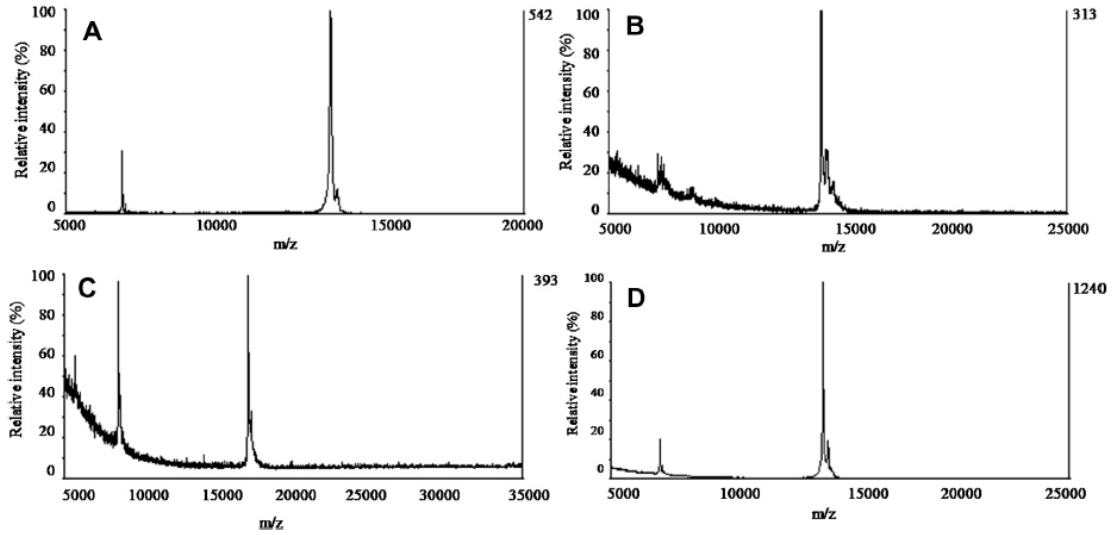

Fig.3. MALDI spectra of proteins dissolved in 0.1 M sodium acetate (pH 5.8) spotted on Vmh2 coating: (A) ribonuclease; (B) lysozyme; (C) myoglobin; (D) α-lactalbumin.

Angle Meter, as described previously [12,13]. Biofilm morphology was examined by scanning electron microscopy (SEM, Quanta 200 FEG scanning electron microscope), operating in low vacuum mode, using a large field detector.

Results and discussion

Hydrophobin coating

The Vmh2 layer coating on steel was prepared and physically characterized following the protocols already established in our previous works [12,14]. Namely, 0.1 μg of Vmh2 protein in 60% ethanol solution was deposited, and after drying several washing steps were performed, including a hot SDS one. Vmh2 coating was homogeneous and compact, as shown by SEM (Fig. 1). Its thickness, estimated by variable-angle spectroscopic ellipsometry measurements, was 9.8 ± 0.7 nm. Analysis of water contact angle of Vmh2-coated steel showed a change of surface wettability from 96 (±2) to 75 (±2)°. The surface concentration G (μg cm^{-2}) of Vmh2 self-assembled on steel can be calculated from ellipsometric data by using the Cuypers formula [27]:

$$\Gamma = 0.1d\frac{M}{A}\frac{n_f^2-1}{n_f^2+2},$$

where A is the molar refractivity (2104 cm^3 mol^{-1}), M is the molecular weight (8563 g mol^{-1}), and d and n_f are the thickness (10 nm) and refractive index (1.384 at l = 1 μm) [28] of the layer, respectively (determined by ellipsometry). The resulting surface concentration was approximately 0.09 μg cm^{-2}, which is comparable to the one reported in the case of the class I hydrophobin FpHYD5 deposited on steel [29]. Based on these data, the amount of Vmh2 that strongly adheres to the well surface was approximately 0.003 μg/well (1 mm radius). Considering that 0.1 μg of protein was initially deposited on each well, we can assume that most of the protein was removed by the washing steps.

To evaluate whether Vmh2 layer was suitable for MALDI plate coating, spectra were acquired from coated wells where only matrices (CHCA, DHB, and sinapinic acid) were deposited. Results showed no signal related to Vmh2 (8563 m/z) and no background interference in any mass range (data not shown). The absence of Vmh2 molecular ion signals can be ascribed to the low amount of protein in the nanometric layer. Actually, a MALDI spectrum of Vmh2 [10] was obtained by co-crystallization of approximately 0.1 μg of protein with sinapinic acid. Finally, the Vmh2 coating can be fully removed by TFA treatment (as detailed above), thereby restoring the physical characteristics of the bare surface.

Peptide analyses

Preliminary experiments were performed using tryptic digests of lysozyme or ovalbumin that were prepared as usually reported in MALDI mapping studies. Here, 5 nmol of proteins, dissolved in

3.1.1 Hydrophobin-coated Plates as Matrix-assisted Laser Desorption/Ionization Sample Support for Peptide/Protein Analysis (Supporting Material)

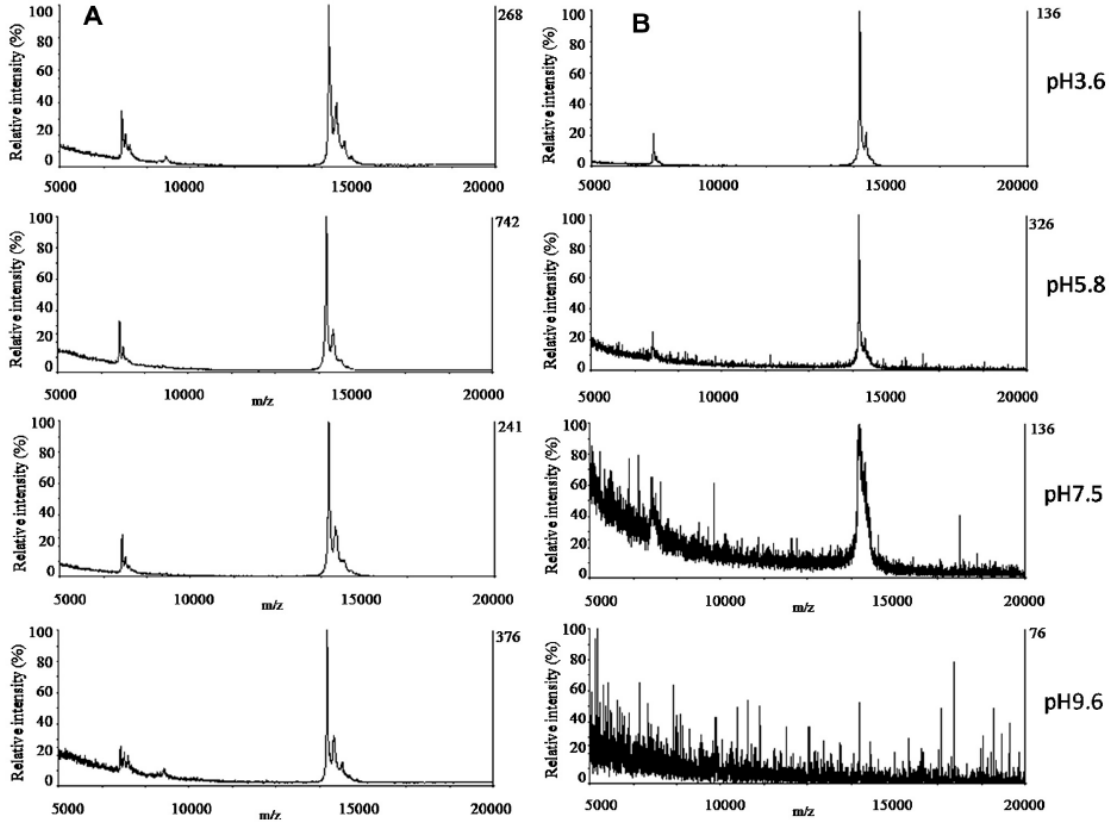

Fig.4. MALDI spectra of lysozyme dissolved in 0.1 M sodium acetate (pH 3.6), 0.1 M sodium acetate (pH 5.8), 0.05 M sodium bicarbonate (pH 7.5), and 0.05 M sodium bicarbonate (pH 9.6) buffers. Shown are samples spotted on Vmh2-coated wells: (A) after washing; (B) unwashed.

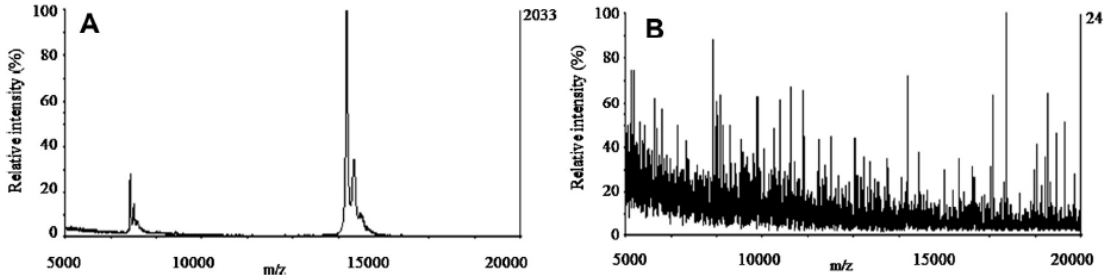

Fig.5. MALDI spectra of lysozyme in denaturing buffer containing 6 M guanidinium chloride. Shown are samples spotted on Vmh2-coated wells: (A) after washing; (B) unwashed.

1 ml of 6 M guanidinium chloride, was reduced and carboxamidomethylated. Samples were desalted before trypsin addition, lyophilized, and dissolved in 1 ml of 0.1% formic acid after hydrolysis. Then, 1 µl of these sample solutions was spotted on bare and Vmh2-coated MALDI wells before 1 µl of CHCA matrix solution was added and dried in air. Very similar spectra were obtained (see Table S1 and Fig. S1 in Supplementary material) in terms of number of signals above the threshold noise and intensity. The same mapping content was found: 21 peptides for lysozyme (94% of sequence coverage) and 18 peptides for ovalbumin (70% of sequence coverage). Therefore no effect was caused by the presence of the hydrophobin layer on the obtained spectra. Then, coated and uncoated wells, after sample loading and before matrix addition, were rinsed three times with 10 µl of distilled water. Few erratic signals of low intensity were observed on bare wells, whereas full spectra, allowing the same sequence coverage, were obtained by laser firing the hydrophobin-coated wells. Therefore, the interaction of Vmh2 coating with peptides allows the on-plate washing

http://dx.doi.org/10.1016/j.ab.2013.11.021

without detectable sample loss. This result suggests, inter alia, that the Vmh2 hydrophobin layers are able to firmly bind peptides with different chemicophysical characteristics.

Tryptic digest samples dissolved in salty buffer or denaturant, namely 100 mM NH_4HCO_3, 1 M NaCl, or 2 M urea, were analyzed on both uncoated and Vmh2-coated wells with or without on-plate washing steps to remove the salts/denaturant excess (see Table S2 and Fig. S2 in Supplementary material). Only few signals with low signal/noise (S/N) ratios (<10) were detected without the washing steps in both cases (coated and uncoated) due to expected suppression of MS signals in the presence of salts or denaturing agents. Many adduct signals severely interfere with detection of signals, especially related to low-molecular-weight peptides (500–1000 *m*/*z*), hiding them in background noise. After on-plate washing, both spectra intensity and peak number dramatically decrease on uncoated wells, whereas spectra characterized by high S/N ratios (>10) were obtained in the presence of Vmh2 coating. The main improvement of S/N ratio occurred at low mass region. As an example, spectra of tryptic peptides dissolved in 2 M urea are reported in Fig. 2. Sequence coverage of 60% for lysozyme and 33% for ovalbumin was obtained in the presence of urea, whereas an increase of S/N ratio from 5- to 10-fold and sequence coverage of 90 and 60%, respectively, were obtained when samples are loaded and washed on Vmh2 coating.

To test the sensitivity of the method, the tryptic digest solutions were serially diluted and spotted on hydrophobin-coated wells. We were able to observe satisfactory sequence coverage (~90% for lysozyme and 60% for ovalbumin) even when 5 fmol of digested proteins was submitted to the on-plate desalting procedure. Furthermore, a more homogeneous sample spread was observed on the Vmh2-coated wells with respect to bare wells. Actually reproducible spectra were acquired accumulating just 50 shots in random positions of the same coated well or in different coated wells.

The sensitivity and practicability of the method were checked in comparison with widely used off-plate and on-plate desalting procedures. Tryptic digest samples, dissolved in salty buffer or denaturant, were desalted by the $ZipTip_{C18}$ microcolumn. Acceptable sequence coverage was obtained only when at least 50 fmol of digested proteins was loaded on the microcolumn. Moreover, the procedure requires some 30 min to process each sample.

Paraffin, mineral oil, and glycerol were used as hydrophobic coating methods, and spectra were recorded by following the procedures described previously [25,26]. The number of signals assigned to the peptides of both proteins in the different conditions is reported in Table 1. When samples containing less than 500 fmol were desalted on other hydrophobin-coated wells, the number of matched peptides dramatically decreased and erratic results were obtained, as already reported by Tannu and coworkers [26]. A comparison of the matched peptides obtained by trypsin hydrolysis of 500 fmol of lysozyme and desalted using the different methods is reported in Table S3 of the Supplementary material.

On the basis of this comparison, the Vmh2 coating method appears to be superior in terms of sensitivity and working time as a sample desalting method for MALDI analysis. Desalting can actually be performed by a simple distilled water rinsing step after some 5 min of sample incubation on the treated surface. We postulate that the observed higher reproducibility as well as sensitivity of the method with respect to the experiments performed by using other hydrophobic coatings such as paraffin may well be due to a stronger interaction of peptides with the assembled hydrophobin layer than with other hydrophobic surfaces.

Protein analyses

Due to the encouraging results obtained with peptide mixtures, and taking into account some previous results showing the binding

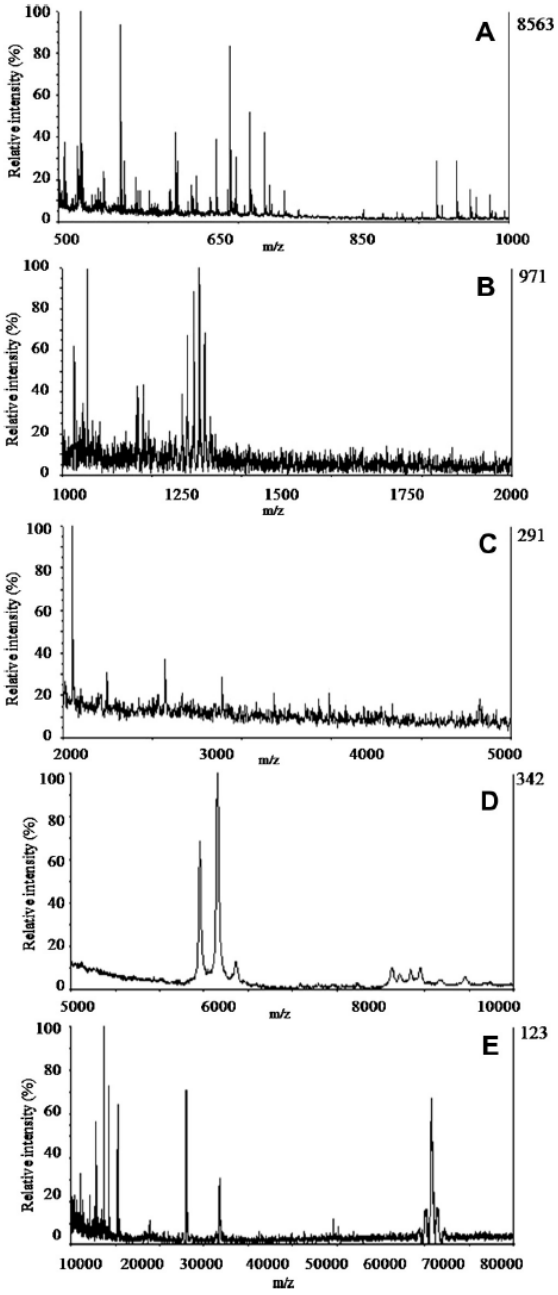

Fig.6. (A, B) 500 to 1000 *m*/*z* range (A) and 1000 to 2000 *m*/*z* range (B) obtained using 100-fold diluted serum and CHCA as matrix. (C) 2000 to 5000 *m*/*z* range obtained using 100-fold diluted serum and DHB as matrix. (D, E) 5000 to 10,000 *m*/*z* range (D) and 10,000 to 80,000 *m*/*z* range obtained using 50-fold diluted serum and sinapinic acid as matrix.

of native proteins on Vmh2 layers [14], we tried to verify whether the above-described procedure could also be used to analyze salty undigested protein samples by MALDI.

Some standard proteins (ribonuclease, lysozyme, myoglobin, and α-lactalbumin), differing in p*I* and/or molecular weight, were

3.1.1 Hydrophobin-coated Plates as Matrix-assisted Laser Desorption/Ionization Sample Support for Peptide/Protein Analysis (Supporting Material)

dissolved at 7 μM in acetate and bicarbonate buffers at different pH levels. Here, 1 μl of sample solutions was spotted on Vmh2-coated MALDI wells, and after 5 min of incubation they were rinsed three times with distilled water, after which the matrix was added and dried. MALDI spectra showed intense signals at the expected m/z values of monoprotonated molecular ions of the proteins dissolved in all of the tested buffers only when the washing step was included. Spectra of the four proteins dissolved in 0.1 M sodium acetate (pH 5.8) and of lysozyme in different buffers are shown in Figs. 3 and 4, respectively. As shown in Fig. 4, when no washing step was performed, pH increase caused a decrease of S/N ratio until no signal was observed at pH 9.0. On the contrary, we were able to detect good signals over threshold noise down to 70 fmol at all of the tested pH levels after on-plate desalting in the presence of Vmh2 coating. High-quality spectra, with intense signals and good S/N ratio, were also obtained when proteins were dissolved in buffers containing denaturing agents, namely in the presence of 6 M guanidinium chloride. As an example, spectra of lysozyme are shown in Fig. 5. Spectra obtained after the proposed on-plate desalting method were similar to those acquired when samples were desalted using standard procedures before MALDI analysis (i.e., PD10, which requires much higher protein amounts and some hours of working time).

Human serum analyses

To verify whether the proposed method is appropriate to a real complex system, the proposed procedure was used to analyze human serum. Serum samples obtained after a simple blood centrifugation were directly incubated for 5 min on Vmh2-coated wells, which were then washed three times with water. After matrix addition, MALDI–TOF spectra ranging from 500 to 80,000 m/z were acquired. Moreover, serum dilutions from 10- to 500-fold were used, and three different matrices (sinapinic acid, CHCA, and DHB) were tested.

Spectra acquired in linear mode from 5000 to 80,000 m/z showed several signals assigned to the most abundant serum proteins (Fig. 6) on the basis of data reported in the literature [30].

The whole, or eventually depleted, serum protein analysis by MS is currently of extreme interest for fast screening in search of possible biomarkers [31–33]. A key factor to attain appropriate standards for clinical laboratory testing is high reproducibility of the data. Using the proposed procedure, serum samples can be directly analyzed, avoiding sample desalting/enrichment pretreatments, thereby reducing variability of results and increasing reproducibility. It is worth noting that signals were detected even in the range of 500 to 3000 m/z, a mass region greatly affected by the presence of contaminants.

These data indicate that the proposed functionalization method can be optimized to analyze, at the same time, high-, medium-, and low-molecular-weight serum proteins, as well as peptides, whereas most of the reported methods are focused on the analysis of molecules in specific mass ranges, usually after serum depletion [34–36].

Conclusions

The ability of Vmh2 to coat a wide range of different surfaces makes it applicable to several types of sample plates and instruments. Moreover, a Vmh2 layer is a low-cost coating, easy to prepare, and easy to remove, allowing reuse of the same plate. In addition, high-quality spectra with excellent levels of sensitivity are achieved under harsh conditions. Vmh2 coating is suitable for analysis of molecules in a wide mass range (from small peptides to intact proteins), thereby demonstrating the high versatility of the system. The wide range of analysis and the good S/N ratio, obtained without sample pretreatment, make the proposed method of interest for the analysis of complex samples such as human serum. Therefore, it should be interesting in future work to exploit the use of hydrophobin-coated plates as a potential proteomics lab-on-a-plate platform in view of the fact that some enzymes retain their activity when deposited on hydrophobin layers [14].

Acknowledgments

We thank Pietro Pucci and Angela Amoresano for the useful discussion, and we thank Cristina Del Barone ("Lamest" laboratory, ICTP–IMCB, CNR) for SEM image acquisition. This work was supported by a grant from the Ministero dell'Università e della Ricerca Scientifica–Industrial Research Project, "Integrated agro-industrial chains with high energy efficiency for the development of eco-compatible processes of energy and biochemicals production from renewable sources and for the land valorization (EnerbioChem)" (PON01_01966), funded in the frame of Operative National Programme Research and Competitiveness 2007–2013 D. D. Prot. n. 01/Ric. 18.1.2010.

Appendix A. Supplementary data

Supplementary data associated with this article can be found, in the online version, at http://dx.doi.org/10.1016/j.ab.2013.11.021.

References

[1] M.B. Linder, Hydrophobins: proteins that self-assemble at interfaces, Curr. Opin. Colloid Interface Sci. 14 (2009) 356–363.
[2] H.A.B. Wösten, M.L. de Vocht, Hydrophobins, the fungal coat unraveled, Biochim. Biophys. Acta 1469 (2000) 79–86.
[3] H.J. Hektor, K. Scholtmeijer, Hydrophobins: protein with potential, Curr. Opin. Biotechnol. 16 (2005) 434–439.
[4] F. Zampieri, H.A.B. Wosten, K. Scholtmeijer, Creating surface properties using a palette of hydrophobins, Materials 3 (2010) 4607–4625.
[5] W. Wohlleben, T. Subkowski, C. Bollschweiler, B. von Vacano, Y. Liu, W. Schrepp, U. Baus, Recombinantly produced hydrophobins from fungal analogues as highly surface-active performance proteins, Eur. Biophys. J. 39 (2010) 457–468.
[6] T. Sun, G. Quing, B. Su, L. Jiang, Functional biointerface materials inspired from nature, Chem. Soc. Rev. 40 (2011) 2909–2921.
[7] M. Qin, L.K. Wang, X.Z. Feng, Y.L. Yang, R. Wang, C. Wang, L. Yu, B. Shao, M.Q. Qiao, Bioactive surface modification of mica and poly(dimethylsiloxane) with hydrophobins for protein immobilization, Langmuir 23 (2007) 4465–4471.
[8] Z. Wang, M. Lienemann, M. Qiao, M.B. Linder, Mechanisms of protein adhesion on surface films of hydrophobin, Langmuir 26 (2010) 8491–8496.
[9] Z.X. Zhao, H.C. Wang, X. Qin, X.S. Wang, M.Q. Qiao, J. Anzai, Q. Chen, Self-assembled film of hydrophobins on gold surfaces and its application to electrochemical biosensing, Colloids Surf. B 71 (2009) 102–106.
[10] A. Armenante, S. Longobardi, I. Rea, L. De Stefano, M. Giocondo, A. Silipo, A. Molinaro, P. Giardina, The *Pleurotus ostreatus* hydrophobin Vmh2 and its interaction with glucans, Glycobiology 20 (2010) 594–602.
[11] S. Longobardi, D. Picone, C. Ercole, R. Spadaccini, L. De Stefano, I. Rea, P. Giardina, Environmental conditions modulate the switch among different states of the hydrophobin Vmh2 from *Pleurotus ostreatus*, Biomacromolecules 13 (2012) 743–750.
[12] L. De Stefano, I. Rea, A. Armenante, P. Giardina, M. Giocondo, I. Rendina, Self-assembled biofilm of hydrophobins protects the silicon surface in the KOH wet etch process, Langmuir 23 (2007) 7920–7922.
[13] L. De Stefano, I. Rea, P. Giardina, A. Armenante, I. Rendina, Protein-modified porous silicon nanostructures, Adv. Mater. 20 (2008) 1529–1533.
[14] L. De Stefano, I. Rea, E. De Tommasi, I. Rendina, L. Rotiroti, M. Giocondo, S. Longobardi, A. Armenante, P. Giardina, Bioactive modification of silicon surface using self-assembled hydrophobins from *Pleurotus ostreatus*, Eur. Phys. J. 30 (2009) 181–185.
[15] P.L. Urban, A. Amantonico, R. Zenobi, Lab-on-a-plate: extending the functionality of MALDI–MS and LDI–MS targets, Mass Spectrom. Rev. 30 (2011) 435–478.
[16] Y.D. Xu, J.T. Watson, M.L. Bruening, Patterned monolayer/polymer films for analysis of dilute or salt-contaminated protein samples by MALDI–MS, Anal. Chem. 75 (2003) 185–190.
[17] C. Pan, S. Xu, H. Zhou, Y. Fu, M. Ye, H. Zou, Recent developments in methods and technology for analysis of biological samples by MALDI–TOF–MS, Anal. Bioanal. Chem. 387 (2007) 193–204.

[18] Y.D. Xu, M.L. Bruening, J.T. Watson, Non-specific, on-probe cleanup methods for MALDI–MS samples, Mass Spectrom. Rev. 22 (2003) 429–440.
[19] Y. Zhang, L. Li, P. Yang, H. Lu, On-plate enrichment methods for MALDI–MS analysis in proteomics, Anal. Methods 4 (2012) 2622–2631.
[20] W. Hutchens, T. Yip, New desorption strategies for mass spectrometric analysis of macromolecules, Rapid Commun. Mass Spectrom. 7 (1993) 576–580.
[21] K.A. Baggerly, J.S. Morris, K.R. Coombes, Reproducibility of SELDI–TOF protein patterns in serum: comparing datasets from different experiments, Bioinformatics 20 (2004) 777–785.
[22] X. Yuan, D.M. Desiderio, Protein identification with Teflon as matrix-assisted laser desorption/ionization sample support, J. Mass Spectrom. 37 (2002) 512–524.
[23] Z. Zeng, Y. Wang, S. Shi, L. Wang, X. Guo, N. Lu, On-plate selective enrichment and self-desalting of peptides/proteins for direct MALDI MS analysis, Anal. Chem. 84 (2012) 2118–2123.
[24] J. Wang, R. Chen, M. Ma, L. Li, MALDI MS sample preparation by using paraffin wax film: systematic study and application for peptide analysis, Anal. Chem. 80 (2008) 491–500.
[25] H.Q. Zhuo, L. Huang, L.J. Feng, H.Q. Huang, Mineral oil-, glycerol-, and vaseline-coated plates as matrix-assisted laser desorption/ionization sample supports for high-throughput peptide analysis, Anal. Biochem. 378 (2008) 151–157.
[26] N.S. Tannu, J. Wu, V.K. Rao, H.S. Gadgil, M.J. Pabst, I.C. Gerling, R. Raghow, Paraffin-wax-coated plates as matrix-assisted laser desorption/ionization sample support for high-throughput identification of proteins by peptide mass fingerprinting, Anal. Biochem. 327 (2004) 222–232.
[27] P. Cuypers, J. Corsel, M. Janseen, J. Kop, W. Hermens, H. Hemker, The adsorption of prothrombin to phosphatidylserine multilayers quantitated by ellipsometry, J. Biol. Chem. 258 (1983) 2426–2431.
[28] I. Rea, P. Giardina, S. Longobardi, F. Porro, V. Casuscelli, M. Gagliardi, I. Rendina, L. De Stefano, Hydrophobin Vmh2–glucose complexes self-assemble in nanometric biofilms, J. R. Soc. Interface 9 (2012) 2450–2456.
[29] T.J. Hakala, P. Laaksonen, V. Saikko, T. Ahlroos, A. Helle, R. Mahlberg, H. Hahl, K. Jacobs, P. Kuosmanen, M.B. Linder, K. Holmberg, Adhesion and tribological properties of hydrophobin proteins in aqueous lubrication on stainless steel surfaces, RSC Adv. 2 (2012) 9867–9872.
[30] J. Villanueva, D.R. Shaffer, J. Philip, C.A. Chaparro, H. Erdjument-Bromage, A.B. Olshen, M. Fleisher, H. Lilja, E. Brogi, J. Boyd, M. Sanchez-Carbayo, E.C. Holland, C. Cordon-Cardo, H.I. Scher, P. Tempst, Differential exoprotease activities confer tumor-specific serum peptidome patterns, J. Clin. Invest. 116 (2006) 271–284.
[31] L. Le, K. Chi, S. Tyldesley, S. Flibotte, D.L. Diamond, M.A. Kuzyk, M.D. Sadar, Identification of serum amyloid A as biomarker to distinguish prostate cancer patients with bone lesion, Clin. Chem. 51 (2005) 659–707.
[32] L. Rossi, B. Martin, G.L. Hortin, R. White, M. Foster, D. Stroncek, E. Wang, F.M. Marincola, M.C. Panelli, Inflammatory protein profile during systemic high dose interleukin-2 administration, Proteomics 6 (2006) 709–720.
[33] A.L. Capirotti, G. Caruso, C. Cavaliere, S. Piovesana, R. Samperi, A. Laganà, Comparison of three different enrichment strategies for serum low molecular weight protein identification using shotgun proteomics approach, Anal. Chim. Acta 740 (2012) 58–65.
[34] M. De Bock, D. de Seny, M.A. Meuwis, A.C. Servais, T.Q. Minh, J. Closset, J.P. Chapelle, E. Louis, M. Malaise, M.P. Merville, M. Fillet, Comparison of three methods for fractionation and enrichment of low molecular weight proteins for SELDI–TOF–MS differential analysis, Talanta 82 (2010) 245–254.
[35] A. Tiss, C. Smith, U. Menon, I. Jacobs, J.F. Timms, R. Cramer, A well-characterised peak identification list of MALDI MS profile peaks for human blood serum, Proteomics 10 (2010) 3388–3392.
[36] Y. Wu, C. Hsieh, M. Tam, Matrix-assisted laser desorption/ionization of peptides on AnchorChip targets with α-cyano-4-hydroxycinnamic acid and nitrocellulose as matrix, Rapid Commun. Mass Spectrom. 20 (2006) 309–312.

Supplementary material

Hydrophobin-coated plates as matrix-assisted laser desorption/ionization sample support for peptide/protein analysis

Sara Longobardi[1], *Alfredo Maria Gravagnuolo*[1], *Ilaria Rea*[2], *Luca De Stefano*[2], *Gennaro Marino*[1] *and Paola Giardina**[1]

[1]Department of Chemical Sciences, University of Naples "Federico II",

Via Cintia 4, 80126, Naples, Italy

[2]Unit of Naples-Institute for Microelectronics and Microsystems, National Council of Research,

Via P. Castellino 111, 80131, Naples, Italy

Short title: Vmh2-coated MALDI plates for high-throughput analysis

Subject category: Mass spectrometry

Corresponding Author

Paola Giardina

Address: Department of Chemical Sciences, via Cintia 4, 80126 Naples, Italy

Tel: +39 081674319

Fax: +39 081674313

Email: giardina@unina.it

3. VMH2 SELF-ASSEMBLED COATING ENHANCES THE SURFACE PROPERTIES OF MATERIALS FOR BIOTECHNOLOGICAL APPLICATIONS

The contents of Supplementary material include the following:

Table S1: List of peptides obtained by trypsin hydrolysis as usually performed in MALDI mapping studies (see text for details).

Table S2: Number of matched peptides obtained by trypsin hydrolysis of lysozyme, dissolved in different buffers. On plate desalting on Vmh2 coating is compared with bare wells.

Table S3: Comparison of matched peptides obtained by trypsin hydrolysis of 500 fmol of lysozyme dissolved in 2M urea, using different desalting methods.

Figure S1: MALDI spectra of tryptic peptide: lysozyme on uncoated (A) and Vmh2-coated (B) wells; ovalbumin on uncoated (C) and Vmh2-coated (D) wells.

Figure S2: MALDI spectra of lysozyme tryptic peptides in 2M urea: without on-plate washing on uncoated (A) and Vmh2-coated (C) wells; after on-plate washing on uncoated (B) and Vmh2-coated (D) wells

3.1.1 Hydrophobin-coated Plates as Matrix-assisted Laser Desorption/Ionization Sample Support for Peptide/Protein Analysis (Supporting Material)

Table S1: List of peptides obtained by trypsin hydrolysis as usually performed in MALDI mapping studies

Lysozyme		Ovalbumin	
Signals (m/z)	sequences	Signals (m/z)	sequences
505.30	^{126}GC*RL^{129}	580.75	^{124}ELYR^{127}
517.36	^{69}TPGSR^{73}	647.86	^{281}VYLPR^{285}
606.86	^{1}KVFGR^{5}	763.95	^{57}VVRFDK^{62}
874.61	^{15}HGLDNYR^{21}	888.56	^{279}IKVYLPR^{285}
993.51	^{62}WWC*NDGR^{68}	957.37	^{52}TQINKVVR^{59}
1030.62	^{14}RHGLDNYR^{21}	1247.45	^{361}ADHPFLFC*IK^{370}
1045.75	^{117}GTDVQAWIR^{125}	1345.61	^{371}HIATNAVLFFGR^{382}
1049.52	^{6}C*ELAAAMKR^{14}	1555.74	^{188}VYLPRMKMEEK^{200}
1333.56	^{115}C*KGTDVQAWIR^{125}	1581.74	^{265}LTEWTSSNVMEER^{277}
1428.98	^{34}FESNFNTQATNR^{45}	1687.92	^{128}GGLEPINFQTAADQAR^{143}
1491.85	^{67}WWC*NDGRTPGSR^{73}	1709.90	^{256}LTEWTSSNVMEERK^{278}
1636.99	^{1}KVFGRC*ELAAAMKR^{14}	1774.02	^{324}ISQAVHAAHAEINEAGR^{340}
1676.10	^{98}IVSDGNGMNAWVAWR^{112}	1858.15	^{144}ELINSWVESQTNGIIR^{159}
1753.12	^{46}NTDGSTDYGILQINSR^{61}	2283.62	^{1}MGSIGAASMEFC*FDVFKELK^{20}
1804.15	^{97}KIVSDGNGMNAWVAWR^{112}	2284.59	^{201}VTEQESKPVQMMYQIGLFR^{219}
2181.53	^{15}HGLDNYRGYSLGNWVC*AAK^{33}	2460.89	^{160}NVLQPSSVDSQTAMVLVNAIVFK^{182}
2337.64	^{14}RHGLDNYRGYSLGNWVC*AAK^{33}	3033.51	^{21}VHHANENIFYC*PIAIMSALAMVYLGAK^{47}
2508.71	^{74}NLC*NIPC*SALLSSDITASVNC*AK^{96}	3238.05	^{341}EVVGSAEAGVDAASVSEEFRADHPFLFC*IK^{370}
2636.89	^{74}NLC*NIPC*SALLSSDITASVNC*AKK^{97}		
2735.84	^{22}GYSLGNWVC*AAKFESNFNTQATNR^{45}		
3164.15	^{34}FESNFNTQATNRNTDGSTDYGILQINSR^{61}		

Table S2: Number of matched peptides obtained by trypsin hydrolysis of lysozyme, dissolved in different buffers. On plate desalting methods on Vmh2 coating are compared with bare wells.

	Bare wells		Vmh2-coated wells	
Buffer	No desalting	On plate washing	No desalting	On plate washing
AMBIC	10	-	11	21
NaCl	9	-	9	18
Urea	8	-	7	17

Table S3: Comparison of matched peptides obtained by trypsin hydrolysis of 500 fmol of lysozyme dissolved in 2M urea, using different desalting methods.

Lysozyme		Desalting methods					
Signals (m/z)	sequences	No desalting	ZipTip µ–column	Paraffin-coating	Mineral oil-coating	Glycerol-coating	Vmh2-coating
505.30	126 -129			+			
517.36	69 -73						
606.86	1-5		+	+	+	+	
874.61	15-21	+	+	+	+	+	+
993.51	62-68	+	+	+	+	+	+
1030.62	14-21		+	+			+
1045.75	117- 125		+	+		+	+
1049.52	6-14			+			+
1333.56	115- 125	+	+	+	+	+	+
1428.98	34- 45	+	+	+	+	+	+
1491.85	67- 73	+	+	+	+		+
1636.99	1-14		+	+			+
1676.10	98 -112	+	+	+	+	+	
1753.12	46- 61	+	+	+	+	+	+
1804.15	97-112	+	+	+		+	+
2181.53	15-33		+		+	+	+
2337.64	14-33						+
2508.71	74-96		+		+		+
2636.89	74-97		+			+	+
2735.84	22-45						+
3164.15	34-61		+				+

Figure S1

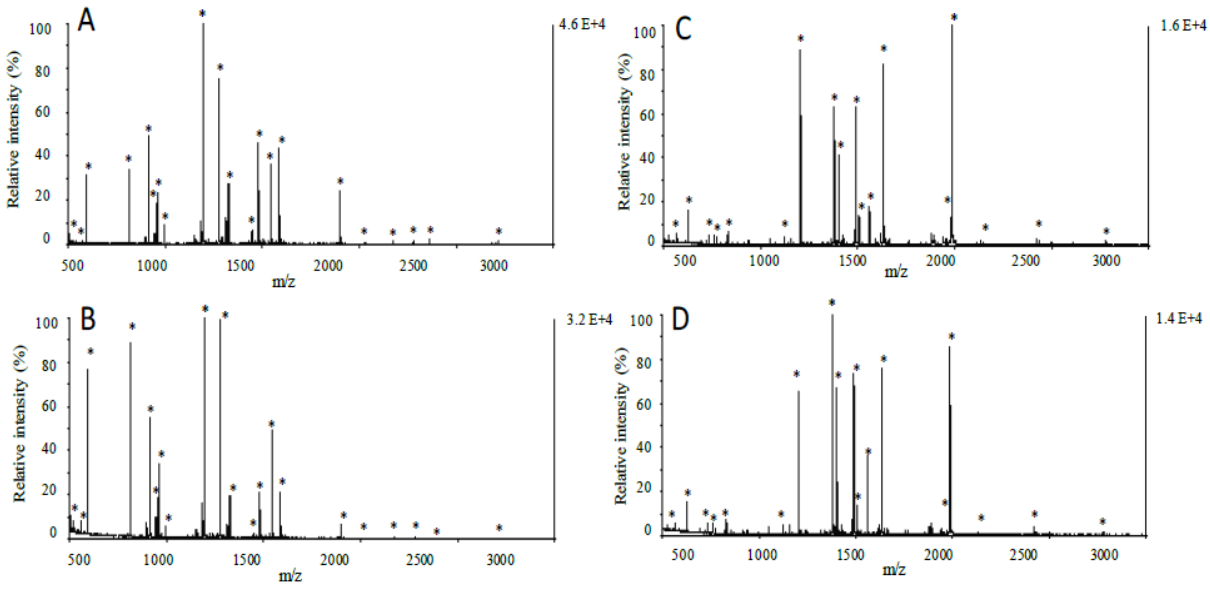

MALDI spectra of tryptic peptide: lysozyme on uncoated (A) and Vmh2-coated (B) wells; ovalbumin on uncoated (C) and Vmh2-coated (D) wells.

Figure S2

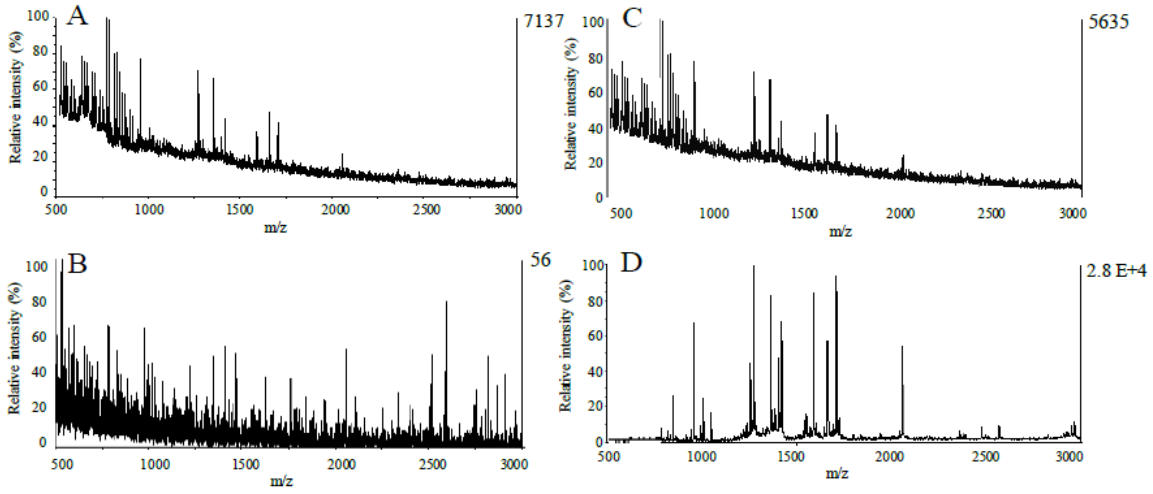

MALDI spectra of lysozyme tryptic peptides in 2M urea on uncoated (A) and Vmh2-coated (C) wells; after on-plate washing on uncoated (B) and Vmh2-coated (D) wells.

Anal Bioanal Chem (2015) 407:487–496
DOI 10.1007/s00216-014-8309-3

RESEARCH PAPER

A simple MALDI plate functionalization by Vmh2 hydrophobin for serial multi-enzymatic protein digestions

Sara Longobardi · Alfredo Maria Gravagnuolo · Riccardo Funari · Bartolomeo Della Ventura · Francesca Pane · Eugenio Galano · Angela Amoresano · Gennaro Marino · Paola Giardina

Received: 10 September 2014 / Revised: 28 October 2014 / Accepted: 30 October 2014 / Published online: 14 November 2014

Abstract The development of efficient and rapid methods for the identification with high sequence coverage of proteins is one of the most important goals of proteomic strategies today. The on-plate digestion of proteins is a very attractive approach, due to the possibility of coupling immobilized-enzymatic digestion with direct matrix-assisted laser desorption/ionization (MALDI)-time of flight (TOF)-mass spectrometry (MS) analysis. The crucial step in the development of on-plate immobilization is however the functionalization of the solid surface. Fungal self-assembling proteins, the hydrophobins, are able to efficiently functionalize surfaces. We have recently shown that such modified plates are able to absorb either peptides or proteins and are amenable to MALDI-TOF-MS analysis. In this paper, the hydrophobin-coated MALDI sample plates were exploited as a lab-on-plate for noncovalent immobilization of enzymes commonly used in protein identification/characterization, such as trypsin, V8 protease, PNGaseF, and alkaline phosphatase. Rapid and efficient on-plate reactions were performed to achieve high sequence coverage of model proteins, particularly when performing multiple enzyme digestions. The possibility of exploiting this direct on-plate MALDI-TOF/TOF analysis has been investigated on model proteins and, as proof of concept, on entire whey milk proteome.

This article is dedicated to the memory of Prof. Alessandro Ballio, a Master of Life and Science.

Electronic supplementary material The online version of this article (doi:10.1007/s00216-014-8309-3) contains supplementary material, which is available to authorized users.

S. Longobardi (✉) · A. M. Gravagnuolo · F. Pane · E. Galano · A. Amoresano · G. Marino · P. Giardina
Department of Chemical Sciences, University of Naples "Federico II", Via Cintia 4, 80126 Naples, Italy
e-mail: sara.longobardi@unina.it

R. Funari · B. Della Ventura
Department of Physics, University of Naples "Federico II", Via Cintia 4, 80126 Naples, Italy

Keywords Functional surface · Deglycosylation · Mass spectrometry · Posttranslational modifications · Self-assembling protein · Enzyme immobilization

Introduction

Mass spectrometry-based proteomics is currently the most valuable analytical tool for identification of proteins present in complex biological samples such as cell lysates, body fluids, or tissues [1]. In a typical bottom-up analytical strategy, proteins are enzymatically digested into peptide fragments, before a mass spectrometric (MS) analysis. Peptide mass mapping and MS/MS sequence analysis are key methods currently used in protein identification [2, 3]. It is generally considered that the in-solution digestion is the most time-consuming step in this workflow. The enzyme/substrate ratio has to be kept low (generally 1:50) to prevent protease autodigested products. For this reason, the incubation with free proteases is usually performed for 12–24 h at 37 °C to achieve an efficient proteolysis.

To try to address the demands of reducing digestion times, while maintaining high sequence coverage, immobilization of proteases onto a solid support has emerged as a promising alternative to the in-solution digestion. Immobilization leads to increased enzyme stability, reduced autolysis, and improved digestion efficiency due to the increased enzyme-to-protein ratio [4–6]. Trypsin is the most widely used enzyme in proteomics [7–10], particularly due to its restricted specificity (Arg-X, Lys-X) [11]. Several methods for trypsin immobilization have been explored, such as adsorption [12–15], encapsulation [16, 17], and covalent binding [18, 19]. Different materials (such as silica, PTFE, magnetic nanoparticles, and so on) have also been tested for both offline digestion and microfluidic devices [20–23].

Despite the many advantages of trypsin, the use of other proteases or other enzymes is often necessary. Tryptic digestion can often result in limited sequence coverage [24] because of the following: (i) lack or excess of Lys and Arg residues, (ii) length of the digested fragments due to missed cleavages, and (iii) the presence of posttranslational modification (i.e., phosphorylation and glycosylation) which can affect the extent of digestion and/or lower the ionization efficiency. To overcome these potential issues, the use of other enzymes, including pepsin [25, 26] chymotrypsin [27, 28], and alkaline phosphatase [28], has been suggested.

The application of matrix-assisted laser desorption/ionization (MALDI)-time of flight (TOF) on-plate digestion is a very attractive strategy due to the possibility of coupling immobilized-enzymatic reactions with direct mass spectrometry analysis [29–31]. However, to the best of our knowledge, no multi-enzymatic digestion directly on MALDI plate has so far been reported. The crucial step in development of on-plate enzyme immobilization is in reality the functionalization of the solid surface.

Design and realization of stable bio/non-biointerfaces able to immobilize biomolecules are key features in several processes. In particular, protein immobilization on surfaces is currently a hot topic in biotechnology, since commercial solutions are of limited availability. It is worth considering that it is extremely difficult to find a common surface suitable for the adsorption of different proteins having a broad range of molecular weights and physicochemical properties, such as charge and hydrophobicity [32].

Recent studies from our research group have demonstrated an efficient surface functionalization by means of a nanostructured layer of amphiphilic proteins, named hydrophobins [33].

Hydrophobins are a family of small amphipathic proteins produced by filamentous fungi, able to self-assemble on hydrophobic or hydrophilic solid surfaces [34]. Due to their interesting properties, several biotechnological applications have been reported [35–37]. In particular, hydrophobin coating has been used as an intermediate layer to attach cells, proteins, or other biomolecules to surfaces for development of several biotools such as biosensors [38–41]. However, the mechanism of binding of proteins to hydrophobin-coated surfaces is still a matter of discussion [40].

A class I hydrophobin secreted by the basidiomycete fungus *Pleurotus ostreatus* (Vmh2) has been extensively studied in our lab [42]. We have demonstrated that Vmh2 spontaneously forms a stable and homogeneous layer on hydrophilic or hydrophobic surfaces, which are able to strongly bind proteins, including enzymes in their active form [33]. Recently, we reported a novel surface biofunctionalization of steel MALDI sample plates by self-assembling of Vmh2, for on-plate high-throughput desalting of proteins and peptides in real samples and offline coupled with MS analysis [43]. No background interference due to Vmh2 molecular ion signals was detected in any mass range, possibly because of the low amount of protein in the nanometric layer. This low-cost, fast, and environmentally friendly strategy allows a remarkable increase of the signal-to-noise ratio of the MALDI mass spectra. Following on from these results, we have investigated a strategy aimed at including the proteolytic steps on the hydrophobin-coated MALDI sample plate. It is worth considering that only few examples of phosphatase or deglycosidase immobilization are reported [28, 44, 45] in comparison with the ample literature concerning trypsin immobilization. As proof of concept, we have used trypsin, V8 protease, PNGaseF, and alkaline phosphatase to achieve high sequence coverage of model proteins, particularly when performing multiple enzyme digestions. Moreover, the possibility of exploiting this technique coupled to MALDI-TOF/TOF sequencing has been applied on both model proteins and on the entire whey milk proteome.

Experimental section

Materials Nα-p-tosyl-L-arginine methyl ester hydrochloride (TAME), lysozyme from chicken egg white, ovalbumin from chicken egg white, α-casein and β-casein from bovine milk were purchased from Sigma (St. Louis, MO, USA). Recombinant human erythropoietin (rhEPO) was purchased in pharmacy (α-darbepoetin from Amgem). Laccase phenol oxidase C (POXC) was purified from cultural broth of *P. ostreatus* (type: Florida no. MYA-2306) [46]. PD-10 desalting columns were purchased from GE Healthcare (Milan, Italy). Calibration mixtures were obtained from AB SCIEX (Framingham, MA, USA).

Stock enzyme solutions Trypsin from bovine pancreas, bovine alkaline phosphatase, and V8 protease were purchased from Sigma (St. Louis, MO, USA). PNGaseF was purchased from Roche. Trypsin stock solution was prepared at 6 mg mL^{-1} in 0.1 % formic acid. The specific activity using TAME as substrate was about 500 U mg^{-1}. Alkaline phosphatase was diluted at 1 U μL^{-1} in 5 mM Tris, 5 mM $MgCl_2$, and 0.1 mM $ZnCl_2$, pH 7.0. PNGaseF was used undiluted (1 U μL^{-1}). V8 protease was dissolved in 0.1 M ammonium bicarbonate, pH 8.0, at 0.5 U μL^{-1}. One unit is defined as the amount of enzymatic activity converting 1 μmol of substrate per minute.

Vmh2 purification Vmh2 was prepared from *P. ostreatus* mycelia as previously described [42]. Preparation basically consists in growing mycelia at 28 °C in static cultures in 2-L flasks containing 500 mL of potato dextrose (24 g/L) broth with 0.5 % yeast extract. After 10 days of fungal growth, hydrophobins released into the medium were aggregated by air bubbling using a Waring blender and collected by centrifugation at 4,000×*g*. The precipitate was freeze dried, left to dissolve under mechanical agitation with trifluoroacetic acid

(TFA) for 2 h, and treated in bath sonicator (operating at 35 kHz and at 240 W) for 30 min. The TFA solution was dried in a stream of air and Vmh2 dissolved in 60 % ethanol, resulting in a stock solution (100 μg mL^{-1}) which was used for further experiments.

Functionalization of steel surface Vmh2-coated steel was prepared and characterized as previously reported [43]. Briefly, 1 μL of Vmh2 solution was spotted on each MALDI plate well. After 1 h, samples were dried for 10 min at 80 °C and washed with 60 % ethanol. Deposition was repeated twice and finally the plate was washed with 2 % SDS at 100 °C for 10 min. The coated MALDI wells were used to noncovalently immobilize a set of four enzymes, usually employed in proteomics. In our current experience, the same coated plate has been used still after 3 weeks storage at room temperature. For trypsin adsorption, the enzyme was diluted in 0.1 % formic acid at different concentrations (from 0.3 to 6 mg mL^{-1} corresponding to 0.15–3 U mL^{-1}). One microliter of these solutions was spotted on Vmh2-coated wells. After 5-min incubation at room temperature, wells were washed three times to remove the excess of enzyme. The adsorbed trypsin was characterized and employed for further experiments. For alkaline phosphatase, PNGaseF, and V8 protease, 1 μL of enzyme stock solutions was spotted on Vmh2-coated wells and immobilized following an identical procedure. Since the immobilization is a very rapid step, we have routinely used freshly immobilized enzymes, to perform the required hydrolytic reaction.

Mass spectral determination of immobilized trypsin activity The enzymatic activity of trypsin in solution was spectrophotometrically determined at 247 nm with 10 mM TAME as a substrate in 50 mM Tris–HCl pH 8.0, by using Beckman DU 7500 spectrophotometer (Beckman Instruments). For quantitative analysis of TAME converted by on-plate trypsin, liquid chromatography–tandem quadrupole mass spectrometry (LC–MS/MS) in the multiple reaction monitoring (MRM) was performed by using a 6420 triple Q system with a HPLC 1100 series binary pump (Agilent, Waldbronn, Germany). The analytical column was a Phenomenex Kinetex 5u 100 A C18. The mobile phase was generated by mixing eluent A (2 % acetonitrile (ACN) and 0.1 % formic acid) and eluent B (95 % ACN and 0.1 % formic acid) and the flow rate was 0.200 mL min^{-1}. The HPLC gradient was from 5 to 95 % B in 8 min then to 100 % for 2 min. Standard solutions were prepared by dissolving the equivalent of 1 mg of TAME in 1 mL of methanol. A standard solution of 500 pg μL^{-1} of each metabolite was used for optimization of the MRM transition. The ideal mass spectrometric parameters for detection were determined via MassHunter Optimizer software, resulting in 343.43 *m/z* as precursor ion, 91.1 and 65.1 *m/z* product ions, and 48 and 92 V optimized voltages.

Quartz crystal microbalance (QCM) determination of immobilized trypsin amount The QCM device is a μLibra from Technobiochip, Italy, and the resonance frequency of the oscillating crystal is monitored by a producer-released software. The oscillators (151218) are AT-CUT quartz with a fundamental frequency of 10 MHz purchased from ICM Oklahoma City (USA). The diameters of the crystal and of the gold sensitive surface are 1.37 and 0.68 cm, respectively. Before the functionalization with Vmh2, the electrodes were cleaned using piranha solution (5:1 sulfuric acid/40 % hydrogen peroxide solution) thus removing any impurity and organic compound from the gold plates. Then, in order to test the Vmh2–trypsin interaction, the protein-coated oscillator is placed in a microfluidic apparatus consisting of the cell which contains the crystal, a GILSON peristaltic pump, and Tygon silicone tubes. The volume of the circuit is 300 μL, while the flow rate is about 50 μL min^{-1}. The volume of the sample to test is 1 mL. Using this experimental setup, it was possible to estimate the amount of trypsin adsorbed onto the Vmh2-coated gold surface at several enzyme concentrations.

Substrate preparation Lysozyme, ovalbumin, POXC, α-darbepoetin, and whey milk proteins were dissolved at 5 μM in 0.5 M Tris–HCl pH 8.0 containing 6 M guanidinium chloride, then reduced in 10 mM dithiothreitol for 2 h at 37 °C, and carboxamidomethylated in 50 mM iodoacetamide for 30 min, in the dark, at room temperature. Samples were desalted on a PD10 column using 10 mM NH_4HCO_3 (AMBIC) as eluting buffer. Fractions containing proteins were pooled and lyophilized before the analyses.

In-solution hydrolysis Trypsin (substrate/enzyme ratio, 50:1 *w/w*) was added to the aliquots of denatured proteins and incubated for 18 h at 37 °C. Then, the reactions were stopped by adding 0.1 % formic acid. Three microliters of stock enzyme solutions was added to the aliquots of boiled tryptic hydrolyzed samples.

Setting up on-plate hydrolysis One microliter of denatured proteins in 10 mM AMBIC was spotted on Vmh2-adsorbed enzyme wells. In the case of trypsin, reaction was carried out for 5 min, 10 min, 3 h, 6 h, or 18 h at room temperature, in a wet atmosphere. The reaction was stopped by addition of matrix solution, α-cyano-4-hydroxycinnamic acid (CHCA) (10 mg mL^{-1} in acetonitrile/0.1 % TFA 7/3 (*v/v*)). Once having set up the best reaction time (see "Results and discussion" section), the serial reactions (trypsin-alkaline phosphatase, trypsin-PNGaseF, and trypsin-V8 protease) were carried out as above described for trypsin (1 μL, 5 min).

MALDI-MS analysis MALDI-TOF/MS spectra were acquired by a Voyager-DE STR MALDI-TOF mass spectrometer (Applied Biosystems, Framingham, MA, USA) equipped

with a nitrogen laser (337 nm). Peptides were detected in reflector mode using CHCA as matrix. Spectra were acquired using a mass range of 500–5,000 amu. Acceleration and voltages were set up as follows: target voltage at 20 kV, grid at 66 % of target voltage, and delayed extraction at 150 ns to obtain the best signal-to-noise (*S*/*N*) ratios and the best possible isotopic resolution. Spectra were accumulated in multiples of 50 laser shots, with 50–2,000 shots in total. The molecular weight standards for the calibration of the Voyager-DE STR system were AB SCIEX calibration mixtures 1 and 2.

MS/MS experiments were carried out on a 4800 Plus MALDI-TOF/TOF™ Analyzer AB SCIEX. All acquisitions were generated automatically in the instrument software and based on averaging 500 shots per spectrum, with 1,000–2,000 shots in total.

Results and discussion

Trypsin immobilization on hydrophobin-coated MALDI sample wells

The ability of the Vmh2-coated MALDI sample plates to bind peptides and proteins has been previously demonstrated [43]. In this work, the most commonly used enzymes in proteomic research, including posttranslational demodifying enzymes, have been adsorbed on this layer and their performances have been exploited.

Preliminary experiments were aimed at evaluating the catalytic activity of the enzyme which was actually adsorbed. Because of the low sensitivity of the spectrophotometric assay, a mass spectrometry method was set up, by using LC–MS/MS MRM ion mode [47]. Two micrograms of trypsin was deposited on the Vmh2 layer and left standing for 5 min. After thoroughly washing the wells with repeated aliquots of 0.1 % formic acid followed by equilibration with AMBIC, the TAME assay was performed. TAME was completely converted in less than 30 s, thus qualitatively indicating that the adsorbed trypsin was fully active. Since we reached the TAME solubility limit (40 mg mL^{-1}), quantitative activity data were obtained by depositing 1 μg of enzyme. Results demonstrated that about 0.1 μmol of substrate was hydrolyzed in 1 min, indicating that 0.1 U of trypsin per well was immobilized. Since Vmh2-coated well surface was equivalent to 7 mm^2, the activity/surface ratio was 14 mU mm^{-2}.

To evaluate the actual amount of trypsin adsorbed on a Vmh2 layer, QCM was used [48]. The QCM gold sensor was coated with hydrophobin, taking into consideration that the physical characteristics of the Vmh2 layer on the gold surface are quite similar to those observed on the steel plate (data not shown). After coating, three different amounts of trypsin (1, 3, and 5 μg in 1 mL of 0.1 % formic acid) were tested by monitoring the resonance frequency of the crystal after the injection of the sample in the fluidic circuit. Since the frequency shifts (Δf) are related to the amount of material adsorbed on sensor [49], we were able to extrapolate the weight of enzyme immobilized. Results (see Electronic Supplementary Material (ESM) Fig. S1) indicated that 100, 220, and 250 ng of enzyme were, respectively, adsorbed, corresponding to 3, 6, and 7 ng mm^{-2}, thus suggesting that the latter value approximately corresponds to that of saturation of the functionalized surface.

In order to evaluate the enzyme-specific activity, we took into account that the QCM gold sensor surface (36 mm^2) is about fivefold wider than that of the MALDI sample plate well (7 mm^2). The specific activity was calculated by dividing the enzyme activity measured by MRM analysis (14 mU mm^{-2}) with the weight measured by QCM (7 ng mm^{-2}), values obtained incubating the same amount of enzyme per square millimeter. Hence, the specific activity of immobilized trypsin was considered to be about 2,000 U mg^{-1}, some fourfold higher than that of the free form. This increase may be ascribed to a greater accessibility of substrate molecules to active sites of immobilized enzyme as reported elsewhere [50, 51].

Protein digestion by on-plate immobilized trypsin

To test the performance of trypsin immobilized on Vmh2-coated MALDI wells, lysozyme and ovalbumin were used as reference proteins. After reduction, carbamidomethylation, and desalting, protein samples were spotted on the trypsin-immobilized wells and incubated for 5 min, 10 min, 3 h, 6 h, or 18 h at room temperature.

Spectra obtained (Fig. 1) showed that the on-plate immobilized trypsin was able to extensively hydrolyze the denatured proteins after 5 min of incubation. As expected, no digestion was observed in the absence of the Vmh2 coating. Eleven unique peptides for lysozyme and 15 unique for ovalbumin (ESM Table S1) were identified, allowing 90 and 60 % of sequence coverage, respectively (ESM Table S2). No improvement of sequence coverage was observed with increases in incubation time, even after incubating for 18 h. It is noteworthy that the spectra used for peptide mapping were recorded without any further sample manipulation. Indeed, the reaction was stopped by addition of the appropriate matrix solution, and spectra were recorded immediately after drying in ambient atmosphere. Therefore, the performance of on-plate trypsin was comparable to that of conventional in-solution digestion (18 h at 37 °C) (ESM Fig. S2) but with a very significant reduction in reaction and sample workup time (about 2 h for plate preparation, which can be used even for 100 hydrolysis, and 5 min for the reaction). These results could be ascribed to the in situ high enzyme/substrate ratios (about 1:1) with respect to those commonly used. In the conventional (in solution) method, this ratio is kept low

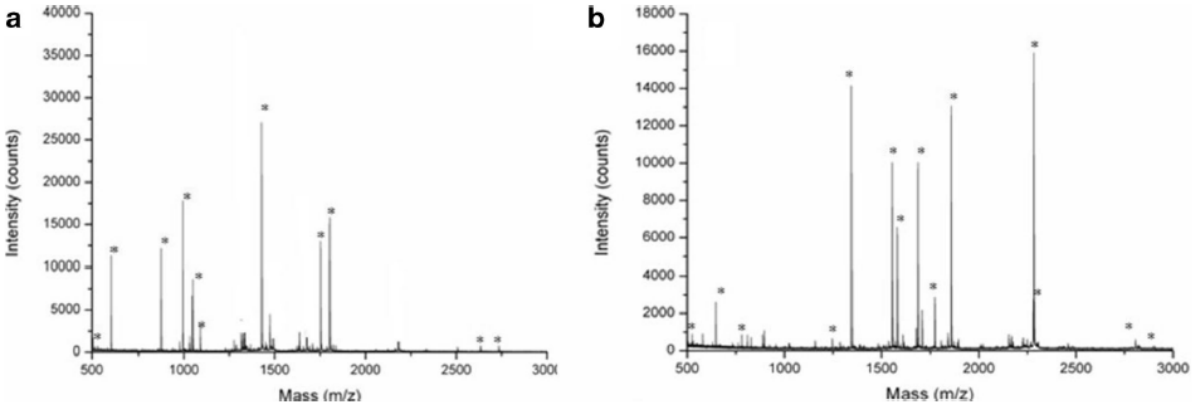

Fig. 1 MALDI spectra of lysozyme (**A**) and ovalbumin (**B**) after 5 min of on-plate hydrolysis. The assigned signals are marked with *asterisks*. List of peptides with their *m/z* values is reported in ESM Table S1

(generally 1:50 *w/w*) to prevent excessive formation of autodigested products. In the reported on-plate method, rapid and efficient proteolysis was achieved with undetectable autodigestion products. As matter of fact, no detectable autoproteolysis product or Vmh2 tryptic peptides were observed in any of the tested conditions (ESM Fig. S3). The absence of autoproteolysis products can be due to the restricted accessibility of an immobilized trypsin molecule to the active site of another one. As expected, Vmh2 was not digested by trypsin because the lone basic amino acid residue is probably hidden in the very compact structure of the layer.

In order to evaluate the reproducibility of the methodology, 10 replicates of each sample were prepared and the MALDI mass spectrometer was set in automatic mode. Spectra accumulated in multiples of 200 laser shots in 10 random positions of the well (2,000 shots in total) were compared. Peaks/spectrum (12.1±0.6) related to lysozyme were detected (1.8 standard deviation). Moreover, all the replicate allowed to obtain the same sequence coverage, thus indicating the reproducibility of these analyses.

Immobilization of other enzymes and on-plate serial reactions

The ionization efficiency of a digested fragment depends on its size, sequence, and, possibly, posttranslational modifications, all factors affecting sequence coverage of the target protein by MS analysis. Therefore, digestion with other proteases, the removal of posttranslational modifications by suitable enzymes, such as phosphatases or deglycosidase often have to be performed to increase the sequence coverage and/or the general sensitivity of the analysis.

Our previous results suggest that the Vmh2 layers are able to bind proteins irrespective of their molecular weights or physicochemical properties [43]. Therefore, once the use of immobilized trypsin was assessed, the on-plate immobilization of other enzymes commonly used in proteomic research was tested in order to further improve sequence coverage, eventually exploiting multiple hydrolysis experiment on the same plate.

V8 protease, N-glycosidase F, and alkaline phosphatase (1 μL of stock solutions) were loaded on Vmh2-coated MALDI wells, using the same procedure described for trypsin. We did not attempt any further investigation on the on-plate enzyme activity as we did in the case of trypsin and directly tested the performance of these enzymes on protein substrates: ovalbumin for V8, ovalbumin and POXC laccase for PNGaseF, and α-casein and β-casein from bovine milk for alkaline phosphatase. Substrate proteins were hydrolyzed first by on-plate immobilized trypsin and then the tryptic digests were transferred by pipetting about 0.8÷0.9 μL on the appropriate immobilized enzyme wells and incubated for 5 min.

Results of V8 activity on the ovalbumin tryptic hydrolyzed are shown in Fig. 2. The detection of 11 new peaks (marked with asterisks) due to the expected hydrolysis after Asp and Glu demonstrated that the enzyme was active and able to hydrolyze the substrate in some 5 min.

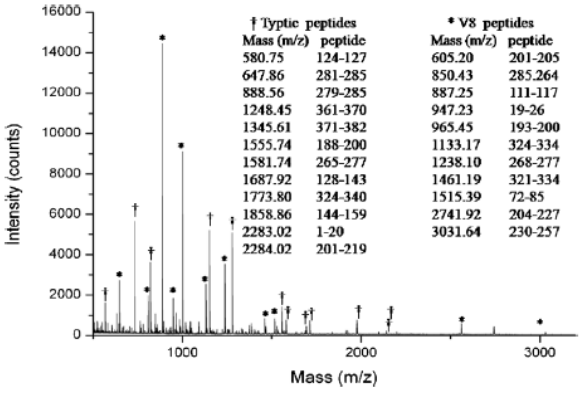

Fig. 2 MALDI-TOF spectra of ovalbumin after trypsin-V8 on-plate hydrolysis. Eleven new peptides that appeared after V8 digestion are marked with *asterisks* and reported in the *inset table*

The performance of immobilized PNGaseF was tested using ovalbumin and POXC laccase (Fig. 3). In the case of ovalbumin, a new signal appeared at 3,294.44 *m/z* which can be attributed to the peptide 292-323 lacking the glycosidic moiety, where Asn293 has been converted into Asp by the PNGaseF reaction. Similarly, in the case of laccase POXC, a new signal appeared at 1,646.77 *m/z* which can be attributed to the peptide 433-448 without glycosidic moiety and with Asn 444 converted into Asp[46]. The identity of these peptides was confirmed by MALDI-TOF/TOF analysis (an example of MS/MS spectra is reported in ESM Fig. S4).

Caseins from bovine milk are phosphoproteins with well-characterized phosphorylated sites [52]. Phosphopeptides are not easily detectable by using MALDI mass spectrometer in positive ion mode, due to the presence of negative charges. Spectra recorded after 5 min of phosphatase reaction on the tryptic peptides showed the presence of the α-casein peptides containing the Ser130-dephosphorylated, 119-134 and 121-134 (1,871.92 and 1,580.76 *m/z*, respectively), and β-casein-dephosphorylated peptide 1-25 (2,802.34 *m/z*) (Fig. 4), confirmed by MALDI-TOF/TOF analysis. Even in this case, tryptic digestion and dephosphorylation were performed in a total time of 10 min.

Since the setup method gives us the opportunity to perform a number of on-plate reactions in very short times, it can be exploited to achieve an even higher sequence coverage of proteins by multiple hydrolytic steps. In addition to the N-glycosylation site at Asn293, ovalbumin has a phosphorylation site at Ser69. As reported above, a 60 % of sequence coverage was achieved after trypsin hydrolysis. When trypsin-digested samples were incubated for 5 min on V8, PNGaseF, and phosphatase-immobilized wells, respectively, new peptides were generated: four new unique peptides (605.43, 850.50, 2,741.48, 3,031.64 *m/z*; peptides 201-205, 258-264, 204-227, 230-257, respectively) by V8 reaction (see Fig. 2), one peptide (3,294.45 *m/z*; peptide 292-323) by PNGaseF reaction, and one peptide (2,282.45 *m/z*; peptide 60-85) by phosphatase reaction, allowed to increase the sequence coverage to some 85 %.

The effectiveness of the setup method has also been tested on a real sample of pharmaceutical interest. α-Darbepoetin is a second-generation rhEPO with five modified amino acids

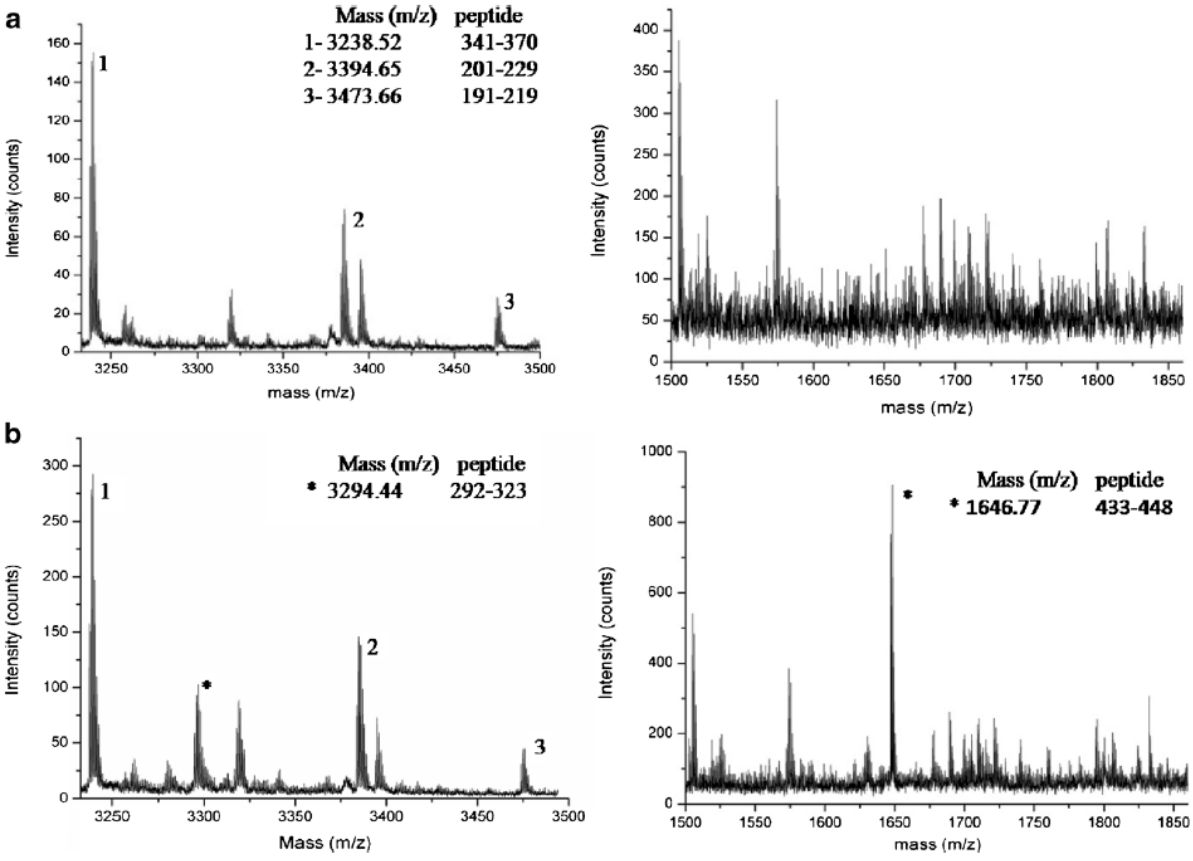

Fig. 3 Section of MALDI-TOF spectra of ovalbumin (*on the left*) and POXC (*on the right*) tryptic peptides, before (**A**) and after (**B**) on-plate deglycosylation. Deglycosylated peptides are marked with *asterisks*

3.1.2. A Simple MALDI Plate Functionalization by Vmh2 Hydrophobin for Serial Multi-enzymatic Protein Digestions

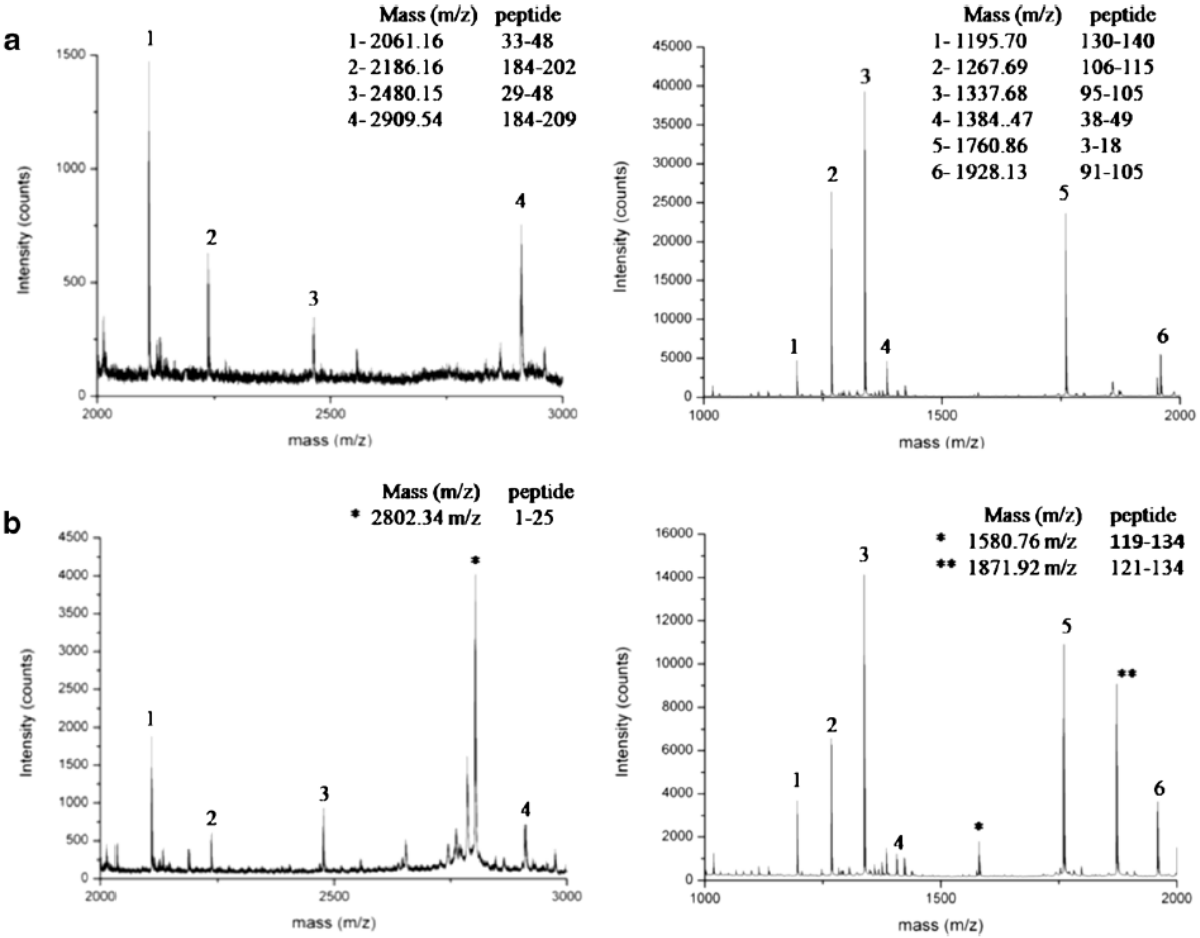

Fig. 4 Section of MALDI-TOF spectra of β-casein (*on the left*) and α-casein (*on the right*) tryptic peptides, before (**A**) and after (**B**) on-plate dephosphorylation. Dephosphorylated peptides are marked with *asterisks*

Table 1 List of unique peptides of rhEPO obtained by on-plate coupled hydrolysis

Signals (*m/z*)	Start	End	Sequences	Trypsin	Trypsin + PNGase	PNGase + trypsin
1,184.68	1	10	(−)APPRLIC*DSR(V)	+	+	+
516.42	11	14	(R)VLER (Y)	+	+	+
736.48	15	20	(R)YLLEAK (E)	+	+	+
2,815.66	21	45	(K)EAE**NI**TTGC***NE**TC*SLNE**NI**TVPDTK(V)			+
1,083.90	46	53	(K)VNFYAWKR(M)			+
2,526.70	54	76	(R)MEVGQQAVEVWQGLALLSEAVLR (G)	+	+	+
2,295.27	77	97	(R)GQALLV**NS**SQV**NE**TLQLHVDK (A)		+	+
602.45	98	103	(K)AVSGLR(S)			+
803.60	104	110	(R)SLTTLLR(A)			+
1,465.93	117	131	(K)EAISPPDAASAAPLR(T)			+
1,052.68	132	140	(R)TITADTFRK(L)	+	+	+
2,481.24	117	140	(K)EAISPPDAASAAPLRTITADTFRK(L)	+	+	+
563.44	140	143	(R)KLFR(V)	+	+	+
2,274.32	144	162	(R)VYSNFLRGKLKLYTGEAC*R(T)	+	+	+

Glycosylation sites are presented in bold

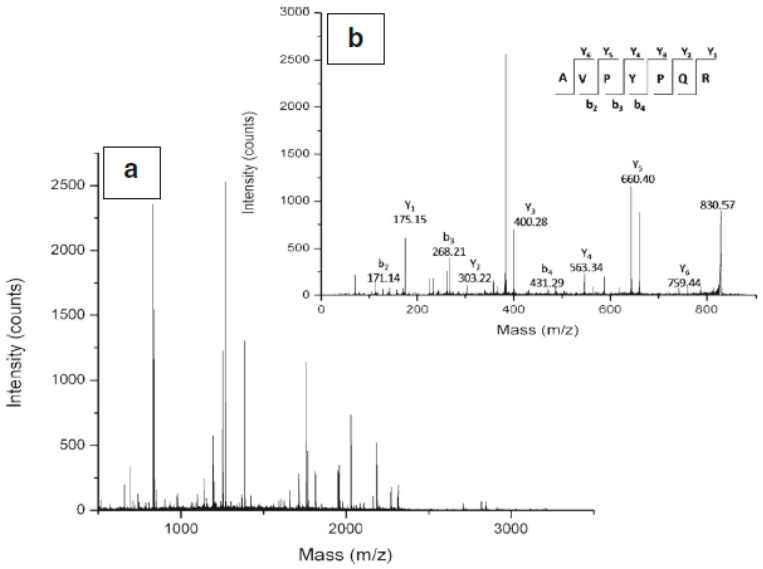

Fig. 5 MALDI-TOF/TOF spectrum of milk proteins after on-plate digestion (**A**). Panel **B** shows the MS/MS spectrum of precursor peptide 830.57 *m/z* (192–198) of β-casein peptide

(Ala30Asn, His32Thr, Pro87Val, Trp88Asn, and Pro90Thr). These amino acidic substitutions insert other two N-glycosylation sites (in addition to the three N-glycosylation sites of human EPO) at positions Asn30 and Asn88. Hyperglycosylation enhances serum half-life, reducing frequency of injections [53]. The presence of high content of carbohydrates, typically tetra-antennary N-glycans containing up to four sialic acids [54], may interfere with proteolysis and MALDI/MS analysis. For this reason, an on-plate digestion protocol for mapping of rhEPO was ad hoc set up. Coupled reactions were performed as already described, and MALDI spectra were acquired after deglycosylation–tryptic digestion or tryptic digestion–deglycosylation steps and compared. Results (Table 1) showed that, when deglycosylation was performed after trypsin hydrolysis, only one deglycosylated peptide was observed (peptide 77-97, two glycosylation sites), while the peptide 21-45 (three glycosylation sites) as well as regions downstream of the glycosylated peptides were not detected. On the other hand, higher sequence coverage (up to 94 %) was obtained when the deglycosylation step was performed prior to trypsin digestion.

Milk proteins

In order to verify the feasibility of our strategy of on-plate coupled reactions on a complex biological sample, whey milk proteins were analyzed. After acetone precipitation, proteins were suspended in denaturing buffer, then were reduced and carbamidomethylated. Finally, samples were incubated for 5 min at room temperature on immobilized trypsin wells. MALDI spectra showed the presence of 48 signals related to 9 milk proteins (ESM Table S3). Because of the complexity of these spectra, the same experiment was performed on MALDI-TOF/TOF plate. Amino acidic sequences of peptides were determined by MS/MS analysis, allowing us to unequivocally identify these proteins. In Fig. 5, the MALDI spectrum of tryptic digested milk proteins is reported, together with an

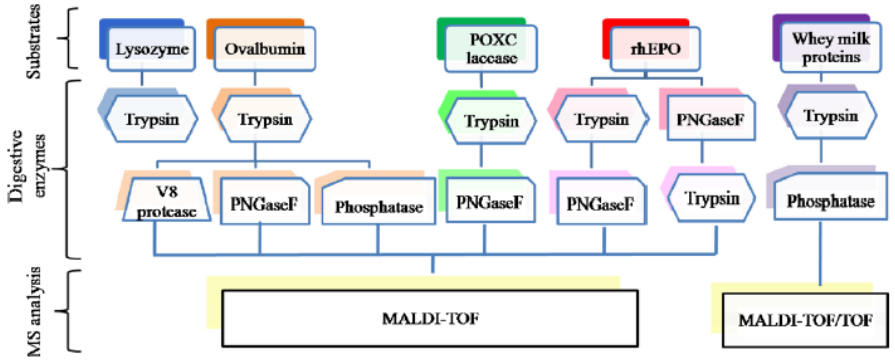

Fig. 6 A graphical overview of the workflow

example of MS/MS spectrum. It is worth noting that some of them are among the less abundant milk proteins.

Whey milk is rich in phosphoproteins (caseins); thus, denatured samples were incubated on trypsin-immobilized well and then on alkaline phosphatase-immobilized well. Spectra acquired after double-reaction steps showed the presence of the expected dephosphorylated peptides for α-casein (1,871.92 *m/z*), and β-casein (2,802.34 *m/z*), confirmed by MS/MS analysis. Results showed that both immobilized enzymes were able to carry out their function in 10 min even in complex samples.

Conclusions

Efficient, fast, and reproducible protein digestion is of utmost importance in bottom-up proteomics. Albeit several trypsin-immobilized systems have been developed for proteolysis, only few studies have described multi-enzymatic immobilized systems [28] and analysis of posttranslational modification in proteins [44, 45]. Our approach is based on the formation of a protein layer on the MALDI sample plate formed by the self-assembling fungal protein hydrophobin. We have demonstrated that this layer is able to immobilize different enzymes involved in proteomic studies, providing a simple and rapid procedure for the analysis of protein sequences, including posttranslational modifications. Several advantages of this in situ procedure can easily be envisaged: (i) rapid analysis, with a reduction of digestion time to few min; (ii) use of very low sample volumes, in the order of magnitude of some microliters; (iii) multi-proteolysis steps directly on the same MALDI sample plate, and (iv) posttranslational modification analysis, thanks to the opportunity of immobilization of different enzymes on the same system. As a consequence, very high sequence coverage has been obtained. Using MALDI-TOF/TOF, the strategy can be extended to protein identification/characterization in complex proteomes, through peptide mass fingerprinting or (selected) peptide sequencing. The potential of this method can be greatly exploited by immobilizing other enzymes and/or setting ad hoc protocols for specific proteins using a combination of proteases and other posttranslational demodifying enzymes (Fig. 6). The demonstration of achieving an almost complete sequence coverage of rhEPO merely by using two immobilized enzymes is highly significant. The strategy demonstrated in this paper can be further developed to be fully automated thus leading to a high-throughput proteome lab-on-plate platform.

Acknowledgments This work was supported by grant from the Ministero dell'Università e della Ricerca Scientifica-Industrial Research Project "Integrated agro-industrial chains with high energy efficiency for the development of eco-compatible processes of energy and biochemicals production from renewable sources and for the land valorization (EnerbioChem)" PON01_01966, funded in the frame of Operative National Programme Research and Competitiveness 2007–2013 D. D. Prot. n. 01/Ric. 18.1.2010.

References

1. Angel TE, Aryal UK, Hengel SM et al (2012) Mass spectrometry-based proteomics: existing capabilities and future directions. Chem Soc Rev 41:3912–3928. doi:10.1039/c2cs15331a
2. Yamaguchi H, Miyazaki M (2013) Enzyme-immobilized reactors for rapid and efficient sample preparation in MS-based proteomic studies. Proteomics 13:457–466. doi:10.1002/pmic.201200272
3. Aebersold R, Mann M (2003) Mass spectrometry-based proteomics. Nature 422:198–207. doi:10.1038/nature01511
4. Switzar L, Giera M, Niessen WMA (2013) Protein digestion: an overview of the available techniques and recent developments. J Proteome Res 12:1067–1077. doi:10.1021/pr301201x
5. Massolini G, Calleri E (2005) Immobilized trypsin systems coupled on-line to separation methods: recent developments and analytical applications. J Sep Sci 28:7–21. doi:10.1002/jssc.200401941
6. Girelli AM, Mattei E (2005) Application of immobilized enzyme reactor in on-line high performance liquid chromatography: a review. J Chromatogr B Analyt Technol Biomed Life Sci 819:3–16. doi:10.1016/j.jchromb.2005.01.031
7. Vestling MM, Fenselau C (1994) Poly(vinylidene difluoride) membranes as the interface between laser desorption mass spectrometry, gel electrophoresis, and in situ proteolysis. Anal Chem 66:471–477. doi:10.1021/ac00076a009
8. Sun J, Hu K, Liu Y et al (2013) Novel superparamagnetic sanoparticles for trypsin immobilization and the application for efficient proteolysis. J Chromatogr B Analyt Technol Biomed Life Sci 942–943:9–14. doi:10.1016/j.jchromb.2013.10.015
9. Bao H, Zhang L, Chen G (2013) Immobilization of trypsin via graphene oxide-silica composite for efficient microchip proteolysis. J Chromatogr A 1310:74–81. doi:10.1016/j.chroma.2013.08.040
10. Fan C, Shi Z, Pan Y et al (2014) Dual matrix-based immobilized trypsin for complementary proteolytic digestion and fast proteomics analysis with higher protein sequence coverage. Anal Chem 86:1452–1458. doi:10.1021/ac402696b
11. Brownridge P, Beynon RJ (2011) The importance of the digest: proteolysis and absolute quantification in proteomics. Methods 54:351–360. doi:10.1016/j.ymeth.2011.05.005
12. Liu Y, Lu H, Zhong W et al (2006) Multilayer-assembled microchip for enzyme immobilization as reactor toward low-level protein identification. Anal Chem 78:801–808. doi:10.1021/ac051463w
13. Liu Y, Zhong W, Meng S et al (2006) Assembly-controlled biocompatible interface on a microchip: strategy to highly efficient proteolysis. Chemistry 12:6585–6591. doi:10.1002/chem.200501622
14. Gao J, Xu J, Locascio LE, Lee CS (2001) Integrated microfluidic system enabling protein digestion, peptide separation, and protein identification. Anal Chem 73:2648–2655
15. Qiao L, Liu Y, Hudson SP et al (2008) A nanoporous reactor for efficient proteolysis. Chemistry 14:151–157. doi:10.1002/chem.200701102
16. Min Q, Zhang X, Wu R et al (2011) A novel magnetic mesoporous silica packed S-shaped microfluidic reactor for online proteolysis of low-MW proteome. Chem Commun (Camb) 47:10725–10727. doi:10.1039/c1cc13969j
17. Qu H, Wang H, Huang Y et al (2004) Stable microstructured network for protein patterning on a plastic microfluidic channel: strategy and characterization of on-chip enzyme microreactors. Anal Chem 76:6426–6433. doi:10.1021/ac049466g
18. Lee J, Musyimi HK, Soper SA, Murray KK (2008) Development of an automated digestion and droplet deposition microfluidic chip for

MALDI-TOF MS. J Am Soc Mass Spectrom 19:964–972. doi:10.1016/j.jasms.2008.03.015
19. Kim BC, Lopez-Ferrer D, Lee S-M et al (2009) Highly stable trypsin-aggregate coatings on polymer nanofibers for repeated protein digestion. Proteomics 9:1893–1900. doi:10.1002/pmic.200800591
20. Dodds ED, Seipert RR, Clowers BH et al (2009) Analytical performance of immobilized pronase for glycopeptide footprinting and implications for surpassing reductionist glycoproteomics. J Proteome Res 8:502–512. doi:10.1021/pr800708h
21. López-Ferrer D, Hixson KK, Smallwood H et al (2009) Evaluation of a high-intensity focused ultrasound-immobilized trypsin digestion and 18O-labeling method for quantitative proteomics. Anal Chem 81:6272–6277. doi:10.1021/ac802540s
22. Casadonte F, Pasqua L, Savino R, Terracciano R (2010) Smart trypsin adsorption into N-(2-aminoethyl)-3-aminopropyl-modified mesoporous silica for ultra fast protein digestion. Chemistry 16:8998–9001. doi:10.1002/chem.201000120
23. Lim LW, Tomatsu M, Takeuchi T (2006) Development of an on-line immobilized-enzyme reversed-phase HPLC method for protein digestion and peptide separation. Anal Bioanal Chem 386:614–620. doi:10.1007/s00216-006-0458-6
24. Guo X, Trudgian DC, Lemoff A et al (2014) Confetti: a multiprotease map of the HeLa proteome for comprehensive proteomics. Mol Cell Proteomics 13:1573–1584. doi:10.1074/mcp.M113.035170
25. Cingöz A, Hugon-Chapuis F, Pichon V (2010) Total on-line analysis of a target protein from plasma by immunoextraction, digestion and liquid chromatography-mass spectrometry. J Chromatogr B Analyt Technol Biomed Life Sci 878:213–221. doi:10.1016/j.jchromb.2009.07.032
26. Geiser L, Eeltink S, Svec F, Fréchet JMJ (2008) In-line system containing porous polymer monoliths for protein digestion with immobilized pepsin, peptide preconcentration and nano-liquid chromatography separation coupled to electrospray ionization mass spectroscopy. J Chromatogr A 1188:88–96. doi:10.1016/j.chroma.2008.02.075
27. Temporini C, Calleri E, Campèse D et al (2007) Chymotrypsin immobilization on epoxy monolithic silica columns: development and characterization of a bioreactor for protein digestion. J Sep Sci 30:3069–3076. doi:10.1002/jssc.200700337
28. Yamaguchi H, Miyazaki M, Kawazumi H, Maeda H (2010) Multidigestion in continuous flow tandem protease-immobilized microreactors for proteomic analysis. Anal Biochem 407:12–18. doi:10.1016/j.ab.2010.07.026
29. Urban PL, Amantonico A, Zenobi R (2011) Lab-on-a-plate: extending the functionality of MALDI-MS and LDI-MS targets. Mass Spectrom Rev 30:435–478. doi:10.1002/mas.20288
30. Jiang B, Yang K, Zhang L et al (2014) Dendrimer-grafted graphene oxide nanosheets as novel support for trypsin immobilization to achieve fast on-plate digestion of proteins. Talanta 122:278–284. doi:10.1016/j.talanta.2014.01.056
31. Li Y, Yan B, Deng C et al (2007) On-plate digestion of proteins using novel trypsin-immobilized magnetic nanospheres for MALDI-TOF-MS analysis. Proteomics 7:3661–3671. doi:10.1002/pmic.200700464
32. De Stefano L, Rea I, Rendina I et al (2011) Organic–inorganic interfaces for a new generation of hybrid biosensors. Biosens Health Environ Biosecurity
33. De Stefano L, Rea I, De Tommasi E et al (2009) Bioactive modification of silicon surface using self-assembled hydrophobins from Pleurotus ostreatus. Eur Phys J E Soft Matter 30:181–185. doi:10.1140/epje/i2009-10481-y
34. Linder MB (2009) Hydrophobins: proteins that self assemble at interfaces. Curr Opin Colloid Interface Sci 14:356–363. doi:10.1016/j.cocis.2009.04.001
35. Hektor HJ, Scholtmeijer K (2005) Hydrophobins: proteins with potential. Curr Opin Biotechnol 16:434–439. doi:10.1016/j.copbio.2005.05.004
36. Zampieri F, Wösten HAB, Scholtmeijer K (2010) Creating surface properties using a palette of hydrophobins. Materials (Basel) 3:4607–4625. doi:10.3390/ma3094607
37. Wohlleben W, Subkowski T, Bollschweiler C et al (2010) Recombinantly produced hydrophobins from fungal analogues as highly surface-active performance proteins. Eur Biophys J 39:457–468. doi:10.1007/s00249-009-0430-4
38. Sun T, Qing G, Su B, Jiang L (2011) Functional biointerface materials inspired from nature. Chem Soc Rev 40:2909–2921. doi:10.1039/c0cs00124d
39. Qin M, Wang L-K, Feng X-Z et al (2007) Bioactive surface modification of mica and poly(dimethylsiloxane) with hydrophobins for protein immobilization. Langmuir 23:4465–4471. doi:10.1021/la062744h
40. Wang Z, Lienemann M, Qiau M, Linder MB (2010) Mechanisms of protein adhesion on surface. Films Hydrophobin 57:8491–8496. doi:10.1021/la101240e
41. Zhao Z-X, Wang H-C, Qin X et al (2009) Self-assembled film of hydrophobins on gold surfaces and its application to electrochemical biosensing. Colloids Surf B Biointerfaces 71:102–106. doi:10.1016/j.colsurfb.2009.01.011
42. Armenante A, Longobardi S, Rea I et al (2010) The Pleurotus ostreatus hydrophobin Vmh2 and its interaction with glucans. Glycobiology 20:594–602
43. Longobardi S, Gravagnuolo AM, Rea I et al (2014) Hydrophobin-coated plates as matrix-assisted laser desorption/ionization sample support for peptide/protein analysis. Anal Biochem 449:9–16
44. Weng Y, Qu Y, Jiang H et al (2014) An integrated sample pretreatment platform for quantitative N-glycoproteome analysis with combination of on-line glycopeptide enrichment, deglycosylation and dimethyl labeling. Anal Chim Acta 833:1–8. doi:10.1016/j.aca.2014.04.037
45. Krenkova J, Szekrenyes A, Keresztessy Z et al (2013) Oriented immobilization of peptide-N-glycosidase F on a monolithic support for glycosylation analysis. J Chromatogr A 1322:54–61. doi:10.1016/j.chroma.2013.10.087
46. Giardina P, Aurilia V, Cannio R et al (1996) The gene, protein and glycan structures of laccase from Pleurotus ostreatus. Eur J Biochem 235:508–515
47. Luo B, Groenke K, Takors R et al (2007) Simultaneous determination of multiple intracellular metabolites in glycolysis, pentose phosphate pathway and tricarboxylic acid cycle by liquid chromatography-mass spectrometry. J Chromatogr A 1147:153–164. doi:10.1016/j.chroma.2007.02.034
48. Cooper MA, Singleton VT (2001) A survey of the 2001 to 2005 quartz crystal microbalance biosensor literature: applications of acoustic physics to the analysis of biomolecular interactions. J Mol Recognit 20:154–184. doi:10.1002/jmr.826
49. Sauerbrey SG (1959) Verwendung von Schwingquarzen zur Wägung dünner Schichten und zur Mikrowägung. Z Phys 155:206–222
50. Kannan K, Jasra RV (2009) Immobilization of alkaline serine endopeptidase from Bacillus licheniformis on SBA-15 and MCF by surface covalent binding. J Mol Catal B: Enzym 56:34–40. doi:10.1016/j.molcatb.2008.04.007
51. Li S, Wu Z, Lu M et al (2013) Improvement of the enzyme performance of trypsin via adsorption in mesoporous silica SBA-15: hydrolysis of BAPNA. Molecules 18:1138–1149. doi:10.3390/molecules18011138
52. Han G, Ye M, Jiang X et al (2009) Comprehensive and reliable phosphorylation site mapping of individual phosphoproteins by combination of multiple stage mass spectrometric analysis with a target-decoy database search. Anal Chem 81:5794–5805. doi:10.1021/ac900702g
53. Egrie JC, Browne JK (2001) Development and characterization of novel erythropoiesis stimulating protein (NESP). Br J Cancer 84(Suppl 1):3–10. doi:10.1054/bjoc.2001.1746
54. Llop E, Gallego RG, Belalcazar V et al (2007) Evaluation of protein N-glycosylation in 2-DE: erythropoietin as a study case. Proteomics 7:4278–4291. doi:10.1002/pmic.200700572

Analytical and Bioanalytical Chemistry

Electronic Supplementary Material

A simple MALDI plate functionalization by Vmh2 hydrophobin for serial multi-enzymatic protein digestions

Sara Longobardi, Alfredo Maria Gravagnuolo, Riccardo Funari, Bartolomeo Della Ventura, Francesca Pane, Eugenio Galano, Angela Amoresano, Gennaro Marino, Paola Giardina

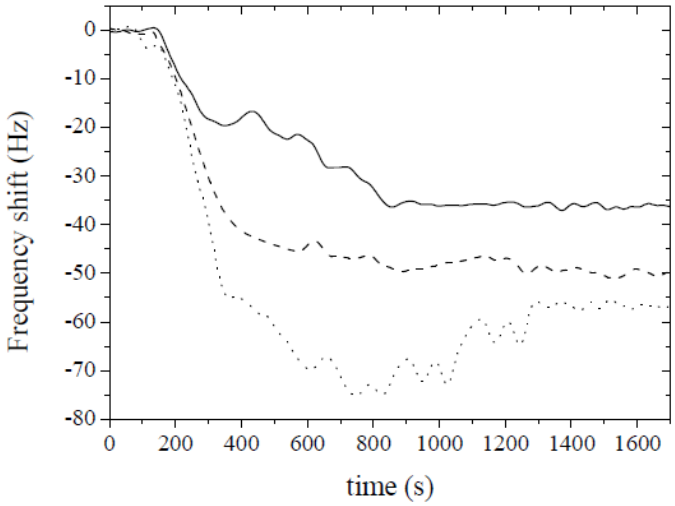

Fig. S1 QCM responses to different concentrations of trypsin solutions injected in measure chamber. 1 µg mL^{-1} (solid line), 3 µg mL^{-1} (dashed line) and 6 µg mL^{-1} (dotted line)

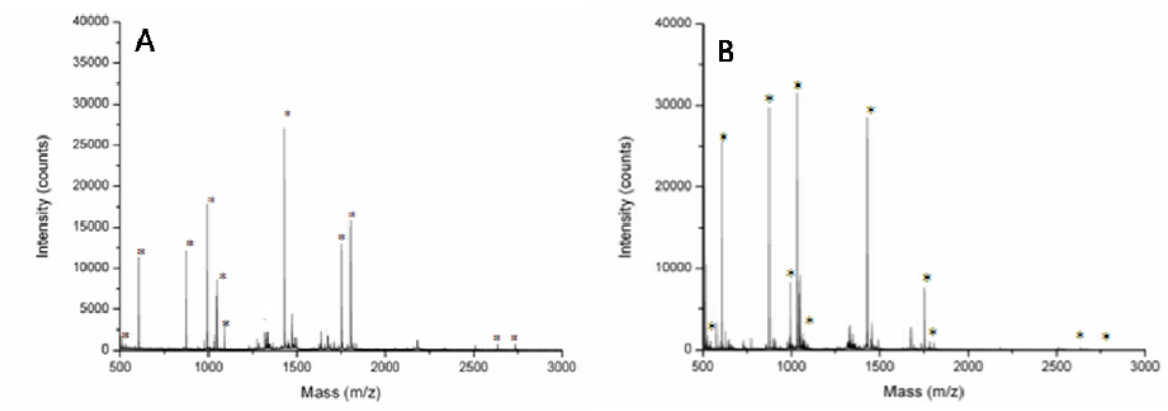

Fig. S2 MALDI-TOF spectra of lysozyme peptides obtained by 5 min on-plate (A) and 18h in solution (B) tryptic hydrolysis. The assigned signals are marked with asterisks. List of peptides with their m/z values is reported in table SM-1

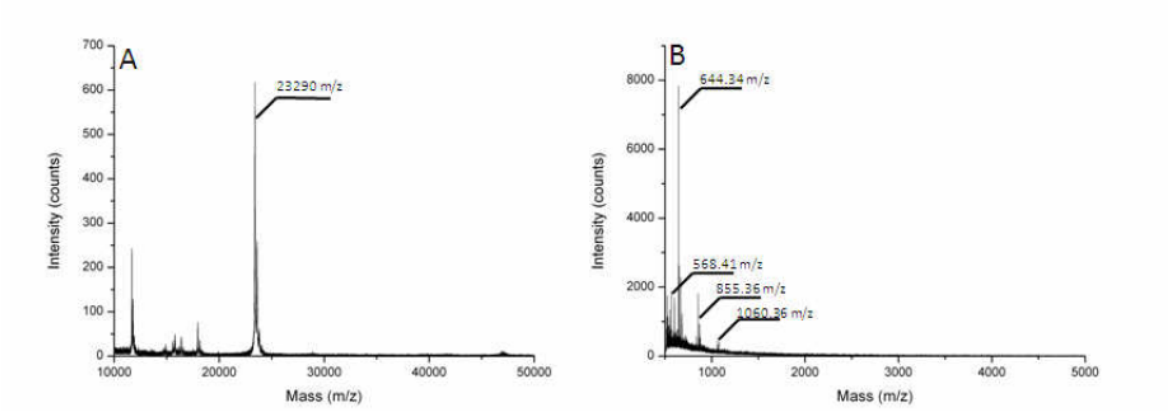

Fig. S3 MALDI-TOF spectra of trypsin immobilized on MALDI sample plate. Panel A: spectrum acquired in linear mode showing a signal at the m/z value of monoprotonated molecular ion of trypsin. Panel B: spectrum acquired in reflector mode showing only the presence of signals related to the matrix (CHCA)

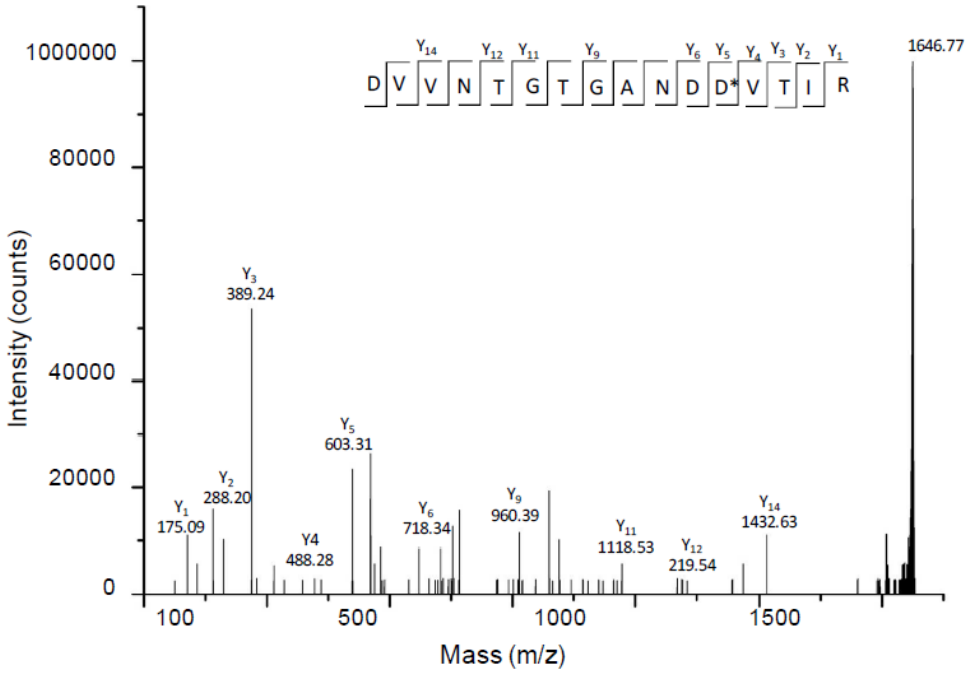

Fig. S4 MALDI-TOF/TOF spectrum of precursor ion 1646.77 m/z (POXC peptide 433-448) without glycosidic moiety. Asn 444 converted into Asp is marked by asterisk (*)

Table S1 List of peptides obtained by on-plate trypsin hydrolysis

Lysozyme		Ovalbumin	
Signals (m/z)	sequences	Signals (m/z)	sequences
505.30	^{126}GC*RL^{129}	580.75	^{124}ELYR^{127}
606.86	^{1}KVFGR^{5}	647.86	^{281}VYLPR^{285}
874.61	^{15}HGLDNYR^{21}	888.56	^{279}IKVYLPR^{285}
993.51	^{62}WWC*NDGR^{68}	957.37	^{52}TQINKVVR^{59}
1045.75	^{117}GTDVQAWIR^{125}	1247.45	^{361}ADHPFLFC*IK^{370}
1049.52	^{6}C*ELAAAMKR^{14}	1345.61	^{371}HIATNAVLFFGR^{382}
1428.98	^{34}FESNFNTQATNR^{45}	1555.74	^{188}VYLPRMKMEEK^{200}
1676.10	^{98}IVSDGNGMNAWVAWR^{112}	1581.74	^{265}LTEWTSSNVMEER^{277}
1753.12	^{46}NTDGSTDYGILQINSR^{61}	1687.92	^{128}GGLEPINFQTAADQAR^{143}
2508.71	^{74}NLC*NIPC*SALLSSDITASVNC*AK^{96}	1774.02	^{324}ISQAVHAAHAEINEAGR^{340}
2735.84	^{22}GYSLGNWVC*AAKFESNFNTQATNR^{45}	1858.15	^{144}ELINSWVESQTNGIIR^{159}
		2283.62	^{1}MGSIGAASMEFC*FDVFKELK^{20}
		2284.59	^{201}VTEQESKPVQMMYQIGLFR^{219}
		3033.51	^{21}VHHANENIFYC*PIAIMSALAMVYLGAK^{47}
		3238.05	^{341}EVVGSAEAGVDAASVSEEFRADHPFLFC*IK^{370}

3.1.2. A SIMPLE MALDI PLATE FUNCTIONALIZATION BY VMH2 HYDROPHOBIN FOR SERIAL MULTI-ENZYMATIC PROTEIN DIGESTIONS (SUPPLEMENTARY MATERIAL)

Table S2 Number of matched peptides and sequence coverage of lysozyme and obalbumin. On plate trypsin hydrolysis is compared with in solution hydrolysis

Protein	hydrolysis	Peptide number (% of sequence coverage)			
		5 min	1h	3h	18h
Lysozyme	In solution	0÷3* (<10)	3 (10)	5 (40)	11 (90)
	On-plate	11 (90)	11 (90)	11 (90)	11 (90)
Ovalbumin	In solution	0÷2* (<10)	6 (30)	9 (35)	15 (60)
	On-plate	15 (60)	15 (60)	15 (60)	15 (60)

*By in solution hydrolysis, erratic data were obtained after 5 minutes. The ranges of peptide numbers observed in the replicates are reported

Table S3 List of identified whey milk proteins with related matched peptides obtained by on-plate trypsin hydrolysis

Protein	Signals (m/z)	peptide	Protein	Signals (m/z)	peptide
α-S1-casein	615.30	135-139	Lactotransferrin	513.25	1-4
	910.45	140-147		746.51	237-243
	1267.68	106-115		946.43	571-578
	1337.65	95-105		1378.66	198-210
	1759.91	23-37		1423.69	532-544
	2316.12	148-166		1457.64	152-163
β-lactoglobulin	837.46	158-164		1627.73	621-633
	903.50	92-99	α-lactalbumin	710.31	128-133
	1193.65	108-117		1090.51	131-141
	1635.77	141-154		1200.64	118-127
	1715.80	165-178		1698.83	99-112
	2313.27	57-76	β-casein	645.34	115-120
α-S2-casein	2707.34	31-56		830.44	192-198
	2818.23	118-140		1013.51	121-128
	2846.26	155-178		2186.14	199-217
	502.29	57-60	K-casein	1250.55	57-67
	572.29	92-05		1608.83	68-81
	690.36	86-91		1735.88	62-82
	746.44	215-220		1980.08	39-56
	979.54	189-196	butyrophilin	1275.60	193-203
	1018.51	168-175		1683.66	79-92
	1195.65	130-140		2312.08	494-515
	1251.67	141-151	Lactoadherin	841.46	122-128
	1367.68	96-106		1221.61	378-387

3.2. NANO-BIOTECHNOLOGICAL APPLICATIONS OF VMH2

In **Section 3.2.1** a one-step method for the exfoliation, stabilization and functionalization of graphene by the class I hydrophobin Vmh2 is described. The process should provide a safe way to produce graphene, leading to a dispersible suspension of protein-coated graphene particles. This strategy devoted to optimize the surface functionality and biocompatibility of Graphene Related Materials (GRMs) can expand the use of carbon nanostructures and the development of new bio-nano-technological devices.

In **Section 3.2.2.** the use of Vmh2 functional layer is tested as a novel coating of glass surface in order to develop an optical (bio)sensing platform. The possibility to integrate nanomaterials such as graphene oxide and quantum dots has also been studied.

The work described in **Section 3.2** has been carried out in collaboration with the Nanobioelectronics & Biosensors Group of Prof. Arben Merkoçi at the Catalan Institute of Nanoscience and Nanotechnology (ICN2), Bellaterra, Spain.

Focus: Bioanalytical Applications of Graphene Related Materials

Biosensors‘s research aims to integrate nanotechnology methods, tools and materials into low cost, user friendly and efficient (bio)sensors with interest for health, safety/security and environment. Nanoparticle based systems are becoming an increasingly relevant alternative to traditional techniques in diagnostics and have been even demonstrated to be very useful for detection of cancer cells (Maltez-da Costa et al., 2012). Compact and cheap devices provided with smart systems, can be developed for diagnostics, exploiting nanotechnology.

One of the major driving forces for the development of biosensors is the biomedical diagnosis of biomarkers. A biomarker is an agent that indicates a biological status. Therefore, a biomarker can reveal biological processes in normal, pathogenic or pathological states and even during pharmacologic or therapy responses. Since biomarkers can provide objective information towards clinical diagnosis, new advantageous devices for biomarker screening are highly desired (Morales-Narváez et al. 2012). Point-of-care detection, high-throughput screening and cheap tests are achievable through biosensor technology.

Biosensors have found also potential applications in the agricultural and food industries. The detection of pathogenic organisms has an important potential in ensuring food safety. Potential applications of biosensors to food quality control include measurement of nutrients, at best, on-line coupled to the processing line through a flow injection analysis system.

Biological polymers (e.g. enzymes and antibodies) are the fundamental active elements of a biosensor, since they interact in a very specific and selective way with a huge assortment of molecules, even nanoparticles, offering the possibility to detect analytes of an incredible variety of sizes and shapes. In fact, the effect of analyte binding can be transduced in every sort of electrical, chemical, optical, physical or a physicochemical signal to be acquired and converted in quantitative data.

3. VMH2 SELF-ASSEMBLED COATING ENHANCES THE SURFACE PROPERTIES OF MATERIALS FOR BIOTECHNOLOGICAL APPLICATIONS

The nanotechnology field is in constant search for new engineered materials for biosensing purposes. Recently, the graphene family of materials has shown great potential and the proposed applications for graphene-based biosensors have shown great variety. Carbon nanotubes and graphene, two categories of closely related carbon nanomaterials, due to their unique mechanical, electronic, chemical, optical and electrochemical properties, represent the most interesting building blocks in various biomedical applications.

A significant number of publications reporting graphene based biosensors which have been used for improving the sensitivity and selectivity of biosensing systems based on the unique chemical, optical, electrical and electrochemical properties of graphene have appeared [Artiles et al. 2011; Pumera et al. 2010; Morales-Narváez and Merkoçi, 2012; Morales-Narváez et al., 2013; Ueno et al., 2013]. Moreover carbon nanomaterials have been extensively explored as drug delivery carriers for the intracellular transport of chemotherapy drugs, proteins, and genes. However, an expanded use of carbon nanostructures in living systems will require strategies to optimize their surface functionality and biocompatibility (Zhang Y et al., 2014).

Many materials of biological source, such as proteins or polypeptides, have emerged as unique building blocks for ordered nanostructures in contexts much broader than those imposed by the original systems due to their ability to self-assemble, and template protein assemblies with nanomaterials. The resultant hybrids can be used to produce nanocomposites with remarkable mechanical properties combining features from both GRMs and proteins. These hybrids are perfectly organized hierarchical structures, characterized by enhanced biocompatibility, allowing their use as cellular growth scaffolds and, thus, expanding the range of applications of graphene in medical/biological fields [Ling et al. 2014].

To explore the many advantages offered by GRMs in biosensor field, it is crucial to improve and optimize the methods by which the bio-recognition layer (i.e. an enzyme) is immobilized onto these nano-structures [Putzbach et al. 2013; González-González et al., 2014]. It is vital that the proteins can be immobilized onto the nanostructure while retaining their native biological structure and function [Zuo et al. 2013]. The ability to render hydrophobic materials soluble in aqueous solution makes hydrophobins attractive as possible coatings for carbon-based nanomaterials [Yang et al., 2013]. By duly exploiting the features offered by these two classes of materials, the application of protein–carbon nanomaterial hybrids may open new strategies in areas as diverse as microfluidics, heterogeneous catalysis, molecular separations, functional nanocomposites, tissue engineering, nanomedicine, nano(bio)electronics, (bio)sensors and in general (bio)analytical chemistry.

ADFM201500016(201500016)

www.afm-journal.de

ADVANCED FUNCTIONAL MATERIALS

In Situ Production of Biofunctionalized Few-Layer Defect-Free Microsheets of Graphene

By *Alfredo M. Gravagnuolo, Eden Morales-Narváez, Sara Longobardi, Everson T. da Silva, Paola Giardina, and Arben Merkoci**

Keywords: biofunctionalized graphene, bionanotechnology, graphene production, self-assembling

Biological interfacing of graphene has become crucial to improve its biocompatibility, dispersability, and selectivity. However, biofunctionalization of graphene without yielding defects in its sp^2-carbon lattice is a major challenge. Here, we set out a process for biofunctionalized defect-free graphene synthesis through the liquid phase ultrasonic exfoliation of raw graphitic material assisted by the self-assembling fungal hydrophobin Vmh2. This protein (extracted from the edible fungus *Pleurotus ostreatus*) is endowed with peculiar physicochemical properties, exceptional stability, and versatility. The unique properties of Vmh2 and, above all, its superior hydrophobicity, and stability allow us to obtain a highly concentrated (≈440–510 μg mL^{-1}) and stable exfoliated material (ζ-potential, +40/ +70 mV). In addition controlled centrifugation enables the selection of biofunctionalized few-layer defect-free micrographene flakes, as assessed by Raman spectroscopy, AFM, scanning electron microscopy, and electrophoretic mobility. This biofunctionalized product represents a high value added material for the emerging applications of graphene in the biotechnological field such as sensing and drug delivery.

1. Introduction

Due to its extraordinary structure and fascinating properties, graphene is definitely the most studied nanomaterial.[1] Being the thinnest object ever known, graphene is a single layer of carbon atoms patterned in a 2D honeycomb network.[2] As the fundamental building block of carbon allotropes, it exhibits unparalleled properties such as high planar surface (≈2630 m^2 g^{-1}),[3] superlative mechanical strength (Young's modulus, ≈1100 GPa),[4] remarkable thermal[5] and electrical conductivity[6] (5000 W m^{-1} K^{-1} and 1738 S m^{-1}, respectively), high absorption of incident white light (2.3%, in spite of its thickness),[7] highly efficient fluorescence quenching capabilities,[8] and impermeability to standard gases.[9] Consequently, graphene can be integrated as the core of cutting-edge technologies and devices related to photonics, electronics, composite materials, sensors, environment, energy, biotechnology, and biomedicine.[10–13]

Since the groundbreaking discovery of the surprising properties of graphene,[14] the industrial and scientific communities have focused their attention on the development of new graphene synthesis methods enabling a variety of options in terms of oxidation grade, number of layers, edge and basal defects, lateral size, quality, and cost for any particular application.[10,15,16] According to the literature,[10,15] the most relevant routes for graphene generation are the chemical vapor deposition, epitaxial growth, mechanical cleavage, wet chemical synthesis, and exfoliation of graphite.

Generally, liquid-phase exfoliation of graphite entails the use of ultrasonication as a key method which promotes the generation of laminated material that is subsequently bound to aggregate due to the lack of hydrophilic groups onto the exfoliated material. In fact, re/aggregation is one of the main challenges to address during the exfoliation procedure and the stabilization of solvent-dispersed graphene flakes.[18] However, re/aggregation is typically minimized by using organic solvents with suitable characteristics[19] or surfactant–water solutions.[20,21]

Biological interfacing of graphene has become crucial to improve its biocompatibility,[22] dispersibility, and selectivity toward various applications in the biotechnological and biomed-

A. M. Gravagnuolo, Dr. E. Morales-Narváez, E. T. da Silva, Prof. A. Merkoçi, ICN2 – Catalan Institute of Nanoscience and Nanotechnology , 08193 Barcelona, Spain
(E-mail: arben.merkoci@icn.cat)
A. M. Gravagnuolo, Dr. S. Longobardi, Prof. P. Giardina, Department of Chemical Sciences, University of Naples "Federico II," 80126 Naples, Italy
Prof. A. Merkoçi, ICREA – Catalan Institution for Research and Advanced Studies 08010 Barcelona, Spain

Correspondence to: Prof. A. Merkoçi (E-mail: arben.merkoci@icn.cat)
10.1002/adfm.201500016

ADVANCED FUNCTIONAL MATERIALS

ical fields.[23–25] However, since chemical functionalization of graphene is generally known to sensitively disrupt its electronic structure,[26] the biofunctionalization of graphene without triggering defects, e.g., disrupting the sp^2-carbon lattice by introducing oxygen-containing groups, is a major challenge. Although graphene modification and biofunctionalization are under active research,[23] the in situ production of biofunctionalized defect-free graphene has been little explored.

Because of their huge range of functions and high responsiveness to a variety of stimuli, proteins are suitable candidates for bioconjugation of nanomaterials for biomedical applications. Protein binding onto pristine carbon lattice is strongly driven by hydrophobic interactions.[27] Besides hydropathicity character of amino acid residues, 3D protein structure also plays a key role in their adsorption onto graphene-based materials (GBMs) and functionality of the resulting bioconjugates. For instance, proteins prone to form amyloid structures strongly interact with carbon nanomaterials, forming bioinspired hybrid materials which show special properties and biodegradability.[28–30]

The use of amphiphilic proteins called hydrophobins from fungal sources has been reported to enable the coating of a wide variety of materials included carbon based materials.[31–34] Hydrophobins are small surface active proteins which play special roles at some stages in the growth and the development of filamentous fungi,[35] being able to self-assemble at hydrophilic–hydrophobic interface to form amphiphilic (mono) layers. Conventional soluble proteins confine hydrophobic residues in the core of the molecular structure and expose the hydrophilic ones to the solvent to reach a minimum of energy in aqueous environment. Conversely, the Janus-faced character of hydrophobins is due to the clustering of hydrophobic residues on one side of the protein surface maximizing the area of interaction with hydrophobic materials. Consequently, these peculiar proteins can tune the wettability of surfaces and improve their properties for biomedical applications such as sensing and drug delivery.[36–40] Moreover, the hydrophobin coating can confer special properties, i.e., prevention of human immune response, [41] specific functionalities trough protein engineering,[32] or molecular adsorption.[42]

The hydrophobin family is split in two classes on the basis of their structure and function;[35] Class I hydrophobins have natural propensity to self-assemble into remarkably stable amyloid-like nanostructures also known as rodlets, which can only be solubilzed in harsh acids.[43–47] Despite the superior stability of coating by Class I hydrophobins, technologies based on their use have been less exploited with respect to the Class II, possibly because of their lower solubility and high propensity to self-assemble which cause several drawbacks in their handling.

Recently, Laaksonen et al. have demonstrated a one-step approach for the ultrasonic wave-based exfoliation and functionalization of layered carbon materials using Class II hydrophobins from the filamentous fungus *Trichoderma reesei*. According to the model proposed by Laaksonen and co-workers, self-assembling hydrophobins at solvent–carbon interface tune the surface energy of the 2D carbon lattice in a surfactant-like system, thus reducing the interlayer stacking which is the driving force opposing to micromechanical exfoliation.

Class I hydrophobin, Vmh2 from the edible white-rot fungus *Pleurotus ostreatus*, has been purified and extensively studied by our research group.[48,49] Solvent polarity, pH, temperature, and the presence of calcium ions trigger the protein transition across structural states. Vmh2 self-assembling into nanometric films has been explored[50,51] as well as its capability to recruit biomolecules, such as glucose or a variety of enzymes in their active form, onto the biohybrid surface.[42,52] Moreover, surface (silicon and steel) functionalization by Vmh2 has been demonstrated to leave unaltered the optical properties and to be effective in technological devices.[51,53,54]

Herein, we explore the ultrasonication-based production of biofunctionalized graphene using the Vmh2 hydrophobin. As depicted in **Figure 1**, we exfoliate a low-cost graphite source (graphite powder, Aldrich 332461) in ethanol–water media by a medium power (125 W, 20 kHz. Inbuilt power meter power output 19 W) tip sonicator. Controlled centrifugation (final steps at 620 and 2500 g) enables us to obtain suspensions of particles of controlled size. They are endowed with exceptional stability in liquid (ethanol–water) due to the hydrophobin coating. Since on one hand the number of graphene layers and their defects significantly modulate the succeeding transport properties,[55] and on the other hand the lateral dimension size controls the maximum dimension and degree of deformability of the material that are paramount parameters for biological interactions,[56,57] we systematically study the quality of the generated graphene sheets in terms of lateral dimension, number of layers per flakes, and defect characteristics. To this aim, we exploit recent advances in graphene Raman spectroscopy in terms of spectral analysis of GBMs[58] and study the self-assembled biohybrid structures by AFM, scanning electron microscopy (SEM) and electrokinetic analysis.

2. Results and Discussion

2.1. In Situ Exfoliation, Functionalization, and Stabilization of GBMs by Vmh2 Hydrophobin

Ultrasonication of graphite powder (1000 μg mL^{-1}) in Vmh2 hydrophobin solution (50–100 μg mL^{-1} in 60%, v/v, ethanol in water, 5 mL volume) resulted in dark and stable dispersions of carbon material, see **Figure 2**A,b. When micromechanical exfoliation was attempted in the absence of the surface active protein, flocculation and settling out occurred in 3 days owing to interlayer stacking of newly formed flakes, see Figure 2A,a. SEM imaging shed light on the starting material, crystallites of ≈1 mm lateral size (Figure 2B), and on the product of Vmh2 assisted exfoliation/stabilization, an heterogeneous mix of GBMs in terms of particles size (up to 2 μm) and shape, see Figure 2C.

Aiming at estimating the amount of GBMs attainable by the Vmh2-assisted exfoliation, the unexfoliated graphite was removed by gentle centrifugation, 40 min at 40 g, then, UV–vis measurements[20,32] indicated a concentration of ≈440–510 μg mL^{-1} of carbon dispersion. This value was one order of magnitude higher than that one previously reported by Laaksonen

www.afm-journal.de

ADVANCED FUNCTIONAL MATERIALS

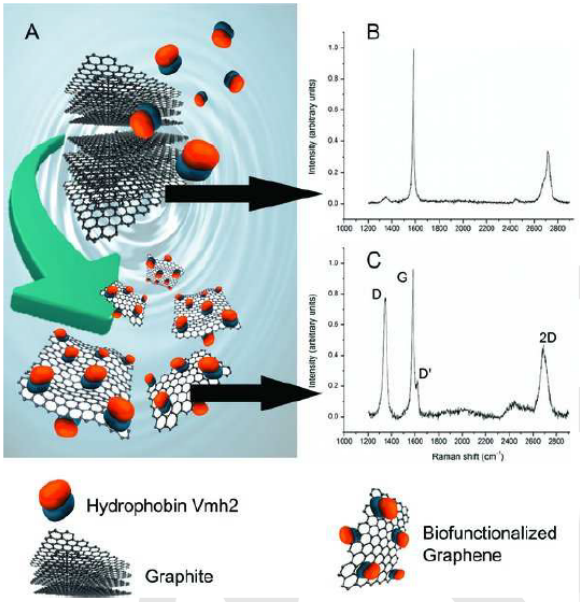

Figure 1. In situ generation of biofunctionalized graphene. A) Schematic representation of the process. Ultrasound waves are applied as a source of mechanical force that brakes and exfoliates the starting material (graphite). Subsequently, the hydrophobic region of the amphiphilic protein hydrophobin Vmh2 is spontaneously adsorbed onto the laminated material (which is also hydrophobic) stabilizing and functionalizing the exfoliated material. B) Raman spectra of the starting material (graphite crystallites). C) Raman spectra of the generated material (biofunctionalized few-layer graphene flake). Experimental conditions as given in the text.

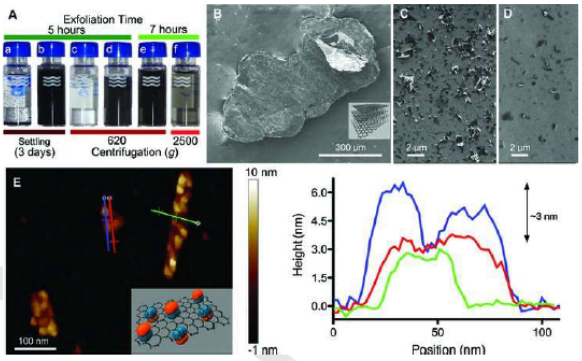

Figure 2. Production of Biofunctionalized Graphene. A,a–f) Samples of the dispersions obtained through (a,c) liquid phase exfoliation in absence of Vmh2 and (b,d,e,f) Vmh2 assisted exfoliation. B) SEM image of the starting material (graphite flake). C) SEM image of the dispersion shown in (A,b). D) SEM image of the dispersion displayed in (A,d). E, left) AFM analysis of biofunctionalized graphene obtained from the sample HC shown in (A,f). E,right) AFM profiles of two flakes showing the graphene–Vmh2 assembly. Experimental conditions as given in the text.

and co-workers using Class II hydrophobins. In addition, they have employed high-class graphitic sources (HOPG and Kish graphite, which are expensive when compared with graphite powder: Kish graphite ≈350 USD, 0.5g; HOPG ≈200 USD, mosaic of 5 × 5 mm, thickness 2.0 mm; graphite powder, ≈72.8 USD, 2.5 kg) in 0.3–1 mL volumes of water solutions, obtaining a 25–40 μg mL^{-1} suspension of exfoliated material.[32] In spite of the considerable differences in the geometry of the proposed processes (see Table S1, Supporting Information), we believe that the unique properties of Vmh2 and, above all, its superior hydrophobicity and stability (as described below) play a significant role in such an advance.

Sequence analysis of hydrophobins and soluble standard proteins with different physicochemical and functional characteristics evidenced that (i) hydrophobins show major contribution of hydrophobic amino acids with respect to the other soluble proteins and (ii) Vmh2 is the most hydrophobic hydrophobin among those that have been used for the stabilization of nanomaterials to date (see Figure S1, Supporting Information). To give insight into its amphiphilic character, the sequence of Vmh2 was compared with that of hydrophobin HFBI used by Laaksonen and co-workers. Hydropathy analysis suggested that Vmh2 brings into play very extended hydrophobic patches that could strongly drive Vmh2 onto GBMs surface (see Figure S2, Supporting Information).

Usually stability to physical and chemical factors deeply limits the use of biological molecules in cutting-edge technology approaches. Irreversible conformational transitions commonly lead to loss of function and aggregation of proteins, often in a temperature dependent kinetics. In contrast, mature Vmh2 is a small (87 amino-acids) and compact protein, particularly resistant to chemical and physical treatments.[51] It is worth mentioning that partial protein unfolding has been reported to occur at 80 °C, however the protein refolds by lowering the temperature at 25 °C.[48] Moreover, batches of Vmh2 protein dissolved in 60 vol%. ethanol solution were soluble and functional at least 18 months at room temperature. This very stable state has been achieved by using a low polar solvent able to solvate the extended hydrophobic patches exposed on the surface of protein. Vmh2 protein showed extreme resistance also in our system, where intensive ultrasonication causes heating of the solution. Likewise, GBM dispersions were stable for at least 6 months at room temperature.

It should be remarked that Vmh2 was also able to stabilize carbon dispersions from different graphite sources by adding the protein either before (see Figure S3, left, Supporting Information) or after exfoliation. Vmh2-assisted ultrasonication of HOPG as well as addition of Vmh2 to a previously exfoliated HOPG or to a commercial GBM allowed the improvement of their dispersibility and their use for surface functionalization. Indeed, drop casting of the obtained dispersions resulted in a very homogenous coating of silicon chips upon solvent evaporation as shown by SEM imaging (see Figures S3, right, and S4, Supporting Information).

The use of smart and self-assembled materials inspired from nature whose properties are dependent on external chem-

ADVANCED FUNCTIONAL MATERIALS

ical or physical stimuli is emerging in biomedical field.[59] The complex behavior of Vmh2 in ethanol/water solvents has been previously elucidated.[48] Its aggregation can be controlled by environmental factors such as solvent polarity, temperature, divalent cations, or base addition.[48] Interestingly, we observed that the biohybrid GBM obtained by Vmh2 assisted exfoliation was endowed with the self-assembling characteristics of the protein moiety which enabled analogous handling of the material morphology. As solvent polarity was increased, by adding water to the water/ethanol solution, the Vmh2 assisted exfoliated GBMs reached the liquid–air or liquid–solid interface forming a homogeneous film (see Figure S5 and the video, Supporting Information). Moreover, ammonia additions triggered the formation of Vmh2–GBM coaggregated in solution, see Figure S5, right, Supporting Information. All these results suggest the wide flexibility of this technology in adding value to carbon materials for an easy handling and applicability.

2.2. Production of Biofunctionalized GBMs

We aim at contributing a cost-effective scalable process for the production of biofunctionalized graphene with well-defined characteristics. We optimized the process parameters to obtain the maximum yield (≈45%–50%) and production rate (≈13–15 μg mL^{-1} h^{-1}): exfoliation time (5–7 h), amount of starting material (≈1 mg mL^{-1}), carbon/protein ratio (w/w 20:1), and Vmh2 concentration (50–100 μg mL^{-1}). Figure S6, Supporting Information, summarizes the most relevant parameters of the optimization process. Selection of GBMs classes on the base of particles size is easily and reliably achievable by controlled centrifugation.[58,60] In particular, after removal of unexfoliated material (40 min at 40 g), consecutive 40 min centrifugations at increased centrifugal force were tested. Since it has been reported that the average number of monolayers per flakes reaches a minimum at ≈2500 g,[58] we characterized the dispersions obtained after medium (620 g), and hard centrifugation (2500 g) steps, named MC and HC samples, respectively. As expected, the applied centrifugal force dramatically influenced the GBMs yield in solution (see Figure 2A). SEM imaging proved an evident reduction of graphite microplatelets and an improvement of homogeneity using both MC and HC (see Figure 2D showing SEM image of MC).

We also characterized the electrokinetic behavior of both MC and HC (see Figure S7, Supporting Information). Pure Vmh2 protein in an electric field migrated toward the negative electrode in solution showing that the protein held a net positive charge, with an electrophoretic mobility (U_e) of 0.55 ± 0.06 μm s^{-1} cm V^{-1} (mean and standard error calculated on 10 sets of measurements). Moreover this value increased in the presence of exfoliated graphene up to 0.71 ± 0.03 μm s^{-1} cm V^{-1} in the case of HC sample and up to 0.80 ± 0.03 μm s^{-1} cm V^{-1} in the case of MC sample. Since the graphene surface is highly nonpolar this change suggested that new species were assembled upon mixing of protein and GBMs through the adsorption of charged Vmh2 molecules onto the surface of carbon particles. The new molecular assemblies showed increased electrokinetic properties probably due to increased surface charge density and to the very unique solvent–sample relationship. We concluded that the interaction between graphene and the amphiphilic protein Vmh2 resulted in the formation of biohybrid assemblies endowed with a positive surface charge density.

The electrostatic repulsion generated by the protein coating could also explain the stabilization of graphene by Vmh2. Indeed, the estimation of ζ-potential from electrophoretic mobility could assess the stability of the graphene dispersion through a model in which the protein act as a surfactant.[20,21] We could estimate the ζ-potential of Vmh2-coated graphene flakes by the Henry equation (see the Experimental Section). Considering the Huckel and Smoluchowski limits of the Henry function, we calculated both the lower and upper bounds of ζ-potential. Values ranged between +40 and +70 mV for Vmh2 assisted exfoliated samples, classifying the biofunctionalized graphene as highly stable.[20]

Evidences of the Vmh2 coating on carbon particles were found out through AFM analysis of HC sample (see Figure 2E). On the basis of the height of the assembly in the AFM profiles and the expected diameter of a hydrophobin molecule (≈3 nm) we could assess that Vmh2 formed a discontinuous, one molecule thick coating. However, since the resolution on the *XY* plane was quite low because of the so-called tip effect, the observed islands could be made of isolated Vmh2 monomers and/or oligomers.

In order to estimate the number of graphene layers per flake, as described below, we used Raman spectroscopy, since AFM analysis provides the top profile of the flakes while the structure of the lower layers is hidden.

2.3. Raman Spectroscopy Characterization and Classification of Biofunctionalized Graphene

Currently, health risk associated to GBMs is under debate.[57,61,62] Establishing the characteristics of the biofunctional graphene is essential to define the structure–safety relationship which is a future challenge concerning the use of graphene materials in biomedical applications. In order to avoid ambiguities in terms of characteristics of GBMs a classification approach has been recently proposed.[57,63] Such a nomenclature is based on the specification of the three most significant characteristics of the GBMs which modulate the chemical, physical, and biological properties: number of graphene layers (N_G); lateral size (*L*, being rectangular-like structures, it generally refers to the maximum lateral dimension of the inspected flake); and defect type. Latest advances in Raman spectroscopy analysis have enabled a simple and consistent estimation of all these parameters.

First, to investigate on the most important parameter, N_G, we fully capitalized on the Raman spectroscopy analysis recently proposed by Paton et al..[58] Characteristics of the classic 2D band are associated with the stacking of carbon layers in GBM. The authors have developed a metric on the base of the consideration that the spectral intensity at the wavenumber corresponding to the 2D peak of graphite (ω_p) and its shoulder ($\omega_s = \omega_p - 30\ cm^{-1}$) is strictly correlated to N_G, see details in the Experimental Section. The result of the Raman analysis on the graphite spectrum (see **Figure 3**F) compared to those of some Vmh2 coated flakes demonstrated that few-layer graphene (2/5 N_G) was produced (see Figure 3A–E).

www.afm-journal.de

ADVANCED FUNCTIONAL MATERIALS

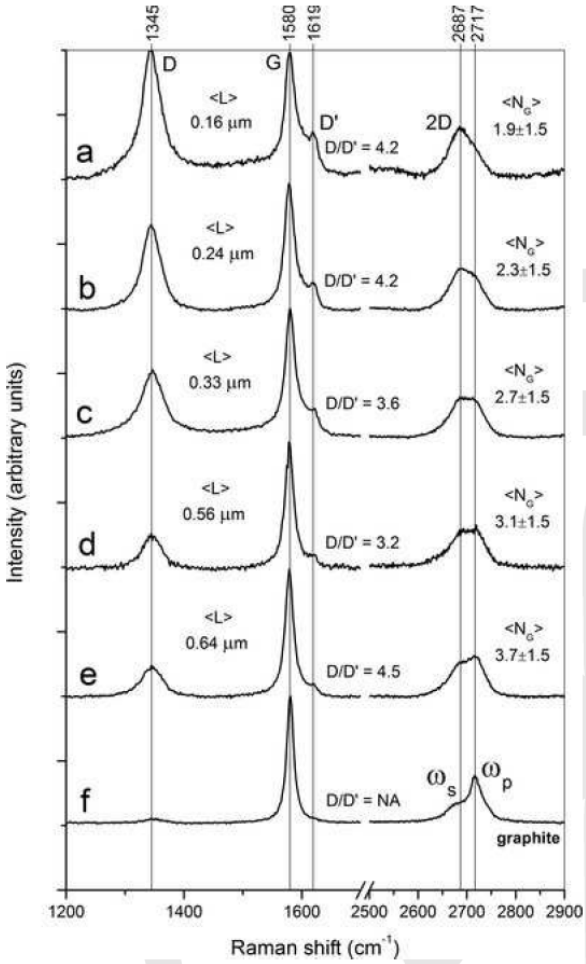

Figure 3. A–E) Quality assessment by Raman spectroscopy analysis of (a,b,c,d,e) biofunctionalized flakes of increasing sizes (from HC sample) and of F) graphite, i.e., the starting material, indicating the wavenumbers corresponding to *D*, *G*, *D′*, 2D peak of graphite (ω_p) and its shoulder ($\omega_s = \omega_p - 30$ cm^{-1}) and the estimated lateral dimension ($\langle L \rangle$), D/D' ratio obtained by fitting and estimated number of graphene layers ($\langle N_G \rangle$). Experimental conditions as given in the text.

Second, to check if the proposed process introduces damages, in the basal plane of graphene we studied defect-activated Raman signals, *D* (≈1345 cm^{-1}) and the *D′* (≈1620 cm^{-1}). Since the reduction of the flakes size determines an increase of the total boundaries, an intrinsic contribution to the *D′* band arises from edge type defects in exfoliated samples. Moreover graphite sources of different qualities could contain natural defects in the basal plane, i.e., sp3 and vacancy-like defects. Herein, the *D* band in spectra of crystallites we used for the synthesis of graphene was scarcely represented, so assessing the good quality of the starting material (Figure 3F). On the other hand, intense *D* signals were detected in the exfoliated flakes (Figure 3A–E). To check if Vmh2 based exfoliation introduced damages in basal plane of graphene, we characterized the defect types analyzing the intensity ratio of the *D* and *D′* peaks through Lorentzian fitting.[64] According to Eckmann et al., values of $D/D' \approx 13$ indicated sp^3 defects, $D/D' \approx 7$ vacancy defects, and $D/D' \approx 3.5$ edge defects. The latter value has been revised by Paton et al. to include the error analysis: $3 \geq D/D'_{\text{edge defects}} \geq 4.5$.[58] All the calculated values of D/D' (Figure 3A–E) in our samples lied in the range indicated for edge type defects. It is worth noting that we set up the maximum ratio of ultrasonication power to reaction volume and the associated solvent heating was attenuated by ice bath cooling. Nevertheless, according to the data acquired experimentally using Raman, defects cannot be ascribed to the basal plane; hence we can conclude that no oxidation of graphene occurred in the course of exfoliation. This is likely due to the essential characteristics of the ultrawave exfoliation technique and to the protection of the Vmh2 coating against surface oxidation.

Third, once demonstrated that only edge type defects were introduced during the exfoliation, Raman spectroscopy analysis enabled the estimation of graphene lateral size ($\langle L \rangle$) through a metric based on the intensity ratio of the *D* and *G* peaks (D/G),[58,65,66] (see details in the Experimental Section). Spectra (Figure 3A–E) evidenced that the analyzed flakes were microsized. Interestingly, a positive correlation between $\langle N_G \rangle$ and $\langle L \rangle$ was observed, although the two properties were estimated by the analysis of separate signals.

Finally, in order to unequivocally assess the quality of material, we performed a complete Raman analysis on 40 biofunctionalized flakes (see **Figure 4**), 16 from MC and 24 from HC sample. The $\langle N_G \rangle$ in both the samples laid in the 2/5 range, with an average value of 3.8 ± 0.4 (standard error) layers in MC and of 2.9 ± 0.3 layers in HC. These data allowed the classification of both materials as few-layer graphene.[63] Furthermore, on the base of the average lateral dimension, 1.0 ± 0.1 μm for MC, 0.49 ± 0.06 μm for HC, we classified the material as micrographene. Moreover, the statistical distribution of $\langle N_G \rangle$ and $\langle L \rangle$ data from all the 40 flakes confirmed their positive correlation (see Figure 4A). Then, the D/D' ratio data distribution definitely characterized the biofunctionalized graphene as defect free, hence lacking in functional groups of oxygen covalently bound to the basal plane (see Figure 4B). All these results are summarized in **Table 1** putting into context both MC and HC materials as biofunctionalized defect-free few-layer micrographene.

3. Conclusion

We have demonstrated a method for the production of biofunctionalized defect-free GBMs by using a unique fungal protein, the hydrophobin Vmh2 extracted from the edible fungus *P. ostreatus*. Due to superior hydrophobicity and stability of Vmh2, we have obtained high concentration of GBMs (≈440/510 μg mL^{-1}) upon Vmh2 assisted exfoliation of raw graphitic material. Furthermore, we have proved through an accurate characterization that controlled centrifugation enables the selection of very stable (>8 months, ζ-potential +40/+70mV), few-layer

ADVANCED FUNCTIONAL MATERIALS

www.afm-journal.de

Table 1. Summary of MC and HC samples characteristics. Analysis of MC and HC performed on 16 and 24 individual flakes, respectively, and reported for each parameter as mean ± standard error. The standard error of $\langle N_G \rangle$ was calculated on the base of a fix error of ±1.5 on the single measurements.

Graphene property	Type of analysis	MC	HC
Average $\langle N_G \rangle$	Raman; 2D based metric[60]	3.8 ± 0.4 layers	2.9 ± 0.3 layers
Average $\langle L \rangle$	Raman; D/G based metric[60]	1.0 ± 0.1 μm	0.49 ± 0.06 μm
Defect type/oxidation	Raman D/D' based classification[60,66]	D/D' 3.8 ± 0.2	D/D' 3.8 ± 0.1
		Edge type defects	Edge type defects
		Not oxidized	Not oxidized
Biofunctionalization	AFM	Vmh2 monolayer	Vmh2 monolayer
	Electrophoretic mobility	Positive surface charge density	Positive surface charge density
Stability	Time	>8 months	>8 months
	ζ-potential[22]	+40/+70 mV	+40/+70 mV
Concentration	UV–vis spectroscopy[22,34]	90/100 μg mL^{-1}	20/30 μg mL^{-1}

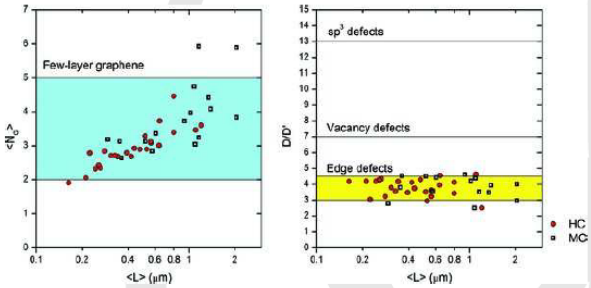

Figure 4. Statistical distribution of (left) the $\langle N_G \rangle$ and (right) the D/D' ratio, in MC and HC samples used for GBM classification. Experimental conditions as given in the text.

(<5 layers), and defect-free graphene (≈90/100 μg mL^{-1}) with an average lateral dimension of 1.0 ± 0.1 μm. Interestingly, the strong interplay between protein and graphene allows also the formation of either thin films on a silicon by the drop casting method or self-assembled biohybrid structures in solution by modulating the environmental conditions. As a potentially scalable approach, this method could enable massive production of biofunctionalized graphene, which could be a valuable material for the upcoming diffusion of new nanobiotechnologies in the global biomedical market.[10,11]

4. Experimental Section

Vmh2 Extraction from P. Ostreatus Mycelia: White-rot fungus, *P. ostreatus* (Jacq.: Fr.) Kummer (type: Florida; ATCC No. MYA-2306) was maintained at 4 °C through periodic transfer on potato dextrose agar (Difco) plates in the presence of 0.5% yeast extract. Mycelia were inoculated in 1 L flasks containing 500 mL of potato-dextrose broth (24 g L^{-1}) supplemented with 0.5% yeast extract, grown at 28 °C in shaken mode (150 rpm). After 10 days of fungal growth, mycelia were separated by filtration through gauze, treated twice with 2% SDS in a boiling water bath for 10 min, washed several times with water and once with 60% ethanol to completely remove the detergent. The residue was dried under nitrogen, grinded and treated with 100% trifluoroacetic acid (TFA) in a water bath sonicator (Elmasonic S30, Elma) for 30 min, and centrifuged (10 min at 3200 g). The supernatant was dried, and then lipids were extracted in a mixture of water–methanol–chloroform 2:2:1 v/v (5 min in bath sonicator). After centrifugation, proteins appeared as a solid aggregate at the interface between the water–methanol and the chloroform phases. They were recovered by liquid phase removal. The aggregated protein was dried, treated with TFA for 30 min in bath sonicator, redried, and dissolved in 80% ethanol. The sample was centrifuged (90 min at 12 000 g) and ethanol was removed from the supernatant under vacuum at 40 °C using rotavapor and the material was freeze-dried, treated with TFA as abovedescribed, and redissolved in 60% ethanol.

Exfoliation and Stabilization Process: Graphite powder (Aldrich, 332461, mesh number of grains +100, >75%) is exfoliated in batches of 5 mL of 60%, v/v, ethanol in MilliQ water (in 10 mL flasks), 17–200 μg mL^{-1} Vmh2, using a medium power tip sonicator (Q125 Sonicator, QSonica, 125 W, 20 kHz, inbuilt power meter power output, 19 W) and cooling the system in an ice bath. Concentration of dispersions is estimated by UV–vis spectroscopy. Absorption spectra are acquired on a UV–vis spectrophotometer SpectraMax M2e using a quartz cell 1 cm optics. Upon the subtraction of the solvent spectrum, we use the absorption coefficient value at 660 nm (1390 g L cm^{-1}) previously established by Lotya et. al.[20] in a surfactant exfoliation process and also used in the hydrophobin-assisted exfoliation reported by Laaksonen et al..[32] Controlled centrifugation is performed using a Sigma 2–16PK FIsher Bioblock Scientific centrifuge (rotor 12072 418/H) in 15 mL tubes.

HOPG (1000 μg mL^{-1}) is exfoliated as previously described, for 2 h in presence of Vmh2 protein (50 μg mL^{-1}) and left to settling for 3 days to remove the unexfoliated material. Alternatively, HOPG is biofunctionalized immediately after ultrasonication by mixing with a Vmh2 solution and treating 10 min in a bath sonicator (Fisherbrand, FB15051). A commercial GBM (Haydale, GNPs-O2) is resuspended in 6/4 (v/v) ethanol/MilliQ

ADVANCED FUNCTIONAL MATERIALS

water solution, Vmh2 (50–400 μg mL^{-1}), sonicated 10 min in bath sonicator and used.

Characterization: Scanning Electron Microscopy (SEM) images are acquired using a FEI Quanta 650 FEG ESEM, 2 kV microscope upon drop casting 3 μL of solution on a silicon chip. AFM measurements are performed on mica using a Nanoscope V Multimode8 AFM (Bruker, Germany) and Si cantilevers (SNL model, k:0.3N/m, Bruker). The SFM are used at a scan rate of 1 Hz and 512 × 512 pixel.

Electrokinetic analysis is carried out in folded capillary cells using a Malvern Zetasizer Nano-ZS system equipped with a 633 nm He–Ne laser. The instrument uses a combination of electrophoresis and laser Doppler velocimetry techniques to measure the electrophoretic mobility (U_e). All measurements are conducted at 25 °C.

ζ-potential is estimated using the Henry equation

$$U_e = \frac{2}{3}\frac{\varepsilon\zeta}{n} f(ka) \quad (1)$$

where U_e is the electrophoretic mobility, ε and η are the dielectric constant and the viscosity of the solvent respectively, ζ is the ζ-potential, and $f(ka)$ is the Henry function. Considering that the approximations for Henry function range between the Huckel and Smoluchowski limits, 1/1.5, we estimate the upper and lower bound for the ζ-potential. Raman spectra are acquired using a Horiba Jobin Yvon LabRAM HR 800, 800 mm focal length, 100× objective, excitation wavelength 532 nm. Exfoliated samples are drop casted for analysis on corning microscope glass slides (Aldrich, CLS294775×25), laser is focused on samples and multiple spectra are accumulated. For estimation of N_G and L we use the Raman metrics reported by Paton et al.[58]

$$\langle N_G\rangle \begin{cases} N_G = 10^{0.84M+0.45M^2} \\ M = \dfrac{I_{G'ene}(\omega=\omega_{p,G'ite})/I_{G'ene}(\omega=\omega_{s,G'ite})}{I_{G'ite}(\omega=\omega_{p,G'ite})/I_{G'ite}(\omega=\omega_{s,G'ite})} \end{cases} \quad (2)$$

$$\langle L\rangle \begin{cases} L = \dfrac{k}{(D/G)_{G'ene}-(D/G)_{G'ite}} \\ (D/G)_{G'ite} = 0.034 \\ k = 0.17 \end{cases} \quad (3)$$

where $I_{Grite}(\omega = \omega_{p,Grite})$ is the intensity of graphite 2D peak, $I_{Grite}(\omega = \omega_{s,Grite})$ is the intensity of graphite 2D shoulder measured at −30cm^{-1} in respect to 2D peak (see Figure 3), $I_{Grene}(\omega = \omega_{p,Grite})$ is the intensity of graphene spectrum at the wavenumber corresponding to graphite 2D peak (2717 cm^{-1}), $I_{Grene}(\omega = \omega_{s,Grite})$ is the intensity of graphene spectrum at wavenumber corresponding to graphite 2D shoulder (1686 cm^{-1}), $(D/G)_{Grite}$ is the value of D/G for graphite, and k is the slope that has been estimated by Paton et al. for the same graphitic material.

Supporting Information

Supporting Information is available from the Wiley Online Library or from the author.Acknowledgements

Acknowledgment

A.M.G. and E.M.-Ná. contributed equally to this work. This work was supported by The European Commission Program, FP7-OCEAN (613844) and MINECO (Spain; BIO2013–49464-EXP and RTC-2014–2619–7); Ministero dell'Università e della Ricerca Scientifica (Italy)—Industrial Research Project PON01_01966 EnerbioChem, funded in the frame of Operative National Programme Research and Competitiveness 2007–2013 D. D. Prot. n. 01/Ric. 18.1.2010; P.O.R. Campania FSE 2007–2013, Project CREMe. ICN2 acknowledges support from the Severo Ochoa Program (MINECO, Grant SEV-2013–0295).

Received: January 2, 2015
Revised: March 4, 2015
Published Online: MM DD, YYYY

[1] A. K. Geim, *Science* **2009**, *324*, 1530.
[2] A. K. Geim, K. S. Novoselov, *Nat. Mater.* **2007**, *6*, 183.
[3] M. D. Stoller, S. Park, Y. Zhu, J. An, R. S. Ruoff, *Nano Lett.* **2008**, *8*, 3498.
[4] C. Lee, X. Wei, J. W. Kysar, J. Hone, *Science* **2008**, *321*, 385.
[5] A. A. Balandin, S. Ghosh, W. Bao, I. Calizo, D. Teweldebrhan, F. Miao, C. N. Lau, *Nano Lett.* **2008**, *8*, 902.
[6] M. F. El-Kady, V. Strong, S. Dubin, R. B. Kaner, *Science* **2012**, *335*, 1326.
[7] R. R. Nair, P. Blake, A. N. Grigorenko, K. S. Novoselov, T. J. Booth, T. Stauber, N. M. R. Peres, A. K. Geim, *Science* **2008**, *320*, 1308.
[8] L. Gaudreau, K. J. Tielrooij, G. E. D. K. Prawiroatmodjo, J. Osmond, F. J. G. de Abajo, F. H. L. Koppens, *Nano Lett.* **2013**, *13*, 2030.
[9] J. S. Bunch, S. S. Verbridge, J. S. Alden, A. M. van der Zande, J. M. Parpia, H. G. Craighead, P. L. McEuen, *Nano Lett.* **2008**, *8*, 2458.
[10] A. C. Ferrari, F. Bonaccorso, V. Fal'ko, K. S. Novoselov, S. Roche, P. Bøggild, S. Borini, F. H. L. Koppens, V. Palermo, N. Pugno, J. A. Garrido, R. Sordan, A. Bianco, L. Ballerini, M. Prato, E. Lidorikis, J. Kivioja, C. Marinelli, T. Ryhänen, A. Morpurgo, J. N. Coleman, V. Nicolosi, L. Colombo, A. Fert, M. Garcia-Hernandez, A. Bachtold, G. F. Schneider, F. Guinea, C. Dekker, M. Barbone, Z. Sun, C. Galiotis, A. N. Grigorenko, G. Konstantatos, A. Kis, M. Katsnelson, L. Vandersypen, A. Loiseau, V. Morandi, D. Neumaier, E. Treossi, V. Pellegrini, M. Polini, A. Tredicucci, G. M. Williams, B. H. Hong, J.-H. Ahn, J. M. Kim, H. Zirath, B. J. van Wees, H. van der Zant, L. Occhipinti, A. Di Matteo, I. A. Kinloch, T. Seyller, E. Quesnel, X. Feng, K. Teo, N. Rupesinghe, P. Hakonen, S. R. T. Neil, Q. Tannock, T. Löfwander, J. Kinaret, A. C. Ferrari, *Nanoscale* **2014**, DOI: 10.1039/C4NR01600A.
[11] *Nat. Nanotechnol.* **2014**, *9*, 737.
[12] E. Morales-Narváez, A.-R. Hassan, A. Merkoçi, *Angew. Chem. Int. Ed.* **2013**, *52*, 13779.
[13] E. Morales-Narváez, A. Merkoçi, *Adv. Mater.* **2012**, *24*, 3298.

ADVANCED FUNCTIONAL MATERIALS

www.afm-journal.de

[14] K. S. Novoselov, A. K. Geim, S. V Morozov, D. Jiang, Y. Zhang, S. V Dubonos, I. V Grigorieva, A. A. Firsov, *Science* **2004**, *306*, 666.

[15] K. S. Novoselov, V. I. Fal[prime]ko, L. Colombo, P. R. Gellert, M. G. Schwab, K. Kim, *Nature* **2012**, *490*, 192.

[16] R. S. Edwards, K. S. Coleman, *Nanoscale* **2013**, *5*, 38.

[17] S. Eigler, A. Hirsch, *Angew. Chem. Int. Ed. Engl.* **2014**, *53*, 7720.

[18] S. Eigler, A. Hirsch, *Angew. Chem. Int. Ed.* **2014**, *53*, 7720.

[19] Y. Hernandez, M. Lotya, D. Rickard, S. D. Bergin, J. N. Coleman, *Langmuir* **2010**, *26*, 3208.

[20] M. Lotya, Y. Hernandez, P. J. King, R. J. Smith, V. Nicolosi, L. S. Karlsson, F. M. Blighe, S. De, Z. Wang, I. T. McGovern, G. S. Duesberg, J. N. Coleman, *J. Am. Chem. Soc.* **2009**, *131*, 3611.

[21] R. J. Smith, M. Lotya, J. N. Coleman, *New J. Phys.* **2010**, *12*, 125008.

[22] K. Yang, Y. Li, X. Tan, R. Peng, Z. Liu, *Small* **2013**, *9*, 1492.

[23] Y. Wang, Z. Li, J. Wang, J. Li, Y. Lin, *Trends Biotechnol.* **2011**, *29*, 205.

[24] C. Chung, Y.-K. Kim, D. Shin, S.-R. Ryoo, B. H. Hong, D.-H. Min, *Acc. Chem. Res.* **2013**, *46*, 2211.

[25] K. V. Krishna, C. Ménard-Moyon, S. Verma, A. Bianco, *Nanomedicine* **2013**, *8*, 1669.

[26] T. S. Sreeprasad, V. Berry, *Small* **2013**, *9*, 341.

[27] M. Calvaresi, F. Zerbetto, *Acc. Chem. Res.* **2013**, *46*, 2454.

[28] C. Li, R. Mezzenga, *Nanoscale* **2013**, *5*, 6207.

[29] M. I. Solar, M. J. Buehler, *Nat. Nanotechnol.* **2012**, *7*, 417.

[30] C. Li, J. Adamcik, R. Mezzenga, *Nat. Nanotechnol.* **2012**, *7*, 421.

[31] W. Yang, Q. Ren, Y.-N. Wu, V. K. Morris, A. a Rey, F. Braet, A. H. Kwan, M. Sunde, *Biopolymers* **2013**, *99*, 84.

[32] P. Laaksonen, M. Kainlauri, T. Laaksonen, A. Shchepetov, H. Jiang, J. Ahopelto, M. B. Linder, *Angew. Chem. Int. Ed.* **2010**, *49*, 4946.

[33] Z. Wang, Y. Wang, Y. Huang, S. Li, S. Feng, H. Xu, M. Qiao, *Carbon* **2010**, *48*, 2890.

[34] K. Kurppa, H. Jiang, G. R. Szilvay, A. G. Nasibulin, E. I. Kauppinen, M. B. Linder, *Angew. Chem. Int. Ed. Engl.* **2007**, *46*, 6446.

[35] J. Bayry, V. Aimanianda, J. I. Guijarro, M. Sunde, J.-P. Latgé, *PLoS Pathog.* **2012**, *8*, e1002700.

[36] X. Wang, H. Wang, Y. Huang, Z. Zhao, X. Qin, Y. Wang, Z. Miao, Q. Chen, M. Qiao, *Biosens. Bioelectron.* **2010**, *26*, 1104.

[37] M. P. Sarparanta, L. M. Bimbo, E. M. Mäkilä, J. J. Salonen, P. H. Laaksonen, A. M. K. Helariutta, M. B. Linder, J. T. Hirvonen, T. J. Laaksonen, H. A. Santos, A. J. Airaksinen, *Biomaterials* **2012**, *33*, 3353.

[38] H. K. Valo, P. H. Laaksonen, L. J. Peltonen, M. B. Linder, J. T. Hirvonen, T. J. Laaksonen, *ACS Nano* **2010**, *4*, 1750.

[39] M. B. Linder, G. R. Szilvay, T. Nakari-Setälä, M. E. Penttilä, *FEMS Microbiol. Rev.* **2005**, *29*, 877.

[40] H. J. Hektor, K. Scholtmeijer, *Curr. Opin. Biotechnol.* **2005**, *16*, 434.

[41] V. Aimanianda, J. Bayry, S. Bozza, O. Kniemeyer, K. Perruccio, S. R. Elluru, C. Clavaud, S. Paris, A. a Brakhage, S. V Kaveri, L. Romani, J.-P. Latgé, *Nature* **2009**, *460*, 1117.

[42] L. De Stefano, I. Rea, E. De Tommasi, I. Rendina, L. Rotiroti, M. Giocondo, S. Longobardi, a Armenante, P. Giardina, *Eur. Phys. J. E. Soft Matter* **2009**, *30*, 181.

[43] A. Zykwinska, M. Pihet, S. Radji, J.-P. Bouchara, S. Cuenot, *Biochim. Biophys. Acta* **2014**, *1844*, 1137.

[44] A. Zykwinska, T. Guillemette, J.-P. Bouchara, S. Cuenot, *Biochim. Biophys. Acta* **2014**, *1844*, 1231.

[45] I. Macindoe, A. H. Kwan, Q. Ren, V. K. Morris, W. Yang, J. P. Mackay, M. Sunde, *Proc. Natl. Acad. Sci. U.S.A.* **2012**, *109*, E804.

[46] V. K. Morris, Q. Ren, I. Macindoe, A. H. Kwan, N. Byrne, M. Sunde, *J. Biol. Chem.* **2011**, *286*, 15955.

[47] I. M. Tucker, J. T. Petkov, J. Penfold, R. K. Thomas, P. Li, A. R. Cox, N. Hedges, J. R. P. Webster, *J. Phys. Chem. B* **2014**, *118*, 4867.

[48] S. Longobardi, D. Picone, C. Ercole, R. Spadaccini, L. De Stefano, I. Rea, P. Giardina, *Biomacromolecules* **2012**, *13*, 743.

[49] A. Armenante, S. Longobardi, I. Rea, L. De Stefano, M. Giocondo, A. Silipo, A. Molinaro, P. Giardina, *Glycobiology* **2010**, *20*, 594.

[50] S. Houmadi, R. D. Rodriguez, S. Longobardi, P. Giardina, M. C. Fauré, M. Giocondo, E. Lacaze, *Langmuir* **2012**, *28*, 2551.

[51] L. De Stefano, I. Rea, P. Giardina, A. Armenante, I. Rendina, *Adv. Mater.* **2008**, *20*, 1529.

[52] I. Rea, P. Giardina, S. Longobardi, F. Porro, V. Casuscelli, I. Rendina, L. De Stefano, *J. R. Soc. Interface* **2012**, *9*, 2450.

[53] S. Longobardi, A. M. Gravagnuolo, R. Funari, B. Della Ventura, F. Pane, E. Galano, A. Amoresano, G. Marino, P. Giardina, *Anal. Bioanal. Chem.* **2014**, *407*, 487.

[54] L. De Stefano, I. Rea, A. Armenante, P. Giardina, M. Giocondo, I. Rendina, *Langmuir* **2007**, *23*, 7920.

[55] V. Georgakilas, M. Otyepka, A. B. Bourlinos, V. Chandra, N. Kim, K. C. Kemp, P. Hobza, R. Zboril, K. S. Kim, *Chem. Rev.* **2012**, *112*, 6156.

[56] K. Kostarelos, K. S. Novoselov, *Science* **2014**, *344*, 261.

[57] P. Wick, A. E. Louw-Gaume, M. Kucki, H. F. Krug, K. Kostarelos, B. Fadeel, K. A. Dawson, A. Salvati, E. Vázquez, L. Ballerini, M. Tretiach, F. Benfenati, E. Flahaut, L. Gauthier, M. Prato, A. Bianco, *Angew. Chemie Int. Ed.* **2014**, *53*, 7714.

[58] K. R. Paton, E. Varrla, C. Backes, R. J. Smith, U. Khan, A. O'Neill, C. Boland, M. Lotya, O. M. Istrate, P. King, T. Higgins, S. Barwich, P. May, P. Puczkarski, I. Ahmed, M. Moebius, H. Pettersson, E. Long, J. Coelho, S. E. O'Brien, E. K. McGuire, B. M. Sanchez, G. S. Duesberg, N. McEvoy, T. J. Pennycook, C. Downing, A. Crossley, V. Nicolosi, J. N. Coleman, *Nat. Mater.* **2014**, *13*, 624.

[59] E. Lurie-Luke, *Biotechnol. Adv.* **2014**, *32*, 1494.

[60] U. Khan, A. O'Neill, H. Porwal, P. May, K. Nawaz, J. N. Coleman, *Carbon* **2012**, *50*, 470.

[61] A. Bianco, *Angew. Chem. Int. Ed. Engl.* **2013**, *52*, 4986.

[62] Y. Ma, H. Shen, X. Tu, Z. Zhang, *Nanomedicine* **2014**, *9*, 1565.

[63] A. Bianco, H.-M. Cheng, T. Enoki, Y. Gogotsi, R. H. Hurt, N. Koratkar, T. Kyotani, M. Monthioux, C. R. Park, J. M. D. Tascon, J. Zhang, *Carbon* **2013**, *65*, 1.

[64] A. Eckmann, A. Felten, A. Mishchenko, L. Britnell, R. Krupke, K. S. Novoselov, C. Casiraghi, *Nano Lett.* **2012**, *12*, 3925.

[65] A. O'Neill, U. Khan, P. N. Nirmalraj, J. Boland, J. N. Coleman, *J. Phys. Chem. C* **2011**, *115*, 5422.

[66] U. Khan, A. O'Neill, M. Lotya, S. De, J. N. Coleman, *Small* **2010**, *6*, 864.

WILEY-VCH

Supporting Information

In situ Production of Biofunctionalized Few-Layer Defect-Free Microsheets of Graphene

*Alfredo M. Gravagnuolo‡, Eden Morales-Narváez‡, Sara Longobardi, Everson T. da Silva, Paola Giardina and Arben Merkoçi**

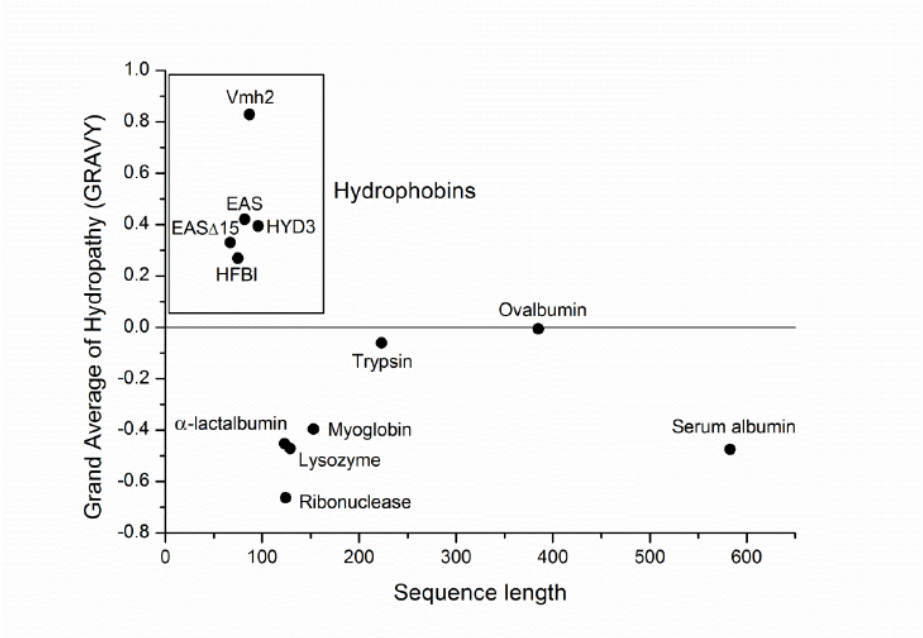

Figure S1. Properties of hydrophobins relevant to carbon based materials interactions. Hydropathic character of some soluble proteins, included hydrophobins that have been used to functionalize carbon based materials. GRAVY index is evaluated on the basis of amino acid composition and Kyte & Doolittle scale.[1]

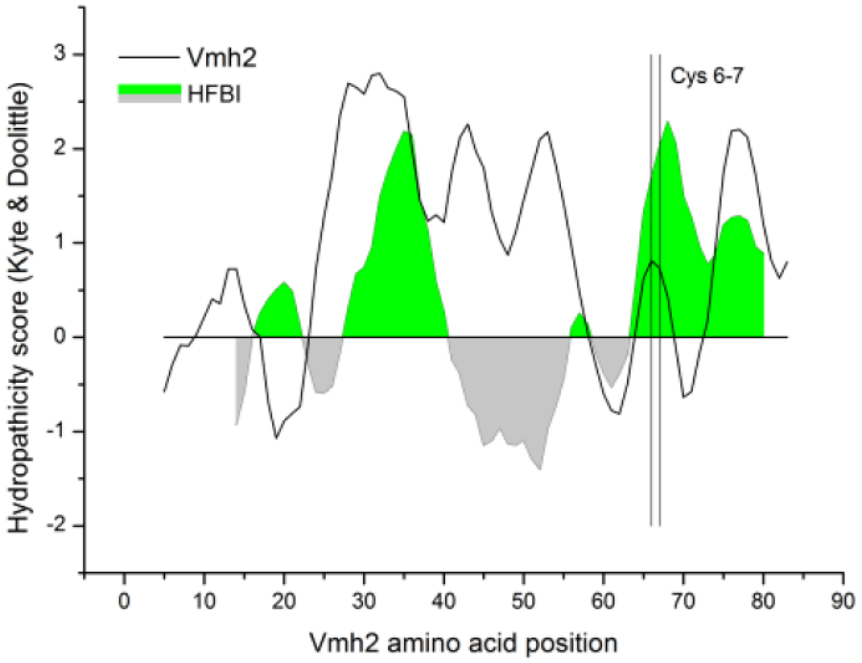

Figure S2. Properties of Vmh2 relevant to GBMs interactions. Hydropathicity pattern of Vmh2 (UniProt[2] Accession Number Q8WZI2; chain 25-111) and HFBI (UniProt Accession Number P52754; chain 23-97) displayed by Prot Scale[1] (parameters: Kyte & Doolittle amino acid scale; 9 amino acids windows size; 20% relative weight of the window edges; linear weight variation model).

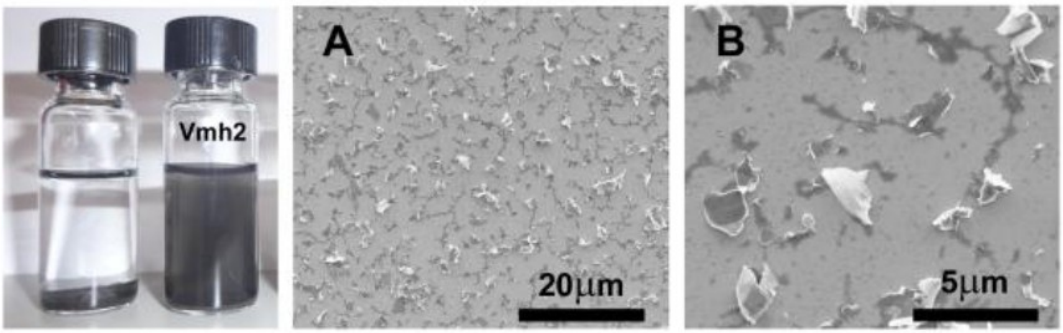

Figure S3. Vmh2 assisted liquid-phase exfoliation of HOPG. (left) Samples of HOPG exfoliated for 2 hours in the presence or absence of Vmh2 and kept to settle out for 3 days. (A, B) HOPG-Vmh2 coating of a silicon chip obtained by drop casting. Experimental conditions as given in the text.

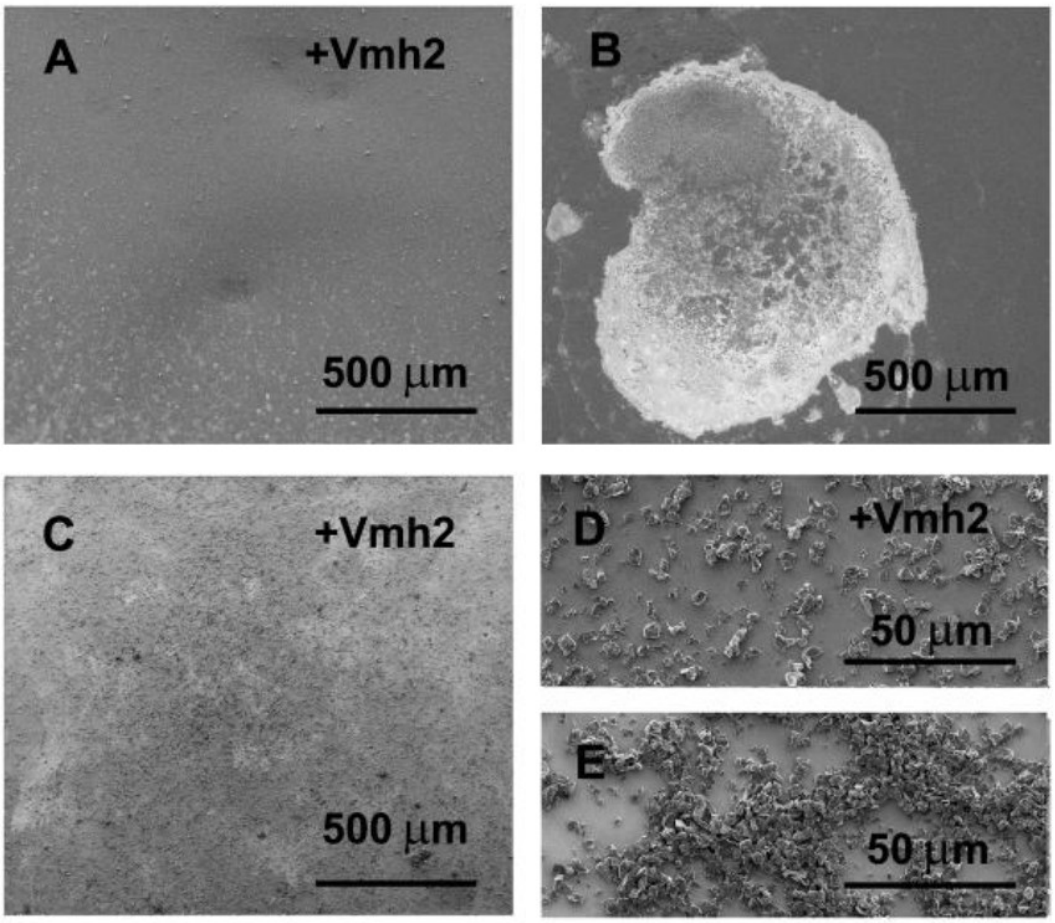

Figure S4. Vmh2 stabilization of GBMs. (A) Silicon chip coated by drop casting with HOPG biofunctionalized after exfoliation. (B) Silicon chip coated with HOPG as in (A) but in the absence of Vmh2. (C, D) Silicon chip coated with a commercial GBM powder stabilized by mixing with Vmh2. (E) Silicon chip coated as in (C, D) using the commercial GBM in the absence of Vmh2.-Experimental conditions as given in the text

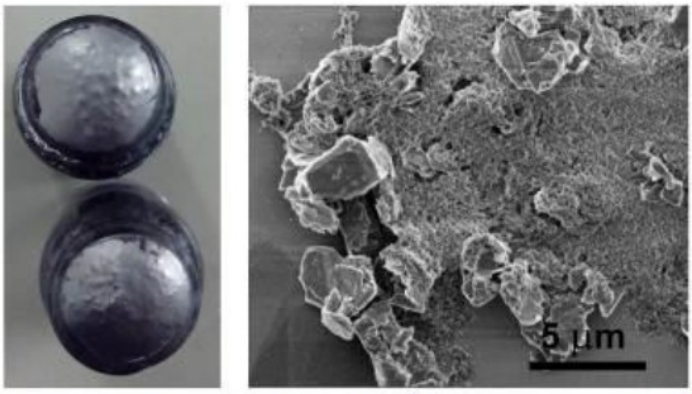

Figure S5. Self-assembled bio-hybrid structures. (Left) Exfoliated Vmh2-GBM at liquid-air interface upon lowering the solvent polarity by water addition (Right) Vmh2-commercial GBM co-aggregate, assembled upon ammonia addition.

WILEY-VCH

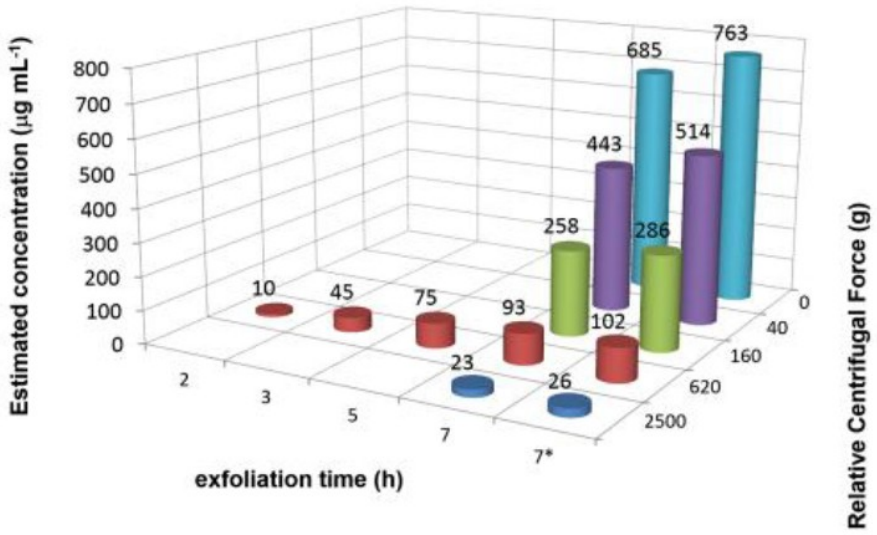

Figure S6. Graphene production assessment. Optimization of the production process by using: graphite flakes 1mg mL^{-1}; Vmh2 50 ug mL^{-1}; 60% (v/v) ethanol in water solution. (7*) effect of using double amounts of starting material (2mg/mL) and Vmh2 (100µg mL^{-1}).

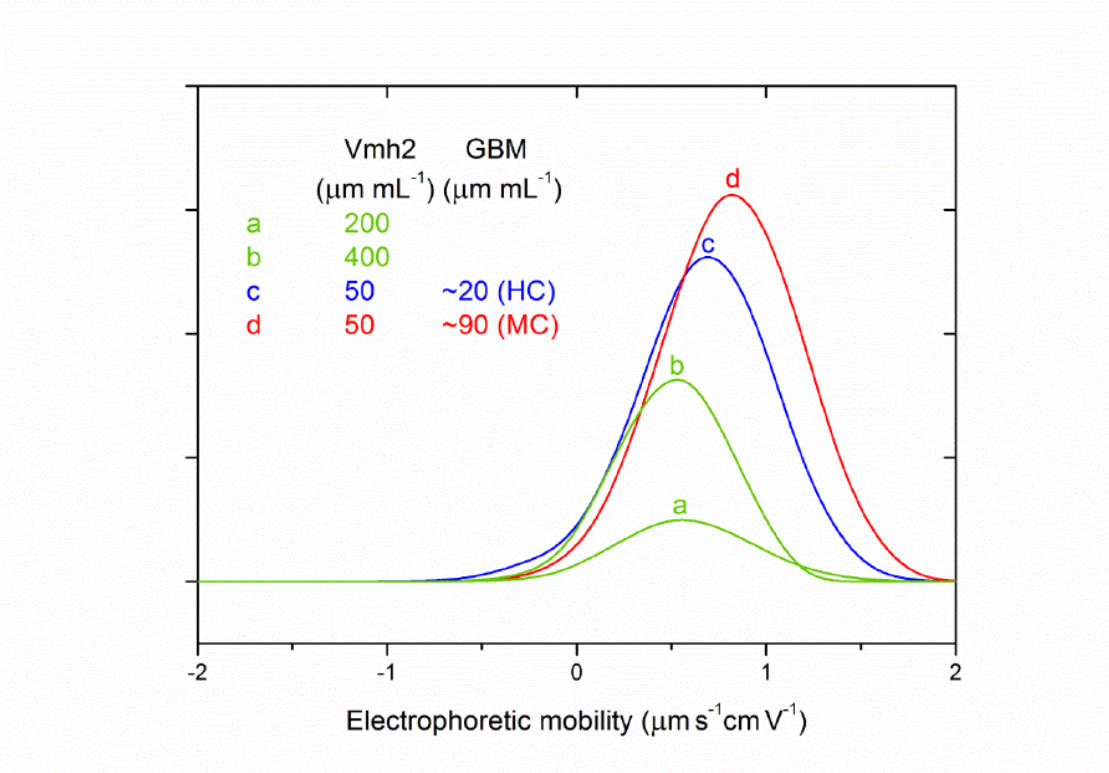

Figure S7. Electrophoretic mobility distribution. (a) Vmh2 200 ug mL^{-1}. (b) Vmh2 400 ug mL^{-1} (c) HC sample; Vmh2 50 ug mL^{-1}, few layer graphene ~20 ug mL^{-1}. (d) MC sample; Vmh2 50 ug mL^{-1}, few layer graphene ~90 ug mL^{-1}. Since the signal intensity of Vmh2 sample was too low at the concentration used for exfoliation, measurements were perforemd at higher concentrations (a, b)

Table S1. Comparison of Hydrophobin assisted exfoliations proposed by Laaksonen *et al.* 2010. Process parameters used for the production of biofunctionalized graphene at the best of their yield.

	This work	Laaksonen *et al.* 2010[3]
Hydrophobin	Vmh2 from *Pleurotus ostreatus* (50 ÷ 100 μg mL^{-1})	HFBI from *Trichoderma reesei* (25 ÷ 2000 μg mL^{-1})
Graphite source	Graphite powder (1000-2000 mg mL^{-1})	Chemically purified Kish graphite (amount not available)
Solvent	60%, v/v, ethanol in MilliQ water	MilliQ water
Tip Sonicator	Q125 Sonicator, QSonica, **125 Watt**, 20kHz. Inbuilt power meter power output = 19 W	Vibra-Cell VCX 750, Sonics & Materials Inc., **750 Watt**, 20KHz
Reaction volume	5 mL	0,3 ÷ 1 mL
Exfoliation Time	7 hours in presence of Vmh2	2 minutes in absence of HFBI and 2 minutes in presence of HFBI
Removal of un-exfoliated material	40 min at 40g using a Sigma 2-16PK FIsher Bioblock Scientific centrifuge (rotor 12072 418/H)	Gentle centrifugation using a National Labnet Co., Mini centrifuge C-1200
Yield	~440 ÷ 510 μg mL^{-1}	~25 ÷ 40 μg mL^{-1}

SUPPORTING REFERENCES

[1] E. Gasteiger, C. Hoogland, A. Gattiker, S. Duvaud, M. R. Wilkins, R. D. Appel, A. Bairoch, In *The Proteomics Protocols Handbook*; Walker, J. M., Ed.; Humana Press: Totowa, NJ, 2005; pp. 571–607.

[2] The UniProt Consortium, *Nucleic Acids Res.* **2014**, *42*, D191.

[3] P. Laaksonen, M. Kainlauri, T. Laaksonen, A. Shchepetov, H. Jiang, J. Ahopelto, M. B. Linder, *Angew. Chemie Int. Ed.* **2010**, *49*, 4946.

Article type: Full Paper (Manuscript in preparation)

On-the-spot Immobilization of Nanomaterials and Proteins Using Hydrophobins

Alfredo M. Gravagnuolo[1,2], Eden Morales-Narváez[1], Sara Longobardi[2], Charlene R.S. Matos[1], Paola Giardina[2] and Arben Merkoçi[1,3]

[1] ICN2 – Catalan Institute of Nanoscience and Nanotechnology, 08193 Barcelona, Spain
[2] Department of Chemical Sciences, University of Naples "Federico II", 80126 Naples, Italy
[3] ICREA – Catalan Institution for Research and Advanced Studies, 08010 Barcelona, Spain

Keywords: biofunctionalized glass, microarray, bio-conjugate, self-assembling, Vmh2 hydrophobin, bio-hybrid material.

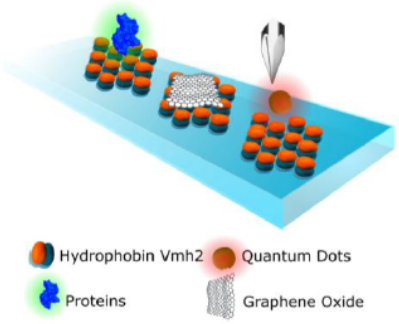

ToC figure

Abstract

Surface modification at the molecular level is a paramount method enabling functional properties in substrates for biotechnological applications. The Class I hydrophobin Vmh2, a peculiar surface active and versatile fungal protein, is known to self-assemble into chemically stable amphiphilic films, able to change wettability of surfaces and to strongly adsorb other proteins in their active form. Herein, glass functionalization by spontaneous self-assembling of Vmh2 at liquid-solid interface is demonstrated in 4 min net time. Vmh2 substrate is feasible for the micropattering immobilization of proteins and home-made quantum dots. Functionality of proteins on Vmh2 layer is shown using an immunoassay in microarray format. Moreover a graphene oxide layer is homogeneously assembled on the Vmh2 substrate. The developed microarray platform could open the way to new strategies in optical sensing.

3. VMH2 SELF-ASSEMBLED COATING ENHANCES THE SURFACE PROPERTIES OF MATERIALS FOR BIOTECHNOLOGICAL APPLICATIONS

Introduction

Surface modification at the molecular level is a paramount method enabling functional properties in substrates for biotechnological applications. In this work, the coating of glass slides through self-assembling biomacromolecules, towards the immobilization of both nanomaterials and proteins in microarray-fashion is studied for the first time.

Nanomaterials - materials with one or more dimensions in the size range between that of bulk materials and of discrete molecules - reveal novel intriguing properties that are world-wide studied with the aim of integrating them in the next-generation technological devices. Consequently, nano(bio)medical research aims to boost the number of breakthrough applications in areas such as nanomedicine, (bio)analytical chemistry, and bioelectronics.[1]

Semiconductor (III-V and II-VI) quantum dots (QDs), are 2-10 nm high performance fluorescent crystals come into play in lieu of classic organic labels because of their high resistance to photobleaching, high brightness and versatility.[2,3] Capable of absorbing radiation in a broad range of wavelengths and showing tunable emission, from UV to mid-IR in dependence of their size, they enable new strategies in sensing and bioimaging.

Graphene Oxide (GOx), is a molecularly flat nanomaterial easily processed in solution and synthesized in large quantity, which has shown outstanding performances in optical sensing.[3] It is a universal long-range superquencer, capable of direct wiring with biomolecules, such as peptides proteins and nucleotides, through its heterogeneous chemical structure. The interplay between GOx, biological molecular assemblies and other nanomaterials can open the avenue to unprecedented opportunities for the development of low-cost and rapid molecular diagnostics tools.[4–6] However their efficient integration in functional devices require strategies to control their assembly without hampering their properties and even enhancing their features.[7]

Self-assembling of proteins, "nanomachines" endowed with a broad variety of functions, is nowadays intensively studied as fundamental and green strategy to build hierarchical

structures in both living systems and hybrid functional assemblies for bio-nano-technological purposes.[8] Hydrophobins (HFB) are self-assembling proteins commonly produced by filamentous fungi that, arising from the typical fungal life style, have evolved "Janus-faced" structures and special functions.[9]. In their soluble forms HFBs are excellent surface active proteins [10] and find applications in industrial and medical biotechnology as foams, emulsions and dispersions stabilizers. HFBs also self-assemble into amphiphilic structured layers able to reverse the wettability of both hydrophilic and hydrophobic materials. Since the layers formed by HFBs of Class I show exceptional chemical stability, i.e. in hot water in the presence of detergents (SDS), they find applications in the biofunctionalization of the surfaces for biomedical devices. Moreover, the adhesive properties of the HFB films, exploited by fungi to grow on hydrophobic surfaces, have been demonstrated to be effective as a "primer" for surfaces bioconjugation of another protein layer on inert surfaces.[11]

Vmh2 from the white-rot fungus *Pleurotus ostreatus* is one of the most hydrophobic HFBs known, soluble in low polar solvents. This Class I HFB has been isolated and studied in our laboratories and used for modification of steel,[12,13] nanostructured silicon[14] and graphene based materials.[15] The nanometric layer (≈2.5 nm tick) of Vmh2 has been characterized on different surfaces as well its self-assembled rod-like structures, typically formed by class I HFBs.[16] The Vmh2 monolayer acts as a bioactive substrate to bind other proteins, which show improved stability and activity when bound on the biohybrid chips.[13,17]

Microarrays are multiple-screening platforms, miniaturized labs-on-a-surface, allowing high-throughput sensing. The disposition of high concentrated selectively sensing molecules in micrometric confined areas analyzed by laser light scanning with micrometric resolution allows bump-up the signal-to-noise ratio and sensitivity, therefore reaching very low limit of detection, and allows the use of very low quantities of detection molecules.

Herein, glass functionalization by spontaneous and rapid self-assembling of Vmh2 at liquid-solid interface is demonstrated. Time needed for surface functionalization is lower than that of

the latest chemical microarray technologies.[18] Relevant surface characteristics of biofunctionalized slides are evaluated and compared with a commercially available, standard aminosilane substrate. Micro-patterning immobilization of labeled proteins and home-made quantum dots are performed obtaining high signal-to-background ratio. Moreover a GOx layer is assembled on the Vmh2 substrate. Functionality of proteins on Vmh2 layer is shown using an immunoassay in microarray format which has been previously developed in our laboratories.[19]

2. Results and Discussion

2.1. Functionalization of glass by self-assembling layers of Vmh2

Immobilization of proteins and nanomaterials on glass was performed in three steps (Figure 1): i) preparation of negatively charged glass surfaces by air plasma treatment (Figure 1A); ii) quick assembly amphiphilic layers of Vmh2 by dip casting method (Figure 1B-1); iii) simple immobilization of proteins (Figure 1B) and nanomaterials (Figure 1C) on Vmh2 substrate by microarray patterning or dip casting.

i) The use of highly homogenous and chemically controlled substrates is essential to develop standard procedures for surface adhesion of molecular layers. Air plasma can be used in surface technology to process glasses at the nanoscale, highly oxidizing a few monolayers of the surface and removing organic contaminants. Since Vmh2 in 60% ethanol solution is endowed with positive electrostatic potential (electrophoretic mobility),[15] negatively charged glass surfaces obtained by air plasma treatment was appropriate to enhance the protein binding.

Precleaned glass slides provided by two manufacturers, MI and MII, showed a water contact angle (WCA) of 18 ± 3° and 31 ± 3° (mean ± standard deviation) respectively.

Following two minutes of plasma treatment, MI and MII were not distinguishable by WCA analysis, showing a very homogenous super-hydrophilic surface (WCA, < 5°).

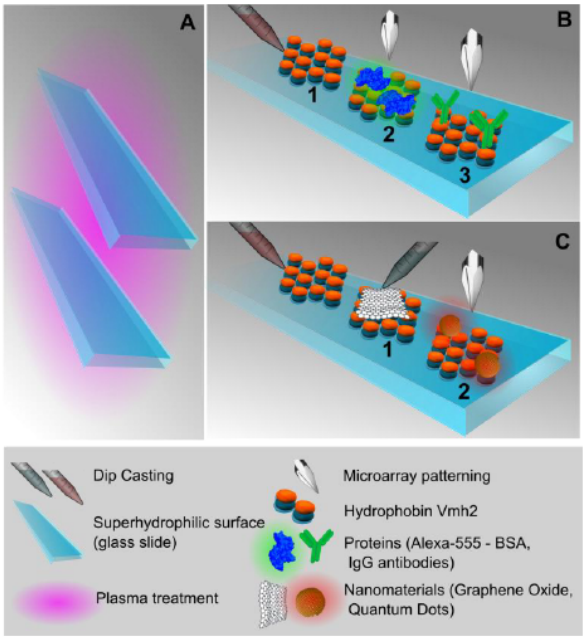

Figure 1. General procedure for hydrophobin Vmh2 based glass slide functionalization (schematic representation, not to scale). A, 2 min plasma treatment of bare glass slides. B, biofunctionalization of glass slide with: B1, Vmh2 layer by drop dip casting; B2, Alexa555-BSA by microarray patterning; B3, anti IgG antibodies by microarray patterning. C, immobilization of nanomaterials with: C1, Graphene Oxide by manual dip coating; C2, CdTe Quantum Dots by microarray patterning.

ii) The high wettable treated glass and the low surface tension of the Vmh2 solvent (60% ethanol), allowed a thin, liquid layer to be readily formed on the whole top area of the slides, 18.8 cm^2, upon drop casting 200 µL of 0÷400 ng $µL^{-1}$ Vmh2 solution. After only two minutes of incubation at room temperature, the excess of Vmh2 was washed out by 60% ethanol and the surface was dried in a steam of nitrogen. The analysis of the WCA shift upon quick-

assembly of Vmh2 showed that the surface saturation was achieved by 100 ng μL^{-1} Vmh2 (Figure 2).

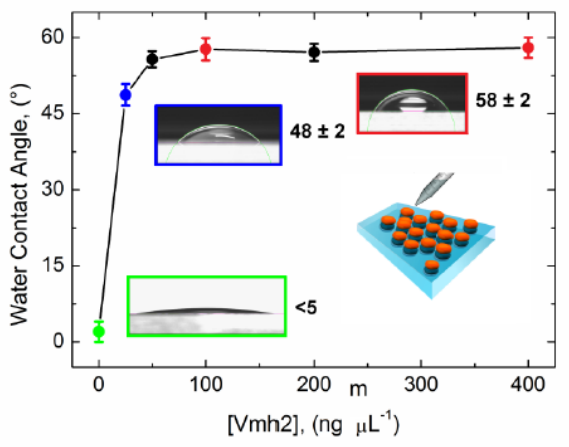

Figure 2. Optimization of superhydrophilic glass slide functionalization analyzed by WCA shift (mean ± standard deviation) in dependence of Vmh2 concentration.

However, ≈80% of saturation was reached, WCA 48 ± 2°, using only 25 ng μL^{-1} Vmh2, corresponding to 270 ng per cm^2 of glass area. On the basis of the diameter of a globular monomer of hydrophobin, ≈30 A°,[20] and the molecular weight of Vmh2, 8563 Da,[21] the estimated amount of Vmh2 necessary to form a monolayer on a flat area of one cm^2 is about 200 ng. This value suggested that a Vmh2 monolayer was formed, also considering the yield of the process and the actual roughness of the glass surface. For further experiments a Vmh2 concentration of 50 ng μL^{-1} was used to optimize the cost-efficiency of the process, achieving ≈90% of surface saturation.

These results highlighted the ability of Vmh2 to self-assemble into amphiphilic mono-layers efficiently modifying the wettability of surfaces. Indeed, only one mg of Vmh2 was able to coat 100 slides (≈200 mg of Vmh2 can be extracted and purified from one Liter of fungal culture) in this process configuration. Remarkably only four minutes were needed for

slides fabrication, the sum of net times for plasma treatment and Vmh2 self-assembling process, demonstrating that a cost-effective process was developed. The electrostatic interaction between Vmh2 and the negatively charged glass surface, enhanced in lower polar solvent with respect to water, could play a key role in this rapid functionalization both increasing the local concentration of Vmh2 at the solid-liquid interface and driving the orientation of the amphiphilic hydrophobin molecules to form a highly ordered amphipilic layer.

The proposed glass biofunctionalization was fast in comparison to standard chemical processes (~13 hours) and to the latest methods for rapid microarray fabrication.[18]. Therefore it was tested for nanomaterial and protein micro-patterning/immobilization.

iii) Home-made quantum dots and proteins were patterned by a microarray robot using a previously optimized protocol [19]. The glass slides were masked using a multiwell microarray cassette to separate the surface in 24 chambers. In each chamber a block of up to 550 micrometric drops can be dispensed. Alternatively, up to 16969 drops per slide can be dispensed in an ordered array of 71 columns and 239 rows in absence of mask. Another nanomaterial, GOx, was deposited in a different arrangement. In this case a second homogeneous layer was assembled on the Vmh2 substrate, and used for further protein patterning. In any case the functionalized surfaces were strongly washed in presence of detergents to test the stability of binding. Analysis of the results obtained by proteins, QD and GOx immobilization is described in the following sections.

2.2. Protein immobilization

Vmh2-glass was tested for protein immobilization, and compared with a commercial available aminosilane substrate as a reference surface. To evaluate protein adsorption and bio-functionality, two proteins, the fluorescent Alexa555-BSA conjugate (A555B) and anti IgG antibodies (αIgG) were micro-patterned in microarray format,[19] upon adsorption onto the

Vmh2 substrate. Morphology and of A555B protein spots, signal-to-background, coefficient of variation (CV) of fluorescence intensity were evaluated (Figure 3). Moreover the effect of the plasma pre-treatment prior to Vmh2 self-assembling on the final results was demonstrated (Figure S1-2).

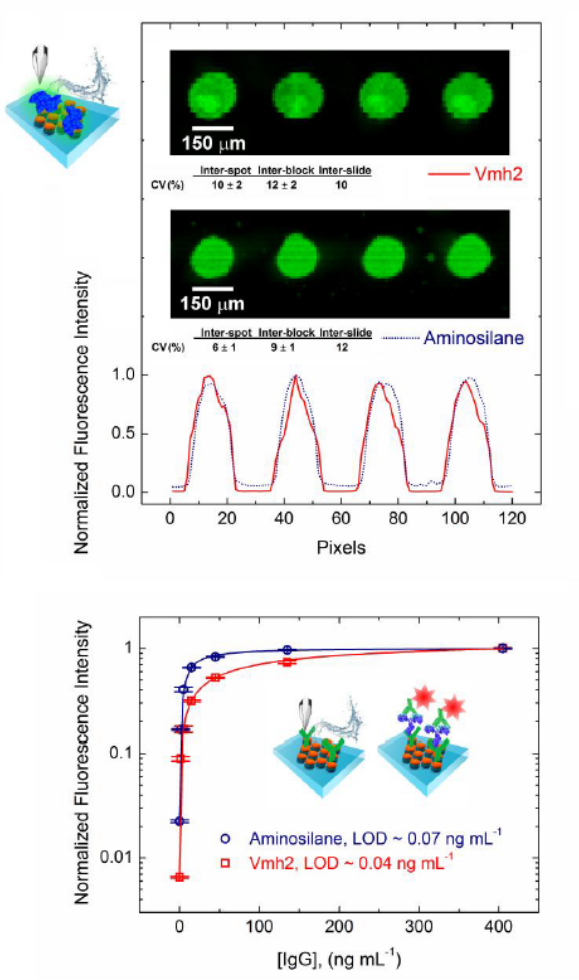

Figure 3. Micro-patterning of proteins on Vmh2 hydrophobin coated glass slides. Top, spot morphology and profile of micro-patterned A555B (excited at 532 nm) on both Vmh2 coated slides MI (750 µg mL^{-1} A555B, 600 PMT gain laser scanner detector) and aminosilane glass slides (200 µg mL^{-1} A555B, 500 PMT gain laser scanner detector), after washing by PBST. Inter-spot (180 spots), inter-block (18 blocks) and inter slide (3 slides) CV are

indicated (details as given in the text). **Bottom**, IgG detection in microarray format. Comparison of aminosilane and Vmh2 coated slides. Bars represent the standard deviation of normalized fluorescence intensity of 4 spots (details as given in experimental section). Detection curves extrapolated by logistic fitting.

Following the incubation of A555B at 750 μg mL^{-1} (the effect of different A555B concentrations on spot morphology is shown in Figure S3) and harsh washing with PBST, fluorescence images of Vmh2-glass surface showed stably immobilized, circularly shaped spots, ~75 μm of radius. Moreover the profile of fluorescence intensity over the surface area evidenced a very high signal-to-background ratio also confirming the good optical properties of the Vmh2 layer.[14] On the other hand, aminosilane exhibited higher binding affinity (A555B was incubated at 200 μg mL^{-1}, to reduce background noise) which resulted in a more homogenous distribution of protein inside a spot, as evidenced by the intensity profile.

The consistency of Vmh2-coating over the whole slide was evaluated comparing the CV of 180 spots intensity with the standard aminosilane substrate. A total number of 18 blocks per slide were printed, each block made of 10 spots for a total of 180 spots per slide in triplicate experiments (see experimental section for details of the statistical comparison). In this configuration, spot-to-spot, block-to-block and slide-to-slide CV evidenced slight higher signal variability on Vmh2 then in aminosilane substrate (Figure3).

Further characterization was performed to evaluate the biological function of the immobilized αIgG upon immobilization on Vmh2-glass. Incubation of αIgG was performed at the same concentration on both Vmh2 and aminosilane substrates. Then IgG detection was carried out according to the previously reported method[19] in microarray format (Figure 3).

Analysis of calibration curves showed that the Vmh2 coated slides, even 45 days after fabrication, were comparable to the commercial standard (Figure S4). Therefore, an easy

method for stable micropatterning of protein in the active form was developed using cheap materials and fast fabrication.

2.3. QDs immobilization

Cadmium Tellurium (CdTe) Quantum Dots (QDs) nanocrystals were synthesized and characterized in our laboratories (Figure S7, S8, S9). Particles showed spherical shape, 4.28 ± 1.94 (mean ± standard deviation) diameter, light absorption from UV to visible and a single fluorescence peak, centered at 660 nm (Figure S10).

Immobilization of QDs on the Vmh2-glass surface was performed as for proteins. Micrometric drops of 10μM QDs dissolved in spotting buffer, were patterned by robot on the Vmh2 and aminosilane substrate, incubated over night and the surfaces were strongly washed by detergent containing buffer. Fluorescence images of the slides surface were acquired by laser scanner (exc 635 nm / em 675 nm) and analyzed to evaluate QDs immobilization (Figure 4).

Micrometric spots, ≈60 μM radius, with excellent signal-to-background were stably adsorbed only on the Vmh2 substrate, whereas only traces of QDs were immobilized on aminosilane. Moreover, spot-to-spot, block-to-block, and slide-to-slide CV evidenced that a quite good reproducibility of immobilized spots were achieved on the Vmh2 substrate. It is worth noting that non optimal excitation wavelength was used, constrained by the instrument coupled light emission filter. Nevertheless by using a 90% photomultiplier gain, very good signal-to-background was obtained.

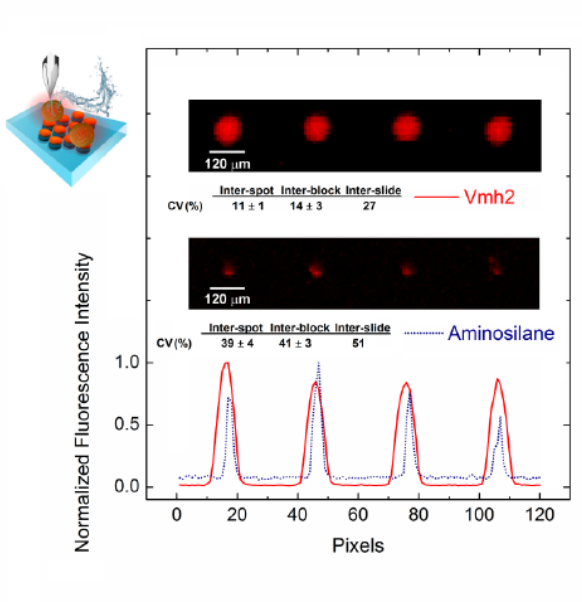

Figure4. Micro-patterning of Quantum Dots on Vmh2 hydrophobin coated glass slides. Spot morphology and profile of micro-patterned CdTe QDs (excited at 635 nm) on both Vmh2 coated slides and aminosilane glass slides (900 PMT), after washing by PBS - 0.05% Tween 20. Inter-spot (180 spots), inter-block (18 blocks) and inter slide (3 slides) coefficient of variation are indicated (details as given in the text).

2.4. Graphene Oxide immobilization

Water-based dispersions of single layer GOx microsheets, with lateral dimensions ranging from 0.18 to 1.2 µm and showing a C/O ratio around 1 (manufacturer's data, approximate values) were casted on the top surface of Vmh2 coated glass slides, incubated for ten minutes at different concentrations, washed five minutes in MilliQ water and dried in a steam of nitrogen. Since the GOx particles are negatively charged, the analysis of surface hydrophobicity offered a first insight into the immobilization extent and reliability (Figure 5A-B).

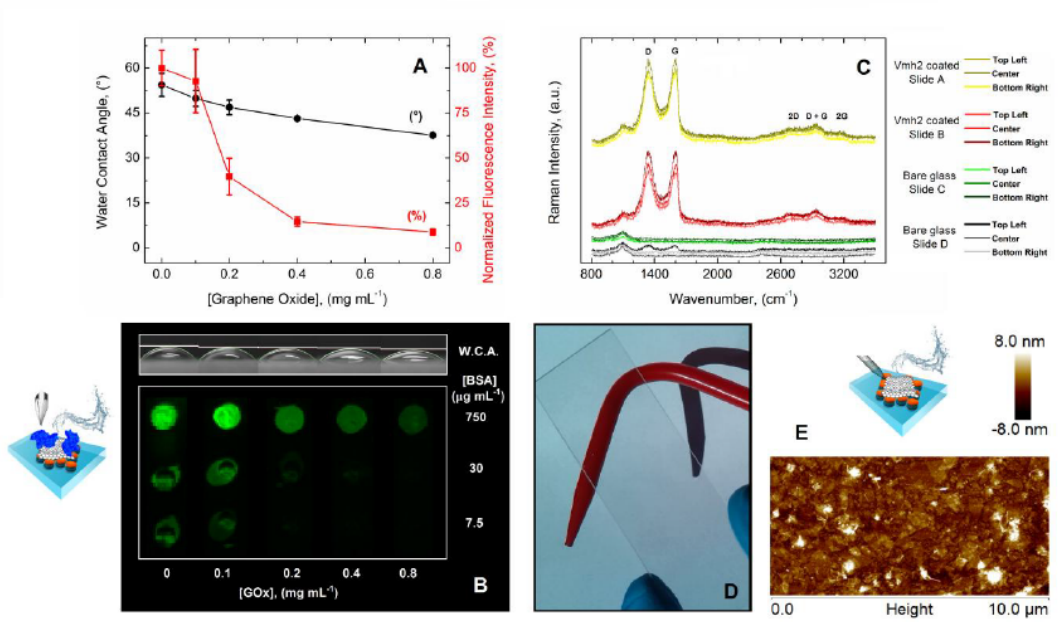

Figure 5. Immobilization of graphene oxide on Vmh2 hydrophobin coated glass slides. A, optimization of GOx immobilization carried out by monitoring surface properties relevant to microarray technology, water contact angle and fluorescence intensity of A555B spots (750 µg mL^{-1}). B, same than A, with spot morphology using different A555B concentration and picture of water drops on functionalized glass. C, Raman spectra (raw data) of Vmh2 coated slides or bare glass slides, incubated with 0.4 mg mL^{-1} graphene oxide and extensively washed with water. D, transparent glass slide functionalized by Vmh2 and GOx. E, AFM image of GOx layer on Vmh2 functionalized MICA support and a schematic representation of functionalized glass slides.

The GOx is an excellent quencher of FRET fluorescence and is able to bind peptides and proteins by a variety of non-covalent interactions with the aminoacids side chains. Therefore the Vmh2 glass surface was incubated with 0÷0.8 mg mL^{-1} GOx and was tested immobilizing 7.5÷750 µg mL^{-1} A555B spots as previously described (Figure 5B). The quantitative analysis of residual fluorescence (Figure 5A) suggested that efficient quenching was obtained upon

incubation with 0.4 mg mL^{-1} GOx. Moreover, the wettability of the hybrid surface was appropriate for drop spotting , even at the highest GOx concentration tested (Figure 5B).

Raman spectroscopy is a powerful technique for the analysis of graphene related materials and their hybrid derivates since scattering response can be observed even from one single sheet of graphene. Therefore this technique was used to compare GOx binding efficiency on bare glass, aminosilane and Vmh2 coated slides. High reproducible spectra (not normalized) were recorded in multiple positions of the Vmh2 (Figure 5C) and aminosilane (Figure S5) glass surface, showing the characteristic D (≈1340cm^{-1}), G (≈1600cm^{-1}), 2D (≈2680cm^{-1}) , D+G (≈2940cm^{-1}), 2G (≈3180cm^{-1}) bands. Conversely, when GOx was tentatively immobilized on the bare glass slides, almost no signal was detected. Additionally, binding stability was demonstrated by strongly washing the Vmh2-GOx glass with PBST (Figure S6). It is worth nothing that Vmh2-GOx glass was transparent to the naked eye (Figure 5D) because a very thin GOx layer was assembled.

Direct observation of the Vmh2-GOx assemblies was performed by AFM imaging in air. Because of the glass roughness, mica was chosen as molecularly flat highly hydrophilic surface for Vmh2 self-assembling. Mica sheets, freshly cleaved by adhesive tape, were coated with 400 ng cm^{-2} Vmh2, and directly dried in a stream of nitrogen. Upon incubation with 0.4 mg mL^{-1} GOx the surface was washed three times for two minutes in MilliQ water, and dried. AFM images showed a layer of homogenously arranged GOx sheets (Figure 5E). Moreover a different hydrophilic surface can be functionalized layer by layer by Vmh2 and GOx.

3. Conclusion

Vmh2 quickly forms bio-adhesive transparent films on glasses both tuning the surface hydrophobicity and allowing facile and homogeneous immobilization of functional proteins and nanomaterials in environmental friendly fabrication process. Time (4 min net time) and materials (1 mg of Vmh2 in water /ethanol solution per 100 slides) needed for glass coating by a Vmh2 self-assembled monolayer allow a cost-effective slide fabrication. The functionalized glass is amenable for microarray technology, in particular for optical sensing. Moreover the combination of protein and nanomaterials on this new microarray platform could provide new biotechnological sensing tools.

4. Experimental Section

Extraction of Vmh2 from the mycelium of P. ostreatus. White-rot fungus, *P. ostreatus* (Jacq.: Fr.) Kummer (type: Florida; ATCC No. MYA-2306) was maintained at 4 °C through periodic transfer on potato dextrose agar, Difco™ (BD Diagnostic Systems; Maryland, USA) plates in the presence of 0.5% yeast extract, Bacto™ (BD Diagnostic Systems; Maryland, USA). Mycelia were inoculated in 1 L flasks containing 500 mL of potato-dextrose broth (24 g/L) supplemented with 0.5% yeast extract, grown at 28 °C in shaken mode (150 rpm). After 10 days of fungal growth, mycelia were separated by filtration through gauze, treated twice with 2% SDS in a boiling water bath for 10 min, washed several times with water and once with 60% ethanol to completely remove the detergent. The residue was dried under nitrogen, grinded and treated with 100% trifluoroacetic acid (TFA) in a Elmasonic S30 water bath sonicator (Elma; Singen, Germany) for 30 min, and centrifuged (10 min at 3200g). The supernatant was dried, then lipids were extracted in a mixture of water-methanol-chloroform 2:2:1 v/v (5 min in bath sonicator). After centrifugation, proteins appeared as a solid aggregate at the interface between the water-methanol and the chloroform phases. They were recovered by liquid phase removal. The aggregated protein was dried, treated with TFA for 30

min in bath sonicator, re-dried, and dissolved in 80% ethanol. The sample was centrifuged (90 min at 12000g) and ethanol was removed from the supernatant under vacuum at 40 °C using rotavapor and the material was freeze-dried, treated with TFA as above-described and re-dissolved in 60% ethanol.

Plasma treatment of glass slides: Pre-cleaned plain glass slides, MI and MII, 75 x 25 mm, were purchased from two different manufactures: Corning (New York, USA) and J. Melvin Freed (Pennsylvania, USA) respectively. MI and MII were washed by isopropanol, dried in a steam of nitrogen and treated for two minutes by air plasma, using a PDC-002 plasma cleaner (Harrick Plasma, New York, USA) 29.2W RF power, equipped with a RV3F vacuum pump (Edwards; Crawley, UK).

Microarray reagents and solutions. Glycerol, PBS, Tween 20, and milk powder were purchased from Sigma-Aldrich (Taufkirchen, Germany). Albumin from Bovine Serum (BSA), Alexa Fluor® 555 conjugate was purchased from Thermo Fisher Scientific (New Hampshire, USA). Monoclonal antibody, and biotinylated detection antibody against IgG were acquired from Abcam (Cambridge, UK). Streptavidin−Alexa 647 was obtained from Invitrogen (California, USA). PBS with 2% (v/v) glycerol was used as spotting buffer. PBS supplemented with 5% (w/v) milk powder and 0.005% (v/v) Tween 20 was prepared as blocking buffer. PBS supplemented with Tween 20 at 0.05% (v/v) was used as washing buffer (PBST). PBS with 0.5% (v/v) Tween 20 containing 1% of BSA fraction V (w/v) was employed as immunobuffer. Water used to prepare the solutions was Milli-Q. Water-based dispersions of GOx were purchuased from Angstron Materials Inc. (Ohio, USA). Quantum dots nanocrystals were synthesized and characterized in our laboratories (details as given in supporting information).

Fabrication of the antibody, A555B and QDs microarrays. The capture anti IgG antibody was spotted at 0.5 mg mL^{-1} and CdTe QDs at 10 µM, over the Vmh2 coated glass or aminosilane glass slides (PolyAn; Berlin, Germany), in spotting buffer using Microgrid II

robot (Digilab; Massachusetts, USA). A555B was spotted at 0.75 mg mL^{-1} and 0.2 mg mL^{-1} on the Vmh2 and aminosilane substrates respectively. Spotting was done at room temperature and at 40 to 60% humidity. The average diameter of the printed spots was ca. 150 μm for proteins and 120 for QDs. After spotting, the slides were incubated at 4 °C overnight in a desiccated environment. The microarray slides were masked and divided by wells through a microarray cassette (Arrayit; California, USA), and each well was washed three times with PBST (150 μL).

Microarray slides quantification: The slides were examined through an AlphaScan™ Microarray Scanner 3.0 (Alpha Innotech Corporation; California, USA) using two different excitation-laser/emission-filter combinations (533exc/570em, or 635exc/670em, wavelength in nm units), depending on the explored fluorophore, and 10 μm resolution (lengths of pixels sides). Fluorescence images of slides were quantified using the AlphaScan™ 3.0 application software and the signal-to-background profile was measured using GenePix Pro 6.0 (Molecular Devices; California, USA). The fluorescence intensities of spots were estimated by measuring the mean intensities of all the pixels inside the area of the spot minus the median value of pixel intensities in the local background, excluding 3 pixels of the neutral zone sorrounding these spots. The fluorescence intensities of blocks (10 spots per block), were estimated by measuring the mean spots intensities, excluding the scattered points spots (spots in the first and forth quartile), the same spots were used for the estimation of CV. The fluorescence intensities over of whole slides (180 spots per slides printed in 18 blocks) were estimated by measuring the mean spots intensities, excluding high scattered spots (spots in the 1÷10 percentile and in the 90÷100 percentile), the same spots were used for the estimation of the CV.

Sandwich Immunoassay Microarray. According to our previous work,[19] the surface of slides with immobilized capture anti IgG antibodies was saturated for 30 min with 100 μL blocking buffer. Subsequently, the masked slides were washed with PBST (100 μL/well, five

times) and the microarrays were incubated for 2 h with solutions of IgG analyte in immunobuffer (100 µL per well) at different concentrations. The masked slides were washed with PBST (150 µL per well, five times), incubated with biotinylated detection antibody (diluted in immunobuffer at 1.5 µg mL^{-1}) for 1 h, and then rewashed with PBST (150 µL per well, seven times). The bound detection antibodies were conjugated (100 µL/well) with Streptavidin−Alexa 647 (diluted in immunobuffer at 0.4 µg mL^{-1}) for 30 min. All incubations were performed with oscillatory agitation at 300 rpm in an MTS 2/4 digital microtiter shaker (IKA; Staufen, Germany). The masked slides were washed with PBST (150 µL per well, five times), twice with PBS, and once with milli-Q water. The slides were then unmasked, subsequently dried by centrifugation (1500 rpm, 1 min) and analyzed by fluorescence imaging with the laser scanner. The limit of detection (LOD) of the respective calibration curve was estimated as the sum of the mean intensity among the spots (incubated in the absence of IgG, excluding the spots in the first and forth quartile) and three times the standard deviation: LOD = MI (Q2;Q3)+ 3SD (Q2;Q3).

Characterization techniques. Contact angle was measured on a DSA25B drop shape analyzer (KRÜSS; Hamburg, Germany) equipped with a CS8420Ci CCD camera (Toshiba Teli; Tokyo, Japan). Images of sessile drops of 5µL Milli Q water, placed in 3÷5 positions of 3÷10 slides, were analyzed with the software package (ver. 1.90.0.14, KRÜSS) using the tangent method. AFM measurements were performed on mica using a Nanoscope V Multimode8 AFM (Bruker, Germany) and Si cantilevers (SNL model, k:0.3N/m, Bruker). The SFM were used at a scan rate of 1 Hz and 512 x 512 pixel. Raman spectra were acquired using a Horiba Jobin Yvon LabRAM HR 800, 800mm focal length, 100x objective, excitation wavelength 532nm.

Bibliography

(1) Biju, V. Chemical Modifications and Bioconjugate Reactions of Nanomaterials for Sensing, Imaging, Drug Delivery and Therapy. *Chem. Soc. Rev.* **2014**, *43*, 744–764.

(2) Kairdolf, B. A.; Smith, A. M.; Stokes, T. H.; Wang, M. D.; Young, A. N.; Nie, S. Semiconductor Quantum Dots for Bioimaging and Biodiagnostic Applications. *Annu. Rev. Anal. Chem. (Palo Alto. Calif).* **2013**, *6*, 143–162.

(3) Morales-Narváez, E.; Merkoçi, A. Graphene Oxide as an Optical Biosensing Platform. *Adv. Mater.* **2012**, *24*, 3298–3308.

(4) Chou, S. S.; De, M.; Luo, J.; Rotello, V. M.; Huang, J.; Dravid, V. P. Nanoscale Graphene Oxide (nGO) as Artificial Receptors: Implications for Biomolecular Interactions and Sensing. *J. Am. Chem. Soc.* **2012**, *134*, 16725–16733.

(5) Pei, H.; Li, J.; Lv, M.; Wang, J.; Gao, J.; Lu, J.; Li, Y.; Huang, Q.; Hu, J.; Fan, C. A Graphene-Based Sensor Array for High-Precision and Adaptive Target Identification with Ensemble Aptamers. *J. Am. Chem. Soc.* **2012**, *134*, 13843–13849.

(6) Morales-Narváez, E.; Hassan, A. R.; Merkoçi, A. Graphene Oxide as a Pathogen-Revealing Agent: Sensing with a Digital-like Response. *Angew. Chemie - Int. Ed.* **2013**, *52*, 13779–13783.

(7) Avvakumova, S.; Colombo, M.; Tortora, P.; Prosperi, D. Biotechnological Approaches toward Nanoparticle Biofunctionalization. *Trends Biotechnol.* **2014**, *32*, 11–20.

(8) Sun, T.; Qing, G.; Su, B.; Jiang, L. Functional Biointerface Materials Inspired from Nature. *Chem. Soc. Rev.* **2011**, *40*, 2909–2921.

(9) Bayry, J.; Aimanianda, V.; Guijarro, J. I.; Sunde, M.; Latgé, J.-P. Hydrophobins--Unique Fungal Proteins. *PLoS Pathog.* **2012**, *8*, e1002700.

(10) Wohlleben, W.; Subkowski, T.; Bollschweiler, C.; von Vacano, B.; Liu, Y.; Schrepp, W.; Baus, U. Recombinantly Produced Hydrophobins from Fungal Analogues as Highly Surface-Active Performance Proteins. *Eur. Biophys. J.* **2010**, *39*, 457–468.

(11) Wösten, H. A. B.; Scholtmeijer, K. Applications of Hydrophobins: Current State and Perspectives. *Appl. Microbiol. Biotechnol.* **2015**, *99*, 1587–1597.

(12) Longobardi, S.; Gravagnuolo, A. M.; Rea, I.; De Stefano, L.; Marino, G.; Giardina, P. Hydrophobin-Coated Plates as Matrix-Assisted Laser Desorption/ionization Sample Support for Peptide/protein Analysis. *Anal. Biochem.* **2014**, *449*, 9–16.

(13) Longobardi, S.; Gravagnuolo, A. M.; Funari, R.; Della Ventura, B.; Pane, F.; Galano, E.; Amoresano, A.; Marino, G.; Giardina, P. A Simple MALDI Plate Functionalization by Vmh2 Hydrophobin for Serial Multi-Enzymatic Protein Digestions. *Anal. Bioanal. Chem.* **2015**, *407*, 487–496.

(14) De Stefano, L.; Rea, I.; Giardina, P.; Armenante, A.; Rendina, I. Protein-Modified Porous Silicon Nanostructures. *Adv. Mater.* **2008**, *20*, 1529–1533.

(15) Gravagnuolo, A. M.; Morales-Narváez, E.; Longobardi, S.; da Silva, E. T. S. G.; Giardina, P.; Merkoçi, A. In Situ Production of Biofunctionalized Few-Layer Defect-Free Microsheets of Graphene. *Adv. Funct. Mater.* **2015**.

(16) Houmadi, S.; Ciuchi, F.; De Santo, M. P.; De Stefano, L.; Rea, I.; Giardina, P.; Armenante, a; Lacaze, E.; Giocondo, M. Langmuir-Blodgett Film of Hydrophobin Protein from Pleurotus Ostreatus at the Air-Water Interface. *Langmuir* **2008**, *24*, 12953–12957.

(17) De Stefano, L.; Rea, I.; De Tommasi, E.; Rendina, I.; Rotiroti, L.; Giocondo, M.; Longobardi, S.; Armenante, a; Giardina, P. Bioactive Modification of Silicon Surface Using Self-Assembled Hydrophobins from Pleurotus Ostreatus. *Eur. Phys. J. E. Soft Matter* **2009**, *30*, 181–185.

(18) Lee, J. H.; Hyun, H.; Cross, C. J.; Henary, M.; Nasr, K. a.; Oketokoun, R.; Choi, H. S.; Frangioni, J. V. Rapid and Facile Microwave-Assisted Surface Chemistry for Functionalized Microarray Slides. *Adv. Funct. Mater.* **2012**, *22*, 872–878.

(19) Morales-Narváez, E.; Montón, H.; Fomicheva, A.; Merkoçi, A. Signal Enhancement in Antibody Microarrays Using Quantum Dots Nanocrystals: Application to Potential Alzheimer's Disease Biomarker Screening. *Anal. Chem.* **2012**, *84*, 6821–6827.

(20) Morris, V. K.; Kwan, A. H.; Sunde, M. Analysis of the Structure and Conformational States of DewA Gives Insight into the Assembly of the Fungal Hydrophobins. *J. Mol. Biol.* **2013**, *425*, 244–256.

(21) Armenante, A.; Longobardi, S.; Rea, I.; De Stefano, L.; Giocondo, M.; Silipo, A.; Molinaro, A.; Giardina, P. The Pleurotus Ostreatus Hydrophobin Vmh2 and Its Interaction with Glucans. *Glycobiology* **2010**, *20*, 594–602.

Supporting Information

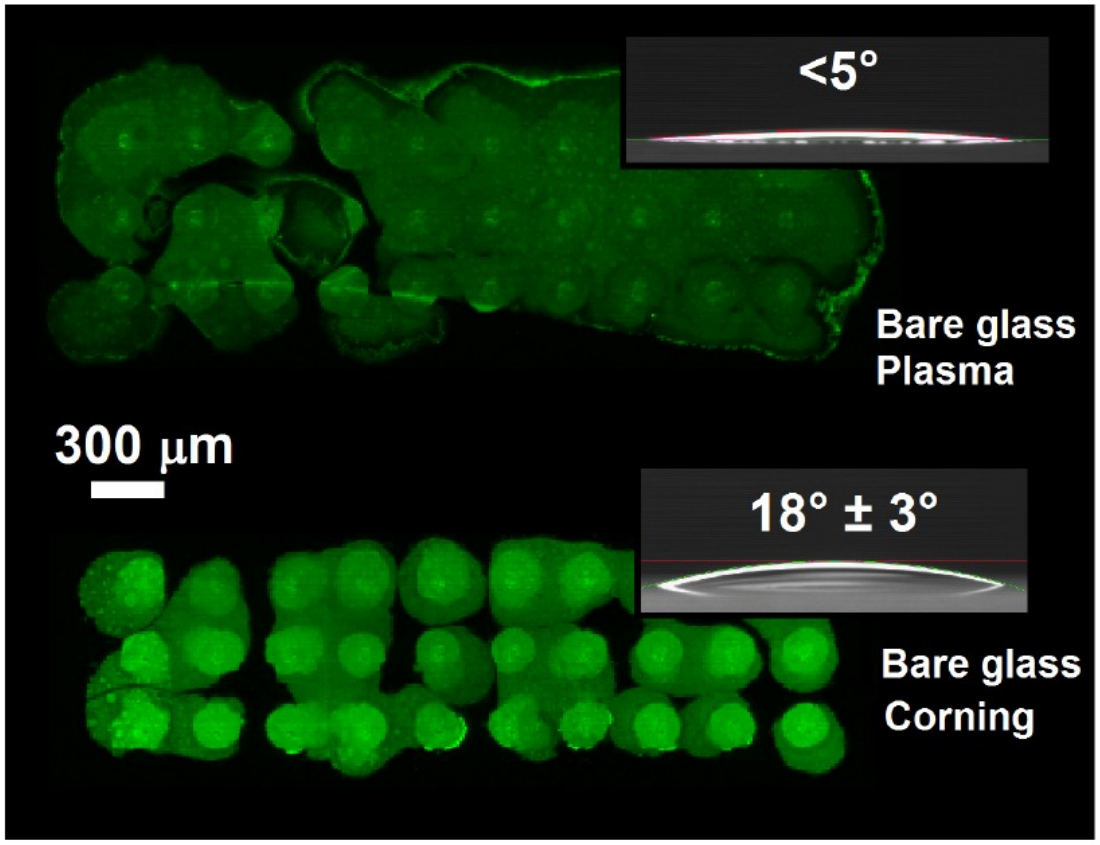

Figure S1. Bare Glass slide Manufacturer I (Corning). Water contact angle (mean ± standard deviation) of bare glass and bare glass after plasma, and morphology of Alexa555-BSA spots after washing by PBS, 0.05% Tween-20.

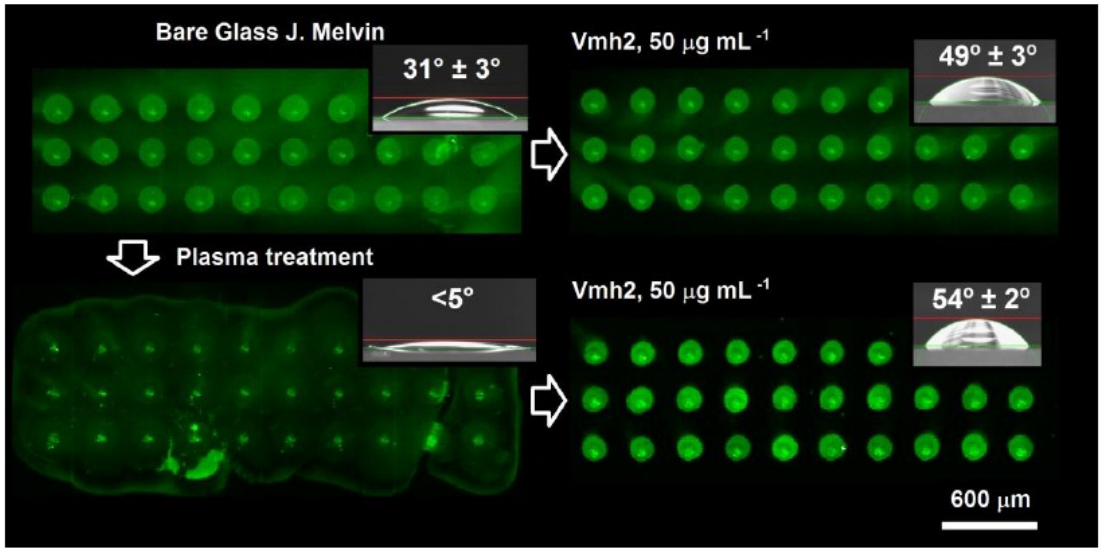

Figure S2. Glass slide Manufacturer II (J.Melvin). Morphology of Alexa555-BSA spots and WCA (mean ± standard deviation) of bare glass type II (J.Melvin), before and after plasma treatment and after Vmh2 functionalization.

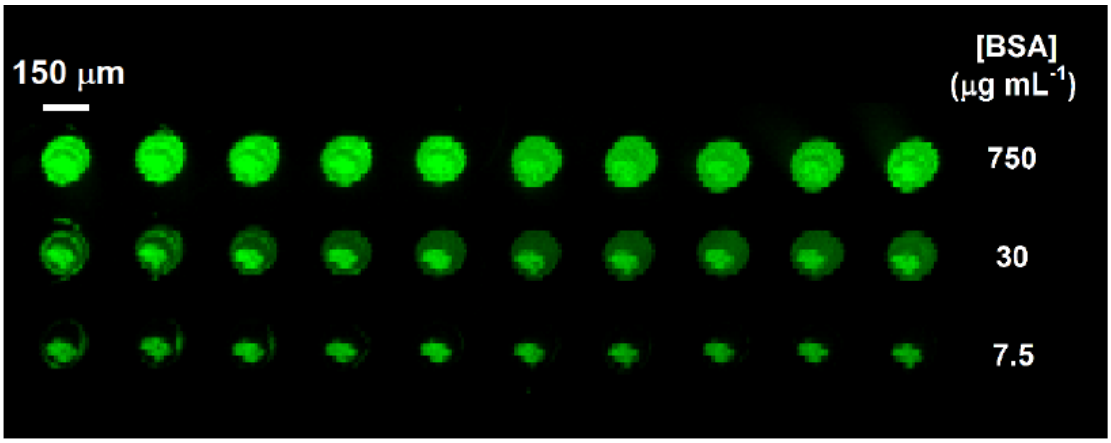

Figure S3. Optimizaion of concentration of Alexa555-BSA on Vmh2 coated glass slide MI.

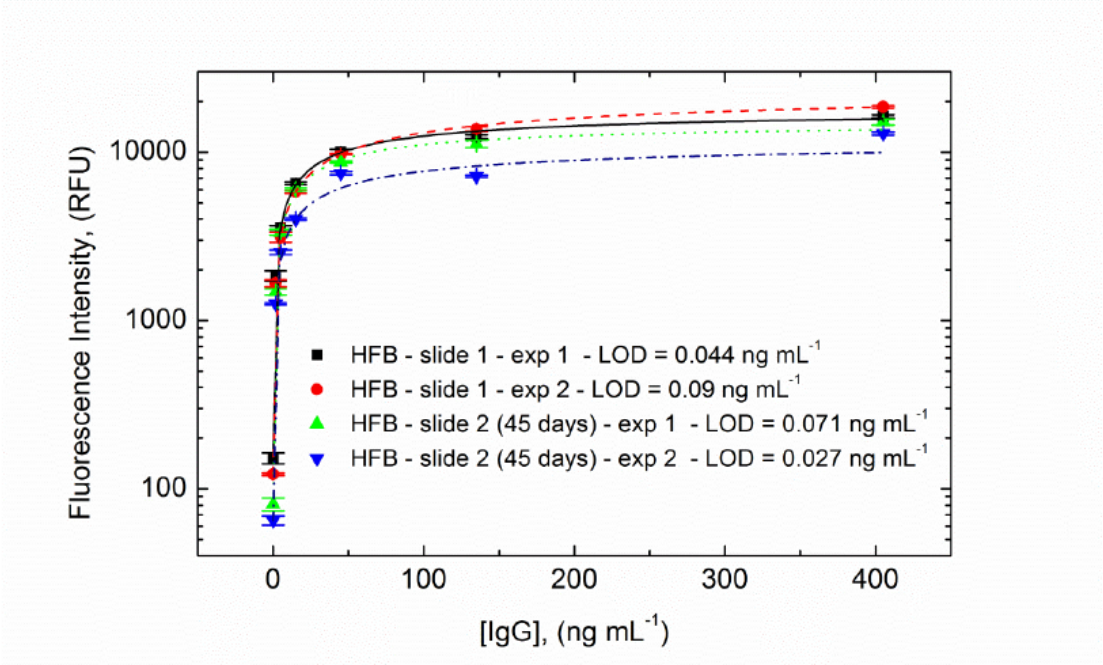

Figure S4. Reproducibility of IgG detection on Vmh2 coated glass slides on fresh slides and 45 days after fabrication.

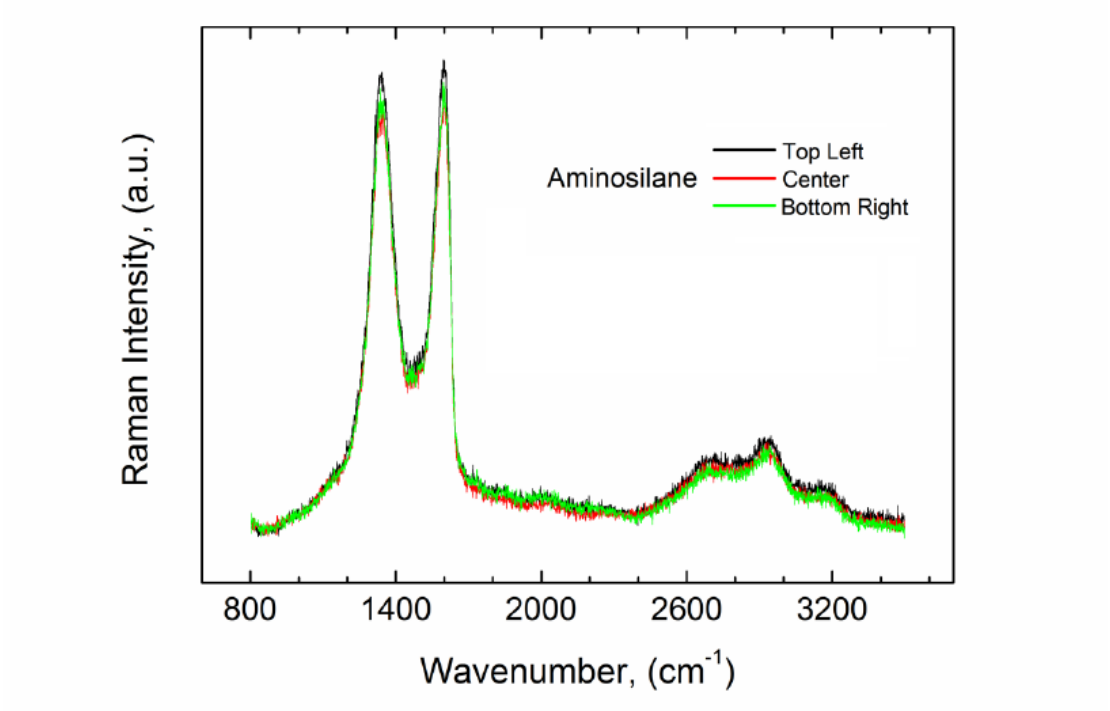

Figure S5. Raman spectra of GOx immobilized on aminosilane slide, acquired in different positions of the slide after washing by water.

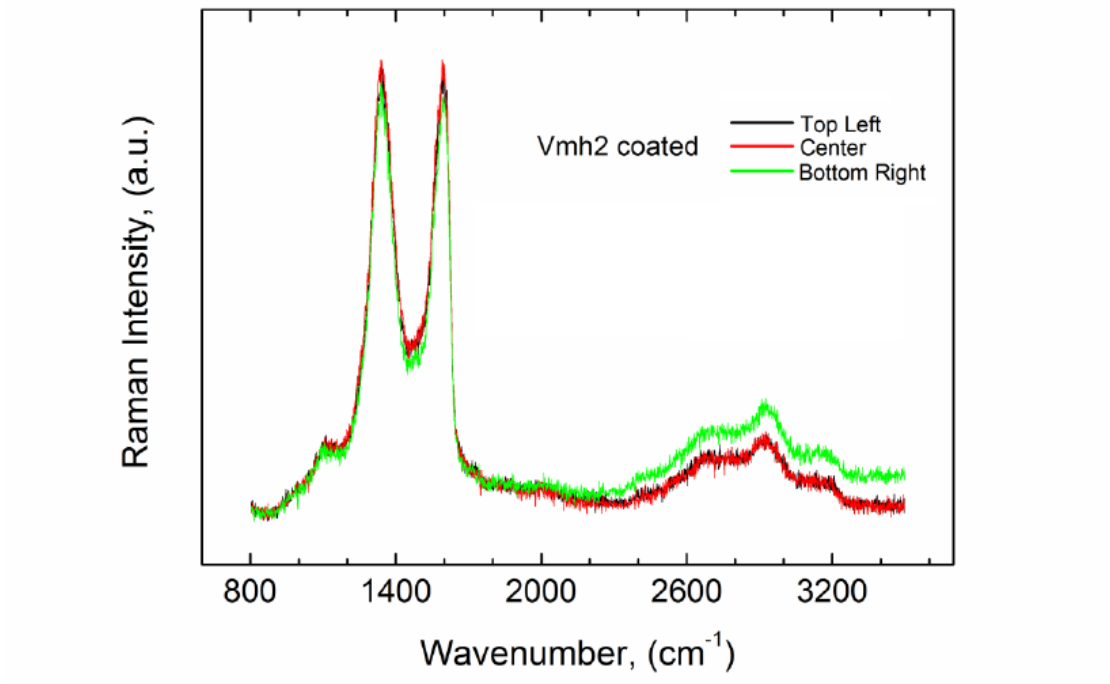

Figure S6. Raman spectra of GOx immobilized on Vmh2 coated glass slides, acquired in different positions of the surface of slide after washing by PBS, 0.05% Tween-20.

Syntesis and Characterization of CdTe Quantum Dots Nanocrystals

Reagents. Tellurium powder (200 mesh, 99.8%), $CdCl_2.H_2O$, (98%), 3-mercaptopropionic acid (≥ 99), were purchased from Sigma and used without further purification. All reactions were carried out with ultrapure water.

Instrumentations. Quatum dots nanocrystals were characterized by FTIR spectra were measured in a Perkin Elmer Spectrum BX. Transmission Electron Microscopy (TEM) images were obtained using TEM-MSC-JEOL 2100 microscope at an accelerating voltage of 200 kV. Samples for TEM observation were prepared by dilution of the colloidal solution of quantum dot in water. The solution is dripped onto a holey carbon-coated copper grid and the solvent is evaporated at room temperature.

Synthesis of CdTe Quantum Dots Nanocrystals. CdTe/MPA: CdTe nanocrystals were prepared by a procedure based on previous.[1,2] In a typical synthesis 50 mL of a 0.1 mol L^{-1} aqueous solution of $CdCl_2$ was added to a three neck round bottomed flask and mixed with 50 mL of aqueous 0.12 mol L^{-1} MPA (stoichiometric ratio was fixed at MPA/Cd = 1.2. The pH was adjusted to 11.5, with 0.1 mol L^{-1} aqueous NaOH, and the resulting solution was stirred at room temperature under N_2 atmosphere for 30 minutes.

Separately, 0.127 g of Te was added to a Schlenk tube along with 5 mL water. A NaBH4 solution (2.5 g/5mL water) was added dropwise under N_2 atmosphere with vigorous stirring at 40 °C for nearly 20 minutes. The resulting colorless solution was injected into the Cd/thiol solution. The Cd/Te/thiol proportion was kept at 1:0.2:1.2. The as-formed orange solution was subsequently heated in a teflon lined stainless steel autoclave for 90 minutes at 100 °C. Nanocrystals could be precipitated when necessary by the addition of 2-propanol following by centrifugation and resuspension in water.

IR Spectra of the CdTe QDs: To verify the existence of MPA on the surface of the prepared QDs as a stabilizer, we compared the FTIR spectra of free MPA and MPA-capped CdTe QDs. As shown in Figure S7, the free MPA spectrum shows characteristic bands such as broad band and unresolved between 3500 and 2500 cm^{-1} assigned to OH stretching of carboxyl group, and the band at 1690 cm^{-1} , associated with the acid carbonyl . The low intensity band at 2560 cm^{-1} may be attributed to stretching -SH . The sample prepared with the CdTe surface functionalized with MPA via hydrothermal synthesis shows characteristic bands of the binder such as OH stretching (wide and centered at 3380 cm^{-1}) bands at 1560 and 1400 cm^{-1} (stretching associated with asymmetric and symmetric carboxylate group , since the samples are prepared in alkaline medium) . The band at 1654 cm^{-1}, together with the OH stretching band, already mentioned suggest that there are residual carboxylic groups in the acid form, together with carboxylate groups . One important observation, according to the literature[3,4] refers to the absence of the band related to stretch -SH, suggesting the interaction of MPA via the hydrogen sulfide -S- group with the Cd^{2+}.

TEM images of nanoparticles. TEM was used to characterize the morphology, size and dispersion degree of QDs and the results are illustrated in Figure S8. The images presented almost spherical shape well defined, but with hard to define contour, which is normal for metal semiconductor. The particles had good crystal structure and monodispersity which is confirmed by the appearance of crystallographic planes. The diameter of the QDs was ~ 4.28± 1.94 nm (see particle size distribution in Figure S9, based on the analysis of 80 nanoparticles).

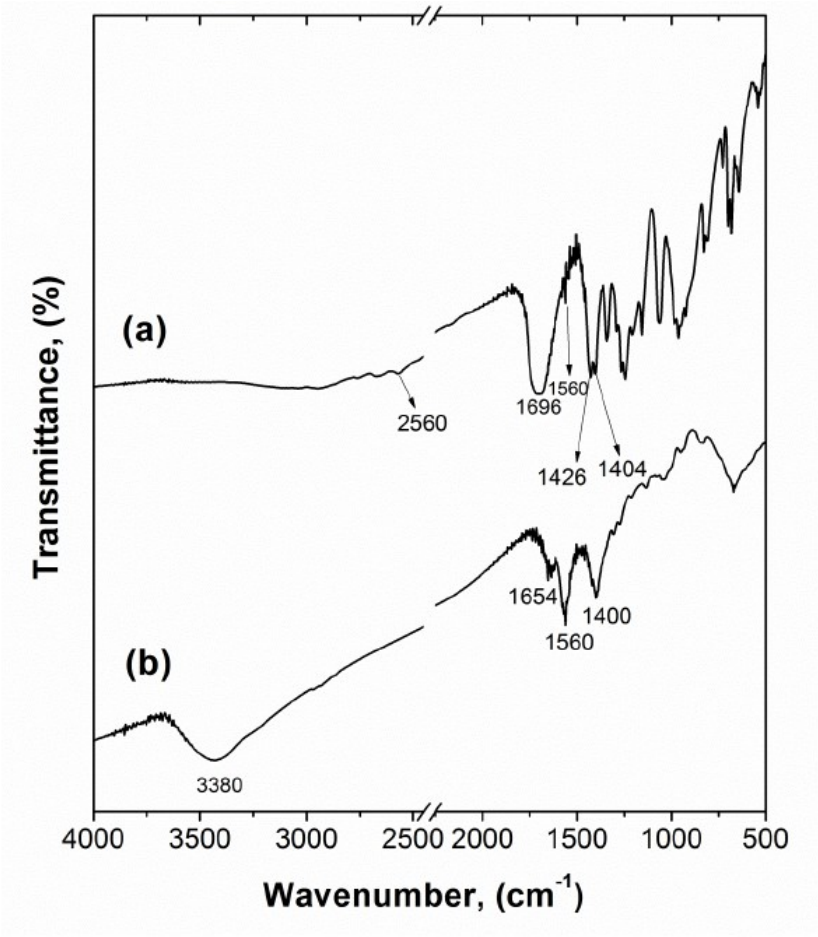

Figure S7. FTIR Spectra (a) free MPA, (b) MPA-capped CdTe QDs

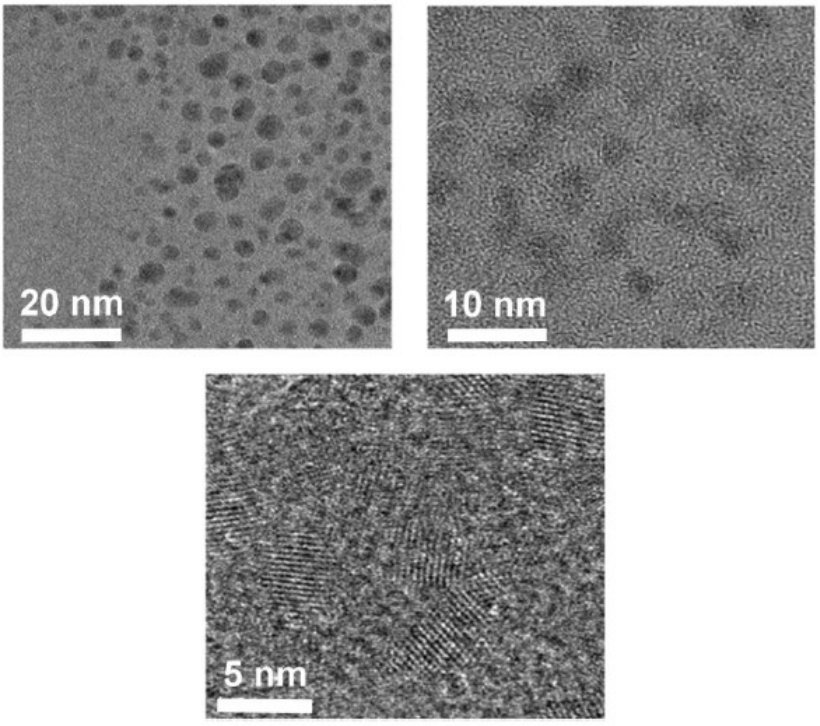

Figure S8. TEM images of CdTe-MPA QDs

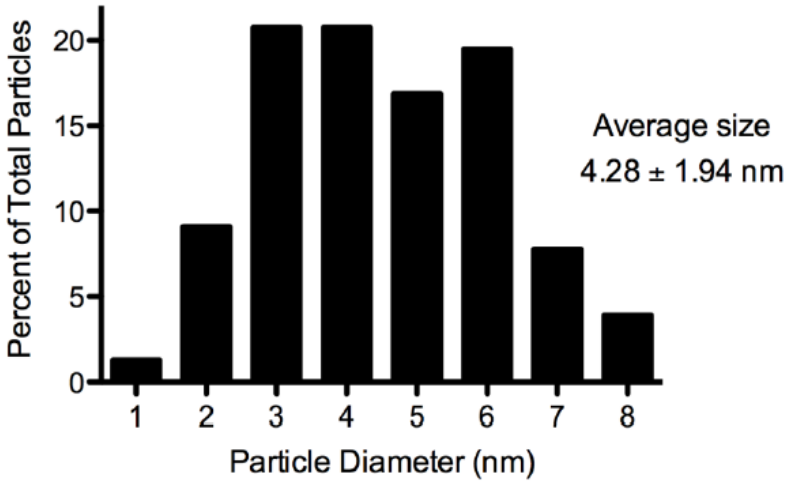

Figure S9. Particle size distribution of the synthesized CdTe QDs.

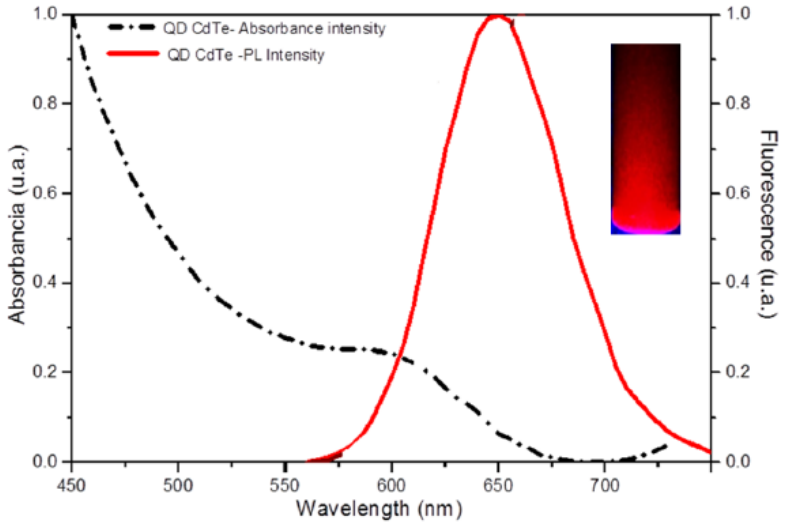

Figure S10. Absorbance and photoluminescent (PL) emission spectra of the synthesized CdTe QDs. UV-Vis absorption and PL spectra were acquired through a Spectramax M2e spectrophotometer (Molecular Devices). A colloidal solution of the synthesized CdTe QDs was excited using a UV lamp (365 nm) to photograph the QDs photoluminescence (figure inset).

References

(1) Zhang, Y.; Zhang, H.; Ma, M.; Guo, X.; Wang, H. The Influence of Ligands on the Preparation and Optical Properties of Water-Soluble CdTe Quantum Dots. *Appl. Surf. Sci.* **2009**, *255*, 4747–4753.

(2) Tian, J.; Liu, R.; Zhao, Y.; Xu, Q.; Zhao, S. Controllable Synthesis and Cell-Imaging Studies on CdTe Quantum Dots Together Capped by Glutathione and Thioglycolic Acid. *J. Colloid Interface Sci.* **2009**, *336*, 504–509.

(3) Abd El-sadek, M. S.; Nooralden, A. Y.; Moorthy Babu, S.; Palanisamy, P. K. Influence of Different Stabilizers on the Optical and Nonlinear Optical Properties of CdTe Nanoparticles. *Opt. Commun.* **2011**, *284*, 2900–2904.

(4) Zhang, H.; Sun, P.; Liu, C.; Gao, H.; Xu, L.; Fang, J.; Wang, M.; Liu, J.; Xu, S. L-Cysteine Capped CdTe-CdS Core-Shell Quantum Dots: Preparation, Characterization and Immuno-Labeling of HeLa Cells. *Luminescence 26*, 86–92.

4. CONCLUSIONS

A) OPTIMIZATION AND SCALE UP OF VMH2 PRODUCTION

- Extraction and purification of Vmh2 from *P.ostreatus* mycelium has been sensibly improved to obtain adequate amount of protein for laboratory scale applications. Yields of ≈230 mg of pure Vmh2 per Liter of culture broth, and productivities of 20÷50 mg of protein per working day have been achieved.
- ATR-FT-IR analysis of purified samples has shown that the set up protocol is efficient in removal of non-protein contaminants.

B) ANALYSIS OF VMH2 SOLUBILITY AND STRUCTURAL STUDIES OF AGGREGATED FORMS

- Vmh2 spontaneously self-assembles into amyloid-like aggregates in aqueous buffers. The aqueous solution of Vmh2 at pH 7 contains a population of soluble oligomers and another one of small amyloid-like aggregates, whose ratio is affected by protein concentration. The aggregation process is promoted by temperature increase, at pH < 6, or in the presence of Ca^{2+} ions, leading to the same final protein conformation.
- On the basis of the 3D structure model of the protein, a self-assembling mechanism can be inferred. Protonation of two aspartates, as well as the interaction with Ca^{2+} ions or increase of temperature would induce a destabilization of a long loop thus triggering a conformational change that in turn would determine rapid and extensive aggregation of the protein and the formation of amyloid-like structures.
- Vmh2 conversion into the β-sheet rich, assembled form occurs in conditions different from those of the other Class I hydrophobins. Exposition of Vmh2 to water-air HHI does not induce self-assembly.
- The layering process of Vmh2 on Teflon membrane has been investigated using ATR-FT-IR. Results, suggesting that a slow aggregation process favours the formation of a more uniform layer with a higher β-sheet contribution, have been validated by SEM imaging.

C) A VERSATILE MALDI MS PLATFORM BASED ON SELF-ASSEMBLED THIN FILM OF HYDROPHOBIN

- The protein film has been exploited to easily and homogenously coat the sample-loading steel plate used in MALDI-TOF mass spectrometry. The coat is easy to remove, allowing reuse of the same plate.
- The functionalized surface is able to stably and homogenously adsorb peptides and proteins whereas salts or denaturants can be washed out allowing fast and high-throughput on-plate desalting prior to MS analysis.
- High-quality spectra (good S/N ratio and reproducibility) with excellent levels of sensitivity are achieved, even under harsh conditions. The wide range of analysis without sample pretreatment makes the proposed method of interest for the high-throughput analysis of complex samples such as human serum.

- The functions of the Vmh2 coating have been expanded immobilizing enzymes of interest in proteomics, on-plate. Efficient, fast, and reproducible multiple enzyme digestions have been performed to achieve high sequence coverage of model proteins, including the analysis of post-translational modifications.
- The possibility of exploiting this technique coupled to MALDI-TOF/TOF sequencing has been applied on model proteins and on the entire whey milk proteome.

D) NANO-BIOTECHNOLOGICAL APPLICATIONS OF VMH2

D1) In Situ Production Of Biofunctionalized Few-Layer Defect-Free Microsheets Of Graphene

- A method for the production of biofunctionalized GBMs by using Vmh2 have been set up. High concentration of GBMs (~440÷510 μg mL^{-1}) have been obtained upon Vmh2 assisted exfoliation of raw graphitic material.
- It has been proved that controlled centrifugation enables the selection of very stable (>8 months, ζ-potential +40 ÷ +70mV), few-layer (<5 layers), graphene (~90÷100 μg mL-1) with an average lateral dimension of 1.0 ± 0.1 μm.
- During the exfoliation/functionalization process the band structure of sp^2-carbon lattice is preserved, as demonstrated by Raman spectroscopy analysis. Therefore, no defects (e.g. oxidiation) are introduced in basal plane of graphene sheets.
- Vmh2 also efficiently stabilizes dispersions of other hydrophobic GBMs. A thin hybrid films of Vmh2/GBMs has been easily assembled on a silicon chip by the drop casting method.

D2) Quick and Simple Immobilization of Nanomaterials and Proteins on Glass Surface Using a Self-Assembled Vmh2 Layer

- Vmh2 self-assembling into a thin amphiphilic layer has been used as a facile and rapid (4 minutes net time) method for glass coating modifying the WCA of super-hydrophilic glass (WCA <5°) up to 60°.
- The optimized procedure allows coating 100 slides, 18.8 cm^2 of surface each, per mg of Vmh2.
- This functionalized surface is highly homogeneous, transparent and able to adsorb proteins and nanomaterials, such as graphene oxide and home-made quantum dots.
- The functionalized slides have been tested in microarray technology. A fluorescent protein and quantum dots have been stably immobilized by micro-patterning. Antibodies immobilized on the Vmh2-glass surface have proved functional in an optical bioassay.

REFERENCES/BIBLIOGRAFIA

Aimanianda V, Bayry J, Bozza S, Kniemeyer O, Perruccio K, Elluru SR, Clavaud C, Paris S, Brakhage AA, Kaveri SV, Romani L, Latge JP. (2009) Surface hydrophobin prevents immune recognition of airborne fungal spores. *Nature.* 460:1117–21.

Armenante A, Longobardi S, Rea I, De Stefano L, Giocondo M, Silipo A, Molinaro A, Giardina P. (2010) The *Pleurotus ostreatus* hydrophobin Vmh2 and its interaction with glucans. *Glycobiology*. 20(5):594-602.

Artiles MS, Rout CS, Fisher TS. (2011) Graphene-based hybrid materials and devices for biosensing. *Adv Drug Deliv Rev.* 63:1352-60.

Askolin S, Nakari-Setälä T, Tenkanen M. (2001) Overproduction, purification, and characterization of the Trichoderma reesei hydrophobin HFBI. *Appl Microbiol Biotechnol* 57(1-2):124-30.

Bayry J, Aimanianda V, Guijarro JI, Sunde M, Latgé JP. (2012) Hydrophobins--unique fungal proteins. *PLoS Pathog.* 8(5):e1002700

Boeuf S, Throm T, Gutt B, Strunk T, Hoffmann M, Seebach E, Mühlberg L, Brocher J, Gotterbarm T, Wenzel W, Fischer R, Richter W. (2012) Engineering hydrophobin DewA to generate surfaces that enhance adhesion of human but not bacterial cells. *Acta Biomater.* 8:1037-47.

Biancalana M, Koide S. (2010) Molecular mechanism of Thioflavin-T binding to amyloid fibrils. *Epub.* 1804(7):1405-12.

Corvis Y, Walcarius A, Rink R, Mrabet NT, Rogalska E. (2005) Preparing catalytic surfaces for sensing applications by immobilizing enzymes via hydrophobin layers. *Anal Chem.* 77(6):1622-30.

Corvis Y, Brezesinski G, Rink R, Walcarius A, Van der Heyden A, Mutelet F, Rogalska E. (2006) Analytical investigation of the interactions between SC3 hydrophobin and lipid layers: elaborating of nanostructured matrixes for immobilizing redox systems. *Anal Chem.* 78(14):4850-64.

De Stefano L, Rea I, Armenante A, Giardina P, Giocondo M, Rendina I. (2007) Selfassembled biofilm of hydrophobins protects the silicon surface in the KOH wet etch process. *Langmuir.* 23:7920–2.

De Stefano L, Rea I, Giardina P, Armenante A, Rendina I. (2008) Protein-modified porous silicon nanostructures. *Adv Mater*. 20:1529-+

De Stefano, L.; Rea, I.; De Tommasi, E.; Rendina, I.; Rotiroti, L.; Giocondo, M.; Longobardi, S.; Armenante, A. and Giardina, P. (2009) Bioactive modification of silicon surface using self-assembled hydrophobins from *Pleurotus ostreatus*. *Eur Phys J.* 30:181-5.

González-González M, Bartolome R, Jara-Acevedo R, Casado-Vela J, Dasilva N, Matarraz S, García J, Alcazar JA, Sayagues JM, Orfao A, Fuentes M (2014) Evaluation of homo- and hetero-functionally activated glass surfaces for optimized antibody arrays. *Anal Biochem.* 450C:37-45.

Hektor HJ, Scholtmeijer K. (2005) Hydrophobins: proteins with potential. *Curr Opin Biotechnol*. 16(4):434-9.

Hou S, Li X, Li X, Feng XZ, Wang R, Wang C, Yu L, Qiao MQ. (2009) Surface modification using a novel type I hydrophobin HGFI. *Anal Bioanal Chem.* 394(3):783-9.

Houmadi S, Ciuchi F, De Santo MP, De Stefano L, Rea I, Giardina P, Armenante A, Lacaze E, Giocondo M. (2008) Langmuir-Blodgett film of hydrophobin protein from *Pleurotus ostreatus* at the air-water interface. *Langmuir*. 24(22):12953-7.

Kisko K, Szilvay GR, Vainio U, Linder MB, Serimaa R. (2008) Interactions of hydrophobin proteins in solution studied by small-angle X-ray scattering. *Biophys J*. 94(1):198-206.

Li X, Hou S, Feng X, Yu Y, Ma J, Li L. (2009) Patterning of neural stem cells on poly(lactic-co-glycolic acid) film modified by hydrophobin. *Coll. Surf. B: Biointerfaces*. 74(1): 370–4.

Linder M, Szilvay GR, Nakari-Setälä T, Söderlund H, Penttilä M. (2002) Surface adhesion of fusion proteins containing the hydrophobins HFBI and HFBII from Trichoderma reesei. *Protein Sci.* 11(9):2257-66.

Linder MB. (2009) Hydrophobins: Proteins that self assemble at interfaces. *Current Opinion in Colloid & Interface Science*. 14:356–363.

Ling S, Li C, Adamcik J, Wang S, Shao Z, Chen X, Mezzenga R. (2014) Directed Growth of Silk Nanofibrils on Graphene and Their Hybrid Nanocomposites. *ACS macrolett.* 3(2):146–52.

Longobardi S, Picone D, Ercole C, Spadaccini R, Stefano LD, Rea I, Giardina P. (2012) Environmental Conditions Modulate the Switch among Different States of the Hydrophobin Vmh2 from *Pleurotus ostreatus*. *Biomacromolecules*. 2012; 13(3):743-50.

Maltez-da Costa M, de la Escosura-Muñiz A, Nogués C, Barrios L, Ibáñez E, Merkoçi A. (2012) Detection of circulating cancer cells using electrocatalytic gold nanoparticles. *Small*. 8(23):3605-12

Morales-Narváez E, Merkoçi A. (2012) Graphene oxide as an optical biosensing platform. *Adv Mater*. 3;24(25):3298-308.

Morales-Narváez E, Montón H, Fomicheva A, Merkoçi A. (2012) Signal enhancement in antibody microarrays using quantum dots nanocrystals: application to potential Alzheimer's disease biomarker screening. *Anal Chem.* 84(15):6821-7.

Morales-Narváez E, Hassan AR, Merkoçi A. (2013) Graphene oxide as a pathogen-revealing agent: sensing with a digital-like response*. Angew Chem Int Ed Engl.* 52(51):13779-83.

Morris VK, Ren Q, Macindoe I, Kwan AH, Byrne N, Sunde M. (2011) Recruitment of class I hydrophobins to the air:water interface initiates a multi-step process of functional amyloid formation. *J Biol Chem.* 286(18):15955-63.

Morris VK, Kwan AH, Sunde M. (2013) Analysis of the structure and conformational states of DewA gives insight into the assembly of the fungal hydrophobins. *J Mol Biol.* 425(2):244-56.

Morris VK, Sunde M. (2013) Formation of amphipathic amyloid monolayers from fungal hydrophobin proteins. *Methods Mol Biol.* 996:119-29

Pan C, Xu S, Zhou H, Fu Y, Ye M, Zou H. (2007) Recent developments in methods and technology for analysis of biological samples by MALDI-TOF-MS. *Anal Bioanal Chem*., 387, 193-204.

Pumera M, Ambrosi A, Bonanni A, Chng ELK, Poh HL (2010) Graphene for electrochemical sensing and biosensing. *Trends in Anal Chem*. 29:954-965.

Putzbach W, Ronkainen NJ. (2013) Immobilization techniques in the fabrication of nanomaterial-based electrochemical biosensors: a review. *Sensors (Basel).* 13(4):4811-40.

Reuter LJ, Bailey MJ, Joensuu JJ, Ritala A. (2013) Scale-up of hydrophobin-assisted recombinant protein production in tobacco BY-2 suspension cells. *Plant Biotechnol J.* doi:10.1111/pbi.

Scholtmeijer K, Janssen MI, Gerssen B, de Vocht ML, van Leeuwen BM, van Kooten TG, Wösten HA, Wessels JG (2002) Surface modifications created by using engineered hydrophobins. *Appl Environ Microbiol.* 68(3):1367-73.

Scholtmeijer K, de Vocht ML, Rink R, Robillard GT, Wösten HA. (2009) Assembly of the fungal SC3 hydrophobin into functional amyloid fibrils depends on its concentration and is promoted by cell wall polysaccharides. *J Biol Chem.* 284(39):26309-14.

Sunde M, Kwan AH, Templeton MD, Beever RE, Mackay JP. (2008) Structural analysis of hydrophobins. *Micron*. 39(7):773-84.

Ueno Y, Furukawa K, Matsuo K, Inoue S, Hayashi K, Hibino H. (2013) Molecular design for enhanced sensitivity of a FRET aptasensor built on the graphene oxide surface. *Chem Commun (Camb).* 49(88):10346-8

Valo HK, Laaksonen PH, Peltonen LJ, Linder MB, JT Hirvonen, Laaksonen TJ. (2010) Multifunctional Hydrophobin: toward functional coatings for drug nanoparticles. *ACS Nano*. 4(3):1750-8.

Wang X, Graveland-Bikker JF, de Kruif CG, Robillard GT. (2004) Oligomerization of hydrophobin SC3 in solution: from soluble state to self-assembly. *Protein Sci*. 13(3):810-21.

Wang Z, Lienemann M, Qiau M, Linder MB. (2010) Mechanisms of protein adhesion on surface films of hydrophobin. *Langmuir*. 26(11):8491-6.

Wohlleben W, Subkowski T, Bollschweiler C, von Vacano B, Liu Y, Schrepp W, Baus U. (2010) Recombinantly produced hydrophobins from fungal analogues as highly surface-active performance proteins. *Eur Biophys* J. 39(3):457-68.

Wösten HA. (2001) Hydrophobins: multipurpose proteins. *Annu Rev Microbiol*. 55:625-46.

Xu, YD, Watson, JT, Bruening, ML. (2003) Patterned monolayer/polymer films for analysis of dilute or salt-contaminated protein samples by MALDI-MS. *Anal Chem*., 75, 185-190.

Yang W, Ren Q, Wu YN, Morris VK, Rey AA, Braet F, Kwan AH, Sunde M. (2013) Surface functionalization of carbon nanomaterials by self-assembling hydrophobin proteins. *Biopolymers*. 99:84-94.

Zampieri F, Wösten HAB, Scholtmeijer K. (2010) Creating surface properties using a palette of hydrophobins. *Materials*. 3:4607-25.

Zhang M, Wang Z, Wang Z, Feng S, Xu H, Zhao Q, Wang S, Fang J, Qiao M, Kong D. (2011) Immobilization of anti-CD31 antibody on electrospun poly(ε-caprolactone) scaffolds through hydrophobins for specific adhesion of endothelial cells. *Colloids Surf B Biointerfaces.* 85(1):32-9

Zhang Y, Petibone D, Xu Y, Mahmood M, Karmakar A, Casciano D, Ali S, Biris AS. (2014) Toxicity and efficacy of carbon nanotubes and graphene: the utility of carbon-based nanoparticles in nanomedicine. *Drug Metab Rev.*

Zhao ZX, Qiao MQ, Yin F, Shao B, Wu BY, Wang YY, Wang XS, Qin X, Li S, Yu L, Chen Q. (2007) Amperometric glucose biosensor based on self-assembly hydrophobin with high efficiency of enzyme utilization. *Biosens Bioelectron.* 22(12):3021-7.

Zhao ZX, Wang HC, Qin X, Wang XS, Qiao MQ, Anzai JI, Chen Q. (2009) Self-assembled film of hydrophobins on gold surfaces and its application to electrochemical biosensing. *Colloids Surf B Biointerfaces.* 71(1):102–106

Zuo G, Kang SG, Xiu P, Zhao Y, Zhou R. (2013) Interactions Between Proteins and Carbon-Based Nanoparticles: Exploring the Origin of Nanotoxicity at the Molecular Level. *Small.* 9(9-10):1546-56.

SCIENTIFIC PUBLICATIONS, COMMUNICATIONS, COURSES, EXPERIENCES IN FOREIGN LAB AND OTHER ACTIVITIES

SCIENTIFIC PUBLICATIONS AND COMMUNICATIONS

P5 - GRAVAGNUOLO AM, Morales-Narváez E, Longobardi S, da Silva ET, Giardina P, Merkoçi A.. (2015). ***In situ*** **Production of Biofunctionalized Few-Layer Defect-Free Microsheets of Graphene.** ADVANCED FUNCTIONAL MATERIALS, Just accepted research paper. doi: 10.1002/adfm.201500016

P4 - Longobardi S, GRAVAGNUOLO AM, Funari R, Della Ventura B, Pane F, Galano E, Amoresano A, Marino G, Giardina P. (2015). **A simple MALDI plate functionalization by Vmh2 hydrophobin for serial multi-enzymatic protein digestions.** ANALYTICAL AND BIOANALYTICAL CHEMISTRY, vol. 407; p. 487-496, ISSN: 1618-2650, doi: 10.1007/s00216-014-8309-3

P3 - Longobardi S, GRAVAGNUOLO AM, De Stefano L, Rea I, Giardina P (2013). **Self–assembling fungal proteins and their biotechnological applications.** RENDICONTI - ACCADEMIA NAZIONALE DELLE SCIENZE DETTA DEI XL. MEMORIE DI SCIENZE FISICHE E NATURALI; p. 65-76, ISSN: 0392-4130, doi: 10.4399/97888548717173

P2 - Longobardi S, GRAVAGNUOLO AM, Rea I, De Stefano L, Marino G, Giardina P (2014). **Hydrophobin-coated plates as matrix-assisted laser desorption/ionization sample support for peptide/protein analysis**. ANALYTICAL BIOCHEMISTRY, vol. 449; p. 9-16, ISSN: 0003-2697, doi: 10.1016/j.ab.2013.11.021 **(front cover)**

P1 - Leo G, Altucci C, Bourgoin-Voillard S, GRAVAGNUOLO AM, Esposito R, Marino G, Costello CE, Velotta R, Birolo L (2013). **Ultraviolet laser-induced cross-linking in peptides.** RAPID COMMUNICATIONS IN MASS SPECTROMETRY, vol. 27; p. 1660-1668, ISSN: 0951-4198, doi: 10.1002/rcm.6610

C5 - Longobardi S, GRAVAGNUOLO AM, Marino G, Giardina P (2014). **Surface functionalization through a fungal hydrophobin for proteomic applications.** In: 8th International Conference on Polymer and Fiber Biotechnology (IPFB 2014). Braga, Portugal, 25-27 May 2014

C4 - Longobardi S, GRAVAGNUOLO AM, Marino G, Giardina P (2013). **Hydrophobin Layer as Versatile Coating of Maldi Plate.** In: 4° MS-J-Day ,"I giovani e la spettrometria di massa 2013". Aula Magna Università della Basilicata, Potenza , 14 novembre 2013

C3 - Longobardi S, GRAVAGNUOLO AM, Rea I, De Stefano L, Giardina P (2014). **Fungal hydrophobin self-assembly: an active layer for multipurpose nanotech devices.** In: Italian Forum on Industrial Biotechnology and Bioeconomy (IFIB 2013) from biotechology new resources for industry. Napoli, Italy, 22-23 Ottobre 2013

C2 - Martín-Quirós A, Nevola L, Eckelt K, Camarero N, GRAVAGNUOLO AM, Llobet A, Giralt E, Gorostiza P (2012). **Photocontrol of endocytosis through engineered inhibitory peptides.** In: Gordon Research Conference on Lysosomes & Endocytosis. Proctor Academy, Aldover, NH, USA

C1 - Martín-Quirós A, Nevola L, Eckelt K, Camarero N, GRAVAGNUOLO AM, Llobet A, Giralt E, Gorostiza P (2012). **Photocontrol of endocytosis through engineered inhibitory peptides.** In: 5th IBEC Symposium on Bioengineering and Nanomedicine. Barcelona, Spain, 11th June 2012

SCIENTIFIC ACTIVITIES IN FOREIGN LABORATORIES

1° year
Visiting student: **Institute for bioengineering of Catalonia (IBEC)**, Barcelona, Spain - Tutor: **Prof. Pau Gorostiza** - Project: **"PHOTOSWITCHABLE PEPTIDES FOR NON INVASIVE REMOTE CONTROL OF CELL TRAFFICKING"** - Period: from the beginning of the PhD activity till April the 13th 2012 (1 month and a half) - Some results of the scientific activity has been presented in two international conferences (see conference list: **Photocontrol of endocytosis through engineered inhibitory peptides**).

2/3° year
Visiting student: **Catalan Institute of Nanoscience and Nanotechnology (ICN2)** campus de la UAB, Edifici ICN2, Bellaterra, (Spain) 08193. - Tutor: **Prof. Dr. Arben Merkoçy (Nanobielectronics & Biosensors Group leader)**. - Project: **"TOWARDS NOVEL BIOSENSING, DIAGNOSTICS AND DRUG DELIVERY SMART SYSTEMS: FUNCTIONALIZATION OF CARBON NANOMATERIALS BY THE HYDROPHOBIN VMH2"** - Period: from October 1st 2013 till September 5st 2014 (11 months) - The scientific visit has been supported by "PROGRAMMA DI MOBILITÁ NELL'AMBITO DELLE RETI DI ECCELLENZA DI CUI AL P.O.R. Campania FSE 2007 – 2013, Asse IV - RETE DI ECCELLENZA: CREME" coordinated by Prof. Maria Furia.

"ATTENDED ONLY" INTERNATIONAL CONFERENCES

"**Young Researchers in Life Sciences**", YRLS 2012, May 14-16th, Université Paris Diderot, Paris, France.

"**19th Transfrontier Meeting of Sensors and Biosensors**", TMSB 2014, September 25-26th, Barcelona, Spain.

ORGANIZED NATIONAL CONFERENCE

"**BIOtecnologie Industriali: UNIone tra uniVERsità e impreSE**", BIO-UNIVERSE 2015, January 30th, Università degli studi di Napoli "Federico II", Naples, Italy.

COURSES AND WORKSHOPS

"Diagnosi di interesse biologico in campo oncologico". Department of Chemical Sciences -University of Naples "Federico II" 27-04-2012. **Tesauro D.**

"Nanosistemi, diagnosi e terapia oncologica". Department of Chemical Sciences -University of Naples "Federico II" 02-05-2012. **Accardo A.**

"Biotecnologie per l'energia". Department of Chemical engineering - University of Naples "Federico II" 09-05-2012 / 16-05-2012 / 23-05-2012 **Marzocchella A. and Olivieri G.**

"On Chemical valorization of rapeseed (Brassica napus) stalk". Department of Chemical engineering - University of Naples "Federico II" 31-05-12 Gravrilescu D.

"About Fate and Behavior of Persistent Pollutants in Romanian Soils: a Condition in Bioremediation". Department of Chemical engineering - University of Naples "Federico II" 31-05-12 **Gravrilescu M.**

"Un Batterio che Viene dal Freddo". Naples - 08-06-2012 **Marino G.**

"Advanced Biotechnology". Faculty of Biotechnology -University of Naples "Federico II" 30-05-2012 / 04-06-2012 / 11-06-2012 / 14-06-2012 / 18-06-2012 **Sannia G, Pane F., Rao R., Pennacchio F. and Cocozza S.**

"Giant Viruses have a sweet tooth". Department of Chemical Sciences -University of Naples "Federico II" 11-07-2012 **Van Etten J. L.**

"Sistemi d'espressione, analisi dell' espressione genica e ingegneria proteica". Department of Structural and Functional Biology - University of Naples "Federico II" 26-06-2012 / 27-06-2012 / 03-07-2012 / 05-07-2012 / 10-07-2012 / 12-07-2012 **Bartolucci S., Fiorentino G. and Contursi P.**

"Caratterizzazione dei materiali: vantaggi ed esempi applicative delle tecniche combinate". Department of Chemical Sciences -University of Naples "Federico II" 25-10-2012 **Garavaglia M. - Pera S. - Raffin P. - "Perkin Elmer" course**

"Biopolimeri per Applicazioni Industriali e per il Biomedicale". Department of Chemical Sciences -University of Naples "Federico II" 28-11-2012 / 04-12-2012 / 06-12-2012 **Malinconico M. and Laurienzo P.**

"Genomica Funzionale" Department of Chemical Sciences -University of Naples "Federico II" 12-12-2012 / 14-12-2012 **Calabrò V.**

"Prokaryotic innate immunity - discovery of a new player" / "Prokaryotic adaptive immunity" / "Prokaryotic gene expression - Jacob & Monod revisited". Department of Structural and Functional Biology - University of Naples "Federico II" 16-04-2013 / 17-04-2013 / 18-04-2013 **van der Oost J.**

"Biomolecular interaction at the aqueous-lipid interface". Department of Chemical Sciences -University of Naples “Federico II” 04-07-2013 **Nylander T.**

"Biofilms in the environment from waste". Department of Hydraulic Geotechnical and Environmental Engineering - University of Naples "Federico II" 24-04-2013 **Van Hullebusch E.D.**

“Dynamic processes in microbial metabolism” Department of Chemical engineering - University of Naples “Federico II” 27-05-2013 **Götz P.**

"Biochemical conversion of biomass for production of value added chemicals". Department of Chemical, Materials and Industrial Production Engineering 03-06-2013 Rehmann L.

"Workshop on material science" Department of Chemical Sciences -University of Naples “Federico II” 19-06-2013 **Netti P. - Menna E. - Contele G. - Di Matteo A. - Pignataro B. - Petrone A. - Mannini P.**

“Graphene Sensors for Bioelectronic Applications”. Catalan Institute of Nanoscience and Nanotechnology (ICN2) 18-10-2013 **Garrido J.A.**

“Scientific Careers in the Life Science High and Technology Industry”. Catalan Institute of Nanoscience and Nanotechnology (ICN2) 7-11-2013 **Bryce P. Nelson** - Manager, Product Management & R&D, Sigma-Aldrich Corporation

“X-Ray Diffraction & Scattering for the Study of Biological Molecules and Human Tissues”. Catalan Institute of Nanoscience and Nanotechnology (ICN2) 22-11-2013 **Siliqi D.**

“Studies on Emissive Chemosensors and Nanoparticles for Applications in Environmental and Biomedical Fields” Catalan Institute of Nanoscience and Nanotechnology (ICN2) 22-11-2013 Lodeiro C.

“Enzyme/graphene - interaction” 13-01-2014 **El Harrad L.**

"Multifunctional Nanostructured Polymeric Multilayers for Biomedical Applications" Catalan Institute of Nanoscience and Nanotechnology (ICN2) 21-03-2014 **Mano J.**

"Technology Transfer Seminar - IP Rights and Spin-Offs". Catalan Institute of Nanoscience and Nanotechnology (ICN2) 29-05-2014 **Etxabe J. / González S. / Gavilanes I. CSIC´s Deputy Vice-Presidency for Knowledge Transfer**

"Europrogettazione" 17-10-2014 / 20-10-2014 / 24-10-2014 / 30-10-2014 **Varchetta G.**

Research Article

Rapid Communications in Mass Spectrometry

Received: 21 January 2013 Revised: 24 April 2013 Accepted: 25 April 2013 Published online in Wiley Online Library

Rapid Commun. Mass Spectrom. **2013**, *27*, 1660–1668
(wileyonlinelibrary.com) DOI: 10.1002/rcm.6610

Ultraviolet laser-induced cross-linking in peptides

Gabriella Leo[1†], Carlo Altucci[2†], Sandrine Bourgoin-Voillard[3], Alfredo M. Gravagnuolo[1], Rosario Esposito[2], Gennaro Marino[1], Catherine E. Costello[3], Raffaele Velotta[2] and Leila Birolo[1*]

[1]Dipartimento di Scienze Chimiche, Università di Napoli 'Federico II', Complesso Universitario di Monte S.Angelo, 80126 Napoli, Italy
[2]Dipartimento di Scienze Fisiche, Università di Napoli 'Federico II', Complesso Universitario di Monte S.Angelo, 80126 Napoli, Italy
[3]Center for Biomedical Mass Spectrometry, Department of Biochemistry, Boston University School of Medicine, Boston, MA 02118, USA

RATIONALE: The aim of this study was to demonstrate, and to characterize by high-resolution mass spectrometry that it is possible to preferentially induce covalent cross-links in peptides by using high-energy femtosecond ultraviolet (UV) laser pulses. The cross-link is readily formed only when aromatic amino acids are present in the peptide sequence.
METHODS: Three peptides, xenopsin, angiotensin I, and interleukin, individually or in combination, were exposed to high-energy femtosecond UV laser pulses, either alone or in the presence of spin trapping molecules, the reaction products being characterized by high resolution mass spectrometry.
RESULTS: High-resolution mass spectrometry and spin trapping strategies showed that cross-linking occurs readily, proceeds *via* a radical mechanism, and is the highly dominant reaction, proceeding without causing significant photo-damage in the investigated range of experimental parameters.
CONCLUSIONS: High-energy femtosecond UV laser pulses can be used to induce covalent cross-links between aromatic amino acids in peptides, overcoming photo-oxidation processes, that predominate as the mean laser pulse intensity approaches illumination conditions achievable with conventional UV light sources. Copyright © 2013 John Wiley & Sons, Ltd.

Cross-linking (CL) with pulsed ultraviolet (UV) lasers has been heralded as a revolutionary technique to increase the photochemical yield of protein-nucleic acid CL by one to two orders of magnitude,[1–9] and to significantly reduce the timescale of the reaction. Protein-DNA photochemical CL reactions proceed in two distinct steps:[10,11] (i) biphotonic UV light absorption and excitation of the DNA bases, in the ns-, ps- or even fs-time scale, and (ii) CL with proteins interacting with the DNA excited site and therefore lying nearby (zero-length CL), which is completed in less than 1 μs.[12] Because conformational transitions of biomolecular complexes usually require more than 100 μs, a ns or ps UV laser pulse can freeze protein-DNA interactions in real time. The exploitation of UV laser-induced CL has allowed investigators to take snapshots at various steps during the assembly of the protein-DNA complexes.[13]

These studies place great emphasis on the nucleic acid side, neglecting the possibility that proteins could also be susceptible to photo-excitation by exposure to a UV laser and that CLs could be generated in proteins. In contrast to nucleic acid–protein cross-linking, peptide–peptide and, more generally, protein–protein cross-linking mediated by laser UV light has not been reported in the scientific literature to the best of our knowledge. Typically, photo–cross-linking is induced between proteins by replacing some amino acids (e.g. leucine and methionine) with their photo-sensitive analogs, which contain photo-sensitive diazirine rings, or by the addition of external reagents,[14–18] or it is considered as a side reaction that follows the exposure of peptides and proteins to reactive oxygen species, namely singlet oxygen $^1O_2$ or hydroxyl radicals HO• on an amino acid side chain.[19–29] We have addressed the feasibility of peptide–peptide photo-cross-linking without any external intervention other than the absorption of UV light, as a way of studying transient interactions between proteins in their most native biological background.

The working hypothesis is that, upon absorption of UV light, the side chains of aromatic amino acids produce radicals that are able to react and generate covalent bonds with nearby residue(s). A UV femtosecond pulsed laser source was chosen from three different types of UV sources: cw-lamps, nanosecond, and femtosecond pulsed lasers, because of its capability to deliver higher radiation doses in shorter irradiation times, while transferring a smaller amount of heat to the irradiated target, thus inducing only minor damage to the biomolecule of interest (see, for instance, Middleton *et al.*[30]).

The experiments reported herein provide proof of concept that it is possible to introduce covalent cross-links in peptides by ultrashort UV laser pulses (i) without any incorporation of unnatural aminoacids, reagents, (ii) within seconds or even less, (iii) with high efficiency, and (iv) only

* *Correspondence to:* L. Birolo, Dipartimento di Scienze Chimiche, Università di Napoli 'Federico II', Complesso Universitario di Monte S.Angelo, 80126 Napoli, Italy.
E-mail: birolo@unina.it

† These authors contributed equally to this work.

Rapid Communications in Mass Spectrometry

with the presence of aromatic side chains. We have demonstrated that cross-links are readily formed and proceed *via* a radical mechanism without extensive photo-damage to the peptides.

EXPERIMENTAL

Xenopsin, angiotensin I, interleukin, Glu-1-fibrinopeptide B, 5,5-dimethyl-1-pyrroline *N*-oxide (DMPO), 2-methyl-2-nitrosopropane (MNP), L-ascorbic acid, matrix-assisted laser desorption/ionization (MALDI) matrix α-cyano-4-hydroxycinnamic acid, and ammonium bicarbonate (AMBIC) were purchased from Sigma (St. Louis, MO, USA). Trifluoroacetic acid (TFA) and acetonitrile (ACN) were HPLC grade solvents obtained from Carlo Erba Reagenti SPA (Arese, Italy), and the other solvents were from Baker (Mallinckrodt Baker, Milan, Italy). The molecular weight standards for the calibration of the Voyager-DE STR system were calibration mixture 1 and calibration mixture 2 purchased from AB Sciex (Framingham, MA, USA).

UV laser peptide-peptide cross-linking.

To induce the cross-link we used a powerful source of UV radiation, a custom-made version of the PHAROS laser system (Light Conversion Ltd., Vilnius, Lithuania) which is a very compact femtosecond amplified laser source – a single-unit integrated system, combining up-to-millijoule pulse energies and high average output power. This system, based on the new Yb:KGW lasing medium and on a very compact Chirped Pulse Amplification scheme, emits 1.3 mJ, 170 fs pulses, centred at 1030 nm, at a repetition rate of 2 kHz, corresponding to an average power of 2.5–2.6 W. The repetition rate can be increased up to 200 kHz, where the average output power reaches nearly 7 W. The IR pulse is then frequency up-converted into a harmonic generator stage (HIRO) where II (515 nm), III (343 nm), and VI (257 nm) harmonic pulses, lasting about 130 fs, are obtained. The system is equipped with a sophisticated pulse picker which allows one to separately select any possible repetition rate, from single-shot to 200 kHz.

Standard peptides (10 nmol of angiotensin I, xenopsin, interleukin), individually or mixed together, were dissolved in 6 μL of ammonium bicarbonate buffer (10 mM pH 7.0) and irradiated with a laser energy of 110 μJ/pulse, at a frequency of 2 kHz and a carrier λ of 257 nm, at room temperature for different time intervals from 0.01 s to 3 min. The reaction was stopped by adding 4 μL of ascorbic acid to achieve a final concentration of 20 mM, dissolved in the same buffer, immediately before use.

The same conditions were used to irradiate the individual peptides in the presence of 5,5-dimethyl-1-pyrroline *N*-oxide (DMPO) (100 mM) or 2-methyl-2-nitrosopropane (MNP) (10 mM). Sample concentration and desalting were performed using C18 reversed-phase ZipTip™ pipette tips (Millipore Corp., Billerica, MA USA). The peptides were eluted with 20 μL of a solution containing 50% ACN, 0.5% formic acid in Milli-Q water at a final concentration of 25 μM.

Maldi-time-of flight mass spectrometry (tof ms) analysis

MALDI-TOF mass spectra were recorded in positive ion mode using a Voyager STR instrument (Applied Biosystems, San Jose, CA, USA) equipped with a nitrogen laser (337 nm, 3 ns pulse width). The analytes were mixed (1:1, v/v) with a 10 mg/mL solution of α-cyanohydroxycinnamic acid in ACN/50 mM citrate buffer (7:3, v/v); for each analysis, 2 μL of this mixture was applied to the metallic sample plate and dried at room temperature. The acceleration and reflector conditions were set as follows: target voltage at 20 kV, grid voltage at 66% of the target voltage, and delayed extraction at 150 ns, to obtain the best signal-to-noise ratios and the best possible isotopic resolution. Mass calibration was performed using external peptide standards purchased from Applied Biosystems. Raw data were analyzed as monoisotopic masses, using the software provided by the manufacturer.

For semiquantitative measurements of the cross-linked peptides, a reference peptide, Glu-1-fibrinopeptide B, EGVNDNEEGFFSAR ($[M_{Glu}+H]^+$ *m/z* 1570.7), was added to the matrix in a concentration (10 μM) that yielded peak intensities of the order of those observed for the abundant analytes. The addition of a reference peptide, whose signal does not overlap with those of the peptides contained in the samples, allows correction for crystallization variability inherent to MALDI sample preparations.[31] Moreover, to average out microheterogeneity in the matrix crystals, the spectra were automatically acquired using uniformly random laser shot pattern with fixed intensity from all over the crystal rim of the matrix-analyte preparation (25 spectra per sample, 200 shots/spectrum).

Tandem mass spectrometry (MS/MS) analysis

The cross-linked products were analyzed in both MS and MS/MS modes by high-resolution mass spectrometry using a hybrid quadrupole-hexapole/Fourier transform ion cyclotron resonance mass spectrometer (Qh/FTICR (SolariX)) equipped with a 12-T actively shielded magnet (Bruker Daltonics, Billerica, MA, USA). This instrument, equipped with a nano-spray source, was operated in positive ion mode. The high voltage used for ionization was between 1000 and 1500 V and nitrogen was used as a counter-current drying gas with its temperature maintained at 180 °C. To record the spectra, an electron capture dissociation (ECD) current of 1.6 A, an ECD bias of 1.5 V and an electron pulse length of 0.07 s were employed. For collision-induced dissociation (CID) spectra, the collision voltage was set between 8 and 15 V. The collision gas was argon at a pressure of 6×10^{-6} mbar. In the electron transfer dissociation (ETD) mode, radical negative ions of fluoranthene, produced in the chemical ionization (CI) source of the SolariX mass spectrometer, were used as the reagent ions. During the ETD experiments, the crucible was heated to about 60 °C to sublimate the fluoranthene. The fluoranthene vapor then passed into the CI chamber where it was ionized *via* chemical ionization with methane. The methane tank was connected to the CI source with stainless steel tubing. Negatively charged fluoranthene ions were extracted from the CI source *via* a set of lenses. The filament was operated with a current of 3 μA. The acceleration time for the reagent was 50–100 ms and the reaction time was 20 ms.

Mass spectra were acquired in the positive-ion mode over the range *m/z* 200–2000 at a mass resolution of 60 000 at *m/z* 400. The mass accuracy was under 1 ppm. Compass Data analysis software (Bruker Daltonics) was used for data analysis; peptide sequencing and cross-linking site assignments were conducted manually employing a ±1 ppm error limit on the product ions.

RESULTS AND DISCUSSION

Three peptides, xenopsin (pyroEGKRPWIL), angiotensin I (DRVYIHPFHL), and interleukin (VQGEESNDK), alone or in combination, were exposed to the UV laser under various irradiation conditions. The first two peptides were selected because they contain one or more aromatic amino acids, whereas interleukin was included because it is devoid of aromatic moieties. Moreover, all of them fall within a molecular weight range adequate to allow direct MS and MS/MS analyses, even when cross-linked, without further manipulation of the sample. The laser setups were inspired by Fecko *et al.*,[32] who studied CL *in vitro* between oligonucleotides and proteins with a femtosecond laser system, although with a much higher repetition rate and lower-energy pulses than those used in our experiments. Our laser system allowed us to span the pulse energy in the range 10–160 μJ and laser pulse repetition rate in the range 30–200 kHz, the irradiation time being only a fraction of a second in some cases. The sample solution was introduced as 6-μL drops with peptide concentrations ranging from 0.5 to 5 mM.

Figure 1 presents the MALDI-TOF mass spectrum of a mixture of xenopsin, interleukin and angiotensin (1.6 mM each) before exposure to the laser (Fig. 1(a)), and after exposure of the mixture to UV laser pulses of 110 μJ for 10 s at a repetition rate of 2 kHz (Fig. 1(b)). The three signals in the spectrum in Fig. 1(a) correspond to the peptide standards (xenopsin $[M_x+H]^+$ *m/z* 980.6; interleukin $[M_i+H]^+$ *m/z* 1005.5; angiotensin I $[M_a+H]^+$ *m/z* 1296.6). In Fig. 1(b), there are two new signals, generated after UV-laser exposure: the peak at *m/z* 1958.4 that could be tentatively assigned as $[(2M_x-2H)+H]^+$ for two molecules of xenopsin cross-linked to one another, and the signal at *m/z* 2274.2 that could correspond to one molecule of xenopsin cross-linked to one molecule of angiotensin I, $[(M_x+M_a-2H)+H]^+$. Signals that can be ascribed to modified products resulting from oxidation of the peptides can be also observed in Fig. 1(b).

It should be noted that interleukin (that has no aromatic residue) does not appear to be involved in any of the species generated upon UV exposure. Each of the three peptides was separately exposed to the UV laser (see Fig. 6 as an example for xenopsin, and Supplementary Figs. S1 and S2 in the Supporting Information for angiotensin and interleukin, respectively), and the results confirmed that only peptides containing an aromatic side chain generated multimeric species upon exposure to UV laser light, thereby demonstrating that the CL reaction requires the presence of aromatic amino acids. These results suggest a reaction mechanism that is triggered by exposure to UV laser light and generates a CL of two aromatic ring centered radicals, analogous to the formation of bis-tyrosine and adducts of two tryptophans as observed in oxidative processes.[27,28,33]

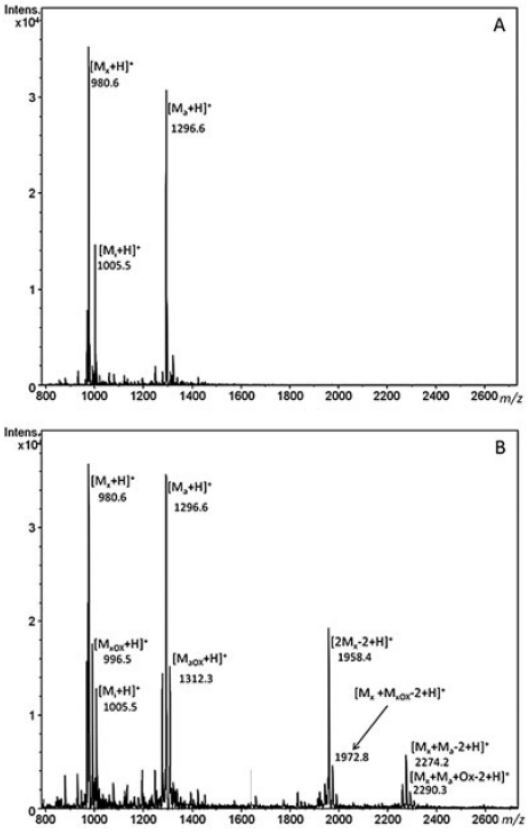

Figure 1. Positive-ion MALDI-TOF mass spectra of a mixture of xenopsin (M_x), interleukin (M_i) and angiotensin I (M_a) not irradiated (A) and irradiated for 10 s (B).

The systematic loss of 2 Da, with respect to the sum of the molecular masses of the two peptides, was observed, suggesting that two hydrogen atoms are lost in the formation of the cross-link, and this assignment was confirmed by high-resolution accurate mass measurements: the mass difference was within 1 ppm of 2.015650, the accurate mass of 2H.

MS/MS spectra of the dimeric species generated upon irradiation with UV laser pulses were obtained on the SolariX 12-T FTICR mass spectrometer in collision-induced dissociation (CID), electron capture dissociation (ECD) and electron transfer dissociation (ETD) fragmentation modes. Displayed in Figs. 2 and 3 are the CID (a) and ECD (b) MS/MS spectra generated from the $[(2M_x-2H)+3H]^{3+}$ ion (*m/z* 653.3759 (CID), *m/z* 653.3757 (ECD); calc. *m/z* 653.3756, see Supplementary Fig. S3, Supporting Information), and the $[(M_a+M_x-2H)+4H]^{4+}$ ion (*m/z* 569.3127 (CID), *m/z* 569.3131 (ECD); calc. *m/z* 569.3128, see Supplementary Fig. S4, Supporting Information), that had been tentatively assigned to the homodimer of xenopsin and the heterodimer of angiotensin I-xenopsin, respectively. Cleavage products originating from both peptide chains can be assigned, and

Rapid Communications in Mass Spectrometry

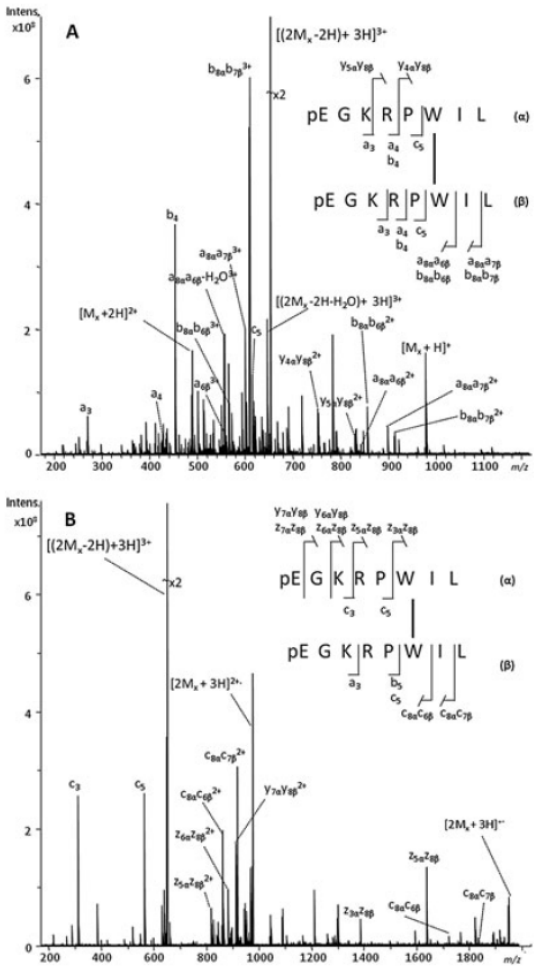

Figure 2. Positive-ion ESI-CID (A) and ESI-ECD (B) MS/MS spectra of xenopsin homodimer. The $[(2M_x - 2H) + 3H]^{3+}$ peaks at *m/z* 653.3759 and 653.3757 were selected as the precursor ions in ESI-CID and ESI-ECD MS/MS, respectively. The cross-linked sites are indicated with a line connecting the linked residues.

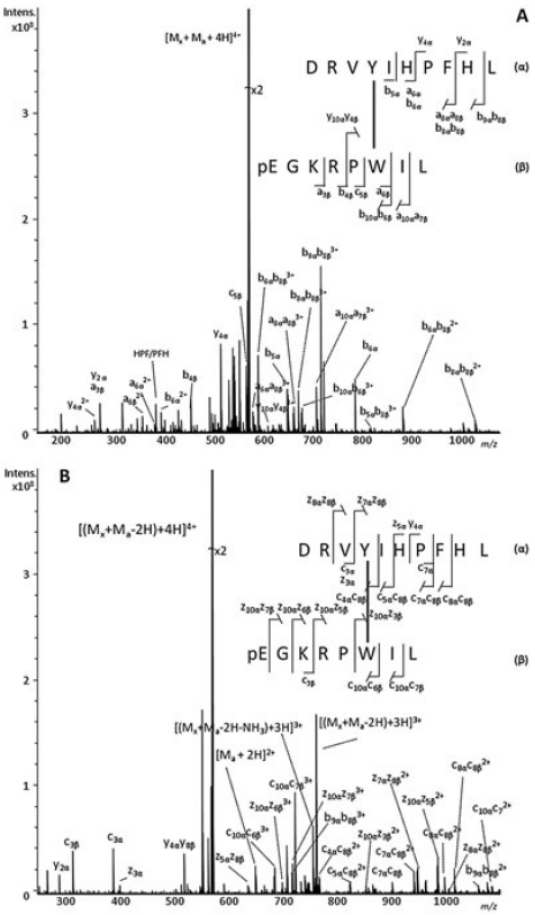

Figure 3. Positive-ion ESI-CID (A) and ESI-ECD (B) MS/MS spectra of the angiotensin I/xenopsin heterodimer. The $[(M_x + M_a - 2H) + 4H]^{4+}$ peaks at *m/z* 569.3127 and 569.3131 were selected as the precursor ions in ESI-CID and ESI-ECD MS/MS, respectively. Product ions arising from angiotensin I (DRVYIHPFHL) are labelled with an α subscript, and those from xenopsin (pEGKRPWIL) with a β subscript. The cross-linked sites are indicated with a line between the sequences.

product ions corresponding to the two peptides are, therefore, designated with either the α or the β subscript to indicate the peptide of origin.

The fragmentation observed in the low-energy CID spectrum of the homodimer (Fig. 2(a)) is dominated by ions corresponding to a-, b- and y-ions whereas, as expected, c- and z•-ion series dominate the corresponding ECD spectrum (Fig. 2(b)). In addition to short z- and a-, b-, c-ion series, it is possible to observe several $y_\alpha y_\beta$-, $z_\alpha z_\beta$-, $b_\alpha b_\beta$-, $c_\alpha c_\beta$-ions detected in their singly, doubly and/or triply charged states, that facilitate assessment of the CL sites as detailed in Supplementary Tables S1 and S2 (Supporting Information). The $z_{3\alpha}z_{8\beta}$- and $c_{8\alpha}c^{2+}_{2\beta}$-ions are key signals to univocally determine that Trp-6 is involved in the cross-link.

Similar considerations allowed the interpretation of the MS/MS spectra (Fig. 3) generated from the $[(M_x + M_a - 2H) + 4H]^{4+}$ ions tentatively assigned to the heterodimer of angiotensin I (α-chain) and xenopsin (β-chain). The MS/MS spectra of the quadruply charged ion at *m/z* 569.3127 consist of dominant b- and y-series ions for the CID spectrum (Fig. 3(a)) while c,z-series ions dominate the ECD MS/MS spectrum (Fig. 3(b)) generated from the ion *m/z* 569.3131, as detailed in Supplementary Tables S3 and S4 (Supporting Information). Several ions that can be interpreted as cross-linked species allowed definition of the location of the CL site within the peptide sequences. The $c_{10\alpha}c^{3+}_{6\beta}$-, $z_{10\alpha}z^{2+}_{3\beta}$-, $z_{7\alpha}z^{2+}_{8\beta}$-, and $c_{4\alpha}c^{2+}_{8\beta}$-ions are key signals to define that Tyr-4 and Trp-6 are involved in the CL. It should be noted that a few cross-link-free product ions were observed in the CID

spectrum and one in the ECD spectrum. To check whether this phenomenon was due to the existence of another cross-linking radical site, we attempted to assign these few product ions in the CID and ECD spectra by considering other radical sites. No ions in the MS/MS spectra could be assigned as having been formed from a differently cross-linked peptide. Moreover, the cross-link-free product ions were formed when the CID mode was employed, whereas the occurrence of such ions was minimal in the ECD spectra; it has been widely established that ECD is a more gentle activation mode than CID. Thus, we suggest that the formation of some low-abundance cross-link-free product ions results from a competition between cleavages of the cross-link and cleavage along the peptide backbone, indicating that the relative stability of the cross-link is comparable with that of the bonds along the peptide backbone. ETD (spectra not shown) confirmed this view by leading to assignments similar to those from ECD.

To test the hypothesis that UV-induced CL is a radical reaction, exposure to the laser was carried out in the presence of spin trap molecules. Spin traps are often used to allow the visualization of transient free radical populations by reacting with short-lived radicals to produce persistent spin adduct radicals that can be studied by electron paramagnetic resonance (EPR)[34,35] or MS since the spin trap molecules covalently label the radical site in the molecule.[36–41] Therefore, the peptides were exposed to the UV laser as described above, for either 10 s or 1 min, but in the presence of either DMPO or MNP.

MALDI-TOF MS analysis of xenopsin irradiated in the presence of 10 mM DMPO (Fig. 4(b)) yielded a signal at *m/z* 1091.6, which is 111.1 *m/z* units higher than the mass of protonated xenopsin ($[M_x+H]^+$ *m/z* 980.5, Fig. 4(a)), thus suggesting that a single DMPO molecule was trapped on the peptide. The ETD spectrum of the $[M_x+M_{DMPO}+2H]^{2+}$ ion (*m/z* 546.8261; calc. *m/z* 546.8256), presented in Fig. 5, yielded the charge-reduced ion $[M_x+M_{DMPO}+2H]^+\cdot$ at *m/z* 1093.6499 (calc. *m/z* 1093.6517) and, more interestingly, c-, z- y- and b-series product ions bearing the DMPO modification. For example, the ion at *m/z* 924.5906 (labelled as y_6*) (calc. *m/z* 924.5903) corresponds in mass to a y_6 ion plus DMPO (+112.0762 *m/z* units) and the ion at *m/z* 865.4914 (labelled as c_6*) (calc. *m/z* 865.4917) corresponds in mass to a c_6 ion containing DMPO (+112.0762 *m/z* units). Moreover, different internal product ions of the peptide also show the addition of DMPO (*e.g.*, $[M_x+M_{DMPO}-H_2O+H]^+$ at *m/z* 537.8209 (calc. *m/z* 537.8203)). The CID spectrum showed complementary ions such as some corresponding to cleavages of amino acids from the N-terminus of the peptide backbone with loss of DMPO (b_4 and c_5) and some corresponding to cleavages of amino acids from the N-terminus of the peptide backbone bearing DMPO (y_4*, b_6*, b_7*, a_7*). The concomitant presence of the y_4*-, c_6*- and c_5-ions indicates that the DMPO adduct is located on Trp-6 in xenopsin. The ECD spectrum (Supplementary Fig. S5, Supporting Information) further confirms the interpretation, showing several internal product ions bearing the DMPO moiety. Similar analyses were performed for the same peptide irradiated in the presence of 10 mM MNP (see Supplementary Fig. S6, Supporting Information, and relative comments).

The interpretation of these data was severely complicated by a significant loss of DMPO and MNP molecules during fragmentation. Possibly the bond between DMPO or MNP and the residue in the peptide is weak and thus susceptible to facile cleavage during MS/MS. To determine the adduct sites, we used CID, ETD and ECD activation modes. The ETD and ECD activation modes are both gentler than CID activation. In the ECD and ETD spectra, the most abundant product ions preserved the spin trap moieties, and a loss of MNP or DMPO could be observed only for a few, usually less abundant, product ions.

The product ions assigned in the CID spectra are indicated in red on the peptide sequence in the ETD or ECD spectra. We can still observe several ions bearing MNP or DMPO although some significant product ions can be attributed to losses of MNP or DMPO. This has been already reported in other cases,[36,42] and interpreted as a cleavage competition between the covalent bond with the spin trap on the side chain and the peptide backbone. Nevertheless, the presence

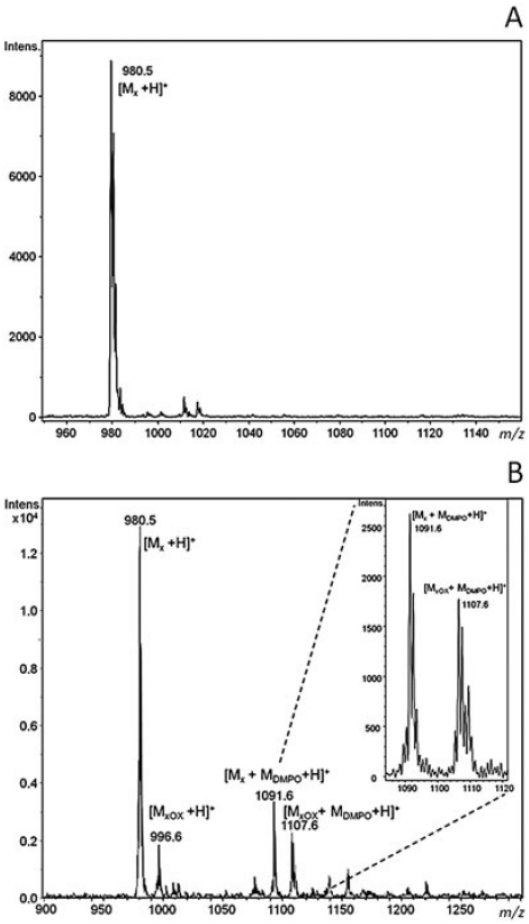

Figure 4. Positive-ion MALDI-TOF mass spectra of xenopsin (A) and xenopsin after exposure to the UV laser in the presence of DMPO (B). The peak at *m/z* 1091.6 corresponds to the $[M+H]^+$ ion of the adduct formed between one molecule of DMPO and one molecule of xenopsin. In the inset, a zoom of the selected *m/z* range.

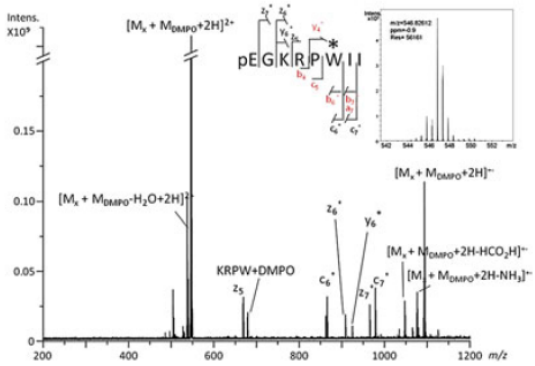

Figure 5. Positive-ion ESI-ETD mass spectrum of xenopsin, exposed to the UV laser in the presence of DMPO. The $[M_x + M_{DMPO} + 2H]^{2+}$ peak at *m/z* 546.8261 was selected as the precursor ion. The asterisk indicates the residue at the adduct site. The members of the ion series detected in the CID spectrum are indicated in red. In the inset, the ESI-FTICR mass spectrum of the precursor ion.

of product ions that retained the DMPO moiety allowed us to suggest the assignment of the DMPO and MNP linkages to the Trp-6 residue of xenopsin, as also validated in the ECD analysis (Supplementary Fig. S5, Supporting Information).

The same experiments with angiotensin I and DMPO and MNP (see SupplementaryFigs. S7 and S8, Supporting Information) suggest DMPO and MNP linkages to the Tyr-4 residue of angiotensin I.

CL has already been reported as a possible type of UV-induced damage in polypeptides.[19–29] It is, however, important to stress that all the photochemical reactions previously described are reported to follow upon the initial addition of singlet oxygen $^1O_2$ or hydroxyl radical HO• to an amino acid side chain. The intermediates then undergo a variety of further reactions which can result in radical formation and ring-opening reactions, including cross-links in proteins.

We then considered comparing the results obtained with our femtosecond laser source with those recorded after exposure of the samples to conventional UV light sources such as a UV lamp. Releasing the same dose (0.5 J) to the target with a typical UV lamp would, however, have taken a very long time, between several hours and 2 days of irradiation, and such a long time would have resulted in deterioration of our sample (even evaporation would no longer be non-negligible). Therefore, we compared our result with those obtained with the femtosecond laser system operated under very different conditions, to make it as close as possible to a standard UV cw-lamp. Xenopsin was exposed to UV light at reduced pulse intensity while extending the exposure time, so as to keep the same total energy amount (0.5 J): thus, the comparison was carried out under the two conditions 6×10^2 μW cm^{-2} and 1.3×10^6 μW cm^{-2} for 58 min (0.75×10^{-3} μJ/pulse, 200 kHz repetition rate) and 1.56 s (160 μJ/pulse, 2 kHz repetition rate). The former are the conditions employed for the result shown in Fig. 6(c), where the same dose was released as in Fig. 6(b), but with laser nano-pulses (carrying very low energy), delivered in a much larger number and for a much longer irradiation time than in the experiment shown in Fig. 6(b).

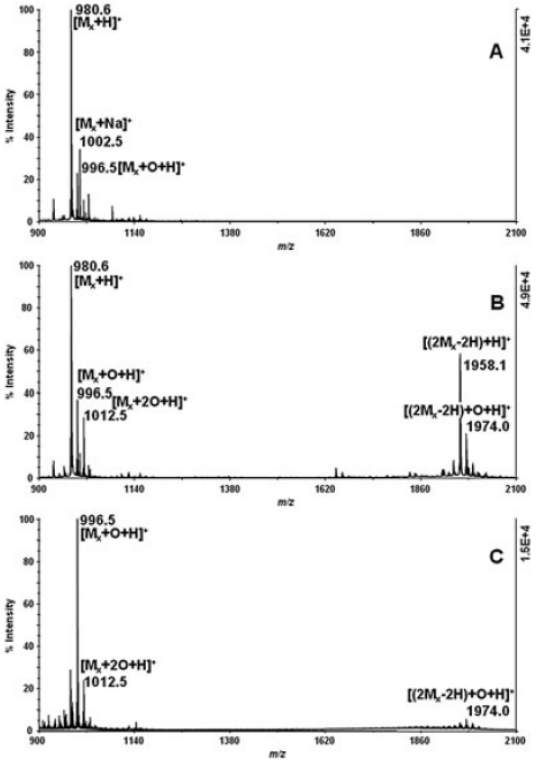

Figure 6. Positive-ion MALDI-TOF mass spectrum of xenopsin after exposure to the high-intensity and low-intensity UV laser. Xenopsin ($[M+H]^+$ *m/z* 980.5) (A, control) was exposed to (B) high-intensity UV light for 1.56 s (1.3×10^6 μW cm^{-2}, 160 μJ/pulse, 2 kHz repetition rate, 1.56 s), so that an energy of 0.5 J was released to the solution. (C) The same energy (0.5 J) was released in 58 min (6×10^2 μW cm^{-2}, 0.75×10^{-3} μJ/pulse, 200 kHz repetition rate, 58 min) .

For the low-energy/pulse sample (Fig. 6(c)), ions arising from side-chain photo-oxidation are the main components of the mass spectrum. The most abundant ion corresponds to the addition of one oxygen atom, probably due to the formation of hydroxytryptophan ($M_x + O$, Δ +16 Da), in agreement with data reported by Grosvenor *et al.*,[19] where a mean intensity of the order of few mW cm^{-2} was used. The signal at *m/z* 1012.5 ($M_x + 2O$, Δ +32 *m/z* units) can be accordingly attributed to *N*-formylkynurenine (NFK)/dihydroxytryptophan. Further signals that can be ascribed to some hydroxyformylkynurenine (M + 3O, Δ +48 Da) can also be detected, as well as a minor dimeric species. In the MS analysis of the high-energy/pulse sample (Fig. 6(b)), the main reaction product is the dimeric form of the peptide (2M – 2H, Δ –2 Da) without notable increase in the signals of the photo-oxidation products with respect to the reference, non-irradiated sample (Fig. 6(a)).

Moreover, when using the high pulse energy irradiation, no notable difference was observed in the mass spectra of xenopsin samples, analyzed immediately or left in the open air for 58 min after irradiation (see Supplementary Figs. S9

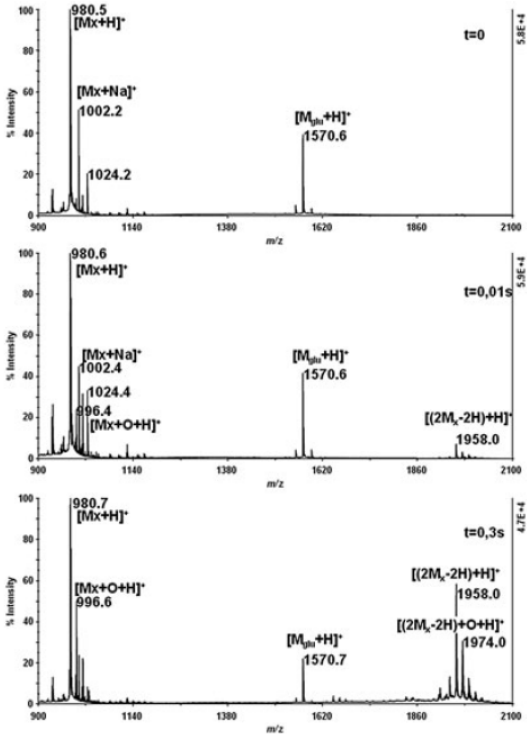

Figure 7. Positive-ion MALDI-TOF mass spectrum of xenopsin after exposure to the high-intensity UV laser as a function of exposure time. Xenopsin ($[M+H]^+$ *m/z* 980.5) (A, control) was exposed to high-intensity UV light (2 kHz, 160μJ/pulse) for 0.01 s (B) and 0.3 s (C). Glu-1-fibrinopeptide B, $[M_{Glu}+H]^+$ *m/z* 1570.7, was introduced as reference peptide in the matrix to provide a semi-quantitative evaluation of the yield of CL.

and S10 Supporting Information). This suggests that the oxidation products detected in the low-energy/pulse sample are a consequence of exposure to the UV laser.

Figure 7 reports examples of a semi-quantitative analysis of the yield of cross-linking as a function of the exposure time. Xenopsin was irradiated with a UV laser (2 kHz, 160 μJ/pulse) for different exposure times starting from 0.01 s and analyzed by MALDI-TOF, with the introduction of a reference peptide (Glu-1-fibrinopeptide B, $[M_{Glu}+H]^+$ *m/z* 1570.6) in the matrix to provide a semi-quantitative evaluation of the yield of CL.[31] Even in the high-energy/pulse regime, some photoxidation products could be observed, and these increased upon increasing the exposure time. However, some consistent cross-linking was achieved with exposure times as low as 0.01 s (corresponding to only 20 laser pulses) and CL was consistently the predominant reaction.

These results suggest that a conventional UV cw-lamp would probably fail to induce the consistent amount of peptide–peptide cross-linking, observed with the irradiation conditions of Fig. 6(b), typical of femtosecond laser sources. As a consequence, we can also conclude that the key parameter in obtaining the observed cross-linking is the peak power of the delivered laser pulses rather than the integrated dose of radiation energy, indicating a possible nonlinear excitation mechanism of the involved molecules at a microscopic level, that will be addressed in forthcoming studies.

CONCLUSIONS

We have demonstrated herein that, upon exposure to pulsed UV laser light of wavelength near 260 nm, a 'zero-length' covalent bond between the aromatic side chains of amino acids in different peptide molecules can be formed with good efficiency on an extremely rapid time scale, probably in the pico- or even femtosecond range. We have determined that photochemical CL is by far the predominant reaction, and that it requires the light intensity that can be generated with pulsed laser sources since, as the average laser intensity is reduced, down to that of conventional UV lamps, photo-damage is observed, similar to damage occurring with conventional UV light sources.[20–28]

We defined a molecular basis for the exploitation of UV-pulsed laser sources as a powerful CL agent, that would certainly have a strong impact on the possibility of studying transient interactions among proteins, and the dynamics of the contacts within multi-protein complexes, and to discover transient interactions which have so far escaped observation in 'molecular sociology of the cell' studies.[43] Although a demonstration that our initial observations of efficient cross-links generated between aromatic amino acids in peptides can be extended to proteins, to freeze biologically significant interactions, will demand further experiments, the results presented here offer the first indications of the feasibility of the development of such an approach.

The extremely fast kinetics of the reactions, the almost instantaneous diffusion of light within the cell, and the absence of exogenous chemical reactants, suggest that, once established, UV laser CL will represent an innovative and important tool well tailored for *in vivo* applications.

SUPPORTING INFORMATION

Additional supporting information may be found in the online version of this article.

Acknowledgements

CA, RE, and RV wish to acknowledge the European Community (ATLAS Contract No. 221952) for the support to set up the laser source experimental apparatus. The BUSM Mass Spectrometry Resource is supported by NIH grant P41 RR10888/GM104603; the SolariX FTMS was acquired with NIH grant S10 RR025082. LB and GL wish to aknowledge the 'Programma per la Breve Mobilità' of the Università di Napoli Federico II, for the financial support to GL in the visit to the CEC laboratory. We thank Prof. Orlando Crescenzi, Dipartimento di Scienze Chimiche, Napoli, for critical discussions.

REFERENCES

[1] C. A. Harrison, D. H. Turner, D. C. Hinkle. Laser crosslinking of *E. coli* RNA polymerase and T7 DNA. *Nucleic Acids Res.* **1982**, *10*, 2399.

[2] J. W. Hockensmith, W. L. Kubasek, W. R. Vorachek, P. H. Von Hippel. Laser cross-linking of nucleic acids to proteins. Methodology and first applications to the phage T4 DNA replication system. *J. Biol. Chem.* **1986**, *261*, 3512.

[3] S. Lejnine, G. Durfee, M. Murnane, H. C. Kapteyn, V. L. Makarov, J. P. Langmore. Crosslinking of proteins to DNA in human nuclei using a 60 femtosecond 266 nm laser. *Nucleic Acids Res.* **1999**, *27*, 3676.

[4] I. G. Pashev, S. I. Dimitrov, D. Angelov. Crosslinking proteins to nucleic acids by ultraviolet laser irradiation. *Trends Biochem. Sci.* **1991**, *16*, 323.

[5] C. Russmann, J. Stollhof, C. Weiss, R. Beigang, M. Beato. Two wavelength femtosecond laser induced DNA–protein crosslinking. *Nucleic Acids Res.* **1998**, *26*, 3967.

[6] C. Russmann, M. Truss, A. Fix, C. Naumer, T. Herrmann, J. Schmitt, J. Stollhof, R. Beigang, M. Beato. Crosslinking of progesterone receptor to DNA using tuneable nanosecond, picosecond and femtosecond UV laser pulses. *Nucleic Acids Res.* **1997**, *25*, 2478.

[7] D. Angelov, M. Charra, C.W. Müller, J. Cadet, S. Dimitrov. Solution study of the NF-kB p50-DNA complex by UV laser protein-DNA cross-linking. *Photochem. Photobiol.* **2003**, *77*, 592.

[8] D. Angelov, V. Yu Stefanovsky, S. I. Dimitrov, V. R. Russanova, E. Keskinova, I. G. Pashev. Protein-DNA crosslinking in reconstituted nucleohistone, nuclei and whole cells by picosecond UV laser irradiation. *Nucleic Acids Res.* **1988**, *16*, 4525.

[9] C. Altucci, A. Nebbioso, R. Benedetti, R. Esposito, V. Carafa, M. Conte, M. Micciarelli, L. Altucci, R. Velotta. Nonlinear protein – nucleic acid crosslinking induced by femtosecond UV laser pulses in living cells. *Laser Phys. Lett.* **2012**, *9*, 234.

[10] P. Kryukov, V. Letokhov, D. Nikogosyan, A. Borodavkin, E. Budowsky, N. Simukova. Multiquantum photoreactions of nudeic acid components in aqueous solution by powerful ultraviolet picosecond radiation. *Chem. Phys. Lett.* **1979**, *61*, 375.

[11] D. N. Nikogosyan. Two-quantum UV photochemistry of nucleic acids: Comparison with conventional low-intensity UV photochemistry and radiation chemistry. *Int. J. Radiat. Biol.* **1990**, *57*, 233.

[12] J. W. Hockensmith, W. L. Kubasek, W. R. Vorachek, E. M. Evertsz, P. H. Von Hippel. Laser cross-linking of protein-nucleic acid complexes. *Methods Enzymol.* **1991**, *46*, 211.

[13] A. K. Nagaich, G. L. Hager. UV laser cross-linking: a real-time assay to study dynamic protein/DNA interactions during chromatin remodeling. *Sci STKE* **2004**, *2004*, 113.

[14] M. Suchanek, A. Radzikowska, C. Thiele. Photo-leucine and photo-methionine allow identification of protein-protein interactions in living cells. *Nat. Methods* **2005**, *2*, 261.

[15] J. W. Chin, P. G. Schultz. In vivo photocrosslinking with unnatural amino acid mutagenesis. *Chembiochem* **2002**, *3*, 1135.

[16] I. Forné, J. Ludwigsen, A. Imhof, P. B. Becker, F. Mueller-Planitz. *Probing the conformation of the ISWI ATPase domain with genetically encoded photoreactive crosslinkers and mass spectrometry.* Mol. Cell. Proteomics **2012**. DOI: 10.1074/mcp.M111.012088.

[17] D. P. Smith, J. Anderson, J. Plante, A. E. Ashcroft, S. E. Radford, A. J. Wilson, M. J. Parker. Trifluoro-methyldiazirine: an effective photo-induced cross-linking probe for exploring amyloid formation. *Chem. Commun.* **2008**, *44*, 5728.

[18] D. Rotili, M. Altun, R. B. Hamed, C. Loenarz, A. Thalhammer, R. J. Hopkinson, Y. M. Tian, P. J. Ratcliffe, A. Mai, B. M. Kessler, C. J. Schofield. Photoactivable peptides for identifying enzyme-substrate and protein-protein interactions. *Chem. Commun.* **2011**, *47*, 1488.

[19] A. J. Grosvenor, J. D. Morton, J. M. Dyer. Profiling of residue-level photo-oxidative damage in peptides. *Amino Acids* **2010**, *39*, 285.

[20] M. J. Davies. Reactive species formed on proteins exposed to singlet oxygen. *Photochem. Photobiol. Sci.* **2004**, *3*, 17.

[21] J. Mizdrak, P. G. Hains, R. J. W. Truscott, J. F. Jamie, M. J. Davies. Tryptophan-derived ultraviolet filter compounds covalently bound to lens proteins are photosensitizers of oxidative damage. *Free Radical Biol. Med.* **2008**, *44*, 1108;

[22] J. A. Aquilina, J. A. Carver, R. J. Truscott. Elucidation of a novel polypeptide cross-link involving 3-hydroxykynurenine. *Biochemistry* **1999**, *38*, 11455.

[23] J. A. Aquilina, J. A. Carver, R. J. Truscott. Polypeptide modification and cross-linking by oxidized 3-hydroxykynurenine. *Biochemistry* **2000**, *39*, 16176.

[24] C. L. Hawkins, M. J. Davies. Generation and propagation of radical reactions on proteins. *Biochim. Biophys. Acta* **2001**, *1504*, 196.

[25] N. Igarashi, S. Onoue, Y. Tsuda. Photoreactivity of amino acids: tryptophan-induced photochemical events via reactive oxygen species generation. *Anal. Sci.* **2007**, *23*, 943.

[26] C. Fonseca, M. R. Domingues, C. Simões, F. Amado, P. Domingues. Reactivity of Tyr-Leu and Leu-Tyr dipeptides: identification of oxidation products by liquid chromatography-tandem mass spectrometry. *J. Mass Spectrom.* **2009**; *44*, 681.

[27] M. R. Domingues, P. Domingues, A. Reis, C. Fonseca, F. M. Amado, A. J. Ferrer-Correia. Identification of oxidation products and free radicals of tryptophan by mass spectrometry. *J. Am. Soc. Mass Spectrom.* **2003**, *14*, 406.

[28] E. R. Stadtman, R. L. Levine. Free radical-mediated oxidation of free amino acids and amino acid residues in proteins. *Amino Acids* **2003**, *25*, 207.

[29] S. D. Maleknia, K. Downard. Radical approaches to probe protein structure, folding, and interactions by mass spectrometry. *Mass Spectrom. Rev.* **2001**, *20*, 388.

[30] C. T. Middleton, K. de La Harpe, C. Su, Y. K. Law, C. E. Crespo-Hernández, B. Kohler. DNA excited-state dynamics: from single bases to the double helix. *Annu. Rev. Phys. Chem.* **2009**, *60*, 217.

[31] C. R. Jiménez, K. W. Li, K. Dreisewerd, H. D. Mansvelder, A. B. Brussaard, B. B. Reinhold, R. C. Van der Schors, M. Karas, F. Hillenkamp, J. P. Burbach, C. E. Costello, W. P. Geraerts. Pattern changes of pituitary peptides in rat after salt-loading as detected by means of direct, semiquantitative mass spectrometric profiling. *Proc. Natl. Acad. Sci. USA* **1997**, *94*, 9481.

[32] C. J. Fecko, K. M. Munson, A. Saunders, G. Sun, T. P. Begley, J. T. Lis, W. W. Webb. Comparison of femtosecond laser and continuous wave UV sources for protein-nucleic acid crosslinking. *Photochem. Photobiol.* **2007**, *83*, 1394.

[33] E. R. Stadtman. Oxidation of free amino acids and amino acid residues in proteins by radiolysis and by metal-catalyzed reactions. *Annu. Rev. Biochem.* **1993**, *62*, 797.

[34] M. J. Davies, C. L. Hawkins. EPR spin trapping of protein radicals. *Free Radical Biol. Med.* **2004**, *36*, 1072.

[35] O. Augusto, S. M. Vaz. EPR spin-trapping of protein radicals to investigate biological oxidative mechanisms. *Amino Acids* **2007**, *32*, 535.

[36] Y.-R. Chen, C.-L. Chen, L. Zhang, K. B. Green-Church, J. L. Zweier. Superoxide generation from mitochondrial NADH dehydrogenase induces self-inactivation with specific protein radical formation. *J. Biol. Chem.* **2005**, *280*, 37339.

[37] L. J. Deterding, S. Bhattacharjee, D. C. Ramirez, R. P. Mason, K. B. Tomer. Identification of the myoglobin tyrosyl radical by immuno-spin trapping and its dimerization. *Anal. Chem.* **2007**, *79*, 6236.
[38] L. J. Deterding, D. C. Ramirez, J. R. Dubin, R. P. Mason, K. B. Tomer. Identification of free radicals on hemoglobin from its self-peroxidation using mass spectrometry and immuno-spin trapping: observation of a histidinyl radical. *J. Biol. Chem.* **2004**, *279*, 11600.
[39] C. W. Fenwick, A. M. English Trapping and LC – MS identification of protein radicals formed in the horse heart metmyoglobin–H_2O_2 reaction. *J. Am. Chem. Soc.* **1996**, *118*, 12236.
[40] M. N. Harris, S. W. Burchiel, P. G. Winyard, J. R. Engen, C. D. Mobarak, G. S. Timmins. Determining the site of spin trapping of the equine myoglobin radical by combined use of EPR, electrophoretic purification, and mass spectrometry. *Chem. Res. Toxicol.* **2002**, *15*, 1589.
[41] O. M. Lardinois, K. B. Tomer, R. P. Mason, L. J. Deterding. Identification of protein radicals formed in the human neuroglobin-H_2O_2 reaction using immuno-spin trapping and mass spectrometry. *Biochemistry* **2008**, *47*, 10440.
[42] C. D. Detweiler, O. M. Lardinois, L. J. Deterding, P. R. O. De Montellano, K. B. Tomer, R. P. Mason. Identification of the myoglobin tyrosyl radical by immuno-spin trapping and its dimerization. *Free Radical Biol. Med.* **2005**, *38*, 969.
[43] C. V. Robinson, A. Sali, W. Baumeister. The molecular sociology of the cell. *Nature* **2007**, *450*, 973.

AKNOWLEDGMENTS

I am absolutely grateful to Prof. Paola Giardina to welcome me in her team and for her profuse, tireless, scientific and moral support.

Thanks to the scientific coordinator of the doctoral programme, Prof. Giovanni Sannia, a guide throughout these years of professional growth.

Moreover I would like to thank the kind people and great scientists I met at the Department of Chemical Sciences, “Federico II”, and at the Catalan Institute of Nanoscience and Nanotechnology and my co-authors from other institutes. Particularly thanks to Prof. Arben Merkoçi, to Dr. Sara Longobardi and to Dr. Eden Morales-Narváez, my major teachers together with Prof. Paola Giardina.

I would also like to thank Prof. Gennaro Marino, for motivating me from the very beginning of my scientific career through his inspiring ideas and exciting interest in science.

Thanks to the PhD students who took part to the organization of the first “Bio-UNIVERSE” meeting, on Industrial Biotechnology, a big success.

Thanks to the nice group of friends of car-pooling who travel with me from my home town, Cava de’ Tirreni, to Naples, and to the friends of my football team “Cava2000” in which I have been playing for many years, enjoying the sport after work.

Thanks to the people who surprise me everyday making my life exciting and giving me energy to work, in particular my family, my friends and not only.

Alfredo Maria Gravagnuolo

The world is so full of a number of things,
I’m sure we should all be as happy as kings.
Robert Louis Stevenson.